

**Modelling of Transport Phenomena for Improved Steel Quality in
a Delta Shaped Four Strand Tundish**

Kinnor Chattopadhyay

Mining and Materials Engineering

McGill University, Montreal

April 2011

A thesis submitted to McGill University in partial fulfilment of the
requirements of the degree of Doctorate of Philosophy

© Kinnor Chattopadhyay 2011

ABSTRACT

Physical and mathematical modelling studies were performed, in order to analyze various transport phenomena occurring during steel making tundish operations. Their effects on liquid metal quality were reported. A full-scale water model of a twelve tonne, delta shaped, four strand, billet caster tundish was used for physical modelling. The commercial code ANSYS FLUENT 12 was used for carrying out mathematical modelling. The tundish used in the present study is a full scale replica of that operated at the RTIT/QIT plant in Sorel Tracy, Canada and is located at MMPC's water modelling laboratory at McGill University.

It is a long lasting fact that the flow pattern within a tundish greatly affects the output metal quality. As such the insertion of flow modifiers in a tundish is a common practice. In the present study, eighteen different arrangements of flow modifier systems (combinations of impact pad and dams) were considered, and mathematical modelling was performed to predict the inclusion removal efficiency for each tundish configuration. A new dimensionless number (Gu) has been proposed, which is a good measure of steel cleanliness.

During melt transfer from the ladle to the tundish, inert gas is injected into the ladle shroud, just below the slide gate, so as to

prevent aspiration of ambient air. The effect of inert gas shrouding on the fluid flow patterns and slag movements have been numerically predicted by using a 3D mathematical model, and then validated with water model experiments.

The effect of the alignment of the ladle shroud during melt transfer was also studied, using a 3D mathematical model, supported by subsequent water model experiments. It was demonstrated that a slight bias from the vertical can be very detrimental to steel quality. Remedial measures have been suggested.

During typical steelmaking tundish operations, conditions are generally non-isothermal. Variable heat losses take place from the free surface and from the walls of the tundish. Similarly, during a ladle change, the steel poured in from the new ladle will tend to be at a higher temperature than the liquid steel remaining in the tundish. Flow patterns change under non-isothermal conditions and hence affect output steel quality. A thorough study has been performed to visualize the effect of thermal gradients on fluid flow patterns, and temperature distributions generated within the delta shaped tundish.

RÉSUMÉ

Dans la présente étude, la modélisation physique et numérique fut utilisée pour analyser l'effet sur la qualité du métal liquide de différents phénomènes de transports ayant lieu dans un panier répartiteur durant les opérations de coulée d'acier. Un modèle physique pleine échelle d'un panier répartiteur de forme triangulaire d'une capacité de douze tonnes comprenant quatre jets pour la coulée de billettes ainsi qu'un modèle mathématique utilisant le logiciel ANSYS FLUENT 12 fut utilisé. Le panier utilisant l'eau comme fluide plutôt que l'acier est une réplique de celui utilisé à l'aciérie RTIT/QIT de Sorel Tracy, Canada.

Il est bien connu que les patrons d'écoulement qui se développent dans le panier affectent grandement la qualité du métal à la sortie et, en conséquence, l'insertion de modificateurs d'écoulements est pratique courante. Dans la présente étude, dix huit arrangements différents de modificateurs d'écoulements (panneaux d'impacts et digues) furent considérés et furent numériquement modélisés pour prédire l'efficacité à limiter l'entraînement d'inclusion lors de la coulée.

Durant le transfert de l'acier de la poche de coulée vers le panier répartiteur, du gaz inerte est injecté dans le jet immédiatement en dessous de la valve coulissante pour prévenir l'aspiration d'air

ambiant. L'effet de l'injection du gaz sur le patron d'écoulement et sur les mouvements du laitier de surface a été estimé grâce à un modèle mathématique en volume (3D) et les résultats furent validés expérimentalement en utilisant le modèle physique à l'eau contenant un laitier de microbilles de verre creuses flottantes.

L'effet de l'alignement du jet provenant de la poche de coulée qui alimente le panier répartiteur fut aussi étudié par modélisation mathématique en trois dimensions et subséquemment, par des tests physiques avec l'eau. Il fut prouvé que les conséquences d'un léger désalignement vertical du jet est catastrophique et des solutions correctrices sont proposées.

Durant les opérations réelles de coulées de l'acier avec panier répartiteur, les conditions ne sont pas isothermes. Il y a des pertes calorifiques provenant de la surface et des côtés du panier. Durant les opérations de changement de poche de coulée, l'acier provenant de la nouvelle poche peut aussi être plus chaud que le restant du panier provenant de la poche précédente. Les patrons d'écoulement change donc sous ces effets non isothermes et affectent aussi la qualité de l'acier sortant. Une étude poussée fut menée pour illustrer l'effet des gradients thermiques sur les patrons d'écoulements et sur la distribution de température dans le panier triangulaire.

ACKNOWLEDGEMENTS

I deeply acknowledge the encouragement, academic advice and support given by my thesis supervisors, Professor R.I.L. Guthrie and Dr M. Isac during my studies at the MMPC. I would like to thank Dr Luis Calzado for helping me in making my experimental setups and carrying out my experiments. I would also like to thank Prof Mainul Hasan for giving me valuable advices on mathematical modelling throughout my study at McGill University.

Special thanks go to our industrial collaborator RTIT/QIT for letting us work on their industrial problems in the full scale water model replica present here at McGill.

My sincere thanks to all the members of the machine shop, and especially Csaba Szalacsi, for fabricating various components of the experimental setup, and also for his great suggestions which made the design better.

I would definitely acknowledge the financial support given to me by the Faculty of Engineering and my supervisors, in the form of the McGill Engineering Doctoral Award (HATCH for 2009-2010 and ERF for 2010-2011), which made it possible for me to study at McGill University.

I would like to thank Patrick Lemieux for his efforts in translating the abstract into French.

I will cherish the warm memories of time well spent with friends and colleagues here at McGill University.

Lastly, but most importantly, I would like to express my gratitude to my loving parents for their constant encouragement and support.

Table of Contents

1.0 Introduction	17
2.0 Literature Review	21
2.1 Physical Modelling	21
2.2 Mathematical Modelling	25
2.3 Research on tundish modelling in the last decade	35
3.0 General Procedures for Physical and Mathematical Modelling	78
3.1 Water modelling procedures	78
3.2 Mathematical modelling procedures	80
3.2.1 Basic equations involved	81
3.2.2 Choice of a proper turbulence model	84
3.2.3 Schemes and algorithms used	89
3.2.4 Grid Independency	90
3.2.5 Modelling of discrete phase and multiphase flows	97
4.0 Effect of Different Flow Modifier Arrangements on Liquid Metal Quality	104
4.1 Introduction	104

4.2 Mathematical modelling procedures	114
4.3 Eighteen different flow modifiers arrangements (in 3D)	116
4.4 Results and discussion	118
4.4.1 Effect of the use of weirs or dams along with the standard impact pad	124
4.4.2 Effect of different sizes of the impact pad on fluid flow and inclusion removal in the tundish	152
4.4.3 Comparative values of (RRI) for all 18 designs	162
4.4.4 Validation of mathematical prediction with water LiMCA studies	164
4.5 Importance of dimensionless numbers and the Guthrie Number (Gu)	165
5.0 Inert Gas Shrouding During Melt Transfer from the Ladle to the Tundish	173
5.1 Introduction	173
5.2 Experimental and mathematical modelling procedures	177
5.3 Results and discussion	181
5.3.1 Bubble trajectories in the tundish	181
5.3.2 Fluid flow patterns in the tundish	188

5.3.3 Modelling of the exposed 'eye' using the multiphase VOF model	195
5.3.4 Effect of inert gas shrouding on residence time distributions	207
6.0 Effect of Ladle Shroud Misalignment on Liquid Metal Quality	
6.1 Introduction	211
6.2 Experimental and mathematical modelling procedures	212
6.3 Results and discussion	216
6.3.1 Slag entrainment	216
6.3.2 Tracer Dispersion and 'Exposed Eye'	220
6.3.3 Bubble and Inclusion Trajectories	224
6.3.4 Contours of turbulent kinetic energy	226
6.3.5 Submerged and non-submerged ladle shroud considerations	235
6.3.6 Preventative measures recommended for the plant	238
7.0 Modelling of Non-Isothermal Melt Flows	240
7.1 Introduction	240
7.2 Experimental procedures	245

7.3 Numerical modelling procedures	248
7.4 Results and discussion	251
7.4.1 Mathematical modelling of tracer dispersion for steady state casting operations.	251
7.4.2 Physical modelling of tracer dispersion for steady state casting operations.	283
7.4.3 Validation of the mathematical model against experimental results.	298
7.4.4 Physical modelling of tracer dispersion during ladle change operations.	309
7.4.5 Effect of heat losses from the tundish walls and free surface.	321
8.0 Conclusions and Recommendations	324
Future Work	328
Contribution to Original Knowledge	329
REFERENCES	333
APPENDIX: Applications of Computational Fluid Dynamics (CFD) in Iron and Steel Making	348

NOMENCLATURE

ρ , Density of the fluid, kg m^{-3}

g , Acceleration due to gravity, m s^{-2}

L , Characteristic length, m

σ , Surface tension, N m^{-1}

u , Fluid velocity, m s^{-1}

Bo , Bond Number, $\frac{\rho g L^2}{\sigma}$

We , Weber Number, $\frac{\rho u^2 L}{\sigma}$

Re , Reynolds number, $\frac{\rho d u}{\mu}$

Fr , Froude number, $\frac{u^2}{gL}$

Courant Number, $\frac{\Delta t}{\frac{\Delta x_{cell}}{u}}$

Gr , Grashoffs Number, $\frac{g \beta \Delta T L^3}{\nu^2}$

β , Coefficient of thermal expansion of the fluid, $\frac{1}{V} \frac{dV}{dT}$, K^{-1}

ΔT_0 , Change in temperature in a fluid due to mixing with a hot fluid,

K , Thermal Conductivity, $\text{W m}^{-1}\text{K}^{-1}$

m , p , Subscripts indicate model and prototype respectively

V_f , Fluid velocity, m s^{-1}

V_r , Stokes rise velocity, m s^{-1}

k , Kinetic energy of turbulence per unit mass, $\text{m}^2 \text{s}^{-2}$

ε , Rate of dissipation of k , $\text{m}^2 \text{s}^{-3}$

ω , Specific rate of dissipation, $\text{m}^2 \text{s}^{-3}$

G_K , Rate of production of k , $\text{kg m}^{-1} \text{s}^{-3}$

$C_1, C_2, C_\mu, \sigma_k$ and σ_ε , Empirical Constants

μ , Viscosity of the fluid, $\text{kg m}^{-1} \text{s}^{-1}$

μ_t , Turbulent viscosity, $\text{kg m}^{-1} \text{s}^{-1}$

μ_{eff} , Effective viscosity, $\text{kg m}^{-1} \text{s}^{-1}$

l_m , Mixing length, m

l_0 , Length scale of turbulence, m

v_0 , Velocity scale, m s^{-1}

d , Distance from nearest wall, m

y^+ , Dimensionless wall distance

f , Constant determined by the shape of the tundish

u , X component of velocity, m s^{-1}

v , Y component of velocity, m s^{-1}

w , Z component of velocity, m s^{-1}

c_i , Concentration of the i^{th} species

θ , Dimensionless time

u_T , Terminal rise velocity, m s^{-1}

S_i , Source term indicating any non-diffusive or non-convective term

Γ_{eff} , Effective diffusivity, m^2s^{-1}

u_p , Particle velocity, m s^{-1}

ρ_p , Density of the particle, kg m^{-3}

F_D , Drag force, N

f_a , Additional acceleration, m s^{-2}

g_x , acceleration due to gravity in x direction, m s^{-2}

\bar{u}_t , Time averaged velocity, m s^{-1}

ζ_i , random number, normally distributed between -1 and 1

C_D , Drag coefficient

d_p , Particle diameter, m

a_1, a_2, a_3 , Constants

FEM, Finite Element Method

FDM, Finite Difference Method

PIV, Particle Image Velocimetry

FCD, Flow Control Devices

SLS/DLS, Swirling Ladle Shroud/Dissipative Ladle Shroud

VOF, Volume of Fluid

TKE, Turbulent Kinetic Energy

DNS, Direct Numerical Simulation

DPM, Discrete phase modelling

LES, Large Eddy Simulation

SIMPLE, Semi-Implicit Method for Pressure Linked Equations

PISO, Pressure Implicit Splitting of Operators

PRESTO, Pressure Staggering Option

SIP, Standard Impact Pad

RRI, Residual Ratio of Inclusions

RTD, Residence Time Distribution

1.0 Introduction

All operations in process metallurgy involve complex phenomena comprising momentum, heat, and/or mass transport: iron and steel making is not an exception. Transport phenomena i.e. fluid flows, heat transfer and mass transfer, play a dominant role in process metallurgy since their respective laws govern the kinetics of the various physical phenomena occurring in iron making and in steel making. These phenomena include such events as three phase reactions, entrainment of slag and gas in liquid steel, vacuum degassing, alloy melting and mixing, the movements and flotation of inclusions, melt temperature losses, residence times in a metallurgical reactor, erosion of refractory linings, etc. In all these aspects, the evolution in our techniques and abilities to model single and multiphase flows and their attendant heat and mass transfer processes has contributed significantly to our understanding and in our effective operation of these processes, to design improvements, and to develop new processes. To be ignorant of these matters can doom a processing operation to the scrap heap of metallurgical failures! Computational fluid dynamics and computational heat and mass transfer has been a very effective tool over the last three decades, for modelling iron and steel making processes, starting from the blast furnace up to continuous casting and beyond. In the continuous casting of steel, the tundish is basically an intermediate

vessel placed between the ladle and the mould. It distributes and supplies liquid steel to different moulds at an approximately constant rate. In recent years, with continuing emphasis on superior steel quality, the tundish has become more of a continuous reactor than merely a distribution vessel. Thus, a modern day steel making tundish is designed to provide a maximum of opportunity for carrying out various metallurgical operations such as inclusion separation, inclusion flotation, alloy trimming of steel, and thermal and chemical homogenization. All these have led to the development of a separate area of secondary steelmaking referred to as “tundish metallurgy”¹. Thus significant efforts have been made by researchers around the globe in the last decade (ie: 1999 to present) to fully exploit and enhance the potential of the continuous casting tundish as a molten steel refining vessel. Research activities concerning the associated theoretical and applied aspects have naturally led to a large number of publications. Mazumdar and Guthrie¹, in 1999, summarized the numerous experimental and theoretical studies that had been carried out using both aqueous models and industrial units to investigate various transport phenomena of relevance to continuous casting tundish systems. A wide range of tundish geometries, along with numerous designs of flow modifiers, have been applied and studied, primarily to investigate the floatation of inclusions from tundishes as a function of operating variables. In addition to these, the roles of increased throughput rate, electromagnetic stirring and auxiliary

heating on tundish performance were also investigated. Flow conditions suitable to facilitate inclusion separation by floatation can be created by insertion of flow modifiers. However, the optimal design of such flow modifiers and their location within the tundish is highly dependent on the tundish geometry, on operating conditions, and on the size range of inclusions present within the molten steel. Mixing, both thermal and material, on the other hand, require significantly different flow conditions. Useful inferences on industrial tundish performance can be made from observations derived from reduced scale water models. Extensive mathematical modelling of fluid flow and transport phenomena and the concurrent validation of mathematical model predictions against laboratory, as well as plant scale experimental data, indicate that a reasonably accurate mathematical framework now exists for effective tundish design and process analysis.

The objective of the present thesis was to carry out an extensive review of research done in the field of modelling of steel making tundish operations in the last decade (1999 to present) and to identify the specific topics which had been ignored or not considered at all, and then to apply physical and mathematical modelling simultaneously in order to study those topics. The tundish considered in the present thesis is a full-scale water model replica of the 12 tonne delta shaped tundish operating at the RTIT/QIT plant in

Sorel-Tracy, Canada. A one third scale water model tundish was also used for some experiments. Mathematical modelling of various transport phenomena was carried out using the commercial code ANSYS FLUENT 12. Apart from qualitative comparisons between the physical and mathematical models, quantitative comparisons were done where possible.

A general literature review on modelling of steelmaking tundish operations in the last ten years is presented in Chapter 2, followed by physical and mathematical modelling procedures in Chapter 3. The effect of different flow furniture on flow patterns and liquid metal quality is discussed in Chapter 4. Chapter 5 deals with the effect of inert gas shrouding on fluid flow, slag movements and residence time distribution. The effect of the alignment of the ladle shroud during melt transfer is presented in Chapter 6. A thorough study on the effect of thermal gradients on fluid flow in a tundish was carried out and discussed in Chapter 7. Finally in Chapter 8, the conclusions and recommendations from the present study are enlisted followed by some future work that could be done. Apart from the general literature review presented in Chapter 2, a specific review is done on the subject of interest in each of the introductory sections to each Chapter.

2.0 Literature Review

2.1 Physical modelling

Physical modelling involves the use of a low temperature aqueous analogue, generally water, to represent molten metal in the tundish. Water flow in a transparent model tundish can be used to observe the melt flows physically. Models can be either reduced scale or full scale. There are certain advantages to using a full scale model over a reduced scale model and these are mentioned by Guthrie and Isaac². For a faithful representation of flow in the model tundish, there should be constant ratios between corresponding quantities in the model and the actual tundish. For melt flows in tundishes, the states of similarity normally include geometric, kinematic, dynamic and thermal similarities. Here, the industrial vessel is known as the prototype, and its laboratory-scale counterpart is known as the model. Laboratory-scale modelling of various secondary steelmaking operations has most frequently used water as the modelling medium to represent molten steel. The most important single property in this context, apart from its ubiquity, is that its kinematic viscosity (that is, molecular viscosity/density) is essentially equivalent to that of molten steel at 1600°C (i.e., within 10%). Flow visualization experiments in aqueous systems using dyes or other tracers have therefore proved to be very helpful in developing a qualitative understanding of various flows in real liquid steel systems. Similarly,

more detailed information on flow characteristics has also been possible by measuring velocity fields by tracking the motion of neutrally buoyant particles or by using hot wire or hot film anemometry, or by laser Doppler anemometry, and, lately, by PIV (Particle Image Velocimetry). In addition, measurements of residence time distributions to characterize mixing in water model experiments using dye, acids, or KCl salt solution, have proved very popular and efficient. Having realized the advantages of using water as the representative fluid, it is now appropriate to discuss the general problem of how to physically model or characterize metallurgical processes. It is important to note here that, if the same forms of dimensionless differential equations and boundary conditions apply to two or more such metallurgical operations, and if an equivalence of dimensionless velocity, temperature, pressure or concentration fields, etc. also exist between the two, then one of them becomes a faithful representation of the other; i.e., one can be termed as a model of the other. This is a general statement of the need for similarity between a model and a prototype, which requires that there be constant ratios between corresponding quantities. The state of similarity between a model and a full-scale system includes geometric, mechanical, thermal, and chemical similarity. Mechanical similarity is further subdivided into static, kinematic, and dynamic similarity. The various states of similarity are discussed in standard texts in great detail³.

Recently a new dimensionless number has gained important recognition in the modelling of steel/slag systems, and that is the Bond number. The Bond number, notated Bo , is a dimensionless number expressing the ratio of body forces (often gravitational or buoyancy) to surface tension forces.

$$Bo = \frac{\rho g L^2}{\sigma} \quad [\text{Eq: 2.1}]$$

The Bond number is a measure of the importance of surface tension forces compared to body forces. A high Bond number indicates that the system is relatively unaffected by surface tension effects; a low number (typically less than one is the requirement) indicates that surface tension dominates. Intermediate values indicate a non-trivial balance between the two effects.

Both the We and Bo similarity criteria become very important when we simulate the slag phase with low temperature oils or emulsions. Different liquids like Benzene, Toluene, CCl_4 , oils, paraffin oil⁴, etc., have been used to simulate the slag phase. G. A. Irons⁵ reported that paraffin oil is the best liquid for simulating the slag phase in water models.

If we use reduced scale models we cannot simultaneously achieve Reynolds number similarity and Froude number similarity, since only one of them can be respected. Since the flows in the tundish are naturally associated with high Reynolds numbers, inertial forces

far exceed laminar viscous forces and correspond to the Newtonian range which is insensitive to Re . By contrast, inertial to gravitational forces are similar in magnitude. As such, flows in the tundish are Froude dominated and hence Froude number similarity is maintained between the model and the prototype for reduced scale models. However, in full scale modelling, both Re and Fr similarities can be achieved simultaneously.

The above mentioned similarity criteria are alright when there are no temperature changes and no effect of buoyancy forces. However, for non isothermal modelling, we have the modified Froude Number which is the ratio of inertial forces to buoyancy forces caused by thermally induced density variations within the liquid.

$$Fr_{modified} = \frac{\rho U^2}{(\rho_l - \rho)gL} \quad [\text{Eq: 2.2}]$$

Damle and Sahai⁶ called the inverse of this, the Tundish Richardson Number (Tu). Tu denotes the ratio of buoyancy force to the inertial force and is expressed as

$$Tu = \frac{Gr}{Re^2} = \frac{gL\beta\Delta T_0}{U^2} = \frac{(\rho_l - \rho)gL}{\rho U^2} \quad [\text{Eq: 2.3}]$$

If inclusion removal modelling is done then another essential modelling requirement is that

$$\frac{V_{f,m}}{V_{f,p}} = \frac{V_{r,m}}{V_{r,p}} \quad [\text{Eq: 2.4}]$$

is to be maintained where V_f and V_r are fluid and Stokes rise velocities respectively.⁷ However, the inclusions rise velocities may not always be in the Stoke's regime. So it is essential to keep them in the same flow regimes.

In modelling heat transfer operations, thermally similar systems are those in which corresponding temperature differences bear a constant ratio to one another at corresponding positions. When the systems are moving, kinematic similarity is a prerequisite to any thermal similarity. Thus, the heat transfer ratio by conduction, convection, and/or radiation at a certain location in the model must bear a fixed ratio to the corresponding rates in the prototype.⁸ Finally, for chemical similarity between a model and a full scale system, the dynamic and thermal similarity first must be satisfied. The former, since mass transfer and chemical reaction usually occur by convective and diffusive processes during motion of reacting material through the system, and the latter since chemical kinetics are normally temperature dependent.

2.2 Mathematical modelling

Mathematical modelling represents an alternative approach to physical models for visualising flow fields inside a tundish. In mathematical modelling, the turbulent Navier-Stokes equation is

solved in a boundary fitted coordinate system, so as to predict the velocity distributions. Analytical solutions to the 3D Navier-Stokes equation are not normally possible in most cases. In practice, therefore, we have to go for numerical methods, and for numerical solutions of these equations. In recent years, a lot of commercial software packages such as FLUENT, CFX, FLOW-3D, PHOENICS, FIDAP, COMSOL, etc. have been marketed, and have allowed CFD to become an increasingly common tool for the non- experts. Various turbulence models are available such as the $k-\epsilon$, RNG $k-\epsilon$, Realizable $k-\epsilon$, etc. An extensive review of the published literature shows that the basic framework of the mathematical modelling used in tundish research can be divided in three sub divisions, namely: (a) 'defining the problem', which is done by expressing the process in terms of some physical variables using partial differential equations, with appropriate operating and boundary conditions, then (b) 'grid generation' of the flow domain and discretization' of those partial differential equations into algebraic form, using different schemes and (c) 'solution to those discretized equations' using numerical techniques. The main physical variable related to any flow field is the velocity. Since other properties follow directly from the velocity field, determination of the velocity field is the prime step in solving a flow problem. For this reason, velocity was chosen as the primary physical variable for all mathematical modelling studies. Realizing the fact that liquid steel flows within a tundish are three dimensional

and turbulent in nature, almost all of the mathematical modelling works published in the literature in the recent past, assume the flow to be three dimensional and turbulent. As the equation of continuity and the equation of “Conservation of momentum” describe the fluid flow in mathematical terms, they are, along with the treatment of turbulence and boundary conditions, used as the starting point for all mathematical modelling studies for a tundish. In addition to using the above equations, different researchers used different equations, to model different parameters. Some included the energy equation to predict temperature distributions under non isothermal conditions.^{9,10,11} Other researchers included additional differential equations to describe inclusion trajectories and inclusion number density distributions.^{12,13} Modelling has also been used to predict parameters such as ‘Residence Time Distributions’¹¹ (RTD), distribution of top surface slag layer¹², etc.. It is practically impossible to solve these equations numerically by Direct Numerical Simulation (DNS) because of its requirement of unrealistically high computational memory, power and time. So, for 99% of the CFD problems that do not attempt to solve the turbulent Navier-Stokes equation in its original form, turbulence modelling is incorporated to capture the critical effects of turbulent flow without having to resolve the actual small length and time scales of real(actual) turbulent motion. One of the most popular practices is of first averaging the ‘Continuity’ and ‘Navier-Stokes’ equations, and then devising means

for solving the resulting system of equations for mean quantities of velocity and pressure. The approach along this line was first proposed by Reynolds and is called the Reynolds Averaged Navier-Stokes (RANS) equation. Here the equations are averaged over a time scale, which is long compared with the time scale of the turbulent motions, but small compared with the unsteady mean flow. In this approach, instantaneous velocity and pressure are decomposed into the mean and fluctuating parts, and incorporated in the continuity and Navier-Stokes equations.

(i) Turbulence Models

Among the different methods, the most widely used concepts in present day turbulence models for practical engineering applications is the “ Eddy viscosity” concept. In analogy to the viscous stresses in laminar flows, Boussinesq suggested that the turbulent stresses are proportional to the mean- gradients of velocity. Of the different turbulence models available in literature, only a few have been used in tundish modelling. Prandtl’s ‘Mixing Length Model’, was one of the early turbulence models used for tundish modelling. In this model, Prandtl defined the eddy mixing length, l_m , as the distance travelled by a fluid lump in the transverse direction before the mean velocity changes by an amount equal to the transverse fluctuation velocity. This momentum transport is equivalent to generating a turbulent shear stress. Prandtl also postulated that: the turbulence length

scale l_0 , is equal to the mixing length l_m , and the velocity scale v_0 , is equal to the mean velocity gradient times the mixing length ($l_m \frac{\partial \bar{u}_x}{\partial y}$).

In a very early modelling attempt, Debroy and Sychterz¹⁴, used this turbulence model for their numerical studies of flow pattern in a tundish and specified a mixing length $l_m = 0.4d$, where d is the distance from nearest wall. But later investigations showed that the mixing length, l_m , which according to the Prandtl's postulate is equal to the turbulent length scale, varies within the turbulent boundary layer itself. So the assignment of a single value for l_m throughout the flow field is questionable and is one of the weaknesses of this approach. Though this model was not used in any further tundish modelling work in later years, the 'Law of the Wall', which is used for boundary conditions for more sophisticated turbulence models, uses this concept and is used frequently.

To date, the most popular approach using the eddy viscosity concept have been the two equation models. In these models, two separate transport equations are solved to determine the length and velocity scales for eddy viscosity. Review of the literature on mathematical modelling in tundish reveals that most of the researchers have used the standard k- ϵ model of Launder & Spalding¹⁵ to calculate eddy viscosity. Later on, many variants of this model were introduced, such as the RNG k- ϵ model of Yakhot and Orszag¹⁶ and the

Realizable k- ϵ model of Shih et al¹⁷. Schwarze et al^{18,19} used different turbulence models in their prediction of flow fields and of dispersed phase behaviour. Though their predicted velocity field using standard k- ϵ vs. the RNG k- ϵ models does not seem to vary much, the mean turbulent quantities do differ significantly. Comparing the results with the available experimental data, they concluded, that the RNG model approximates the turbulence in flow situations with a high curvature of streamlines better than other models. While the literature survey shows, that most of the simulation works were done using the standard k- ϵ turbulence model, they²⁰ argued that this model, over- predicts k values, because it does not take into account the fact that the strain rate of the flow field influences turbulence. Hou & Zou²⁰ came to the same type of conclusion. They compared the standard k- ϵ turbulence model with the RNG k- ϵ turbulence model, while numerically simulating swirling flows in a tundish. They also obtained converged results more easily using the RNG k- ϵ turbulence model and concluded that this model is more appropriate for swirling motions. By far the most elaborate computational study on tundish performance predictions was done by Jha et al.²¹ They studied the effect of different turbulence models on residence time distribution predictions. Apart from these, they also applied the LES model (large eddy simulation) in tundish modelling. Models such as the standard k- ϵ , RNG k- ϵ , Chen – Kim k- ϵ , LES, etc. predict gross flow properties fairly well. Others such as Lam- Bremhorst low

Reynolds number k - ϵ model, predicts initial variation better than the others.

Nonetheless, the most widely used model of turbulence is the standard k - ϵ model. In general, as stated earlier, the standard k - ϵ model tends to overestimate mixing situations where highly turbulent and essentially laminar regions coexist, such as in a tundish. To adequately predict such situations, the model must be able to represent the existence probability of the turbulent fluid at a particular location. Realizing this fact, Ilegbusi et al.²² used a two fluid model of turbulence to predict the flow behaviour in a tundish. This model essentially considers the system to be composed of two interpenetrating fluids (a turbulent and a non turbulent fluid). These fluids are allowed to exchange mass, momentum and energy at the interface. At any location, transport equations would be solved for the characteristics of each fluid, including velocity components, temperature, and volume fractions. The volume fraction of the turbulent fluid provides a measure of the intermittency or turbulence. The model is therefore well suited to represent the whole tundish domain, the intermittency factor being high in the turbulent inlet region and low in the quiescent region.

In wall-bounded turbulent flows, as in a tundish, the presence of solid walls also has a strong effect on flow characteristics. So, all the researchers who tried to model the flows within the tundish, had to

use special treatments like the wall function approach, or the low Reynolds number model approach, to tackle the boundaries. However, when there are strong reattaching and separating flows, the wall function approach is not recommended.

Only a few researchers^{23,24} have used the Low Reynolds number method. In this approach, computations are carried out all the way to the walls and hence a very fine grid is required near the wall. Some researchers²⁴ used the low Reynolds number model of Launder & Jones to study residence time distributions in a 6-strand tundish, and found better agreement with experimental results. The low Reynolds number models like the model of Lam & Bremhorst (used by ref.^{23,24}) and the Chen-Kim low Reynolds number (with and without the Yap correction) (used by ref. ²¹) were used only for comparison purposes.

The capabilities of RANS models are limited. Under certain conditions these models can be very accurate, but these are not suitable for transient flows, because the averaging process wipes out most of the important characteristics of a time-dependent solution. On the other hand, ' Direct Numerical Simulation '(DNS), which is the direct solution of the turbulent Navier-Stokes equation, is not practical for 99.9% of CFD problems because of its requirement of unrealistically high computational power and time. As a result a new simulation technique, called 'Large eddy simulation'

(LES) has also become very popular. In LES, the contribution of the large scale eddies to the momentum and energy transfer is computed exactly through DNS ,while the effect of the small eddies are modeled. The distinction between the large and small eddies is done by a filtering operation. But an exhaustive survey of literature shows only Jha et al ²¹ applied the LES technique during their modelling of tundish flows.

(ii) Solution of the PDE's

Due to the complex nature of the governing equations and geometries of the tundishes, analytical solutions for the equations are not possible in a practical sense. So different numerical techniques have been developed to solve these transport equations. The numerical solution aims to provide the values of the variables at some discrete number of points in the domain of interest. These points are called grid points, nodes or cell centroids, depending on the scheme it follows. The conversion of differential equations into a set of discrete algebraic equations requires the discretization of domain. This is called mesh generation or meshing.

- The different techniques used are:
- Finite Difference Method (FDM)
- Finite Element Method (FEM)
- Spectral Methods

- Hybrid Methods (such as Control Volume Finite Element Method, Control volume Finite Difference Method etc.)

All the techniques perform three basic steps i.e. approximation of unknown flow variables by means of simple functions, followed by discretization by substitution of the approximations into the governing flow equations, and subsequent mathematical solutions.

Close examination of the three components of the momentum equation and continuity equation shows that they are closely coupled, because all velocity components appear in each momentum and continuity equation. The most complex issue is to know the pressure term in the momentum equations. This is because there is no equation available for pressure for the case of incompressible fluid flows such as the flows in a tundish. These problems are generally tackled by the use of different iterative solution strategies like SIMPLE, SIMPLER, SIMPLEC, PISO^{25,26} etc. All these techniques are iterative methods and use either the Tri Diagonal Matrix Algorithm (TDMA) introduced by Spalding or the Gauss-Siedel method, for solution. Several other techniques like the Penta Diagonal Matrix Algorithm, the implicit under-relaxation scheme of Patankar, etc. are also used.

2.3 Research in the last decade

Having given a brief description of physical modelling and mathematical modelling in the last section, this section provides a comprehensive review of the work of different researchers in the last decade. The review is done in ascending order of chronology. FAN and HWANG²⁷, in 2000, developed a mathematical model to analyze fluid flow phenomena of liquid steel in the tundish, during its filling stage and subsequent casting operation in the continuous casting process of steel. The ultimate goal was to ensure smooth initial casting operations without nozzle clogging. The mathematical model was developed using a CFD technique, named SOLA-MAC and the famous $k - \varepsilon$ turbulence model. SOLA-MAC (Solution Algorithm Marker And Cell) has the capability to handle transient flow problem with highly distorted free surfaces. The SOLA-MAC technique uses a finite-difference scheme for the mathematical analysis of the fluid flow problems. Like most numerical techniques, it first divides the system, which is the configuration of the tundish under consideration, into a number of volume elements. Then a set of imaginary markers is introduced into the system to represent the location of the fluid at any instant. The velocity field of the moving fluid domain can be calculated by the application of fluid dynamics principles. Next, the markers are moved according to the calculated velocity field in order to represent the new location of the fluid

domain. The procedure can be repeated from the beginning when the tundish is empty until it is filled to a predetermined height in the tundish. The mathematical model was first tested on a one fourth scale water model and good consistency was observed when the simulated filling patterns were compared with the water model experiments. Inclusion distribution and the amount of “dirt” exiting through the outlets of the various strands in the tundish were also analyzed by a fluid particle method. The simulated results showed that for the tundish, inclusion contamination was not uniform at the different strands, which was also confirmed by actual experience in the plant.

Odenthal et al²⁸. reported results of Digital Particle Image Velocimetry (DPIV) on a one fourth scale model of a single strand tundish. The data lead to a good interpretation of the dynamic flow phenomena. The flow separated at the bottom of the tundish and a recirculating region was developed. Simultaneously, the jet coming out of the shroud induced a counter-rotating lateral double vortex and a short circuit flow around the side walls. A two equation model was developed in order to describe turbulence and the results obtained with this model corresponded well with the DPIV data. They concluded that DPIV can be used as an effective tool to determine two dimensional velocity fields and transient velocity fields. They also suggested the use of 3D DPIV and Laser Doppler Anemometry

(LDA) for the future. LDA has an advantage is that it can measure turbulent fluctuations.

A transient two fluid model was developed by Sheng and Jonsson²⁹ to simulate fluid flow and heat transfer in a non isothermal water model of a continuous casting tundish. Thermal stratification in the bath was evident and the results, predicted by the two fluid approach adopted, made the effect of natural convection more clear compared with the generally used single fluid k- ϵ model. The overvaluation of the conductive heat transfer in the transition region of the system found by using the single fluid approach was eliminated by using the two fluid k- ϵ model. The two fluid approach was also found to be better in describing the counter gradient diffusion phenomenon caused by the thermal buoyancy force.

J.H. Ann et al.³⁰ predicted a concentration change during grade transition operations during steel thin slab casting based on computer simulations, a water model, and plant trials. Fluid flow and mixing patterns in various tundish levels and flow rates were analyzed through 3D mathematical modelling. They correlated their results with water model experiments and developed a simple, efficient and accurate computational model which could predict the concentration profile at the outlet of the tundish. Based on the model, mixing in/below the mould was analyzed considering EMBR (electromagnetic breaking). The total amount of mixed grade steel

only depended on the mixing in the tundish when EMBR was applied. They also concluded that the optimum tundish operating condition to minimize intermixed slabs greatly depends on tundish geometry.

A systematic study was conducted by S.K.Sinha et al.³¹ of the National Metallurgical Laboratory in India on the fluid flow behaviour in a two strand tundish under conditions of submerged entry nozzle (SEN) and open entry nozzle (OEN) with different levels of water in the tundish. Flow was characterized by the profiles of tracer responses at the tundish outlets. Two configurations of entry nozzle (ladle shroud), the straight tube (for SEN and OEN) and the T-shaped (for SEN only) were applied. At 34 mm immersion depth of the straight ladle shroud, the optimal level of mixed flow in the tundish was produced and thus uniformity in composition was obtained. With the OEN configuration, the more was the height of the entry nozzle, the less was the dead volume and the mixing increased. They suggested that tracer response profiles from different outlets should be nearly the same to have unity A-ratio and vessel dispersion number.

Y. Sahai³² made a summary on modelling of melt flows in continuous casting tundishes at the Brimacombe Memorial Symposium. He emphasized the importance of proper melt flow in tundishes for the production of high quality clean steel and stated that this can be

achieved by good tundish design and optimum volumetric flow rate of liquid metal. In a full scale model, the Reynolds and Froude similarities can be satisfied simultaneously. However, in a reduced scale model, both similarities cannot be satisfied for a water model. Thus, only Froude similarity is sufficient and convenient similarity criterion for water modelling. In non isothermal systems where buoyancy forces become important, the tundish Richardson number is the sufficient and necessary similarity criteria for modelling. Sahai also mentioned that the solution of the turbulent Navier-Stokes equation with an appropriate set of boundary conditions provides detailed information about the velocity and turbulence fields in the tundish. A coupled solution with the heat transfer equation also provides the temperature field existing in the melt.

Robert and Mazumdar²⁴ developed a steady state, three dimensional, turbulent flow model for analyzing melt flow and RTD in steelmaking tundish systems. They used a control volume based, finite difference procedure and the SIMPLE algorithm. To ensure that their model is consistent and sufficiently robust, they tested the model on several standard systems and obtained satisfactory results. Accordingly, the turbulent model was applied to simulate flow and RTD in four different tundishes. The results were compared with equivalent water model experiments. Except for the single strand tundish system, large differences between measurements and

prediction were noted for the other three tundish geometries. Numerical modelling of RTD in the rectangular, six strand tundish system embodying the low Reynolds number $k - \varepsilon$ model of Launder and Jones, was found to produce estimates of RTD parameters that are in reasonable agreement with the corresponding experimental results and superior to those deduced via the high Reynolds number $k - \varepsilon$ model.

Sergio. P. Ferro et al.³³ presented mathematical models for the evaluation of residence time distribution curves for a large variety of vessels. They introduced a new volume called convection diffusion volume to obtain a good representation of RTD curves. Two numerical models for simulation of RTD curves in different vessels were presented. The comparison of measured RTD curves with numerical results from the proposed model shows that these models can successfully represent the general behaviour of a fluid inside a variety of systems. The first of the two models proved to be efficient to describe most of the one-peaked RTD curves, in spite of its simplicity. The second one, slightly more complex, successfully represented all the different RTD curves under consideration including those with double peaks. The key feature of these models was the use of a new type of volume, the convection diffusion volume. In order to find the parameters of the model for a given experimental RTD curve, a numerical algorithm was developed and

also some simple mathematical relations were found, that allowed the estimation of the parameters of the model from the characteristic parameters of the RTD curve.

P. Gardin et al.³⁴ carried out an experimental and numerical CFD study of turbulence in a tundish container. Extensive mean and fluctuating velocity measurements were performed using LDA, in order to determine the flow field and these data formed the basis for the numerical model validation. CFD modelling of this problem apparently seems easy but actually it was not. Accurate description of the jet is the most important and requires a localized fine grid, but also a turbulence model that predicts the correct spreading rates of the jet and impinging wall boundary layers. The velocities in the bulk of the tundish are generally much smaller than those of the jet, leading to damping of turbulence, or even laminar flow. They started the work with the objective of applying and validating the $k - \omega$ model of Wilcox to a tundish flow problem. This model was thought to have advantages over the $k - \epsilon$ model. After initial 2D studies, they found that the $k - \omega$ model was diffusing the wall jet too quickly. Medium grid density 3D computations, confirmed this finding. The authors developed several low- Reynolds number $k - \epsilon$ model variants to compute the flow and compare against measurements. The $k - \epsilon$ modifications proved to be very successful, with the newly developed $k - \epsilon$ D1 model being the best. This indicated there is no

need to use more sophisticated differential Reynolds stress models, which are more difficult and take longer to converge. From the grid refinement they concluded that certain turbulence models were more grid-sensitive than others. They also concluded that the LES model might still have certain limitations for practical use.

Guthrie and Isaac² reported on the importance of using full-scale models for studying the fluid flow and transport phenomena in ladle-tundish-mould operations. They mentioned that reduced scale models are convenient to simulate first order simulations of inertially dominated flows, but the finer details are better analyzed in full scale models where Re, Fr and Tu can be simultaneously respected.

Jha and Dash³⁵ employed different turbulence models to the design of optimum steel flows in a tundish. The Navier-Stokes equation and the species continuity equation were solved numerically in a boundary fitted coordinate system comprising the geometry of a large-scale industrial size tundish. The solution of the species continuity equation predicted the time evolution of the concentration of a tracer at the outlets of a six-strand billet caster tundish. The numerical prediction of the tracer concentration using six different turbulence models: [the standard $k-\epsilon$, the $k-\epsilon$ RNG, the Low Re number Lam-Bremhorst model, the Chen-Kim high Re number model (CK), the Chen-Kim low Re number model (CKL) and the simplest constant effective viscosity model (CEV)] which compared favourably with that of the

experimental observation for a single strand bare tundish. It was found that the overall comparison of the $k-\epsilon$ model, the RNG, the Lam-Bremhorst and the CK model was much better than the CKL model and the CEV model as far as gross quantities like the mean residence time and the ratio of mixed to dead volume were concerned. However, the $k-\epsilon$ model predicted the closest value to the experimental observation compared to all other models. The prediction of the transient behaviour of the tracer was best done by the Lam-Bremhorst model and then by the RNG model, but these models did not predict gross quantities very accurately as did the $k-\epsilon$ model for a single strand bare tundish. With the help of the above six turbulence models, mixing parameters, such as the ratio of mix to dead volume and the mean residence time, were computed for the six strand tundish for different outlet positions, height of advanced pouring box (APB) and shroud immersion depth. It was found that three turbulence models show a peak value in the ratio of mixed to dead volume when the outlets were placed at 200 mm away from the side wall as shown in Figure 2.1 below.

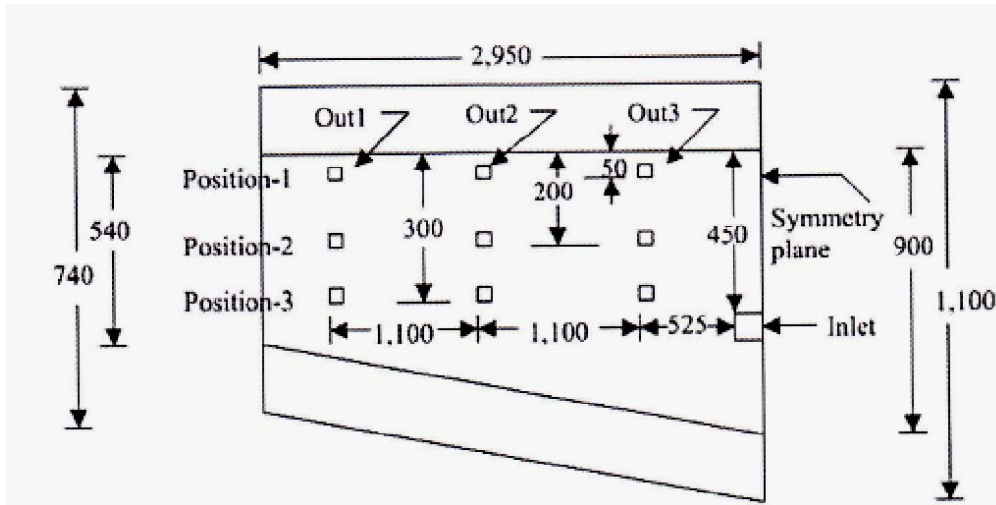


Figure-2.1 Top view of the tundish showing outlets on the bottom plane³⁵

An advanced pour box (APB) was put on the bottom of the tundish surrounding the inlet jet when the outlets were kept at 200 mm away from the wall. It was also found that there exists an optimum height of the APB where the ratio of mixed to dead volume and the mean residence time attain further peak values signifying better mixing in the tundish. At this optimum height of the APB, the shroud immersion depth was made to change from 0 to 400 mm. It was also observed that there exists an optimum immersion depth of the shroud where the ratio of mixed to dead volume still attains another peak, signifying slightly better mixing. However, none of the turbulence models predict the same optimum height of the APB and the same shroud immersion depth, as the optimum depth. The optimum height of the APB and the

shroud immersion depth were decided when two or more turbulence models predicted the same values.

P. K. Jha et al.²¹ also performed large eddy simulation to study mixing in a tundish. They took the solution of the k- ϵ model as a starting guess for the large eddy simulation (LES). A solution for the LES could be arrived at after adapting a local refinement of the cells (twice), so that the near wall y^+ could be set less than 1. Such a refined grid gave a time independent solution for the LES, which was used to solve the species continuity equation. The LES solution slightly over predicted the mean residence time but could predict the mixed volume fairly well. However, the LES was unable to predict both the peaks in the tracer concentration, like the k- ϵ , RNG and Lam-Bremhorst models were able.

S. Lopez. Ramirez et al.⁹ studied the influence of input temperature changes on molten steel flow in tundishes by physical and mathematical modelling. In their study, the difference between considering and not considering the thermal influence changed the parameter values in approximately 5% of the relative standard deviation. The thermal response obtained from an input step temperature change reproduced the real behaviour of the molten steel flow in a tundish dominated by buoyancy forces. A comprehensive process model for fluid flow and heat transfer in the tundish was developed by R. Pardeshi et al.³⁶ which had the

capability to capture the transient process dynamics. The model was based on a conjugate thermal analysis of the tundish, accounting for simultaneous heat transfer through the liquid steel, refractory, steel shell and dams. The model was validated by comparing model predictions for laminar and turbulent fluid flow conditions cited in the literature. Plant campaigns were undertaken to collect plant data for tuning and validation of the model.

Kumar, Koria and Mazumdar³⁷ from their experimental and computational study on flow modelling and RTD, indicated that a sufficiently small grid resolution (control volume of the order of 10^{-6} m³) is necessary to arrive at a practical grid independent solution. They also reported that the Reynolds Stress model was found to simulate RTD in the system somewhat better to the standard coefficient k- ϵ model. Their mathematical model was validated with experimental results and proved sufficiently robust and reliable to predict mixing parameters in tundishes with and without flow control devices.

A. V. Zamora et al.³⁸ studied inertial and buoyancy driven water flows under gas bubbling and thermal stratification conditions in a model tundish. Steel flow dominated by inertial and buoyancy flows under gas bubbling and thermal stratification conditions, in a one-strand tundish, was studied, using a 2/5 scale water model. The use of a turbulence inhibitor yielded plug flow volume fractions well above

40% for a simulated casting rate of 3.12 tons/min under isothermal conditions. Small flow rates of gas injection ($246 \text{ cm}^3/\text{min}$), through a gas curtain, improved the fluid flow by enhancing the plug flow volume fraction. Higher flow rates caused an increase in back-mixing flow, forming recirculating flows on either side of this curtain. Step inputs of hot water drove streams of this fluid towards the bath surface due to buoyancy forces. A rise in gas flow rate led to thermal homogenization within the two separated cells of flow located on either side of the gas curtain. Step inputs of cold water drove input streams of colder fluid along the tundish bottom. The use of the gas curtain homogenized the lower part of the tundish as well as the upper part of the bath to the left side of the curtain. However, the temperature at the top corner of the tundish, in the outlet box, remained very different than the rest of the temperatures inside this tundish. High gas flow rates ($912 \text{ cm}^3/\text{min}$) were required to homogenize the bath after times as long as twice the mean residence time of the fluid.

A. Ramos Banderas et al.³⁹ performed mathematical simulation and physical modelling of unsteady fluid flows in a water model tundish mould. The LES approach used by them was able to predict, qualitatively, the instantaneous upper recirculating flow fields of water in the physical model. Agreement of simulated and measured jet parameters such as the jet angle and the impingement position of the entry jets in the narrow wall of the mould were acceptably good.

Thus they suggested that the LES approach is well recommended to estimate jet characteristics. Changes of flow pattern with time were generated as a result of the vertical oscillation motion of the jet core. This motion was promoted by the residual Reynolds stresses that characterize turbulent flow. The fluid flow pattern in the jet root was unaltered by changes of the flow rate of the liquid. The asymmetry of fluid flows caused by these stresses yielded biased flows. Mass transfer in the mould also yielded asymmetric flow patterns as a consequence of the fluid flow characteristics.

Tripathi and Ajmani⁴⁰ reported on a numerical investigation of fluid flow phenomena in a curved shape tundish (Fig 2.2). A 3D mathematical model was developed by them. The results were compared with a conventional delta shaped tundish. The strong role of curvature in improving fluid flow characteristics and enhancing inclusion floatation was evident from their results. They also reported a considerable increase in the plug volume and mean residence time through the use of contour shaped pouring chambers as compared to those with sharp corners. The mathematical model was validated with experimental results for a single strand bare tundish.

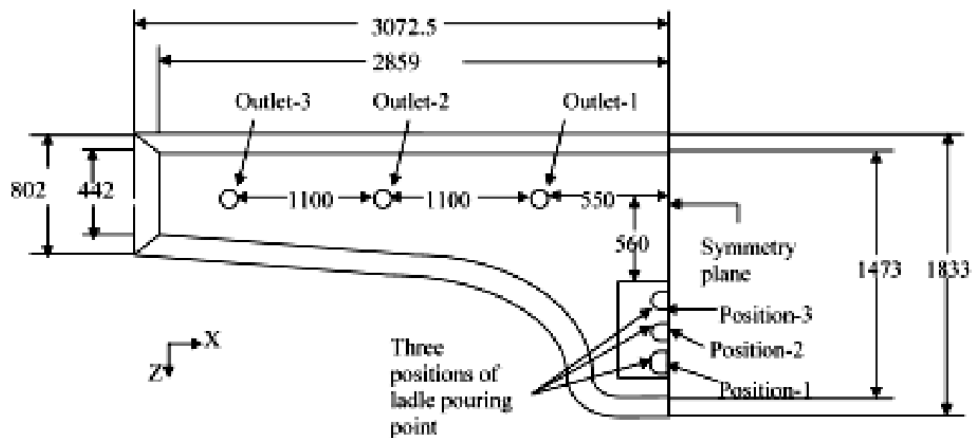


Figure-2.2 Curved shaped tundish of Tripathi and Ajmani⁴⁰

A novel tundish mixing model was proposed to predict the outlet concentration of the tundish during a grade transition by Cho and Kim⁴¹. To enhance the efficiency and replication performance, the present model was designed to minimize the number of parameters to only one that needs to be tuned for easier application to new situations whereas the Huang and Thomas⁴² model had six parameters to be tuned. Two types of water model were employed to verify Cho and Kim's model, and the real grade mixed blooms were produced through a grade transition continuous casting. When the present tundish mixing model was applied to the cases of the water models and real bloom casting, the numerical results of the present model were found to be in good agreement with the experimental data, and the constant parameter f of the present model was found to be determined according to the tundish shape.

Alkishriwi, Meinke and Schroder⁴³ carried out large eddy simulations of a continuous casting tundish to investigate the turbulent flow structure and vortex dynamics. The method used an implicit time accurate dual time stepping scheme in conjunction with low Mach number preconditioning and multigrid acceleration. To validate the scheme, large-eddy simulations of turbulent pipe flow at $Re_T = 1280$ and cylinder flow at $Re_D = 3900$ were performed. The results showed the scheme to be efficient and to improve the accuracy at low Mach number flows. The findings from the LES showed the presence of many intricate flow details that have not been observed before by customary RANS approaches. Fluid flow dynamics during ladle drainage operations of steel under isothermal and non-isothermal conditions were studied using the turbulence shear stress transport $k-\epsilon$ model (SST $k-\omega$) and the multiphase volume of fluid (VOF) model by O. Davila et al.⁴⁴ At high bath levels, the angular velocity of the melt, close to the ladle nozzle, was small, rotating anticlockwise, while intense vertical-recirculating flows were developed in most of the liquid volume due to descending steel streams along the ladle vertical wall. These streams ascended further downstream driven by buoyancy forces. At low bath levels, the melt, which was close to the nozzle, rotated in a clockwise direction with higher velocities for shorter ladle stand still times (holding time). Figure 2.3 to 2.6 shows draining operations under isothermal and non-isothermal conditions. These velocities were responsible for the formation and development of a

vortex on the bath free surface, which entrained slag into the nozzle by shear-stress mechanisms at the metal-slag interface. The critical bath level or bath height for this phenomenon was 0.35 m (in this particular ladle design) for a ladle standstill time of 15 minutes and decreased with longer ladle stand still times. At these steps, the vertical-recirculating flows were substituted by complex horizontal-rotating flows in most of the liquid volume. Under isothermal conditions, the critical bath level for vortex formation on the melt free surface was 0.20 m, which agrees very well with that determined with a 1/3 scale water model of 0.073 m. It was concluded that buoyancy forces, generated as a result of thermal gradients, as the ladle cools, were responsible for increasing the critical bath level for vortex formation.

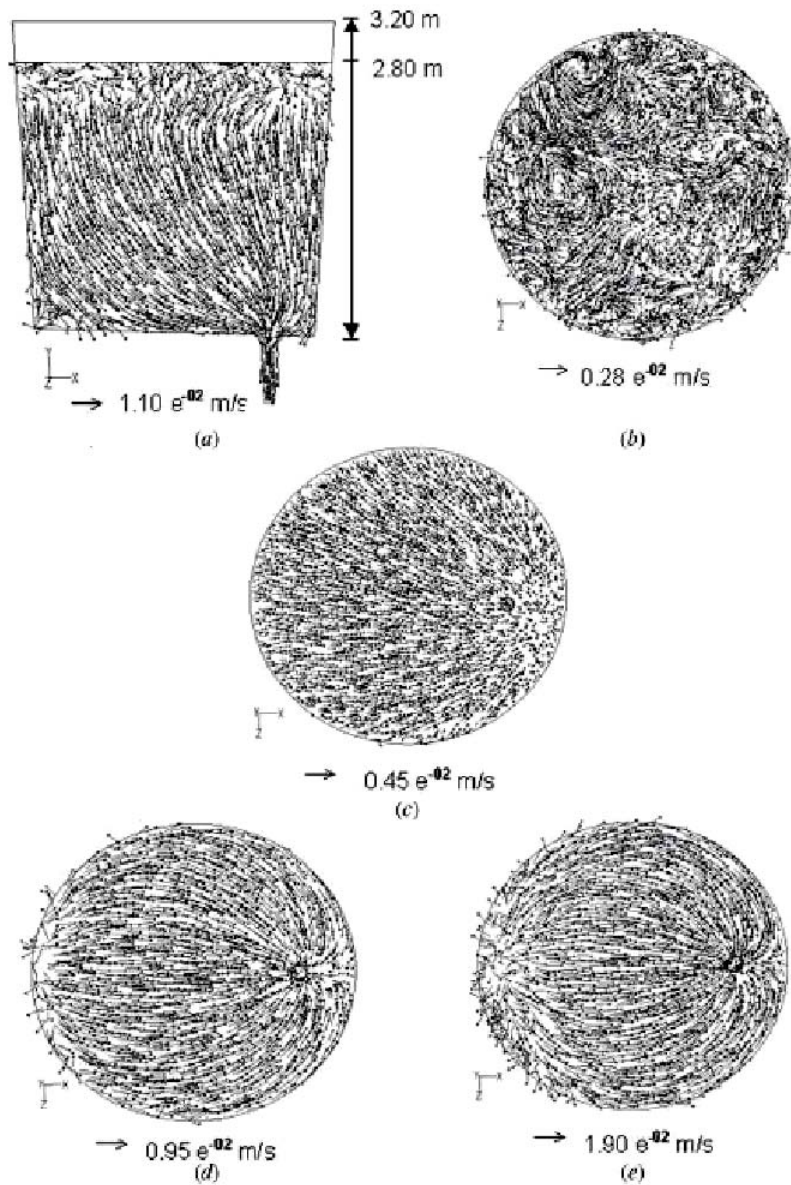


Figure- 2.3 Velocity fields in different planes during isothermal drainage of liquid steel from a ladle at a throughput of 2.1 ton/min for a bath level of 2.80 m: (a) vertical plane, (b) horizontal plane at 2.50 m from the bottom, (c) horizontal plane at 1.50 m from the bottom, (d) horizontal plane at 0.35 m from the bottom and (e) horizontal plane at 0.20 m from the bottom.⁴⁴

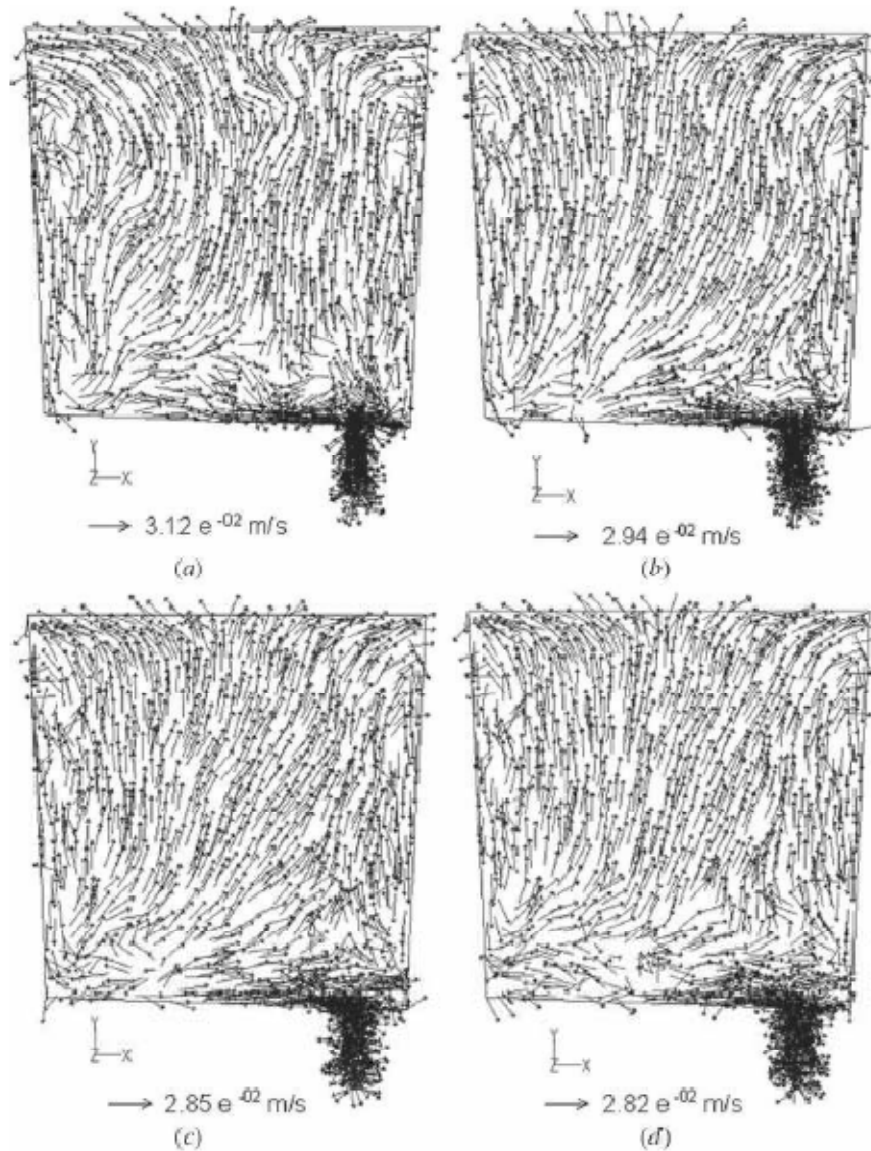


Figure- 2.4 Velocity fields developed during thermal stratification of liquid steel at different standstill times of the ladle: (a) 15 min, (b) 30 min, (c) 45 min, and (d) 60 min.⁴⁴

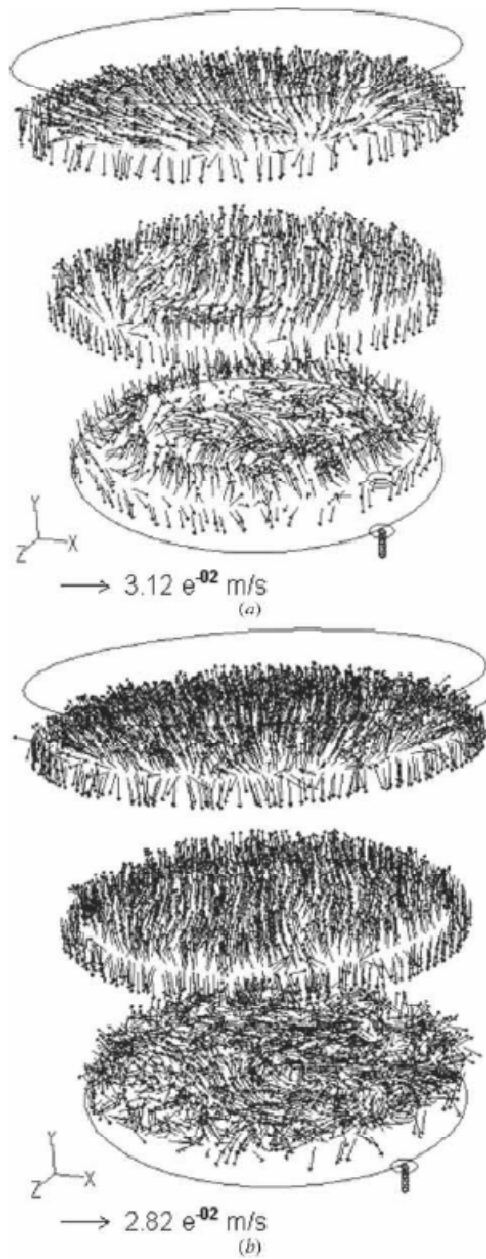


Figure- 2.5 Velocity fields at different horizontal planes located at 2.80, 1.50, and 0.30 m from the bottom: (a) after a standstill time of 15 min and (b) after a standstill time of 60 min.⁴⁴

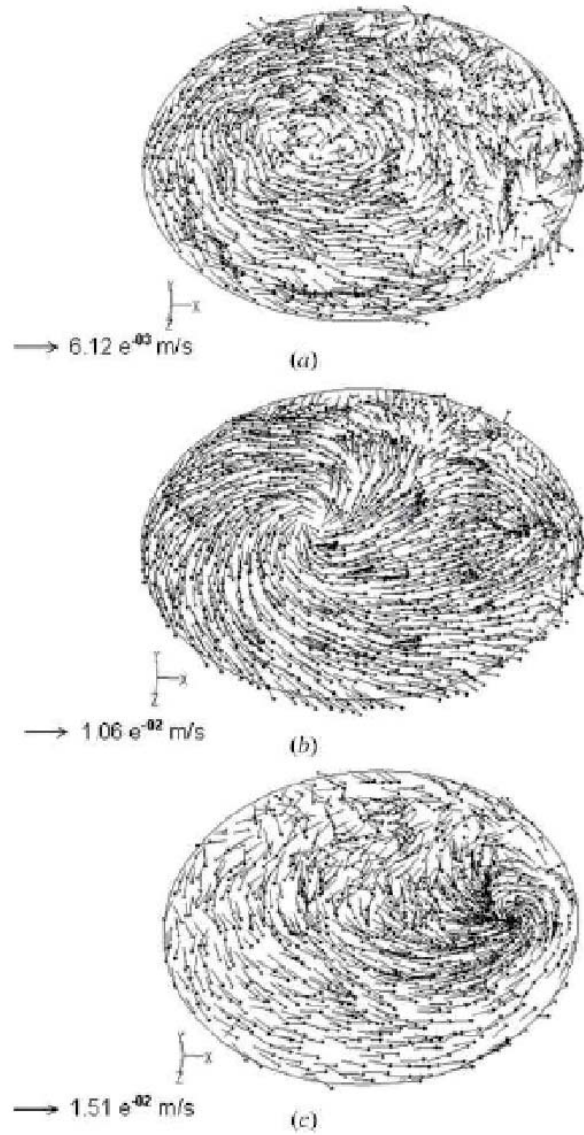


Figure-2.6 Velocity fields at horizontal planes during non isothermal drainage of liquid steel from a ladle at different horizontal planes for a bath level of 1.50 m: (a) 0.80 m from the bottom, (b) 0.40 m from the bottom, and (c) 0.20 m from the bottom.⁴⁴

Sankanarayan and Guthrie^{45,46} showed that the diameter ratio of the outlet nozzle and the ladle is important and this ratio and the critical height for vortex formation are proportional. For a constant ratio of outlet diameter to ladle diameter, the critical height becomes larger with higher initial bath heights. Understanding vortex mechanisms will be useful to design simple and efficient devices to break down the vortex flow during steel draining even at very low metal residues in the ladle.

P. Vayrynen et al.⁴⁷ modeled steady state and transient casting situations. Their work was focused on tuning and validation of a commercial CFD package which will be used to simulate tundish operations. They concluded that the software was not able to simulate the downscaled water model accurately, but on the other hand both temperature and transient casting situation results of the full scaled tundish were satisfactory. They mentioned that one possible reason for this behaviour is that areas of clearly turbulent flow in the water model are much smaller than in actual tundish and this transition of flow type is very difficult for the present turbulence models to calculate accurately.

M. Zorzut et al.⁴⁸ developed a mathematical model which could predict steel grade change. The model was set up using dilution interconnecting elementary cells that describe the shroud and each strand. The cells were considered with uniform concentration. Such

a model was very useful in the definition of the technological practice for the steel grade change operation.

Fluid flow and mixing of molten steel in a twin-slab-strand continuous casting tundish were investigated using a mixing model under non isothermal conditions by ALIZADEH et al.⁴⁹ This model led to a set of ordinary differential equations that were solved with a Runge-Kutta algorithm. Steady state water modelling was carried out under non-isothermal conditions. Experimental data obtained from the water model was used to calibrate the mixing model. As a result of the presence of mixed convection phenomena in the non-isothermal tundish, parts of the primary fluid were mixed with the warm incoming fluid. Due to the density difference between the two fluids, fluid channelling was evident within the tundish. The volume flow rate of the fluid in the channel was found to depend on the ratio of inertial to buoyancy forces inside the tundish. They mentioned that if Re_T and Tu between two tundishes are same the RTD curves would be in absolute accordance with each other. However, the mixing model results showed that the total mixing flow volume fraction in the non-isothermal tundish was lower than that in the isothermal one.

Wang et al⁵⁰ analyzed fluid flow phenomena in a centrifugal flow tundish. They particularly emphasized on dam spacing and rotation speed of flow structure. Their results revealed that the bias flow,

originating from the rotary outflow, leads to the formation of transversal circulation behind the dam. Such transversal flow could effectively diminish the conventional dead volumes. Small dam spacing helped to form a large-scale transversal circulation, and thus the prolonged flow path and relatively low velocity lead to an increased plug volume. With the increase of dam spacing, the intensity of transversal circulation decreased and the increased fluid velocity caused a diminished plug volume. The highest ratio of plug to dead volume was obtained under the dam spacing when transversal circulation was strongest. Furthermore, under lower magnetic intensities, the weaker fluid momentum leads to relatively large dead volume. With the increasing of magnetic intensity, the fluid mixing became better. They concluded that much larger magnetic intensity will lead to decreased ratio of plug to dead volume and recommended a rotation speed of 30r/min.

Warzecha et al.⁵¹ investigated fluid flow characteristics in a six strand tundish using plant measurements, physical modelling and numerical predictions. The aim of their study was to obtain the mass exchange characteristics in the tundish of interest. Plant measurements were done directly at the steel plant during normal working conditions. By controlling the changing content of manganese in steel, the residence time distribution (RTD) characteristics were acquired. The RTD curves were also obtained

with a one third scale water model tundish. Numerical simulations were carried out with the finite-volume commercial code FLUENT using the standard k-e turbulence model. The primary purpose of the investigations carried out is to present the characteristics describing the transitory zone in a six-strand tundish. Tracer dispersion characteristics for the tundish obtained from both modelling techniques - physical as well as mathematical were very similar in nature.

Inclusion removal in the tundish is a very important operation and a lot of work has been in literature till date. Mazumdar & Guthrie¹ had discussed the studies on inclusion separation where Stokes terminal rising velocity of the inclusion particles were vectorially added to the vertical component of the fluid motion in the partial differential equation which is basically convection – diffusion equation for species transfer [Eq:2.5]

$$\frac{\partial(\rho c_i)}{\partial t} + \frac{\partial(\rho u c_i)}{\partial x} + \frac{\partial(\rho[v + u_{T,i}]c_i)}{\partial y} + \frac{\partial(\rho w c_i)}{\partial z} = \frac{\partial}{\partial x} \left(\Gamma_{eff} \frac{\partial c_i}{\partial x} \right) + \frac{\partial}{\partial y} \left(\Gamma_{eff} \frac{\partial c_i}{\partial y} \right) + \frac{\partial}{\partial z} \left(\Gamma_{eff} \frac{\partial c_i}{\partial z} \right) + S_i$$

[Eq: 2.5]

After obtaining a steady state velocity field, equation 2.5 is solved for inclusion concentration. Generally each group of inclusions is characterized by their diameter. They also discussed the source term S_i that represents generation or destruction of a particular size of inclusion by coalescence and the boundary conditions. Details of

these are not repeated here. Recent studies showed the use of different models to study inclusion separation phenomenon. Hamill and Lucas⁵² used an algebraic slip model (ASM) which basically is a simplified form of a multi-phase model to study inclusion motion and its removal. Assuming that the small particles (40 μ m-300 μ m) always move at their slip velocity, which basically comes from a balance between the buoyancy and drag forces, they solved separate scalar volume fraction equation for each particle species along with the basic conservation equations for multiphase flows (the equations are not given here). They used the software CFX to compute the results and compared their results with previously published results of Joo et al.⁵³, who used equation 2.5 which is based on single phase modelling approach. Joo et al.⁵³ used the METFLO 3D software (a code developed in McGill university) to solve those equations. For the flow conditions modelled, they showed that most inclusions greater than 100 microns should float out, independent of flow control devices while all those less than 40 microns would not be helped by flow modifying devices, and would be retained in liquid steel exiting to the strands.

More recently, Huelstrung et al.⁵⁴ studied the influence of tundish volume, while Schwarze et al.¹⁸ studied the influence of different weir & dam arrangements on predicting the degree of inclusion separation. Huelstrung et al.⁵⁴ used a “discrete phase model” to

predict the degree of inclusion separation and used the results as a tool for designing a higher capacity tundish. Better macroscopic cleanliness of steel slabs produced during abnormal casting conditions caused due to the stopping of one of the strand slab caster, led them to design a tundish with a higher volume. They investigated the behaviour of solid alumina particles using an Euler-Lagrangian method. In this method, the particle trajectories were computed in a Lagrangian reference frame. The equations involved in this method are discussed in the later part of the thesis. Schwarze et al.¹⁸, in their isothermal and non isothermal studies of a V-shaped tundish, also considered the effect of added mass (Figure 2.7), which should be included when a thin film of liquid surrounds a moving particle (equation 2.6).

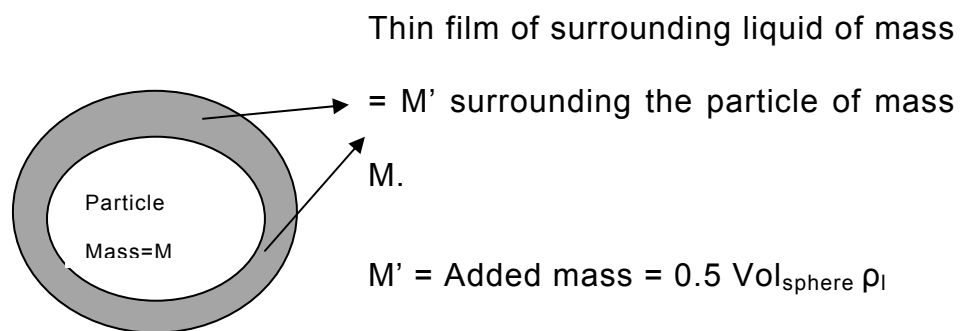


Figure-2.7 showing added mass due to thin film of liquid surrounding the particle¹⁸

$$\frac{du_p}{dt} = \frac{18 \mu C_D Re}{24 \rho_p d_p^2} u_{rel} + \frac{g(\rho_p - \rho)}{\rho_p} + \frac{1}{2} \frac{\rho}{\rho_p} \frac{d}{dt} u_{rel} \quad [\text{Eq. 2.6}]$$

To simulate the chaotic effect of the turbulence eddies of the liquid phase on the inclusion trajectories; a discrete random-walk model was applied by S. Diaz et al.⁵⁵ In this model, a fluctuant random-velocity vector (u'_i) is added to the calculated time-averaged vector (\bar{u}_i), in order to obtain the inclusion velocity (u_i) at each time step, as particles travels through the fluid. Each random component of the inclusion velocity is proportional to the local turbulent kinetic energy level(k_p), according to the following equation (2.7)

$$u'_i = \zeta_i \sqrt{\bar{u}_i'^2} = \zeta_i \sqrt{\frac{2k}{3}} \quad [\text{Eq: 2.7}]$$

Where ζ_i is a random number, normally distributed between -1 and 1, which changes at each integration step.

Lifeng Zhang et al.⁵⁶ proposed three modes of inclusion removal from molten steel in the tundish viz. floatation to the free surface, collision and coalescence of inclusions to form larger ones and adhesion to the lining solid surfaces. They studied the 3D fluid flow with and without flow control devices. The results indicated that flow control devices effectively limit the strong stirring energy to within the inlet zone. Flow control devices were also favourable for inclusion removal. The total removal ratio was 51% without flow control devices where inclusions with radii greater than 72 microns

were totally removed. This increased to 79% with flow control devices where inclusions with radii greater than 61 microns were totally removed. Out of this 79%, removal by floatation was 49.5% and removal by adhesion was 29.5%. The collision and coalescence mode was a better way to remove smaller size inclusions as the number of collisions per unit time per unit volume of steel was much higher for smaller inclusions than bigger inclusions.

M. Javurek et al.⁵⁷ considered the removal of non metallic inclusions due to buoyancy forces in continuous casting tundishes. They found the reasons why the particle separation is worse than the calculated maximal possible removal rate. The reasons were unfavourable fluid flow pattern and the turbulent particle diffusion. They also concluded that RTD curves are inappropriate to estimate the particle separation in tundishes. The use of direct calculation and CFD simulation was recommended.

R. Schwarze et al.¹⁸ studied the degree of inclusion separation in different (V shaped) tundish configurations by numerical modelling. The numerical model was based on the Euler-Lagrange approach. The flow was described by the Reynolds averaged transport equations for mass, momentum and energy in conjunction with the RNG - $k - \epsilon$ model. They considered both isothermal and non isothermal flows. Only small differences between the isothermal and non isothermal flows were observed for the conditions modelled.

Thermal natural convection was not that significant. The results of the numerical model were in good agreement with corresponding data from water model studies. The highest degree of inclusion separation was reached when a dam was positioned just at the beginning of the tundish arm (Figure 2.8).

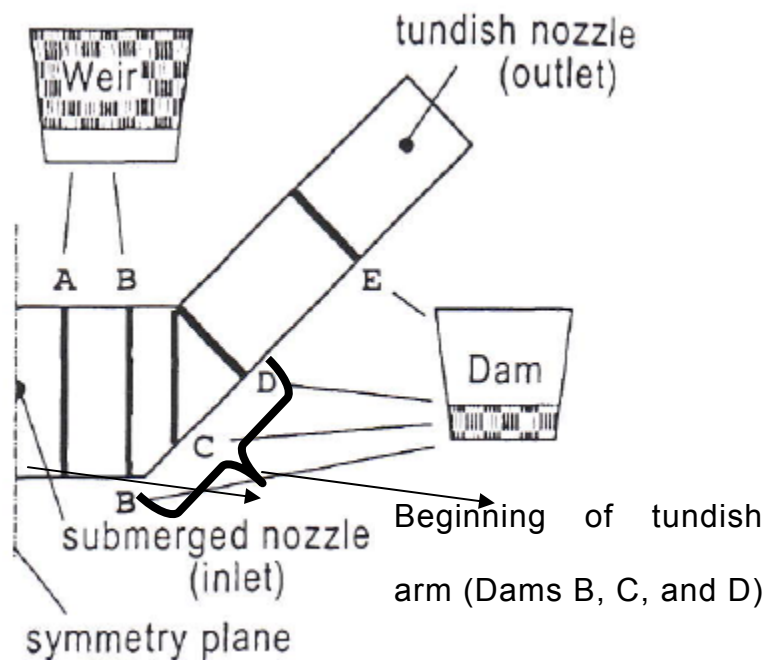


Figure-2.8 Showing V shaped tundish with different arrangements of weir and dams¹⁸

Thomas and Bai⁵⁸ summarized the formation mechanisms, detection methods and prevention of tundish nozzle clogging, focusing on the role of computational models in quantifying the non-composition-related aspects. They classified tundish clogging into four main

types viz. the transport of oxides present in the steel to the nozzle wall, air aspiration into the nozzle, chemical reaction between the nozzle refractory and the steel and steel solidified in the nozzle. However, in practice, a clog can be a combination of two or more of the above types. They mentioned that clogging can be best detected during casting by simultaneous monitoring of several different parameters like argon back pressure, nitrogen pickup, mould level fluctuations and flow control position relative to casting speed. Solutions to clogging problems were also mentioned by them. They are minimizing inclusions by improved steelmaking practices, optimizing fluid flow and transfer processes, controlling steel alloy additions, slag and refractory compositions, improving nozzle material design and avoiding air aspiration. J. P. Rogler et al.⁵⁹ reported the probability of inclusion removal in a tundish by gas bubbling. They developed a simple mathematical model and concluded that the probability of particle/bubble attachment (P_{at}) is the product of the probabilities of three fundamental steps of this process including thinning, rupture and three-phase contact stability⁶⁰ (Figure 2.9).

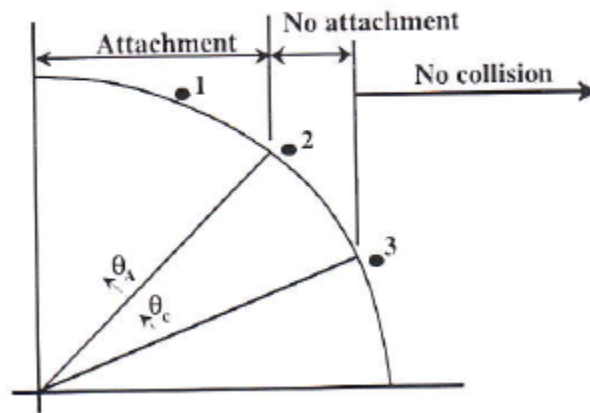


Figure- 2.9 (a) Schematic diagram of critical angles.⁶⁰

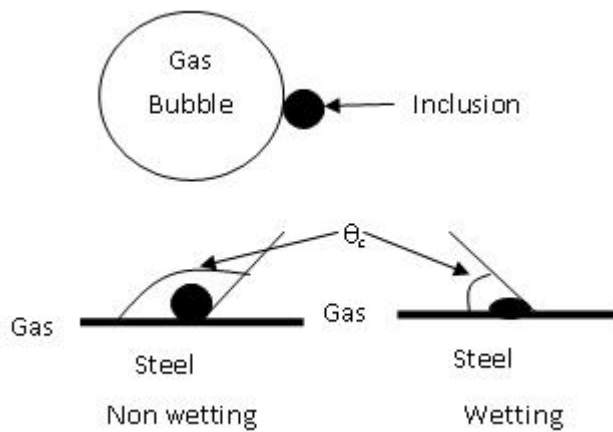


Figure- 2.9(b) Schematic diagram of steel gas and inclusion system

However, only the probability of film thinning can be calculated by any known method and they suggested that the probability of the last two steps could be assumed to be unity. P_{at} increases with decreasing particle size and increases with increasing bubble size. But for attachment collision is necessary and hence the particle

collection probability (P) is the product of P_{at} and the collision probability P_c . A semi-analytical solution of the Navier-Stokes equation gives a rough estimate of P_c . This analysis shows that the collection probability (P) increases with decreasing bubble size and increases with increasing particle size. The removal of exogenous non-metallic inclusions by optimization of hydrodynamic characteristics was reported by A. V. Kuklev et al.⁶¹ The suggested methods are increasing tundish size to allow more residence time and the use of flow control devices. Most of the researchers mentioned above did mathematical modelling of inclusion removal. J. P. Rogler et al.⁶² performed physical modelling of inclusion removal in a tundish by gas bubbling. They used water as the analogue of steel and linear low density polyethylene (LLDPE, $\rho=0.92 \text{ kg m}^{-3}$) as an analogue of inclusions. A layer of kerosene oil was used on the top of the tundish, to simulate the slag phase. This kerosene layer was also very efficient in collecting any LLDPE particles that float up. A 400 mesh sieve (38 μm openings) with an upward extending wall was used as a particle collector, and was placed in the outlet stream of the tundish. Before each experiment, the particle collector was completely dried and weighed. A 6g sample of LLDPE was weighed and placed in a syringe and then the remaining of the syringe was filled with isopropyl alcohol in order to form stable slurry of LLDPE particles. At time = 0, the particle slurry was injected into the ladle shroud from the syringe. At the conclusion

of the experiment, the particle collector was removed and completely dried under a hot lamp. Once dried the particle collector containing the particles was weighed again, and the mass of the collected particles was easily determined by subtracting the weight of the collector itself. The main reason for choosing LLDPE over hollow glass micro-spheres was that the latter is extremely difficult to sieve and also is not collected by kerosene on the top of the tundish. However, in terms of the density ratio, a hollow glass microsphere to water is very similar to that of aluminate inclusions to liquid steel. They concluded that separation efficiency of inclusion particles within the flowing liquid bath in a tundish is influenced by a number of factors such as the overall fluid flow behaviour, the chemical and physical nature of the inclusion, size of the inclusions, and the rates and mechanisms of particle capture by various potential particle sinks. From their study, they concluded that FCD enhanced particle separation efficiency and properly sized bubbles induced the highest particle separation efficiencies. Ruckert et al.⁶³ performed physical and mathematical modelling to study inclusion separation from a continuous casting tundish. In their experiments, the principle of the particle counter is that of a photoelectric barrier with a laser diode as light source and a CCD sensor as receiver. The particles flow through a channel and influence the light signal from the laser diode. The signal received by the CCD sensor is analysed and the particle size can be evaluated. For these experiments a Quantel Twins

Nd:YAG laser with a pulse energy of 140mJ was used. The laser beam from the front lens spans a plane of green laser light through the tundish. A mixture of particles and water are sucked down to the shroud from a container. Particles are added continuously from the beginning of the measurement. For each group of particles and for measurements with and without impact pad, series of ten pictures are taken after one quarter, one half and after each resident time (RT) till the eighth. Pictures are made with two cameras located parallel to the tundish, one takes a photo from the first half of the tundish and a second one takes a photo of the second half. The illuminated particles are represented by pixels with a strong white colour. To separate them from the rest of the picture, the inhomogeneous background has to be subtracted from the pictures. A mesh is applied to all pictures in which particles are counted. Particles which are represented by pixels were counted using a threshold technique. A histogram shape-based approach was used as the threshold technique. They concluded that with high inflow rates of liquid into the tundish the separation rate of inclusions is lowered down to a great extent. They also considered a tundish fitted with an impact pad and reported that the separation rates of inclusions are much better as compared to a bare tundish. At the MMPC, Guthrie and co-workers^{64,65,66,67,100} developed the LiMCA technique, which is capable of monitoring inclusions online. The system consists of a probe, which has two electrodes and the probe

is submerged in the liquid. As soon as a particle passes through the electric sensing zone of the two electrodes, there is a change in the resistance, and that is identified as a voltage peak in the signal. The height of the peak corresponds to diameter of the inclusion. So far three Aqueous Particle Sensors (APS I,II and III) have been developed and a significant amount of research have been done. LiMCA for Aluminum and LiMCA for steel are also commercially available.

An extensive review of the literature shows a large number of modelling efforts covering various aspects, such as fluid flow , RTD, effects of FCD on flow pattern, inclusion removal, thermal energy transport, etc, have been reported. However, most of the modelling did not consider refractories, slag, and fluxes; in their predictions. Henrik Solhed et al.¹² did include these in their modelling effort, and studied slag-steel interactions in continuous-casting tundishes. A model was developed that took into account the steel, slag and refractory phases. The model was also used to determine the optimal location of flow devices, rendering the temperature distribution in the steel more uniform and enhancing the removal of inclusions to the upper slag phase. In that study, the focus was to study the slag/steel interface. Predictions showed that slag is dispersed into the steel close to the interface, as well as close to the ladle shroud. A momentary interfacial solidification sampling (MISS)

method was developed to confirm these predictions with plant tests. Analysis of the samples by ultrasonic testing, optical microscopy and SEM confirmed the presence of non metallic particles close to the slag steel interface and close to the ladle shroud. The analyses also showed that the slag steel interface is very irregular despite low velocities. They concluded that the slag/steel interface is unstable and that the liquid steel at the interface can engulf slag and may lead to the formation of inclusions in the final cast product. In another investigation, slag floatation and entrapment was studied by Henrik Solhed et al.¹³ using fluid flow simulations, sampling and physical metallurgy. A model of a continuous casting tundish was developed, which considers refractory, slag and flux phases in addition to the steel phase. The model was verified with velocity and temperature measurements in the liquid steel and temperature profiles in the refractory walls.. The agreement between the measured velocities and temperatures and the corresponding predictions were good. From their computational results it was seen that slag concentrations were very low in the regions near the walls, where flows were upwardly directed, but that near to the shroud and the stopper rod, slag concentrations were higher and the downwardly directed velocity components caused the slag to penetrate the steel. It is evident that not much work has been done on slag entrainment. So more work on slag entrainment using both physical and mathematical modelling needs to be done. Here at the

MMPC, modelling slag entrainment both physically and numerically is being done by some researchers. In the numerical model the VOF approach is currently used.

The effect of flow control devices have also been extensively studied by a number of researchers^{68,69,19,70,71,72,73}. The research on FCD has been so vast in the past decade that perhaps it needs a separate review on the effect of FCD on the performance of tundish. However it has been seen that a FCD can have a positive effect on tundish performance if its design is properly optimised and positioning within the tundish is proper. But for inclusion removal FCD have failed to show their efficiency either in physical or mathematical modelling^{74,75,76}. Also improper positioning of a FCD may result in detrimental flow patterns inside the tundish. Also in large tundishes which allow sufficient residence time for inclusion floatation FCD are not recommended because they are inconvenient to sustain hot cycle tundish practice, which is quite economical. With a large tundish, the deep melt bath does not require a pour pad either.⁷

A swirling ladle shroud may be very useful to reduce turbulent kinetic energy within the inlet zone. A new design of ladle shroud (Figure-2.10), obtained through water modelling, that controls turbulence of the entry jet in continuous casting tundishes has been proposed by G. S. Diaz et al.⁷⁷ Particle Image Velocimetry (PIV) measurements indicated that this design decreased the impact velocity on the

tundish bottom close to 1/3 of that provided by a conventional ladle shroud. This achievement was due to a swirling jet that promoted a recirculatory flow in the horizontal planes of the tundish. The swirling effects helped to dissipate the turbulence energy of the jet before it hit the tundish bottom thereby decreasing fluid velocities impacting the back and front walls of the tundish.

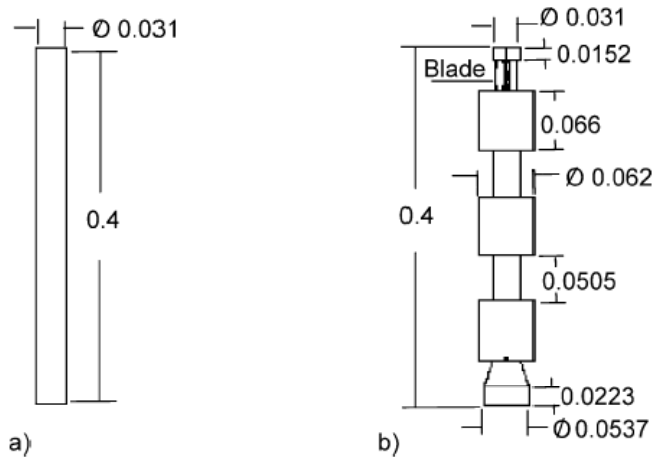


Figure-2.10 Geometric dimensions of the experimental shrouds (a) Conventional and (b) Swirling Ladle Shroud (SLS).⁷⁷

Turbulence models such as $k-\epsilon$, $k-\omega$ and RSM were applied to simulate the experimental PIV measurements of velocities in the fluid flow. Only the RSM model yielded predictions that agreed remarkably well with the experimental determinations. These results were sufficiently good as to avoid the employment of flow control devices such as dams, weirs, turbulence inhibitors and the like, in tundishes.

G. S. Diaz et al.⁷⁸ in another study concluded that the SLS efficiently avoids the formation of vortexes and recirculating flows either under isothermal and non isothermal conditions. The SLS enhances floatation of inclusion and makes the floatation rate less dependent on particle size. The trajectories of inclusions in the water flow are shown in Figures 2.11, 2.12 and 2.13.

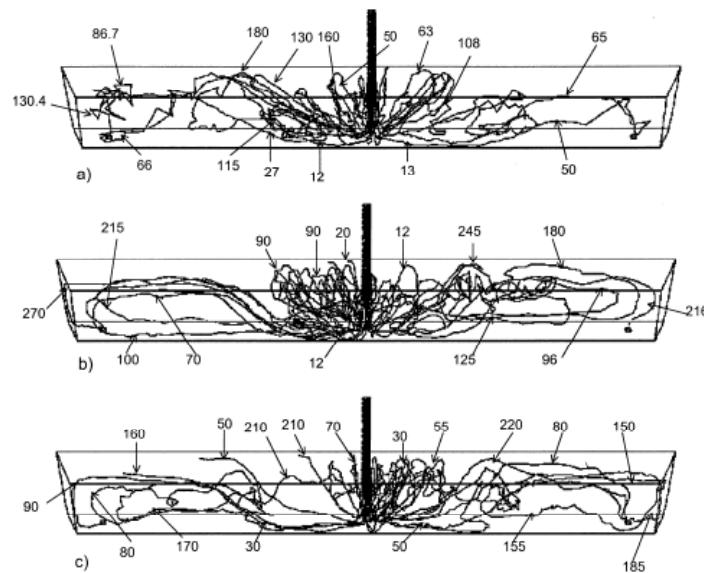


Figure 2.11 Trajectories of inclusions in the water flow obtained by mathematical simulation. Isometric view using conventional ladle shroud and particle of $20\mu\text{m}$ for: (a) 27 s after the thermal step up input, (b) 120 s after the thermal step up input, (c) 240 s after the thermal step up input.⁷⁸

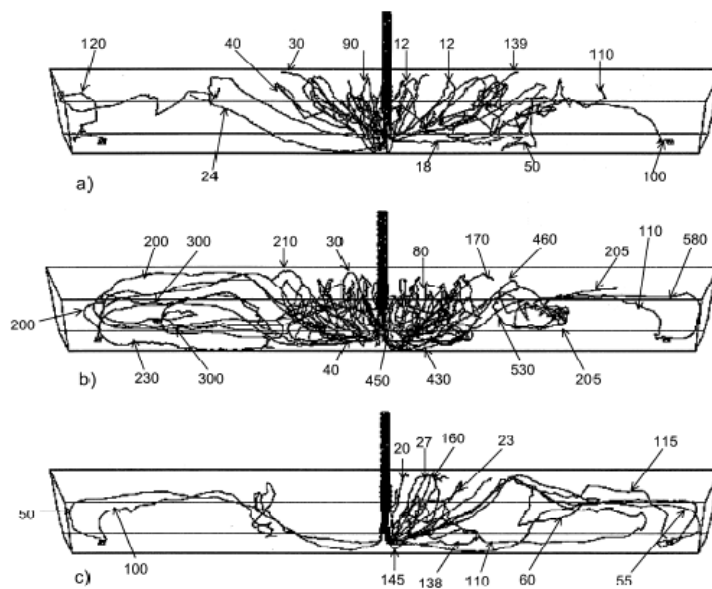


Figure 2.12 Trajectories of inclusions in the water flow obtained by mathematical simulation (isometric view) for a conventional ladle shroud and particle of $100\mu m$ for:(a) 27 s after the thermal step up input, (b) 120 s after the thermal step up input, (c) 240 s after the thermal step up input.⁷⁸

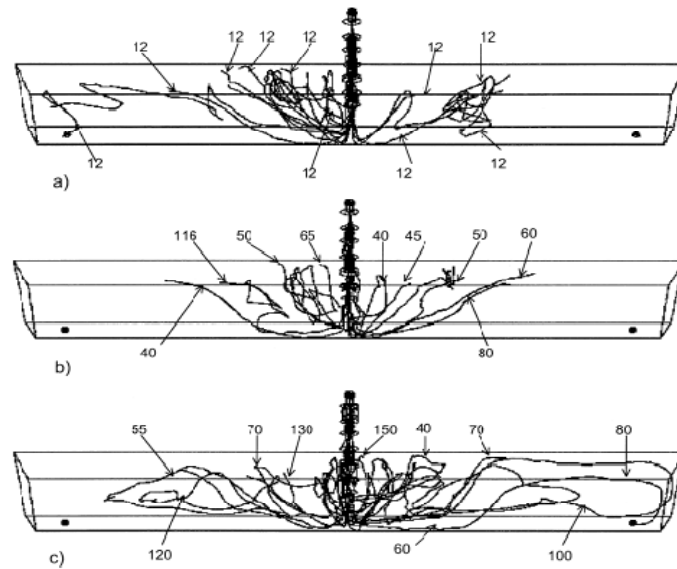


Figure 2.13 Trajectories of inclusions in the water flow obtained by mathematical simulation at the isometric view using swirling ladle shroud and particle of $20\mu\text{m}$ for: (a) 27 s after the thermal step up input, (b) 120 s after the thermal step up input, (c) 240 s after the thermal step up input.⁷⁸

Thus the SLS is a good alternative to substitute the FCD available in the market. The SLS may have many advantages but from the flow fields it appears that the flows are highly complex and certainly cause erosion of refractory inside the shroud which is not economical and detrimental for the steel quality.

In summary, it is seen that a lot of work has been done on the development of mathematical models for studying fluid flow patterns in tundishes, to study the effect of FCDs, to evaluate mean residence times, RTD, and inclusion removal ratios. This R&D effort

has been possible, thanks to the increase in computational power and the logarithmic decreases in computational costs (MOHR's Law). However, slag entrainment, one of the most important issues in continuous casting, has not gained much attention and only few researchers have reported that in the literature. Also, it is essential to validate these numerical models with actual experiments. The review also shows a recent trend in modelling considering non isothermal conditions. In reality tundish operations are inevitably non-isothermal to some extent,(unless plasma heated tundishes are practised). Hence, there are effects of inlet steel temperatures and buoyant forces. So isothermal modelling predictions may not be sufficiently correct since tundish flows are very sensitive to even minor fluctuations in steel/slag temperature (ie.~5⁰C). Many researchers are now advocating against the use of FCDs and are proposing increased tundish volumes for sufficient residence times and better inclusion removal. This practice has already started in Japan some twenty years ago together with the adoption of plasma heating for maintaining isothermal conditions during casting. Although, DNS seems to be impossible, at least one research centre of a Japanese Steel Company is doing this with the aid of parallel processing, with over 300 computers in synergy.

3.0 General Procedures for Physical and Mathematical Modelling

3.1 Water Modelling Procedures

For performing the physical modelling experiments, a full-scale water model and its one third scale equivalent of the QIT four strand tundish was used to simulate various physical phenomena. Liquid steel was replaced by its low-temperature aqueous analogue (water) which was maintained at around 293K for all experiments. A schematic diagram of our full-scale water model and its dimensions are given in Figures 3.1 and 3.2. Figure-3.3 shows the actual picture of the full scale water model system present at the MMPC laboratory.

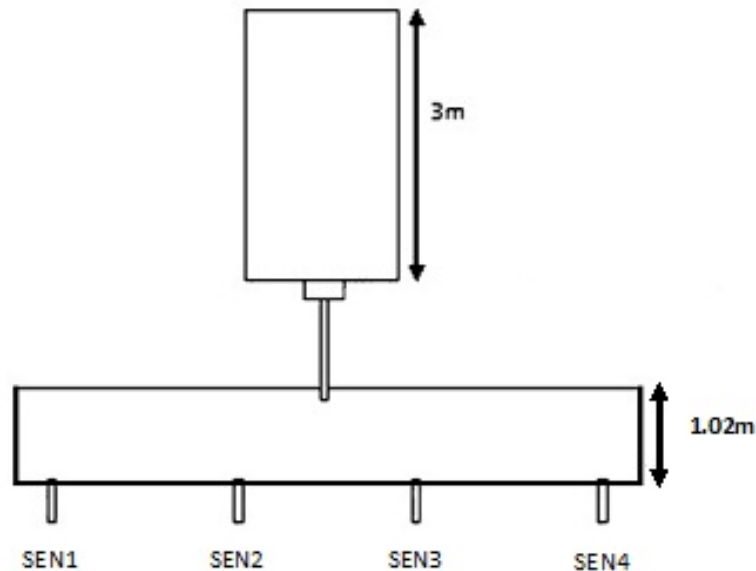


Figure-3.1 Schematic diagram of the full-scale water model tundish

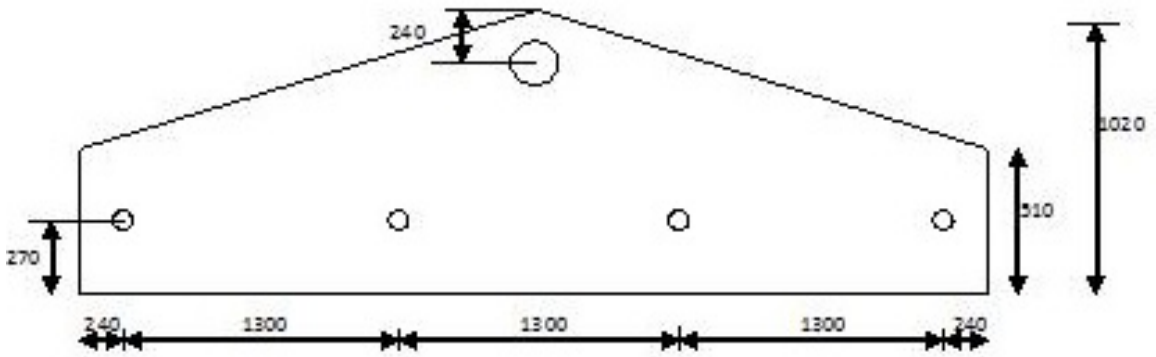


Figure-3.2 Key dimensions (mm) of the full-scale water model tundish



Figure-3.3 Full-scale water model system at the MMPC laboratory

The square tank above the tundish was used to provide the 3-m head pressure of water, and was used to control the inflow rate of water into the tundish. A flow rate of $0.17 \text{ m}^3/\text{min}$ was maintained through the ladle shroud, so as to maintain a steady-state height of 500 mm of water within the tundish. The immersion depth of the ladle shroud was 60 mm. For the one third scale model, a flow rate $0.01 \text{ m}^3/\text{min}$ was maintained from the inflow, so as to obtain a steady

state height of 167mm, determined on the basis of Froude ($\frac{U^2}{gL}$) similitude. For full-scale water modelling the slag phase was simulated using polyethylene beads (density = 920 kg m⁻³, diameter = 2.5mm to 3mm) that were poured uniformly over the free surface of water in the tundish, prior to the experiment. The thickness of the polyethylene bead layer in the vicinity of the ladle shroud was 0.02m ± 0.002m. A 0.01m thick layer of mineral oil (density= 870kg m⁻³, viscosity = 0.017 Pa.s) was used to simulate the slag phase in the one third scale water model. In order to simulate inert gas injections, compressed air was used as an analogue to argon. For simulating inclusions, hollow glass microspheres of density 300-400 kg m⁻³ were used based on Stokes' rise velocity similarity criterion. High Definition video photography was used to visualize bubble plume movements, slag layer motions and tracer dispersions.

3.2 Mathematical modelling procedures

The following steps were involved in the mathematical modelling;

- a) drawing of the tundish (the calculation domain) using basic CAD tools,
- b) discretization of the whole domain into tiny tetrahedral cells (commonly called meshing),
- c) exporting the mesh to an appropriate CFD package (ANSYS FLUENT 12.0),
- d) setting up of material properties and boundary conditions,
- e) setting up of solution parameters,
- f) iterative solution of the discretized equations until

convergence is achieved, g) post processing and graphical representation.

Calculations were performed in one half of the tundish, assuming a vertical symmetry plane between the two sides of the tundish, and ignoring any potential large scale transient turbulent motion.

In general, the velocity inlet boundary condition was used for the inlet, and outflow boundary conditions were used for the outlets. The top surface was set as a free surface with zero shear stress, and all other surfaces were walls with the no-slip condition. For specific cases like modelling non-isothermal conditions, and modelling discrete and multiphase flows, the boundary conditions are discussed in the respective Chapters.

3.2.1 Basic equations involved

For the simulation of most transport phenomena, the general convection-diffusion transport equation applies and is given below.

$$\frac{\partial(\rho\phi)}{\partial t} + \text{div}(\rho\mathbf{u}\phi) = \text{div}(\Gamma\text{grad}\phi) + S \quad [\text{Eq. 3.1}]$$

Here, Φ is the variable of interest (u, v, w, c, T, k, ϵ , etc.) according to the type of phenomena being considered (momentum, continuity, turbulence, species conservation, energy, temperature, etc.). S

represents a source term for the partial differential equation, allowing for non-convective and non-diffusive terms, to be incorporated. In the present study the basic equations considered are the continuity equation, the Navier-Stokes equation, the energy equation and the scalar transport equation.

$$\text{Continuity:} \quad \frac{\partial \rho}{\partial t} + \nabla \cdot (\rho \mathbf{u}) = 0 \quad [\text{Eq. 3.2}]$$

$$\text{Navier-Stokes:} \quad \frac{\partial(\rho \mathbf{u})}{\partial t} = -[\nabla \cdot \rho \mathbf{u} \mathbf{u}] - \nabla P - [\nabla \cdot \boldsymbol{\tau}] + F_b \quad [\text{Eq. 3.3}]$$

$$\text{Energy:} \quad \frac{\partial(\rho c_p T)}{\partial t} + \frac{\partial}{\partial x_i} (\rho c_p T u_i) = \frac{\partial}{\partial x_i} \left(k_{eff} \frac{\partial T}{\partial x_i} \right) + Q_v \quad [\text{Eq. 3.4}]$$

$$\text{Scalar Transport:} \quad \frac{\partial(\rho \psi)}{\partial t} + \frac{\partial}{\partial x_i} \left(\rho u_i \psi - \Gamma_\psi \frac{\partial \psi}{\partial x_i} \right) = 0 \quad [\text{Eq. 3.5}]$$

As the equations of “conservation of mass” (continuity equation) and “conservation of momentum” (Navier-Stokes equation) describe the fluid flow in mathematical terms, they, along with treatment of turbulence and boundary conditions define all mathematical models, including those of tundishes. Due to the complexity of the engineering flows, such as flow in tundish, it is practically impossible to solve these equations analytically. Also, as the flow is associated with turbulence, turbulence modelling is incorporated to capture the critical effects of turbulent flows, without having to resolve the actual small scale turbulent motions. So instead of using the conservation equations in their original forms, the ‘Reynolds Averaged Navier Stokes’ (RANS) equation and the averaged continuity equation is

solved for mean quantities of velocity and pressure. Direct numerical solution, (DNS) of the conservation equations will require extremely high computational power and time and this has already been stated in the literature review section.

To model the turbulence, the standard k - ε model of Launder and Spalding⁷⁹ was used along with the basic conservation equations. In the k - ε model, k is the kinetic energy of turbulence per unit mass of fluid, while ε is the rate of turbulence energy dissipation. Thus,

$$k = \frac{1}{2} \sum \overline{u_i'^2} \quad [\text{Eq. 3.6}]$$

So, in addition to the continuity and momentum equations, two extra equations for k and ε are solved.

$$\frac{Dk}{Dt} = \frac{\nu_t}{\sigma_k} \nabla^2 k + G_k - \varepsilon \quad [\text{Eq. 3.7}]$$

$$\frac{D\varepsilon}{Dt} = \frac{\nu_t}{\sigma_\varepsilon} \nabla^2 \varepsilon + \frac{\varepsilon}{k} (C_1 G_k - C_2 \varepsilon) \quad [\text{Eq. 3.8}]$$

Here G_k is the rate of production of k and is given by the following equation:

$$G_k = \nu_t \left[\frac{\partial v_i}{\partial x_j} + \frac{\partial v_j}{\partial x_i} \right] \frac{\partial v_i}{\partial x_j} \quad [\text{Eq. 3.9}]$$

The turbulent and effective viscosity is calculated by the following equations:

$$\mu_t = \frac{c_\mu \rho k^2}{\varepsilon} \quad [\text{Eq. 3.10}]$$

$$\mu_{eff} = \mu + \mu_t \quad [\text{Eq. 3.11}]$$

The recommended values of the constants for the standard k - ε model were $C_1= 1.44$, $C_2= 1.92$, $C_\mu= 0.09$, $\sigma_k = 1$ and $\sigma_\varepsilon=1.3$ as proposed by Launder and Spalding⁷⁹. There are other variants of the k - ε model, and each of them has been tested for specific cases. The reason for choosing the standard k - ε model is justified in the subsequent section.

3.2.2 Choice of a proper turbulence model

Choosing an appropriate turbulence model is very essential and this depends highly on the type of phenomena taking place, and also on the parameters predicted. For example, some researchers are interested in bulk properties where as others are more concerned about local variations. Seyedein et al⁸⁰ employed various turbulence models to study turbulent jet impingement in a confined slot. They considered a single jet and performed 2D mathematical modelling. They concluded that the standard k - ε model is not the best model for simulating confined turbulent impinging jets. The standard k - ε model underestimated the Nusselt number profile along the whole impingement surface. They reported that the accuracy of the standard k - ε model greatly depends on the model parameters and near wall treatment. They also used the low Re k - ε models viz. Launder and Sharma, Lam and Bremhorst, and Chien. The predictions from the low Re k - ε model of Launder and Sharma seemed to

be closest with the experimental results. Jha and Dash²³ employed the standard k- ϵ model, the RNG k- ϵ model and the low Re k- ϵ model of Lam and Bremhorst to predict gross flow properties like mean residence time and ratio of mix to dead volume. They performed 3D mathematical modelling. All the three turbulence models predicted the gross flow properties quite well and were in accordance with experimental results. The standard k- ϵ model predicted the closest value. All the turbulence models were able to predict the two peaks in the temporal variation of tracer concentration for a single exit tundish, while the Low Reynolds number Lam-Bremhorst model predicted the initial transience much better than the other two models. So from the above discussion it is clear that the choice of the turbulence model really depends on what people are interested to predict. Following the above footsteps, different turbulence models were used viz. Standard k- ϵ model with standard wall functions, Realizable k- ϵ model, RNG k- ϵ model, and low Re k- ϵ models of Launder-Sharma, Lam-Bremhorst and Yang-Shih to predict the velocity profile in the plane of the ladle shroud. 3D mathematical models were developed and the four strand billet caster tundish was considered. The RNG k- ϵ model and the low Re k- ϵ model of Lam-Bremhorst did not converge because of numerical instability. Figures 3.4-3.7 shows the predicted velocity contours in the plane of the ladle shroud with four different k- ϵ models. It is clearly seen that the four different k- ϵ turbulence models predict the local jet behaviour differently. The

standard k- ϵ model cannot capture additional high velocity areas in the vicinity of the jet which is clearly predicted by the other three turbulence models. However, the difference is not very significant.

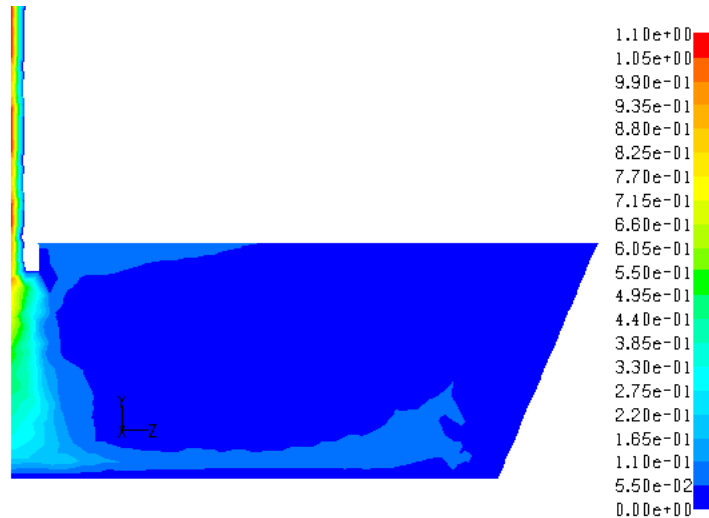


Figure-3.4 Standard k- ϵ model used to predict velocity ($m s^{-1}$) contours in the jet entry region in the plane of the ladle shroud.

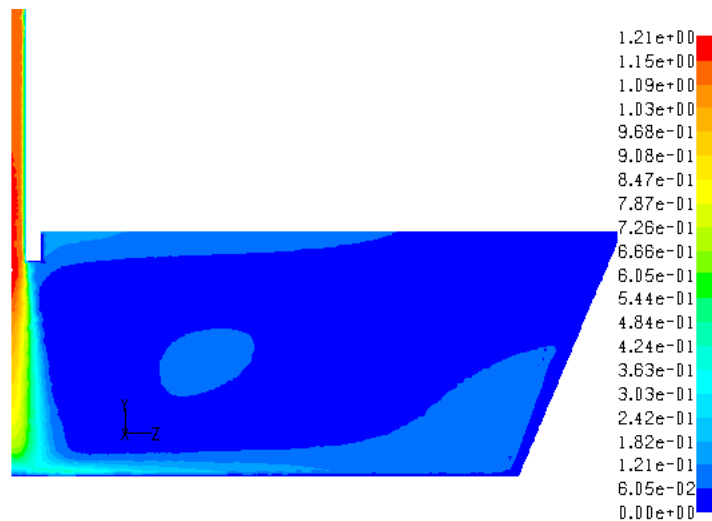


Figure-3.5 Realizable k- ϵ model used to predict velocity (ms^{-1}) contours in the jet entry region in the plane of the ladle shroud.

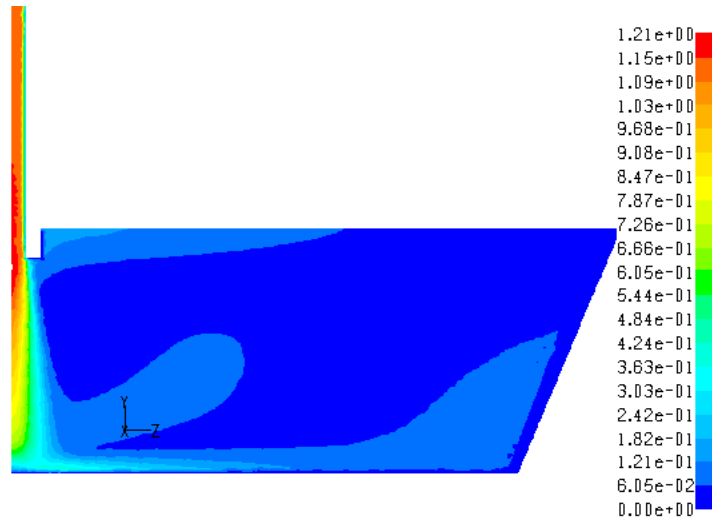


Figure-3.6 Launder-Sharma $k-\epsilon$ model used to predict velocity (ms^{-1}) contours in the jet entry region in the plane of the ladle shroud.

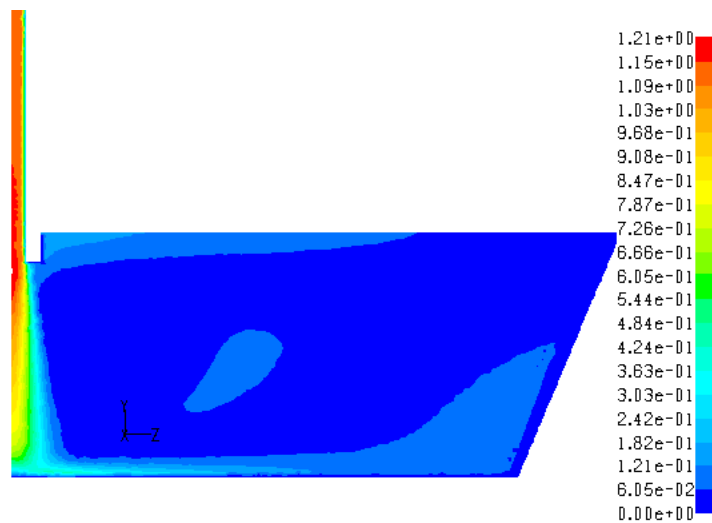


Figure-3.7 Yang-Shih $k-\epsilon$ model used to predict velocity (ms^{-1}) contours in the jet entry region in the plane of the ladle shroud.

To assess the effect of different turbulence models on bulk properties, residual ratio of inclusions (RRI) was predicted using these four variants of the $k-\epsilon$ turbulence model. For predicting RRI,

the discrete phase model was used, which is explained in the later part of this Chapter. Figure- 3.8 shows the predicted values of RRI with different turbulence models. All the four variants of the k- ϵ model predict the RRI% in the same range with the realizable model slightly under predicting the RRI% for the inner strand. So, in summary, our study is in accordance with the results of Seyedein et al.⁸⁰ and Jha et al.²³ and it is clear that the standard k- ϵ model can be used effectively to predict gross properties.

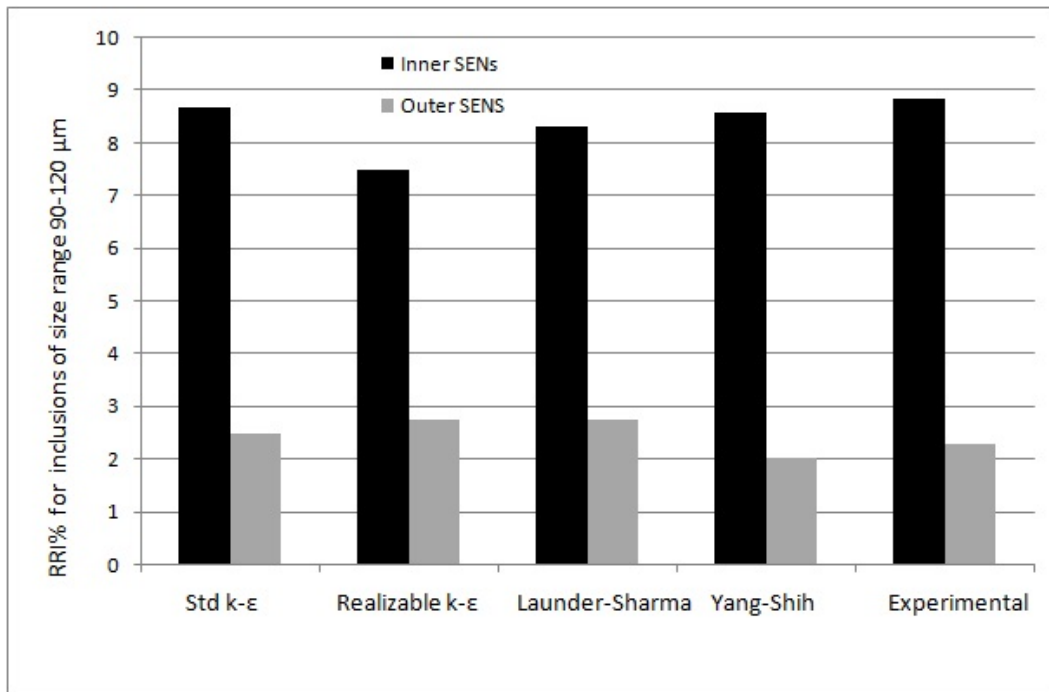


Figure- 3.8 Predicted RRI values for inclusions in the size range of (90-120 μ m) and comparison with experimental results.

The standard k- ϵ model has a major advantage over the low Re k- ϵ model, that the former converges much faster (takes almost one third the time) than the latter. This is because, in the low Re k- ϵ model, wall functions

cannot be used and hence finer grids are used near the wall to perform calculations up to the wall, making it longer to converge. Also, when using low Re k - ϵ models, often they need to be severely under-relaxed. So, if local properties are not of great importance, the standard k - ϵ model can be effectively used as long as it is validated with physical experiments.

3.2.3 Schemes and algorithms used

Now that the turbulence model is decided, it is customary to mention the solution methods and discretization schemes used. For most of the cases, a steady state flow field was first obtained before proceeding any further. The fluid considered was incompressible and Newtonian and hence the pressure based solver was used. During the initial steady state calculations, the SIMPLE^{81,82} algorithm was used for pressure –velocity coupling, along with the first order upwind scheme for momentum, k , and ϵ equations. Default values of the under relaxation factor were used i.e. unity for body forces, density and turbulent viscosity; 0.8 for the k and ϵ equations; 0.7 for the momentum equation. For pressure, the standard scheme was used, with an under relaxation of 0.3. Then for subsequent unsteady simulations, the steady state flow field was used as the initial solution and the PISO⁸² algorithm was used along with the second order upwind scheme for momentum, k , ϵ , energy, and species equations and PRESTO for the pressure. The PISO performs a neighbouring correction and a skewness correction and thus

facilitates faster convergence at every time step. The equations for k , ε , and momentum were under-relaxed to 0.5-0.6 as compared to those for the initial steady state solution.

When the first order upwind scheme is employed, first order accuracy is achieved. The quantities at the cell faces are determined by assuming that the cell centre values of any field variable represent a cell average value and hold throughout the entire cell. The face value Φ_f is set equal to the cell center value of Φ in the upstream cell. When second order accuracy is desired, the second order upwind scheme is applied. Here, quantities at the cell faces are calculated using a multidimensional linear reconstruction approach. In this approach higher order accuracy is achieved at the cell faces through a Taylor series expansion of the cell centered solution about the cell centroid⁸³.

When modelling cases which involve discrete or multiphase flows, other methods were used and these are mentioned in section 3.2.5.

3.2.4 Grid Independency

Having mentioned on the choice of turbulence models and solution methods, it is now obvious to perform grid independency tests. It is already a proven fact that the finer the mesh used, the closer is the numerical solution to the exact solution. In the calculation domain (tundish), various sizes of mesh (tetrahedral cells) were generated

and the flow field was analyzed. The plane on which the flow field was visualized is shown in Figure- 3.9.

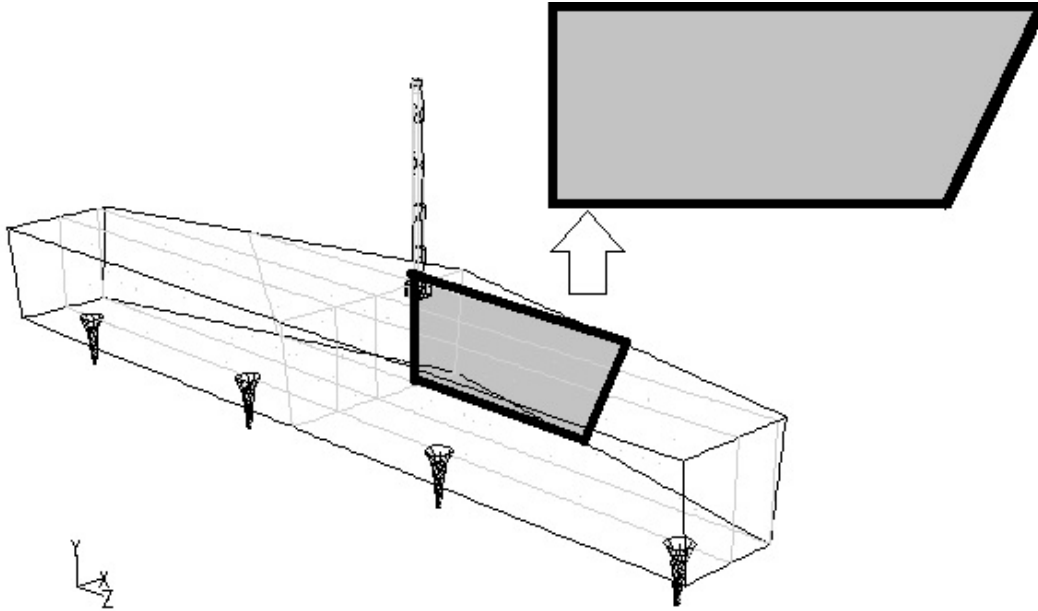


Figure-3.9 Plane on which velocity field was examined

As the mesh size is reduced, the number of cells generated inside the domain increased. A colour map of the velocity magnitude is given in Figure 3.10.

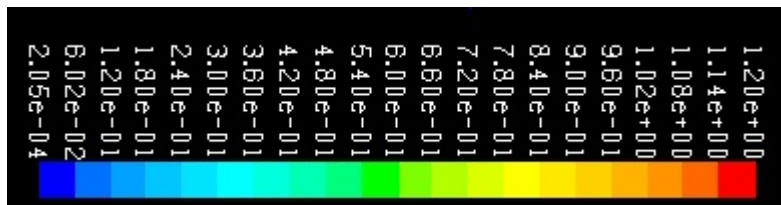


Figure-3.10 Colour map of velocity magnitude ($m s^{-1}$) for figures 3.11 to 3.19

Figures 3.11 to 3.19 show the velocity field in the plane of the ladle shroud.

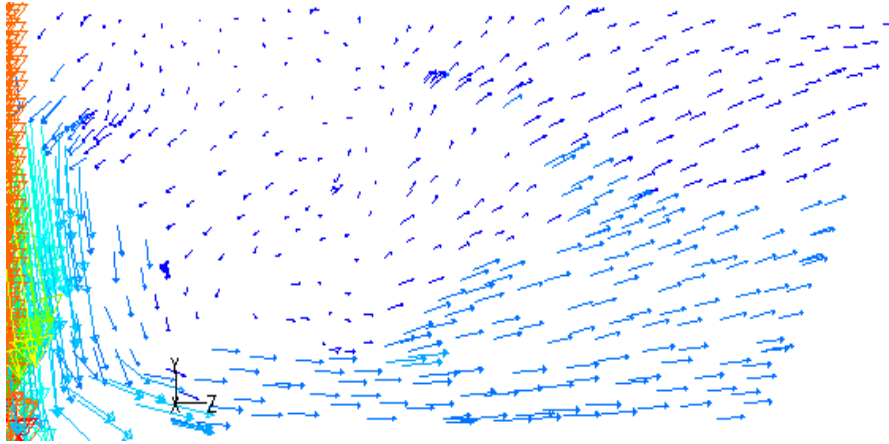


Figure-3.11 Tetrahedral mesh with 7392 cells generated inside the tundish to predict velocity vectors in the plane of interest

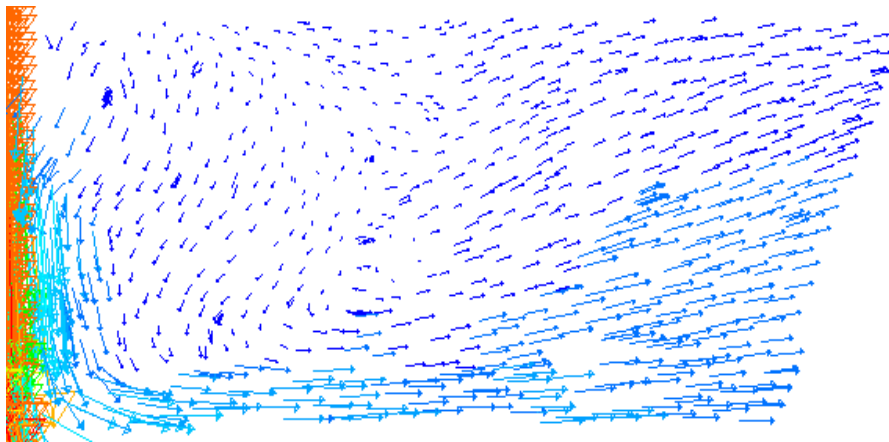


Figure-3.12 Tetrahedral mesh with 15372 cells generated inside the tundish to predict velocity vectors in the plane of interest

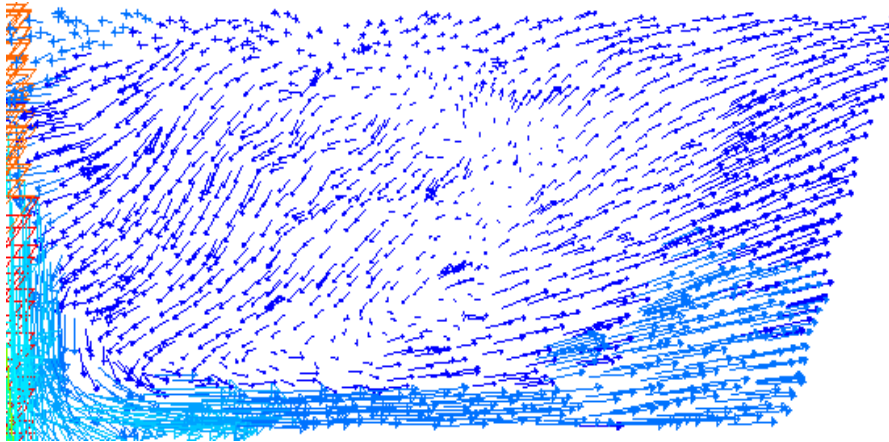


Figure-3.13 Tetrahedral mesh with 35188 cells generated inside the tundish to predict velocity vectors in the plane of interest

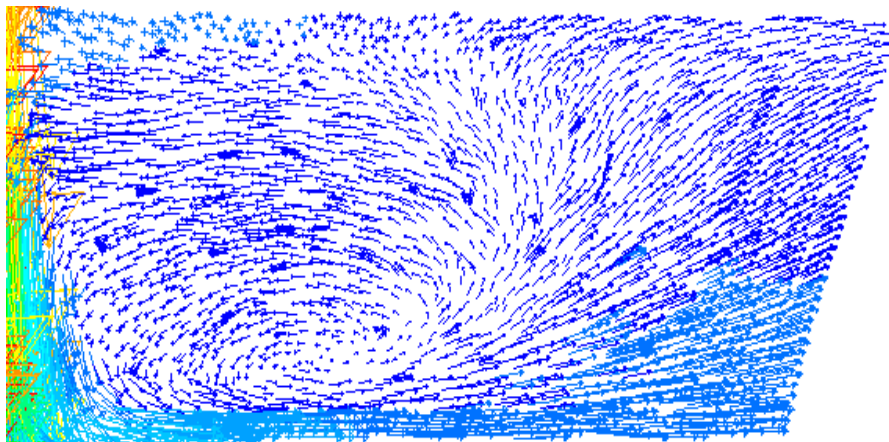


Figure-3.14 Tetrahedral mesh with 80268 cells generated inside the tundish to predict velocity vectors in the plane of interest

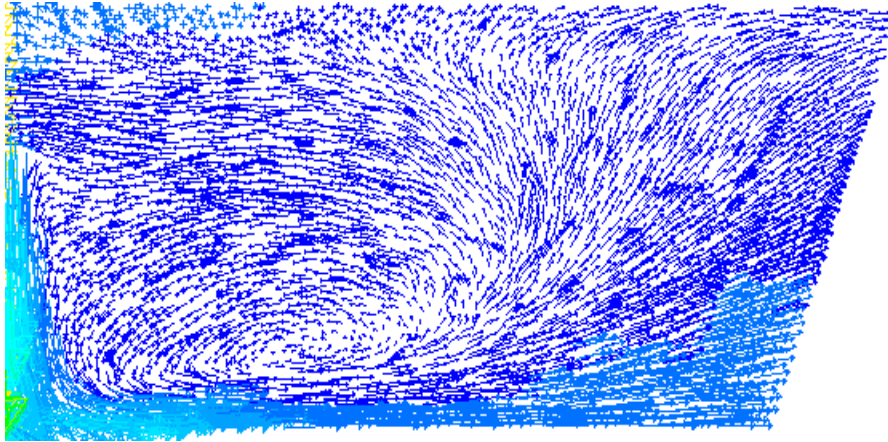


Figure-3.15 Tetrahedral mesh with 184012 cells generated inside the tundish to predict velocity vectors in the plane of interest

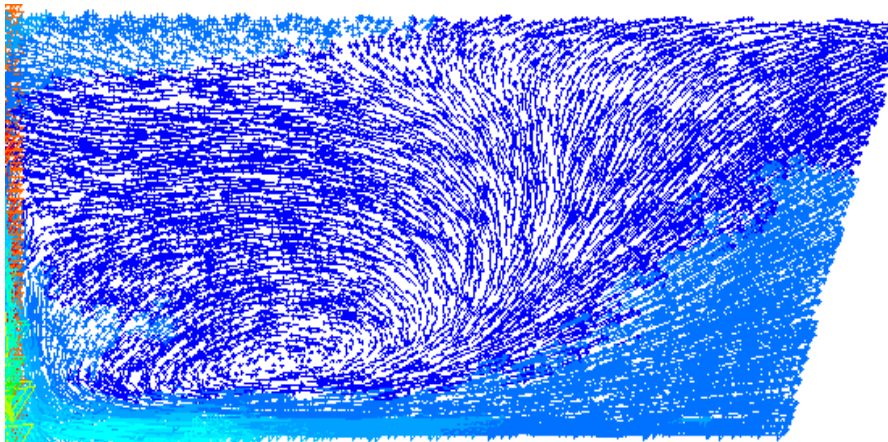


Figure-3.16 Tetrahedral mesh with 367050 cells generated inside the tundish to predict velocity vectors in the plane of interest

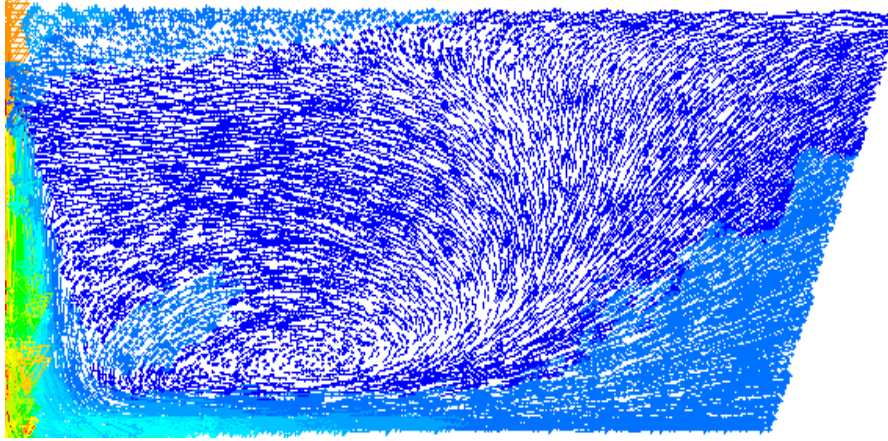


Figure-3.17 Tetrahedral mesh with 571189 cells generated inside the tundish to predict velocity vectors in the plane of interest

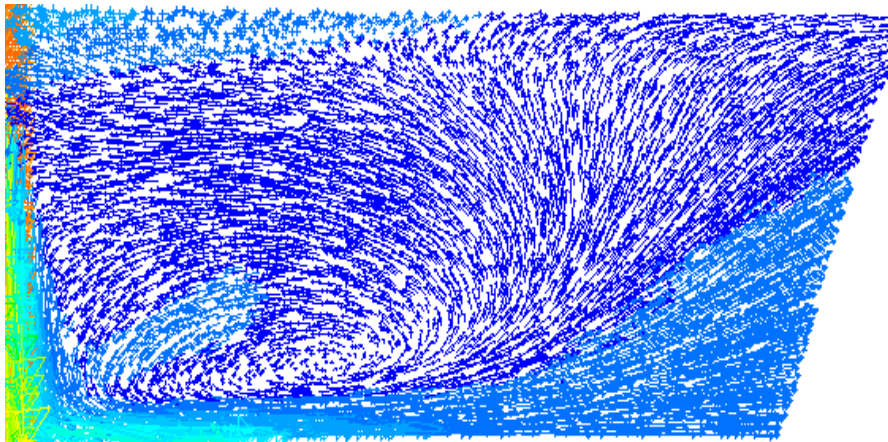


Figure-3.18 Tetrahedral mesh with 1643196 cells generated inside the tundish to predict velocity vectors in the plane of interest

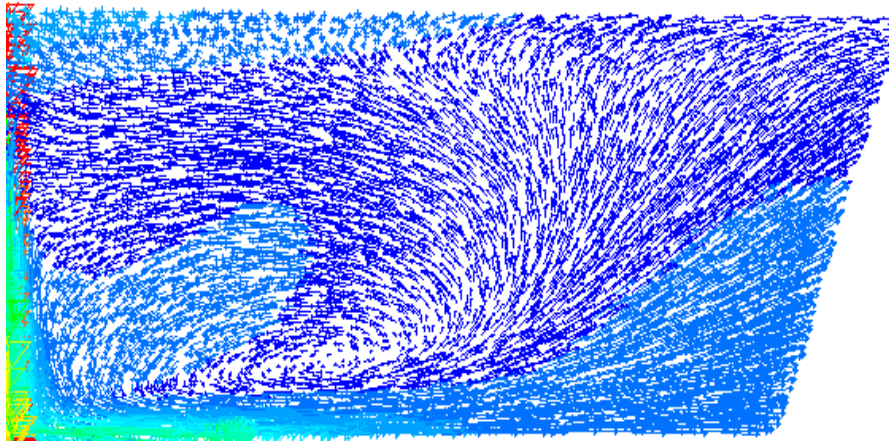


Figure-3.19 Tetrahedral mesh with 3877232 cells generated inside the tundish to predict velocity vectors in the plane of interest

If the above figures are carefully examined, the velocity field does not change significantly from Figure-3.15 –Figure-3.19. In Figures 3.11 – 3.14, the velocity field changes with the number of grid points (cells). So a minimum of 184012 cells are required to obtain a grid independent solution. In order to have a quantitative assessment of grid independency, residual ratio of inclusions (size range 90-120 μm) were numerically calculated in the tundish, with different number of grid points, and this is shown in Figure-3.20. It is clearly observed that prior to grid point index 6, which corresponds to 184012 cells, the RRI% values are fluctuating and highly dependent on the number of grid points. On the contrary, the RRI% values after from grid point index 6 to 10, are very stable and are in the same range. So it is quite evident that a minimum of 184012 grids are required for obtaining grid independent solutions. For all our subsequent simulations involving various transport phenomena, 250,000 to 300,000

cells were used, with the exception while modelling multiphase flows where 3.8×10^6 grid points were used.

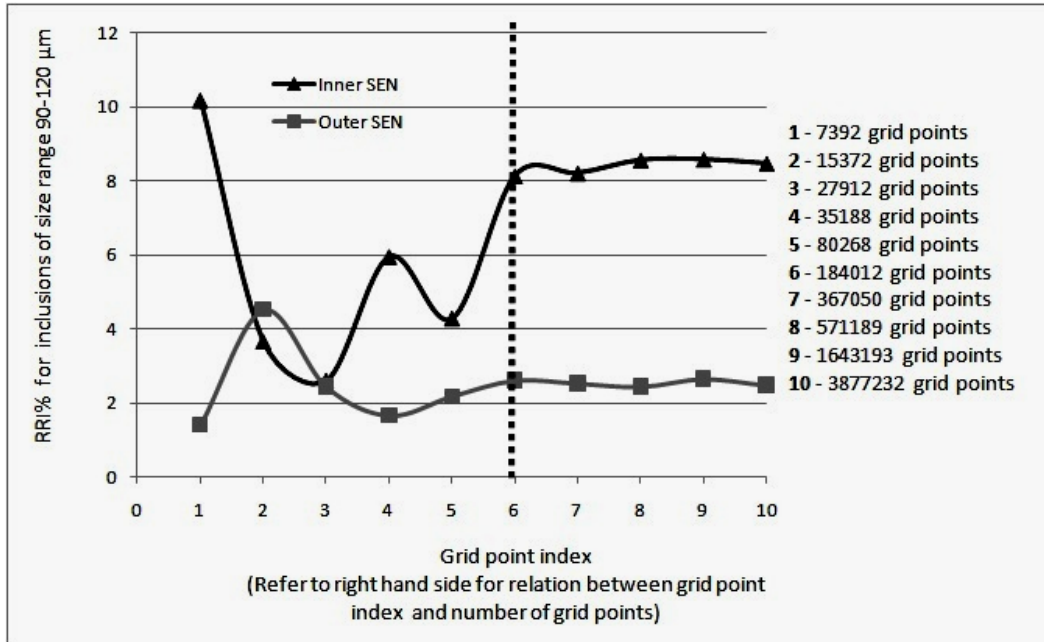


Figure-3.20 Effect of cell size on RRI%

3.2.5 Modelling of discrete phase and multiphase flows

In liquid metals processing, most of the flows are multiphase in nature and modelling of these is highly complex. Usually a tundish consists of multiple phases such as liquid steel, slag, entrained air, inclusions and gas bubbles. Since liquid steel occupies most of the volume of the tundish, it is considered to be the primary phase where as slag, gas bubbles, inclusions etc. are considered as the secondary and tertiary phases. When the secondary phase is dispersed in nature (gas bubbles and inclusions) and its volume fraction is less than 10-12% of the volume of the primary phase, the

discrete phase modelling approach holds true. However, if the secondary phase is more than 10-12% by volume then multiphase models like the mixture model or the VOF model needs to be applied. If it is necessary to track a free surface or an interface between two phases then the VOF method is proved to be good.

In the discrete phase modelling procedure, the fluid phase is treated as a continuum by solving the Navier-Stokes equations, while the dispersed phase is solved by tracking a large number of particles, bubbles, or droplets, through the previously calculated flow field in a Lagrangian frame of reference. The dispersed phase can then exchange momentum, mass, and energy with the fluid phase. The particle or droplet trajectories are computed individually at specified intervals during the fluid phase calculation. The dispersed secondary phase can affect the flow in the primary phase and for that two way turbulence coupling needs to be used. In the two way turbulence coupling, as the trajectory of a particle is computed, a track of the momentum gained or lost by the particle stream that follows that trajectory is kept, and these quantities are then incorporated in the subsequent continuous phase calculations. Thus, while the continuous phase always impacts the discrete phase, we can also incorporate the effect of the discrete phase trajectories on the continuum phase. This two-way coupling is accomplished by alternately solving the discrete and continuous phase equations,

until the solutions in both phases have stopped changing⁸³. The basic equations involved in discrete phase modelling are as follows.

$$\frac{du_p}{dt} = \frac{18 \mu C_D Re}{24 \rho_p d_p^2} u_{rel} + \frac{g(\rho_p - \rho)}{\rho_p} + \frac{1}{2} \frac{\rho}{\rho_p} \frac{d}{dt} u_{rel} \quad [\text{Eq. 3.12}]$$

$$Re = \frac{\rho d_p |u_{rel}|}{\mu} \quad [\text{Eq. 3.13}]$$

$$u_{rel} = u - u_p \quad [\text{Eq. 3.14}]$$

$$C_D = a_1 + \frac{a_2}{Re} + \frac{a_3}{Re^2} \quad [\text{Eq. 3.15}]$$

The original derivation of equation 3.12 was done by Y. A. Buevich⁸⁴ in 1966, and a simplistic derivation of the equation is furnished below.

The forces acting on a particle of mass m_p are the drag force, the buoyancy force and the force due to added mass. For a sphere the volume of the added mass of liquid is half the volume of the particle.

$$m_p \frac{du_p}{dt} = F_D + F_B + F_a \quad [\text{Eq. 3.16}]$$

$$m_p \frac{du_p}{dt} = \frac{1}{2} \rho (|u - u_p|)^2 C_D A + m_p \frac{g(\rho_p - \rho)}{\rho_p} + \frac{1}{2} v_p \rho \frac{d}{dt} (u - u_p) \quad [\text{Eq. 3.17}]$$

$$m_p \frac{du_p}{dt} = \frac{1}{2} \rho (|u - u_p|)^2 C_D A + m_p \frac{g(\rho_p - \rho)}{\rho_p} + \frac{1}{2} m_p \frac{\rho}{\rho_p} \frac{d}{dt} (u - u_p) \quad [\text{Eq. 3.18}]$$

[Replacing v_p by $\frac{m_p}{\rho_p}$]

$$m_p \frac{du_p}{dt} = \frac{1}{2} \rho |u_{rel}|^2 C_D A + m_p \frac{g(\rho_p - \rho)}{\rho_p} + m_p \frac{1}{2} \frac{\rho}{\rho_p} \frac{d}{dt} (u - u_p) \quad [\text{Eq. 3.19}]$$

$$m_p \frac{du_p}{dt} = \frac{1}{2} \rho |u_{rel}| |u_{rel}| C_D \frac{\pi d_p^2}{4} + m_p \frac{g(\rho_p - \rho)}{\rho_p} + m_p \frac{1}{2} \frac{\rho}{\rho_p} \frac{d}{dt} (u - u_p) \quad [\text{Eq. 3.20}]$$

$$m_p \frac{du_p}{dt} = \frac{1}{8} \rho |u_{rel}| |u_{rel}| C_D \pi d_p d_p + m_p \frac{g(\rho_p - \rho)}{\rho_p} + m_p \frac{1}{2} \frac{\rho}{\rho_p} \frac{d}{dt} (u - u_p)$$

[Eq. 3.21]

$$m_p \frac{du_p}{dt} = \frac{1}{8} \rho |u_{rel}| \cdot d_p \cdot |u_{rel}| C_D \pi d_p \frac{\mu}{\mu} + m_p \frac{g(\rho_p - \rho)}{\rho_p} + m_p \frac{1}{2} \frac{\rho}{\rho_p} \frac{d}{dt} (u - u_p)$$

[Eq. 3.22]

$$m_p \frac{du_p}{dt} = \frac{1}{8} \left(\frac{\rho |u_{rel}| d_p}{\mu} \right) \cdot |u_{rel}| C_D \pi d_p \mu + m_p \frac{g(\rho_p - \rho)}{\rho_p} + m_p \frac{1}{2} \frac{\rho}{\rho_p} \frac{d}{dt} (u - u_p)$$

[Eq. 3.23]

$$m_p \frac{du_p}{dt} = \frac{1}{8} Re |u_{rel}| C_D \pi d_p \mu \frac{\frac{d_p^2}{6}}{\frac{d_p^2}{6}} + m_p \frac{g(\rho_p - \rho)}{\rho_p} + m_p \frac{1}{2} \frac{\rho}{\rho_p} \frac{d}{dt} (u - u_p) \quad [\text{Eq. 3.24}]$$

[Replacing $\frac{\rho |u_{rel}| d_p}{\mu}$ by Re]

$$m_p \frac{du_p}{dt} = \frac{6}{8 d_p^2} Re |u_{rel}| C_D \mu \frac{\pi d_p^3 \rho_p}{6 \rho_p} + m_p \frac{g(\rho_p - \rho)}{\rho_p} + m_p \frac{1}{2} \frac{\rho}{\rho_p} \frac{d}{dt} (u - u_p)$$

[Eq. 3.25]

$$m_p \frac{du_p}{dt} = \frac{6}{8 d_p^2 \rho_p} Re |u_{rel}| C_D \mu \frac{\pi d_p^3 \rho_p}{6 \rho_p} \frac{3}{3} + m_p \frac{g(\rho_p - \rho)}{\rho_p} + m_p \frac{1}{2} \frac{\rho}{\rho_p} \frac{d}{dt} (u - u_p)$$

[Eq. 3.26]

$$m_p \frac{du_p}{dt} = \frac{18\mu C_D}{24d_p^2 \rho_p} Re |u_{rel}| m_p + m_p \frac{g(\rho_p - \rho)}{\rho_p} + m_p \frac{1}{2} \frac{\rho}{\rho_p} \frac{d}{dt} (u - u_p) \quad [\text{Eq. 3.27}]$$

$$[\text{replacing } g, \frac{\pi d_p^3 \rho_p}{6} = m_p]$$

$$\frac{du_p}{dt} = \frac{18 \mu C_D Re}{24 \rho_p d_p^2} u_{rel} + \frac{g(\rho_p - \rho)}{\rho_p} + \frac{1}{2} \frac{\rho}{\rho_p} \frac{d}{dt} (u - u_p) \quad [\text{Eq. 3.28}]$$

The volume of fluid method⁸⁵ was first proposed to track free boundary (surface). In this method a function G , is defined in such a way that its value is unity (1) at any point occupied by fluid and zero (0) otherwise. The average value of G in a cell then represents the fractional volume of the cell occupied by the fluid. So unit value of G will correspond to a cell full of fluid, while a zero value would indicate that a cell contained no fluid. Cells with G values between zero and one must then contain a free surface and is a boundary cell. It also gives the information about the location of the fluid in the boundary cell. The normal direction of the boundary lies in the direction in which the value of G changes most rapidly. The derivatives of this G can be used to determine the boundary normal. Once both the normal direction and the value of G in a boundary cell are known, a line cutting the cell can then be constructed that can approximate the interface. This method is also can be used to track interface between two or more phases. The VOF formulation relies on the fact that two or more fluids (or phases) are not interpenetrating. For each additional phase added in the system a

variable, the volume fraction of the phase, is introduced in the computational cell. In each control volume, the volume fractions of all phases sum to unity. The fields for all variables and properties are represented as volume-averaged values. Thus the variables and properties in any given cell are either purely representative of one of the phases, or representative of a mixture of the phases, depending upon the volume fraction values.

For tracking interfaces between phases, continuity equations (Equation 3.29) for the volume fraction of one or more phases are solved⁸³.

$$\frac{1}{\rho_q} \left[\frac{\partial}{\partial t} (\alpha_q \rho_q) + \nabla \cdot (\alpha_q \rho_q \vec{v}_q) \right] = S_{\alpha_q} \quad [\text{Eq. 3.29}]$$

The volume fraction for the primary phase is not solved. Rather it is computed based on the constraint:

$$\sum_{q=1}^n \alpha_q = 1 \quad [\text{Eq. 3.30}]$$

In the present doctoral thesis, the VOF method was used to track the upper slag phase during inert gas injections. For the VOF calculations, the transient solver was used with the explicit scheme for time discretization. The face fluxes were interpolated using the Geo-Reconstruct interface reconstruction scheme⁸³. The geometric reconstruction scheme represents the interface between the fluids

using a piece wise linear approach. This scheme is very useful for unstructured meshes. It assumes that the interface between two fluids has a linear slope within each cell, and uses this linear shape for calculation of the advection of fluid through the cell faces. The first step in this reconstruction scheme is to calculate the position of the linear interface relative to the center of each partially-filled cell, based on information about the volume fraction and its derivatives in the cell. The second step is to calculate the advecting amount of fluid through each face using the computed linear interface representation and information about the normal and tangential velocity distribution on the face. The third step is to calculate the volume fraction in each cell using the balance of fluxes calculated during the previous step⁸³. Low values of under relaxation were used for all the equations to achieve convergence.

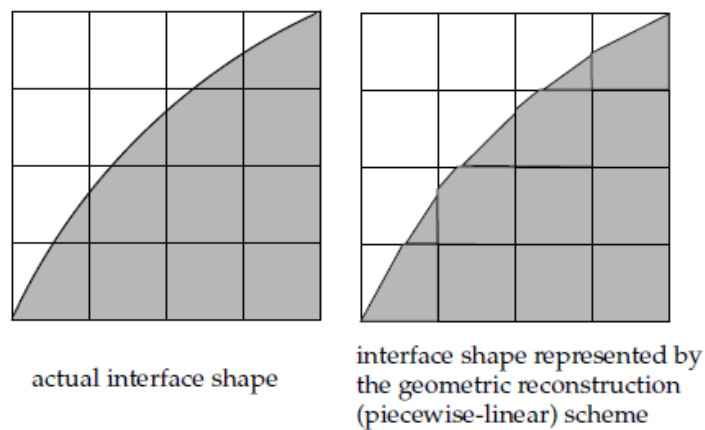


Figure – 3.21 Schematic representation of the Geo-Reconstruct scheme

4.0 Effect of Different Flow Modifier Arrangements on Liquid Metal Quality

4.1 Introduction

The overall performance of a tundish is dominated by melt flow patterns generated within it. As the laws of fluid mechanics govern the flow of liquid steel, they affect gas and slag entrainment within the steel, and affect the floatation and separation of non metallic inclusions⁷. Many research articles have been published to date on the use of flow control devices, of turbulence inhibitors and suppressors and of flow modifiers. A wide range of tundish geometries along with numerous designs of flow modifiers have been applied, in order to primarily investigate the floatation of inclusions from tundishes as a function of operating variables. Flow conditions suitable to facilitate inclusion separation by floatation can be created by insertion of flow modifiers. However, the optimal design of such flow modifiers and their location within the tundish is highly dependent on the tundish geometry, tundish operating conditions, and the size range of inclusions present within the molten steel. Chattopadhyay et al.⁸⁶ in 2010 concluded that much work had been done in the past ten years on the development of physical and mathematical models for studying flow fields in tundishes, to study the effect of FCD's, to evaluate mean residence times, RTD's and inclusion removal. Flow control devices are

generally dams, weirs, baffles, impact pads, turbulence inhibitors, etc., and any combination of these. For physical modelling of a tundish with FCD's, usually a plexi-glass aqueous model (full scale or reduced scale) of the tundish is built, and flow modifiers are inserted in the tundish according to choice. The FCD's are usually made of wood or acrylic material. Similarity criteria (geometric, dynamic, chemical and thermal) are respected during construction and operation of the model. These FCD's act as resistive walls to the fluid flow, thereby changing the fluid flow patterns as compared to a bare tundish.

The major methods to visualize these flow fields in physical modelling are Laser Doppler Anemometry (LDA), Particle Image Velocimetry (PIV), tracer dispersion studies, and video photography. In the first two cases, the flow field can be visualized on any particular plane with the aid of a laser and in the last case i.e. tracer dispersion studies, a coloured liquid is injected into the tundish and its overall mixing behaviour is photographed with a high speed camera . Odenthal et al.⁶⁹ carried out 3D LDA and 2D PIV investigations for different “ turbostops” in a reduced scale water model of a 16 ton single strand tundish. Quantitative laser optical studies (PIV and LDA) indicated that the fundamental flow related effects are identical for Reynolds and Froude similarity. Detailed measurements of the mean velocity and turbulence intensity in the

tundish, with and without turbo-stops, were done. It was found that with suitable turbo-stop geometry, the recirculation area in the tundish centre and the short circuiting flows near the wall, can be avoided and thus a more favourable residence time distribution can be obtained. It was shown that the turbo-stop produces higher turbulence in the inlet region of the tundish which is spatially more limited, however, in relation to the flow without a turbo-stop. Thereby a more homogeneous flow was created at the discharge of the tundish, with better conditions for particle separation. The experimental data gave a good understanding of the flow phenomena in a tundish using a turbostop, and were used to validate the numerical results obtained from FLUENT 5.5. R.D. Morales et al.⁷⁰ performed physical modelling of steel flow in a three strand billet tundish using a turbulence inhibitor. They emphasised the design of the turbulence inhibitor (TI) and clearly mentioned that the role of a TI is not only to reduce turbulence in the pouring zone, but also it has to act like a redirecting flow device, so as to distribute molten steel uniformly to each strand. They concluded that a tailor made turbulence inhibitor is useful to accomplish control of fluid turbulence and to redirect melt evenly to all strands. In steelmaking practise, the turbulence inhibitor also helped to decrease nitrogen pick up during ladle changes and to float out inclusions towards the covering slag. As a consequence, rod operations to take of alumina deposits from nozzle walls are considerably decreased using a

turbulence inhibitor. Yanping Bao et al.⁸⁷ studied different flow patterns in a tundish, caused by different arrangements of weirs and dams on a 1/3 scale tundish. He showed that the RTD curves varied with different tundish configurations as per the Table below. The combination of weir and dam was beneficial for the flow pattern in the tundish, in that the weir could prevent the upper recirculating flow and the dam could cut off the bottom flow and turn it upwards. This was advantageous for separating the non metallic inclusions from the melt. They also gave an optimum arrangement of weir and dam, and also mentioned that it was important to exceed the critical depth of bath during a ladle change, not only for inclusion floatation but also for avoiding early slag entrainment. J.P. Ramos et al.⁸⁸ designed and constructed a typical water model of a 60t slab tundish to determine flow patterns when using turbulence inhibitors and dams. Their tundish geometry and arrangement of flow control devices are shown below. The use of turbulence inhibitors produced better melt flow control by reducing the turbulence at the entry pour box and the mixed volume component. The arrangement using a turbulence inhibitor and low dams showed the highest fraction of plug flow, lowest dead volume and the greatest axial dispersion. They also concluded that as the flow rate decreases, the volume fraction of plug flow increases. Thus, at the start of a grade change, when the tundish depth is reduced and the flow rate is increased to reach the working level, the fraction of mixed volume will be higher.

The minimum residence time of the tracer compatible with the steel is considerably increased by using the combination of a turbulence inhibitor and a pair of dams. Redirecting the flow upwards helps to remove inclusions.

The effect of turbulence inhibitors on slag emulsification in the continuous casting tundish was reported by J. A. Morales Pereira et al.⁸⁹. They concluded that there is slag emulsification occurring during a ladle change, because of a high throughput rate of steel during the tundish re-filling. Also slag accumulation on the side walls due to the turbulent energy of the incoming jet facilitated slag emulsification. So they recommended maintaining only a small thickness of slag before the ladle change. When a turbulence inhibitor was used with an overhang flange around its top exit area, it helped to concentrate the emulsification between the shroud and the back wall far from the casting region. Also the open eye was smaller. Thus it helped to reduce re-oxidation and slag entrainment. Sinha and Vassilicos⁹⁰ carried out physical modelling to study the effect of a turbulence suppressor device on flow and mixing in a dual strand tundish. They used a "dogbowl" device in place of dams, weirs or baffles. Experiments were conducted to evaluate steel splashing during fill-up, reduction of intermixed liquid during grade changes and effectiveness of the 'dogbowl' device in maintaining symmetry of flow in each strand of the tundish. The 'dogbowl' device

did a good job in suppressing steel splashing during initial tundish fill-up compared to other flow control devices. For the standard “pour-on-pour” practice, the 'dogbowl' generated about 8% less intermix. The 'dogbowl' device was not very useful for unequal strand casting rates. For all cases, the 'dogbowl' device showed a higher than expected sensitivity to positional misalignment, leading to non-repeatable flow patterns in the tundish. Piccone, Sinha and Madden⁹¹ performed some intermix trials using different tundish configurations and concluded that intermix could be improved by using turbulence suppression devices in the tundish. K.J Craig et al.¹¹ presented the results of a design optimization study, performed on the steady-casting operation of the Columbus Stainless single strand stainless steel caster tundish. Three case studies were performed of which the first two were water models and the last one was with liquid steel to investigate the effect of temperature and the buoyancy on the resulting flow patterns and optimum design. Two separate tundish configurations were considered. The first one had one dam and one weir while the second configuration was comprised of a baffle with angled holes and an impact pad. Significant improvements of up to 34% in minimum residence time were reported for the second configuration. S.L. Ramirez et al.⁹² performed a modelling study of the influence of turbulence inhibitors on the molten steel flow, tracer dispersion and inclusion trajectories in tundishes. Physical and mathematical modelling were used in a

complementary fashion. They concluded that the use of a turbulence inhibitor and low dams provided the best flow characteristics i.e. high plug flow with low dead volume. The combination of a turbulence inhibitor and dam reduced the turbulence and the fluid velocity in the jet entry zone and thus reduced lining erosion near the tundish walls. This arrangement also improved flow patterns, promoting more symmetrical flow fields along the length of the tundish. The minimum residence time also considerably increased in a large tundish using this arrangement. They also mentioned that a turbulence inhibitor improved steel cleanliness by two mechanisms. For small particles, it traps them inside its walls and for large particles; it drives them upwards to the top surface where the molten slag layer absorbs them. A.V. Zamora et al.¹⁰ physically and mathematically simulated fluid flow; heat and mass transfer of liquid steel in a trough type tundish. Flow fields were determined by PIV. Under isothermal conditions, the fluid flow approached the “ideal” plug flow condition, and mass transfer phenomena yielded concentration distributions that followed the same pattern. Under non-isothermal conditions, the fluid flow deviated from plug flow and fluid velocities were larger close to the bath surface, owing to the presence of buoyancy forces. Larger fluid velocities near the bath surface increased a bypass flow carrying tracer from the inlet directly to the outlet along the bath surface. Consequently, the minimum residence time of the tracer inside the vessel decreased.

This was detrimental for small inclusions, but for large inclusions, thermal buoyancy forces enhanced flotation. However flow control devices like turbulence inhibitors play the major role in eliminating inclusions. The effects of centred and off-centred positions of the ladle shroud in a two strand slab caster on steel flow was studied using water modelling with injection of a tracer, PIV and video recording techniques by A. A. Corona et al ⁹³. When the ladle shroud was in a centred position, the arrangement with an inhibitor and a dam (proposed system) yielded flows with higher volumes of fluid under plug flow regime than the arrangement using only a pair of baffles (current system). With the ladle shroud in an off-centred position, the current system yielded better flow characteristics than the tundish with a centred ladle shroud. However, the proposed system yields better flow characteristics than the current system. At low flow rates, the proposed arrangement offered considerably better fluid characteristics than the current one. The proposed arrangement under any operating conditions showed a higher stability at the oil layer (slag) interface due to reduction of the shearing stresses at the water-oil interface. Thermal stratification of steel flow in a tundish with off-centred ladle shrouds using two flow control arrangements was studied by A. A. Corona et al.⁹⁴ using a non-isothermal water model. One of the flow control arrangements consisted of a pair of baffles and the other one consisted of a turbulence inhibitor and a pair of dams (TI-D). Positions of the ladle shroud were centred,

off-centred one ladle shroud diameter (1D) and off-centred two ladle shroud diameters (2D). Thermal experiments involved feeding higher temperature water and monitoring the effects at various locations within the liquid. For any position of the ladle shroud and casting rate, the TI-D arrangement yielded smaller thermal gradients of liquid inside the vessel and higher plug flow volumes. Particle image velocimetry (PIV) measurements demonstrated a close relationship between the velocity fields and the buoyancy number, relating thermal buoyancy forces to inertial forces for a given casting rate. Buoyancy forces were estimated through the thermal responses at the outlet and it was found that the TI-D arrangement prolonged the lifetime of the buoyancy effects to a greater extent than the pair of baffles arrangement, owing to the effects of the turbulence inhibitor. A one-strand slab tundish was water modelled by A. R. Banderas et al.⁹⁵ to study the influence of gas bubbling curtains on the fluid flow patterns produced by turbulence inhibitors. The study included the bare tundish, the employment of half dams, and the combination of half dams with gas bubbling without a Turbulence Inhibitor (TI). A combination of a TI with gas bubbling derived in complex recirculating flows of liquid steel. Higher flow rates of gas led to a decrease of the plug flow fraction of the fluid inside the vessel. The best results, for the purpose of flotation of inclusions, were obtained for a tundish with the TI, followed by gas bubbling, with 596 ml/min and with the half dams and without the TI. The worst case, for the same objective, was

the bare tundish. Thus, gas bubbling itself yielded very good results for floating inclusions, but is not superior to a well-designed TI for the same purpose. A tundish without gas bubbling and without a TI, but equipped with half dams provided acceptably high performances for inclusions flotation. They also suggested that if optimum flotation conditions are not required, then the simple arrangement of half dams is acceptable. P. Kovac et al.⁹⁶ also reported on improvement of steel cleanliness through tundish configuration optimization. They employed the commercially known TURBOSTOP together with a pair of baffles and a flat impact pad to improve steel cleanliness and fluid flow phenomenon in a two-strand tundish. Liu Jin Gang et al.⁹⁷ performed water model experiments in a bare tundish, a tundish equipped with a turbulence inhibitor and a rectangular tundish equipped with weirs (dams) and a turbulence inhibitor. After comparison of the RTD curves, inclusion separation and the result of the streamline experiment, it was concluded that the tundish equipped with weirs (dams) and a turbulence inhibitor had a great effect on the flow field and the inclusion separation when compared with the sole use, or no use, of the turbulence inhibitor or weirs (dams).

At the McGill Metals Processing Centre, two researchers Dr H. B. Kim⁹⁸ and Dr S. Ray⁹⁹, worked extensively on a project given by RTIT/QIT and did a lot of modelling to design a suitable flow control

device. After all their hard work, they came up with a standard QIT impact pad which was again improved as the standard impact pad + 2 inches. This pad proved to be highly efficient and was finally adopted by QIT for both Al- killed and Si –killed grades, after comparing with many other FCDs.

In the present project, RTFT/QIT wanted to know if along with the standard impact pad, other dams or weirs could be used in combination, so as to yield better results. Also, they wanted to know if the size of the pad matters. Dams of different heights were placed between the inner and outer strands along with the standard impact pad. Eighteen different configurations of the tundish were considered and 3D mathematical simulations were done to visualize the vector fields, turbulent kinetic energy (TKE) contours and also to calculate the residual ratio of inclusions.

4.2 Mathematical modelling procedures

As the performance of eighteen different tundish designs needed to be evaluated, it was obvious to perform mathematical simulations for all of them. Finally a couple of these models were validated with water model experiments. The operating level of the tundish was 0.5m from the base of the tundish. The standard k- ϵ model of Launder and Spalding⁷⁹ was used, coupled with the discrete phase model. The steady state velocity field was first obtained and then the

RRI was calculated. For evaluating the residual ratio of inclusions (RRI), around one million (10^6) inclusions of linear size distribution between 50 - 200 μm were injected through the shroud and the number of inclusions coming out of each SEN was calculated, under steady state conditions. The size distribution of inclusions is shown in Figure 4.1 below.

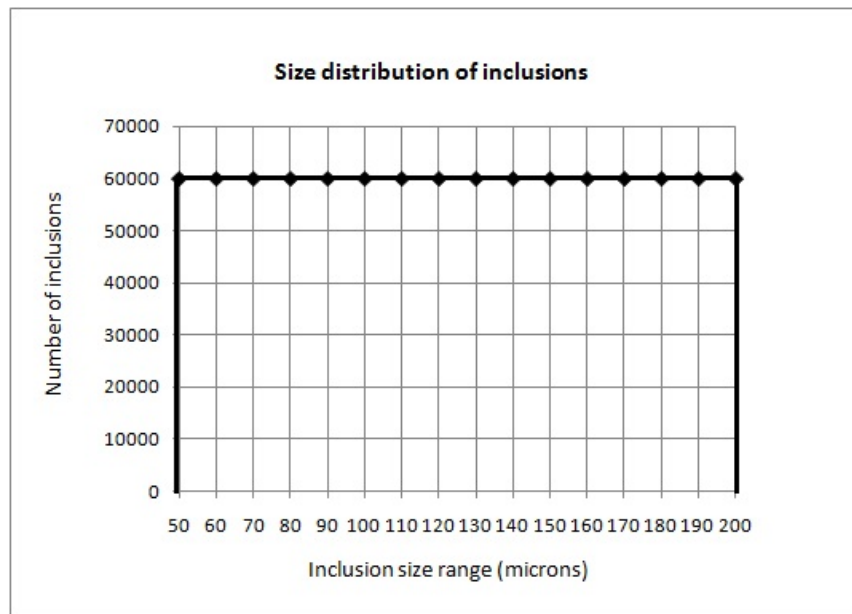


Figure - 4.1 Size distribution of inclusions

The RRI is calculated using the following relation.

RRI (%)

$$= \frac{\text{Number of inclusions of a particular size range coming out of each SEN}}{\text{Number of inclusions of a particular size range injected within the tundish}} \times 100$$

4.3 Eighteen different arrangements of flow modifiers (in 3D)

Eighteen arrangements of flow furniture was considered and named as d1 to d18 to represent design 1 to design 18. Design 1 is the bare tundish whereas design 2 is the tundish with the standard impact pad. These are shown in Figure 4.2. The length of the standard impact pad is shown in a top view in Figure 4.3. In all subsequent designs from d3 to d14, the standard impact pad is kept intact, plus a dam is placed between the inner and outer SEN's and the height and position of the dam is varied. In designs 15, 16 17, and 18 the size and height of the impact pad is changed, and no dam is used. Detailed dimensions and locations of the dams used are given in Table 4.1 below.

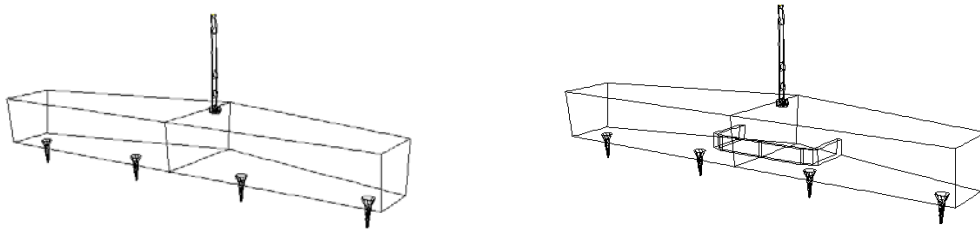


Figure- 4.2 Bare tundish and the tundish fitted with SIP

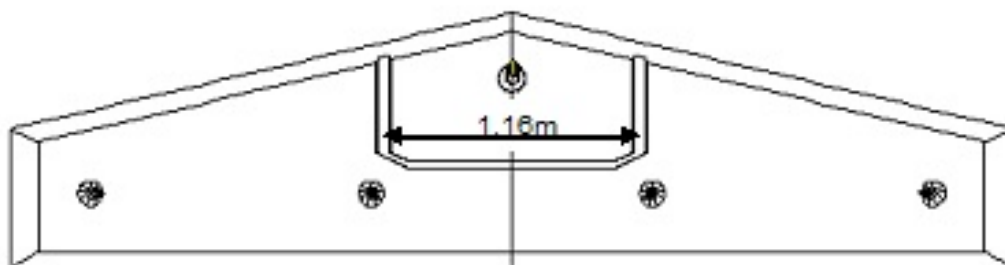


Figure- 4.3 Top view of the tundish d2 showing length of the SIP

Detailed dimensions of the eighteen designs		
Design number	Distance from the impact pad (m)	Height of the dam (m)
d3	0.69	0.254
d4	0.37	0.254
d5	1	0.254
d6	1.26	0.254
d7	0.69	0.152
d8	0.37	0.152
d9	1	0.152
d10	1.26	0.152
d11	0.69	0.08
d12	0.37	0.08
d13	1	0.08
d14	1.26	0.08
d1 (bare tundish)	Refer Figure-3.2	

d2 (tundish with Standard impact pad)	Length of the pad 1.16m, Height of the pad 0.152m
d15	Length of the pad 1.16m, Height of the pad 0.3m
d16	Length of the pad 0.8m, Height of the pad 0.152m
d17	Length of the pad 0.6m, Height of the pad 0.152m
d18	Length of the pad 1.392m, Height of the pad 0.152m

Table- 4.1 Detailed dimensions and locations of flow furniture

4.4 Results and Discussion

Flow control devices significantly change the fluid flow patterns within a tundish, which again affects inclusion motion within the tundish. So for all the eighteen configurations of the tundish, the flow field and inclusion trajectories were reported. The velocity field was shown on a longitudinal plane (0.51m from the apex of the tundish) and is shown in Figure-4.4. Since the flow is symmetrical, only one half of the tundish is considered.

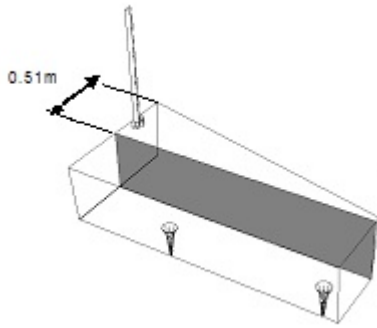


Figure-4.4 Plane of interest

The inclusion trajectories in the bare tundish are shown in Figure-4.5 below. It is very clear that the inclusions are clustered near the inner strands and hence much more inclusions are passing through the inner SENs as compared to the outer SENs. This fact is also evident in the RRI calculations (Figure-4.6). The RRI values for the outer SEN are much less than those for the inner SENs. Inclusions of size $140\mu\text{m}$ and above float up and do not pass through the SENs.

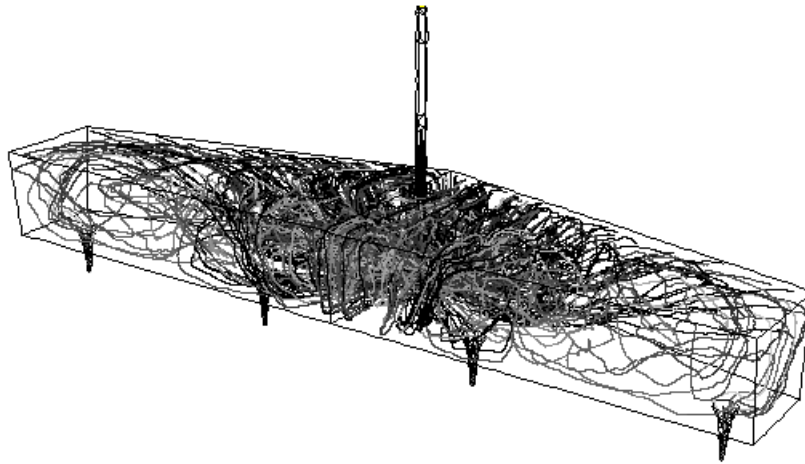


Figure-4.5 Inclusion (50-200 μ m) trajectories in the bare tundish

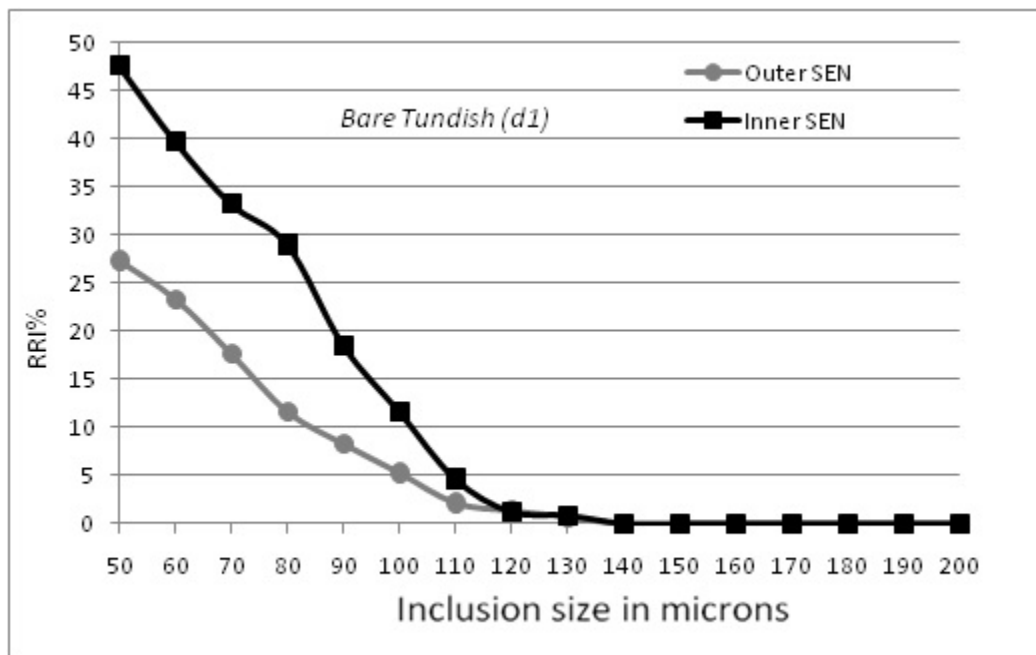


Figure-4.6 RRI calculations in the bare tundish

In order to inhibit the TKE in the entry region and to improve the performance of the tundish in terms of inclusion removal, the standard impact pad was inserted. The flow field in the tundish with the standard impact pad is shown in Figure-4.7. The flow field within the impact pad region changes. A huge recirculation is present in the pad region. This recirculation carries all the inclusion upwards, which in turn gets attached to the slag phase. Thus, inclusion float out is highly enhanced by the use of this pad. This is also evident in Figure 4.8, which shows the RRI calculations. The RRI values for a particular size range of inclusions are lower in the tundish with the SIP than the corresponding values in the bare tundish. Inclusion trajectories are shown in Figure-4.9.

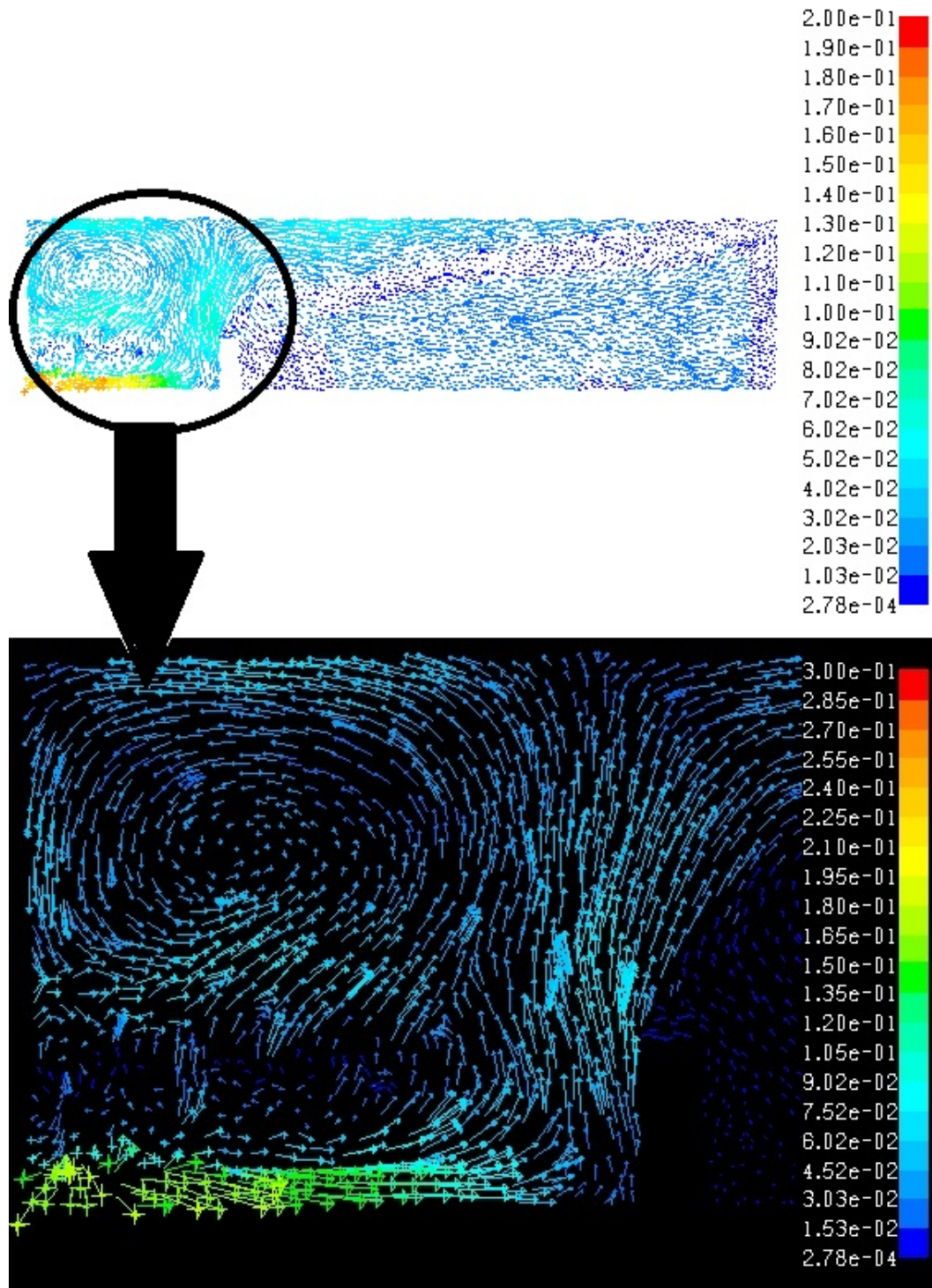


Figure-4.7 Velocity field ($m s^{-1}$) in the tundish with impact pad

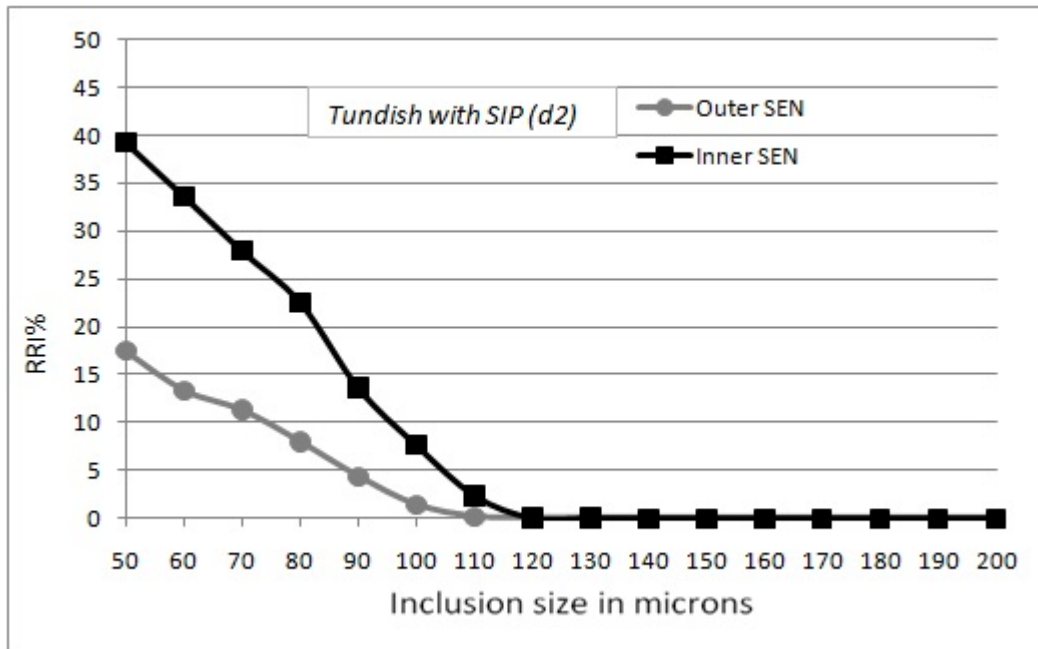


Figure-4.8 RRI calculations in the tundish fitted with the SIP

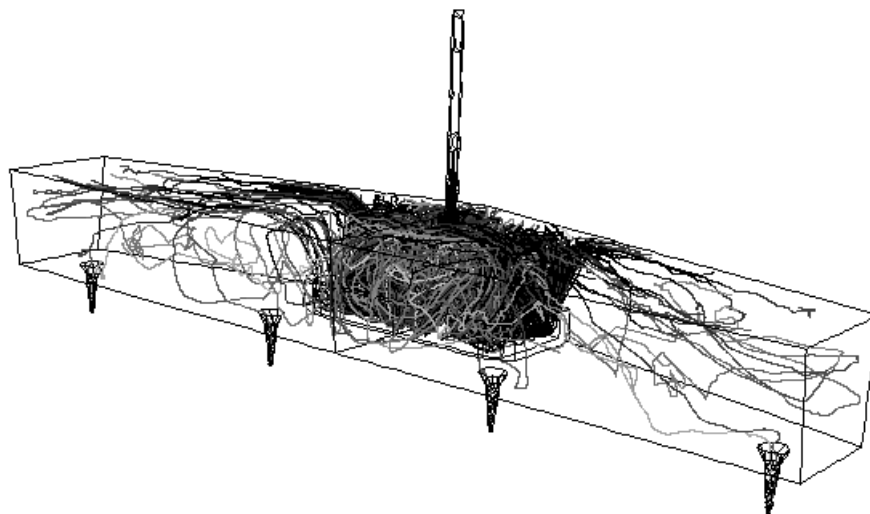


Figure-4.9 Inclusion (50-200 μ m) trajectories in the tundish with SIP

Here, it is clearly observed that the inclusions are confined within the impact pad region and amount of inclusions passing through the

SEs is much less. So, to sum up, the tundish with the standard impact pad performs much better in terms of inclusion removal than the bare tundish.

4.4.1 Effect of the use of weirs or dams along with the standard impact pad

Now, the fact has been established, that the tundish with the standard impact pad is better than the bare tundish in terms of inclusion removal efficiency. However, using a dam (weir) in conjunction with the standard impact pad may yield better results. The detailed dimensions of the flow furniture used are already given in Table-4.1. In this section, a schematic diagram of each tundish configuration is given, along with the flow field on the plane of interest (Figure-4.4), and inclusion trajectories. RRI calculations for the designs are given in groups of four. The groups are based on the height of the dam, and hence three groups (height of the dam= 0.254m, 0.152m, and 0.08m) are presented.

(a) Design 3

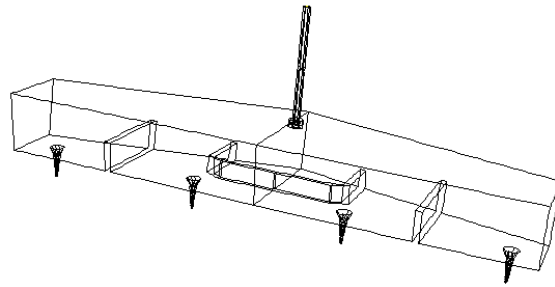


Figure-4.10 Tundish of design 3

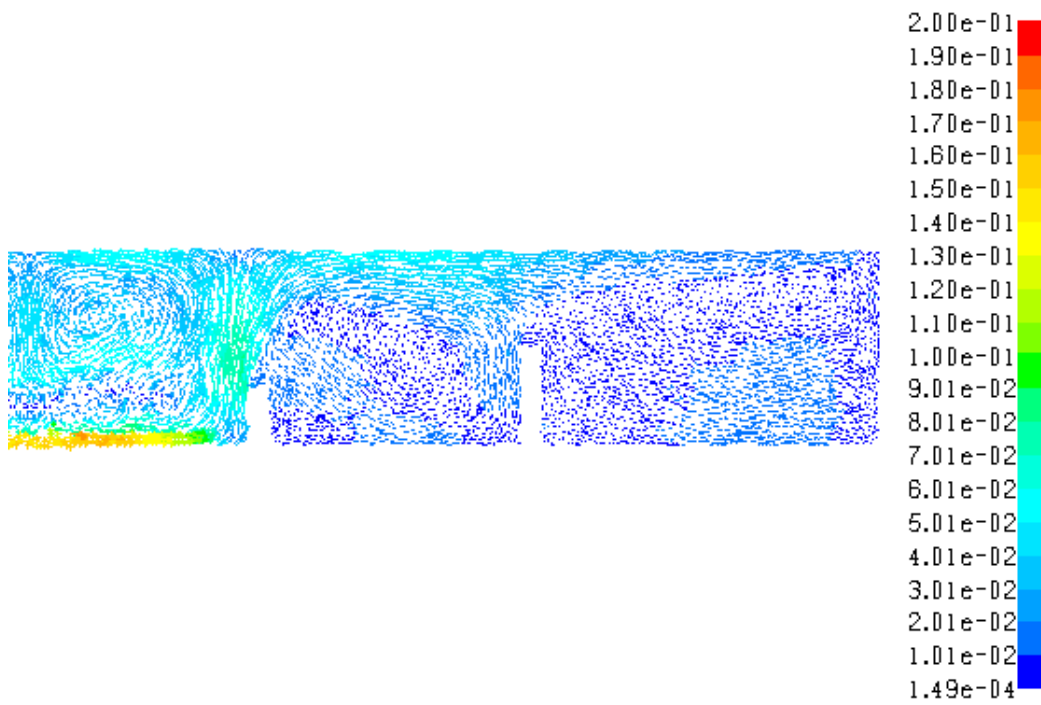


Figure-4.11 Velocity field ($m s^{-1}$) in the tundish of design 3.

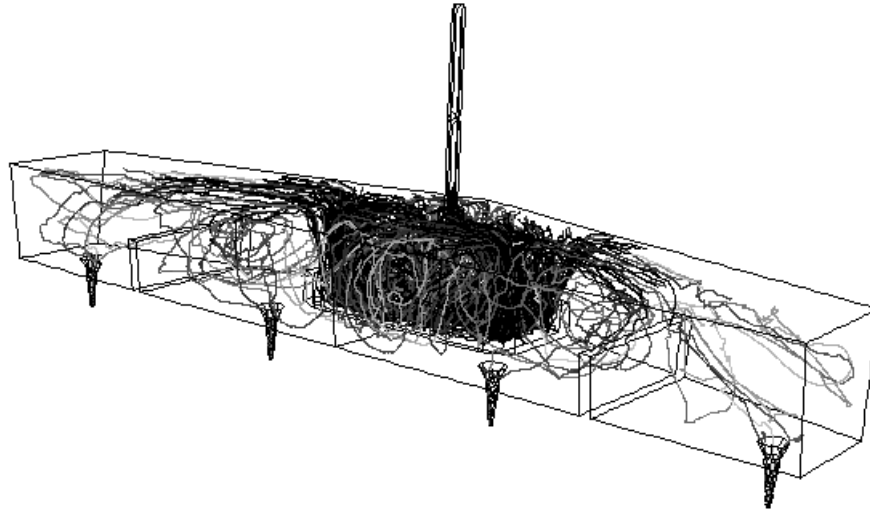


Figure-4.12 Inclusion (50-200 μ m) trajectories in the tundish of design 3.

Due to the presence of a dam in the middle of the inner and outer SEN, the flow pattern changed significantly. The flow field within the pad region remained unchanged, but another recirculation of opposite sense was formed in the region between the pad and the dam. This recirculation basically constrained the inclusions in the inner strand region. Also, if the inclusion trajectories are examined, it is observed that the presence of the dam prevents the inclusions from coming near the outer SENs.

(b) Design 4

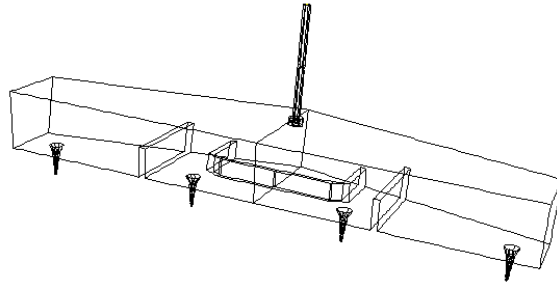


Figure-4.13 Tundish of design 4

In design 4, the dam was brought closer to the impact pad. As a result of this, the recirculation between the pad and dam got smaller. If the inclusion trajectories are examined, it is similar to that in design 3. Inclusions are constrained in the inner SEN region. Some inclusions could get reflected as they hit the dam, and were then entrained into the inner SEN.

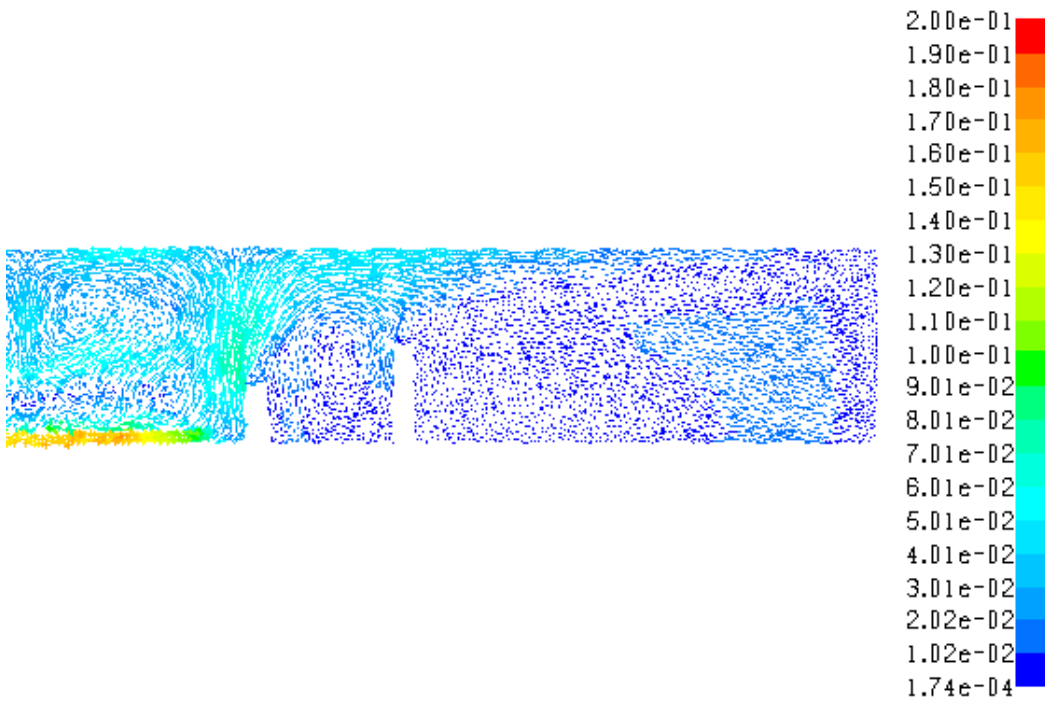


Figure-4.14 Velocity field ($m s^{-1}$) in the tundish of design 4

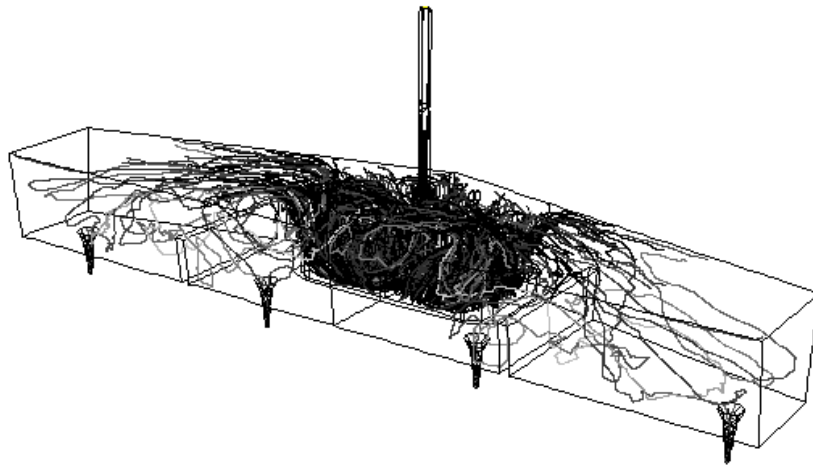


Figure-4.15 Inclusion ($50-200\mu m$) trajectories in the tundish of design 4.

(c) Design 5

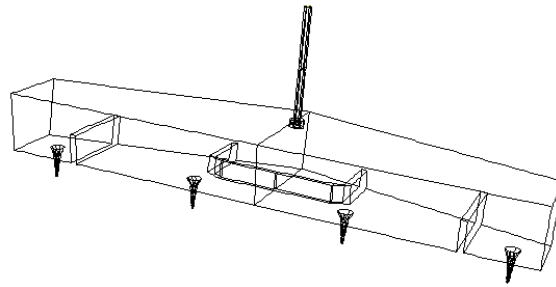


Figure-4.16 Tundish of design 5

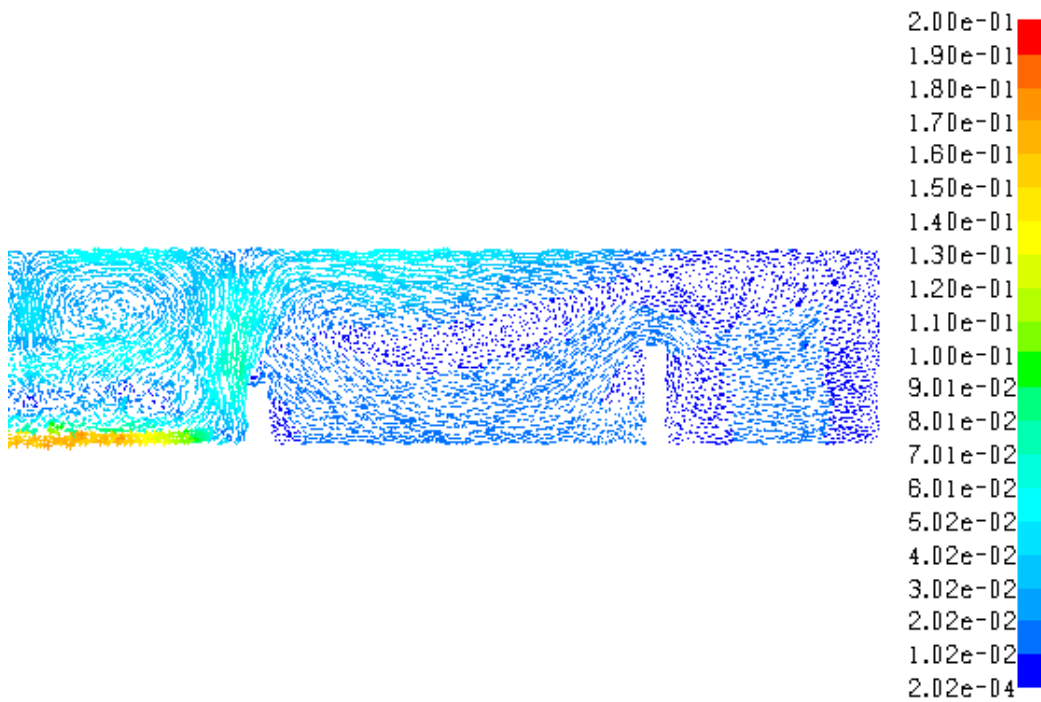


Figure-4.17 Velocity field ($m s^{-1}$) in the tundish of design 5.

In design 5, the dams were moved further away from the pad and were closer to the outer SEN. Here, the recirculation between the pad and the dam was not completely formed because of the relatively larger distance between them. So, the inclusions were no longer clustered near the inner SENs, but were allowed to flow towards the ends of the tundish. Since, the dam was quite high (0.254m), the flow guided the inclusions towards the upper slag phase and they were trapped there. This phenomenon is also evident in Figure 4.18 below.

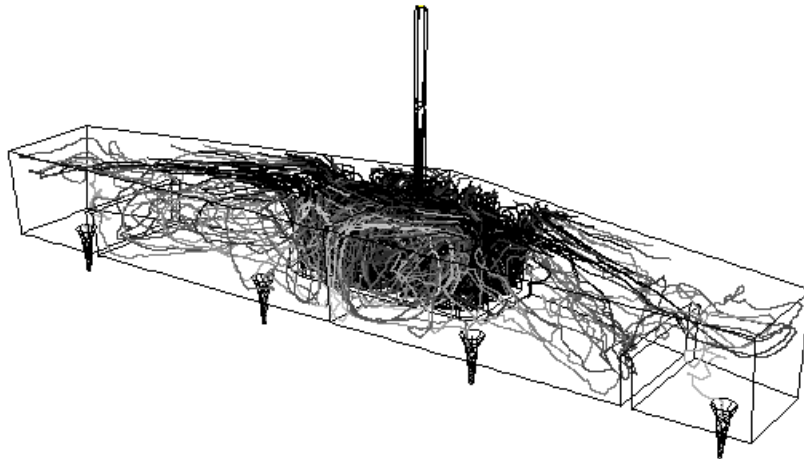


Figure-4.18 Inclusion (50-200 μ m) trajectories in the tundish of design 5.

(d) Design 6

In design 6, the dams were now moved very close to the outer SENs. Since the distance between the pad and the dam was very large now, the recirculation between the pad and dam was not formed at all. So more inclusions could move towards the outer SENs. Also, since the dam was just adjacent to the SEN, more inclusions could drop in the outer SENs as compared to the previous design.

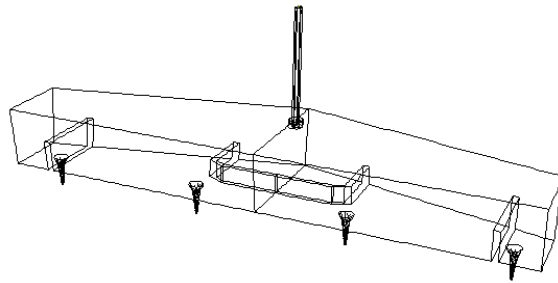


Figure-4.19 Tundish of design 6

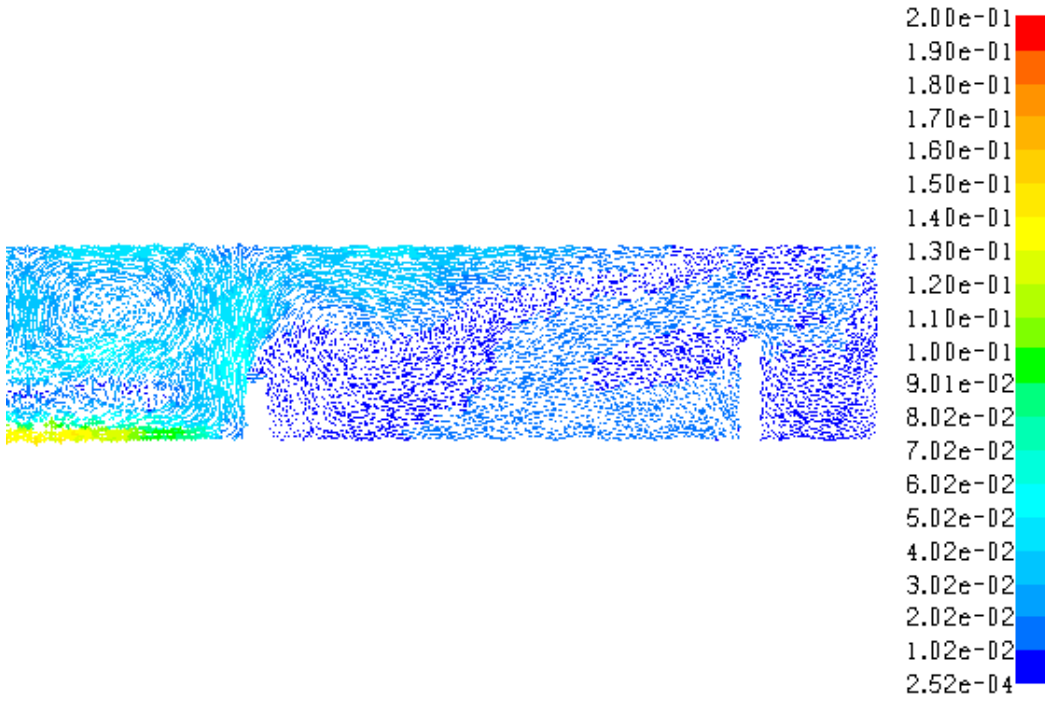


Figure-4.20 Velocity field ($m s^{-1}$) in the tundish of design 6.

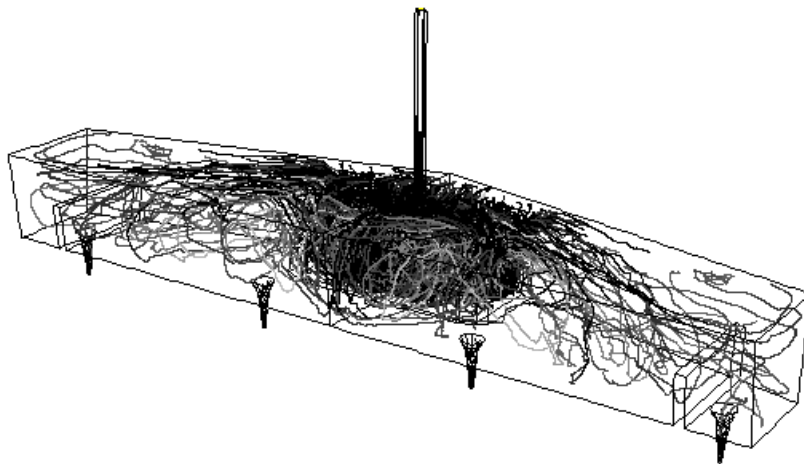


Figure-4.21 Inclusion ($50-200\mu m$) trajectories in the tundish of design 6.

Figures 4.22 (a) and (b) shows the RRI% for the tundish fitted with an impact pad and a 0.254m high dam between the inner and outer SEN.

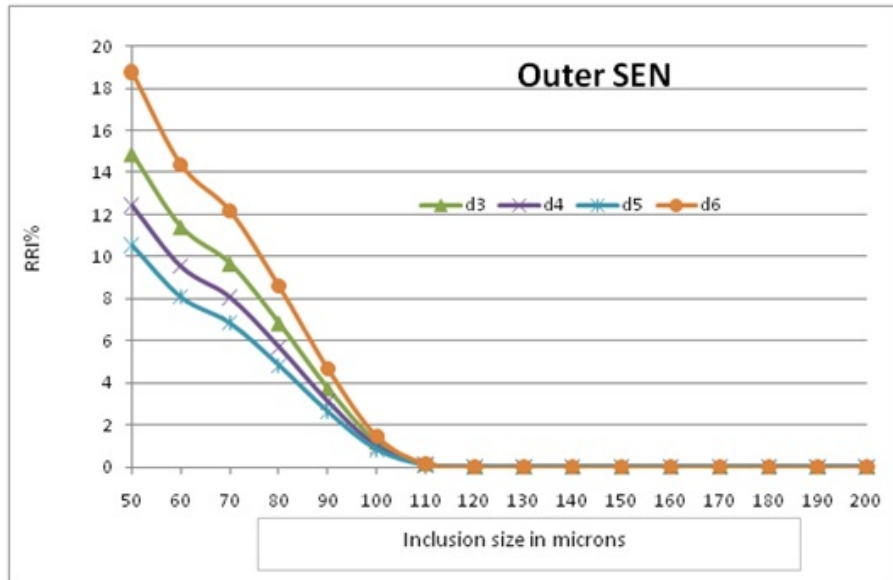


Figure- 4.22(a) Showing RRI% for d3,d4,d5 and d6 in the outer SEN

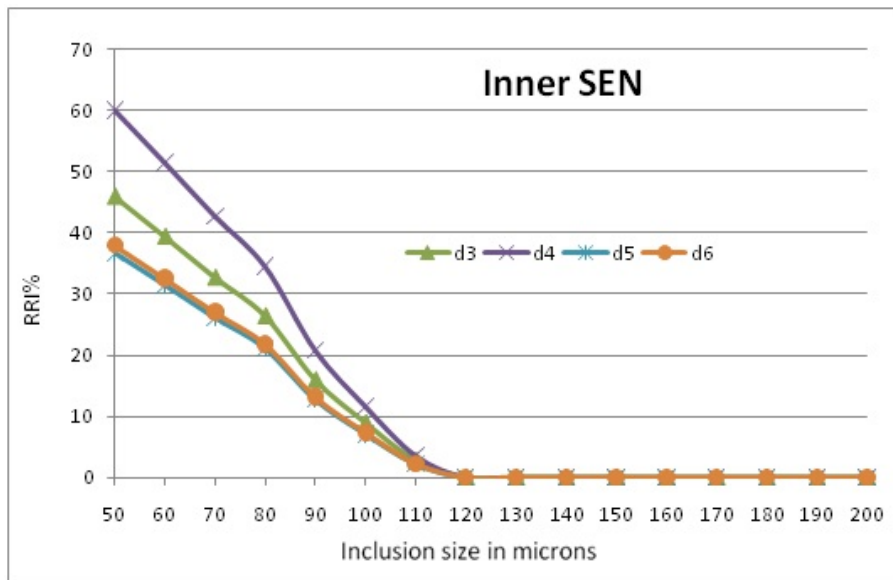


Figure- 4.22(b) Showing RRI% for d3,d4,d5 and d6 in the inner SEN

From the above figures it is clear that bringing the dam closer to the inner SEN (d4) deteriorated the steel quality in the inner strands. Placing the dams away from the inner SEN was good, and the further away the dams were placed, the better was the liquid metal quality in the inner strand. However, placing the dam very close to the outer SEN (d6) was not good for the steel coming out of the outer strands as indicated from figure 4.22(a). Overall, when a 0.254m high dam was used, the best results were obtained for d5, i.e. when the dam was placed at a distance of 1m from the impact pad.

(e) Design 7

The height of the dam was now reduced and was same as the height of the impact pad. The dam was positioned exactly in the middle of the inner and outer SENs. Figure 4.24 shows the velocity field within the tundish on the plane of interest. As the height of the dam here was almost half that in design 3, the recirculation between the pad and dam was not completely formed. So the inclusions were not constrained in the inner strand region as it was in design 3, but were allowed to move towards the outer SENs. If the inclusion trajectories are visualized in Figure- 4.25, it is seen that the inclusions have a tendency to pass through the outer SENs, rather than floating up, towards the end of the tundish. The reason for this may be attributed to the height of the dam. Since it is half the height of the dam in

design 3, the flow could not guide the inclusions all the way up to the slag phase.

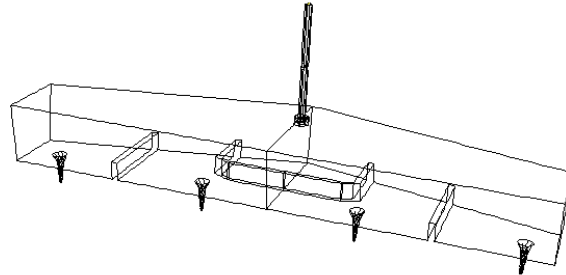


Figure-4.23 Tundish of design 7

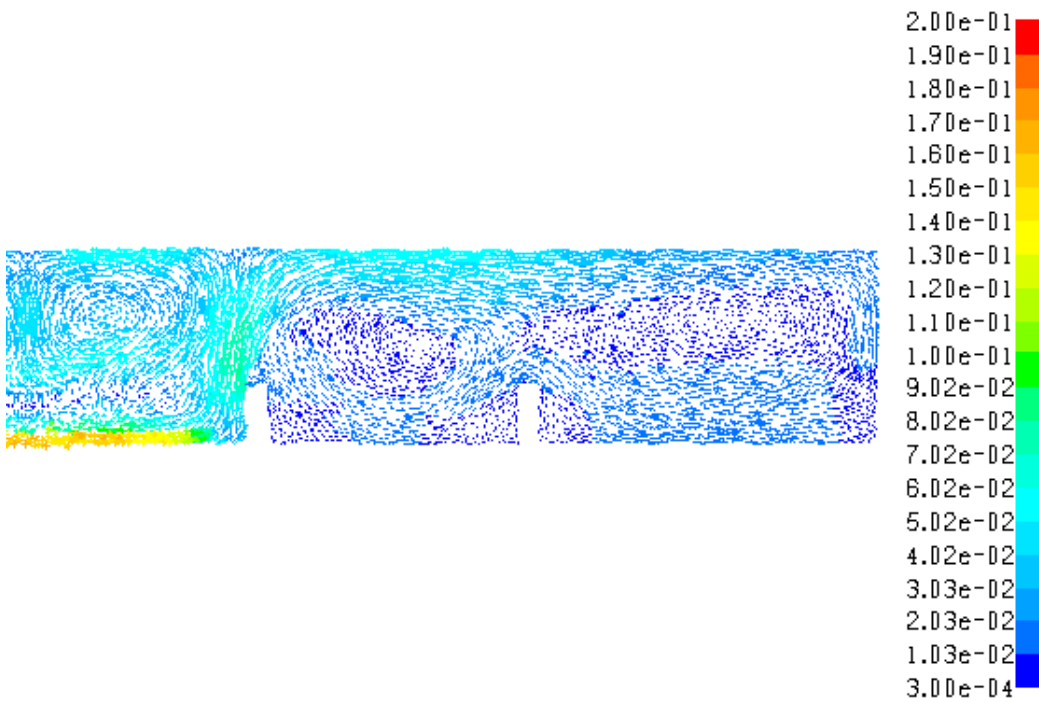


Figure-4.24 Velocity field ($m\ s^{-1}$) in the tundish of design 7.

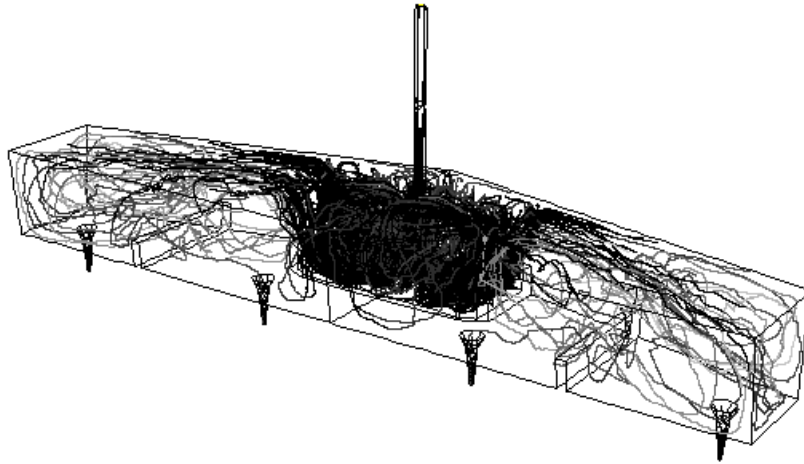


Figure-4.25 Inclusion (50-200 μ m) trajectories in the tundish of design 7.

(f) Design 8

The dam was now brought closer to the inner SENs. Since the distance between the dam and the impact pad is reduced, a recirculation is formed in between them. The inclusions were now retained in the inner strand region and less number of inclusions passed through the outer SENs. Also, a lot of inclusions after hitting the dam, back flowed and entrained in the inner SEN. Again as the height of the dam was less, the flow field was such that, it could not drag the inclusions all the way to the slag phase before it reached the outer strand. So inclusion removal efficiency was not good with this tundish configuration. More inclusions were expected to entrain

in the inner SENs. The above fact is supported in Figure- 4.28, where the inclusion trajectories are represented.

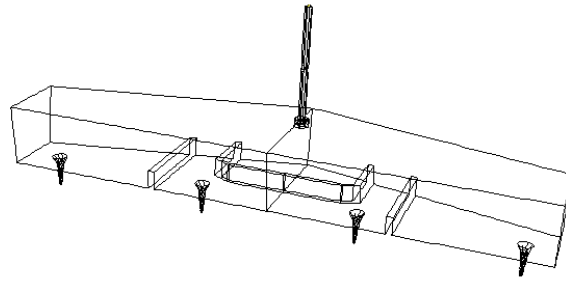


Figure-4.26 Tundish of design 8

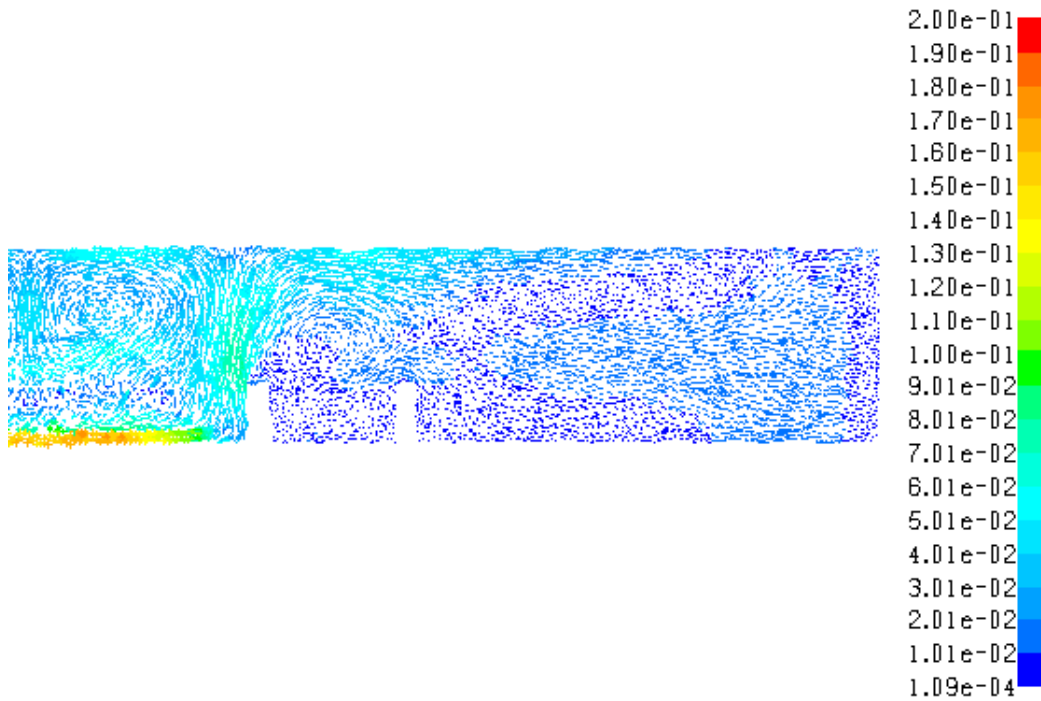


Figure-4.27 Velocity field ($m s^{-1}$) in the tundish of design 8.

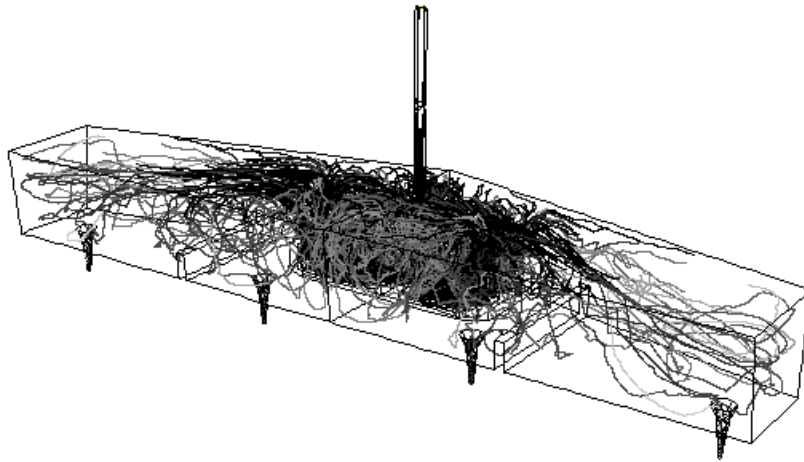


Figure-4.28 Inclusion (50-200 μ m) trajectories in the tundish of design 8.

(g) Design 9

The dam was now moved away from the inner strand and was at a distance of 1m from the pad. Because of this large distance, no recirculation was formed, and so inclusions were allowed to flow until the end of the tundish and were not grouped near the inner SENs. Since the height of the dam was not as high as in design 5, the fluid flow could not result in efficient inclusion floatation and this fact is shown in the inclusion trajectories in Figure- 4.31.

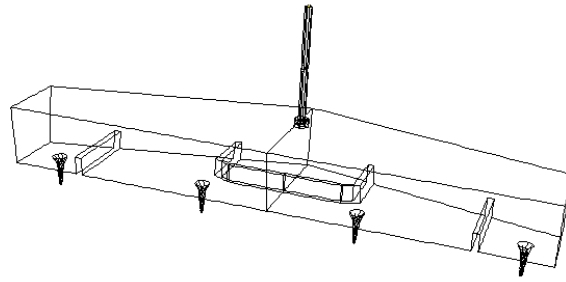


Figure-4.29 Tundish of design 9

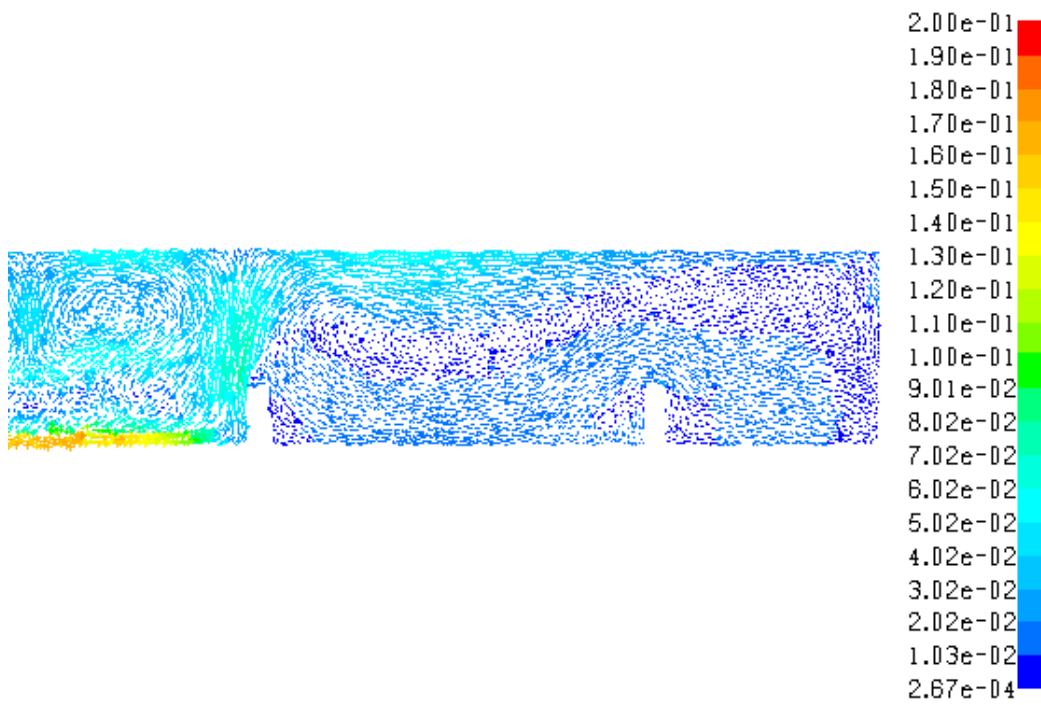


Figure-4.30 Velocity field ($m s^{-1}$) in the tundish of design 9

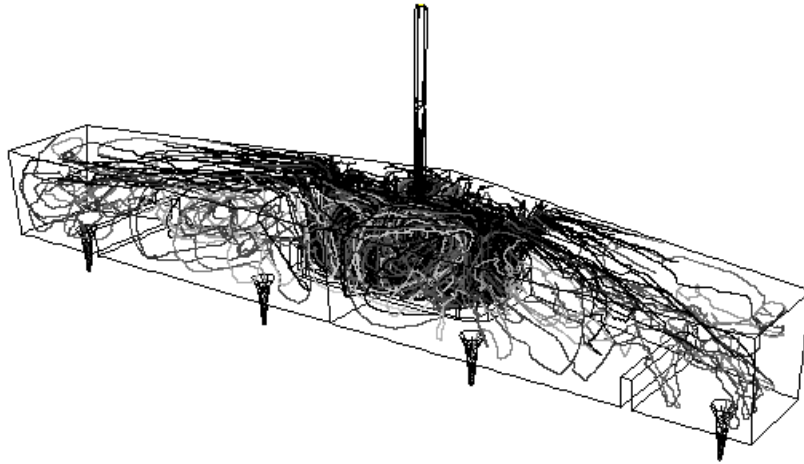


Figure-4.31 Inclusion (50-200 μ m) trajectories in the tundish of design 9.

(h) Design 10

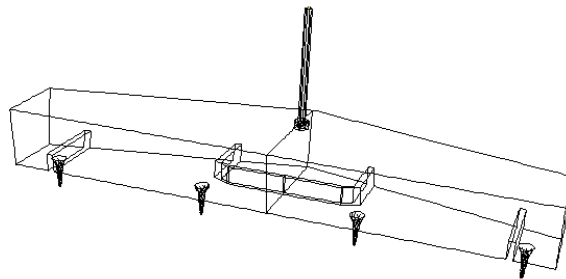


Figure-4.32 Tundish of design 10

The dams were placed just adjacent to the outer strands. So, more inclusions were entrained in the outer SENs as compared to d9.

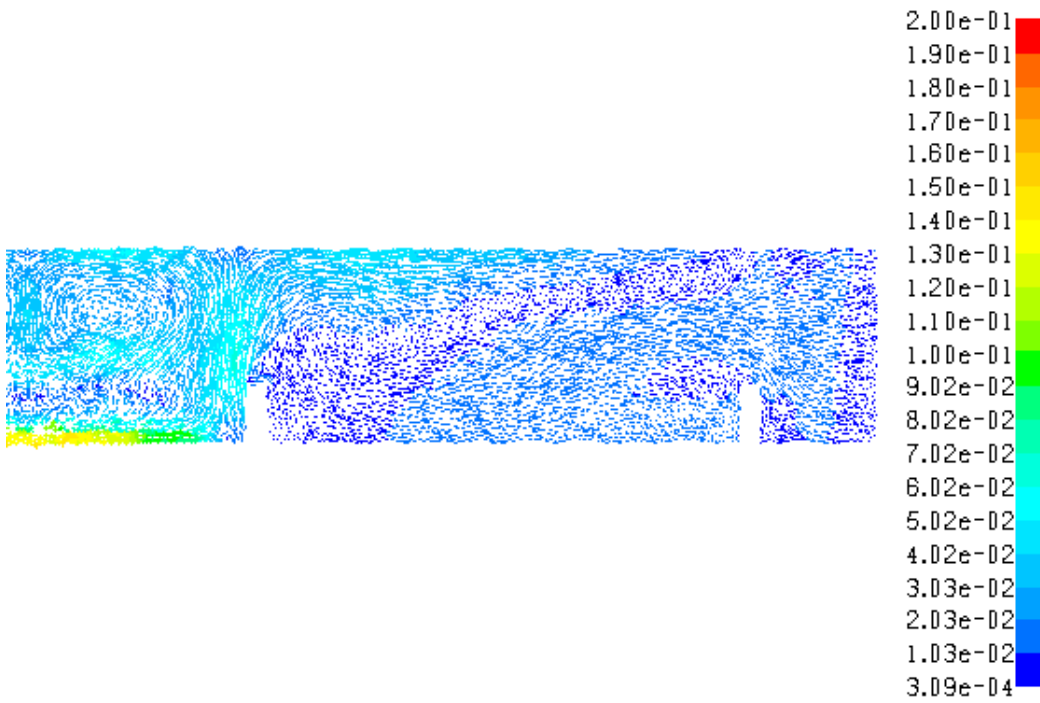


Figure-4.33 Velocity field ($m\ s^{-1}$) in the tundish of design 10.

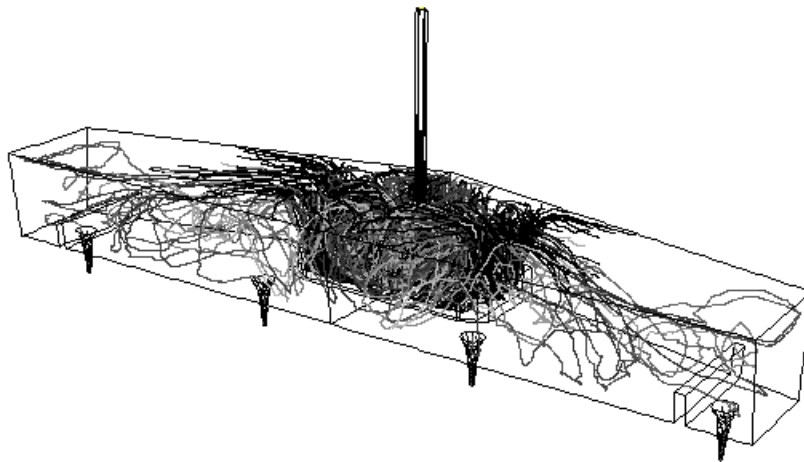


Figure-4.34 Inclusion (50-200 μm) trajectories in the tundish of design 10.

Figures 4.35 (a) and (b) shows the RRI% values for the tundish fitted with the impact pad, and a 0.152m high dam

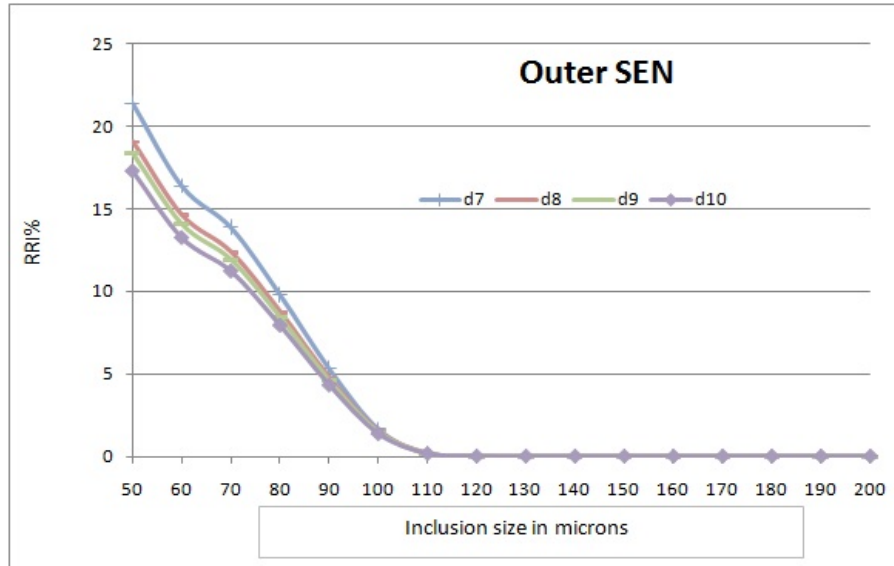


Figure- 4.35(a) Showing RRI% for d7, d8, d9 and d10 in the outer SEN

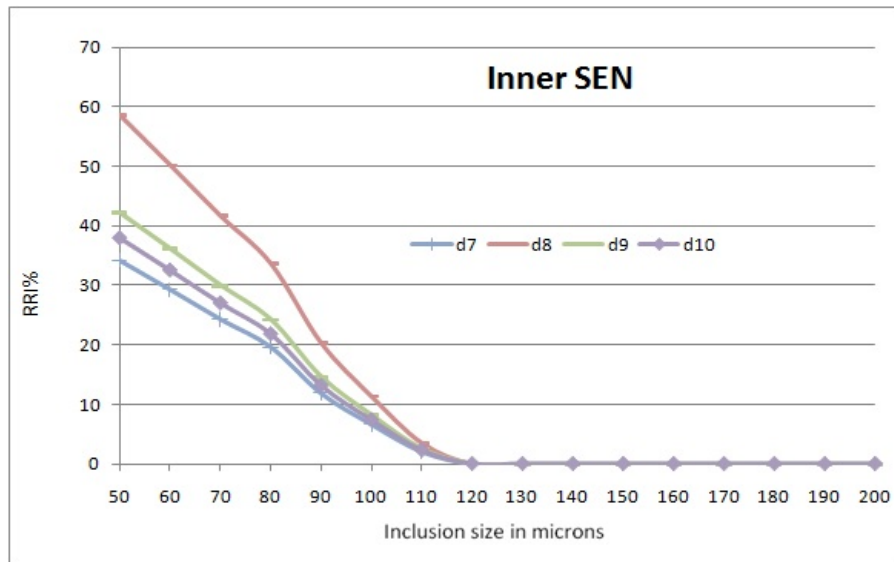


Figure- 4.35(b) Showing RRI% for d7, d8, d9 and d10 in the inner SEN

For designs 7 – 10, when the 0.152m high dam was brought closest to the inner SEN (d8), the steel quality coming out of the inner SEN degraded. However, when the dam was placed furthest away from the pad (d10), i.e. adjacent to the outer SEN, the steel quality was good for both inner and outer strands. When the dam was positioned exactly in the middle of the inner and outer SEN (d7), the steel quality in the inner strand was the best, but was worst for the outer strand. So overall, when using a 0.152m high dam, placing it adjacent to the outer SENs yielded best results.

(i) Design 11

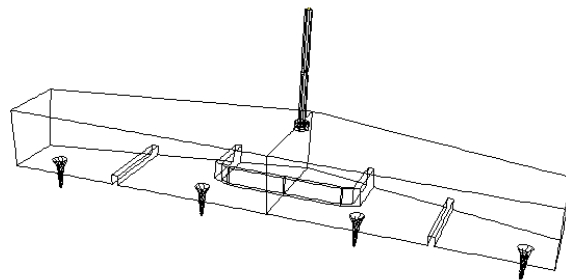


Figure-4.36 Tundish of design 11

The height of the dam was further reduced to 0.08m, i.e. almost half the height of the pad. This low dam could not restrict the inclusions in the inner SEN region and thus a lot of inclusions reached up to the outer strand and passed through it.

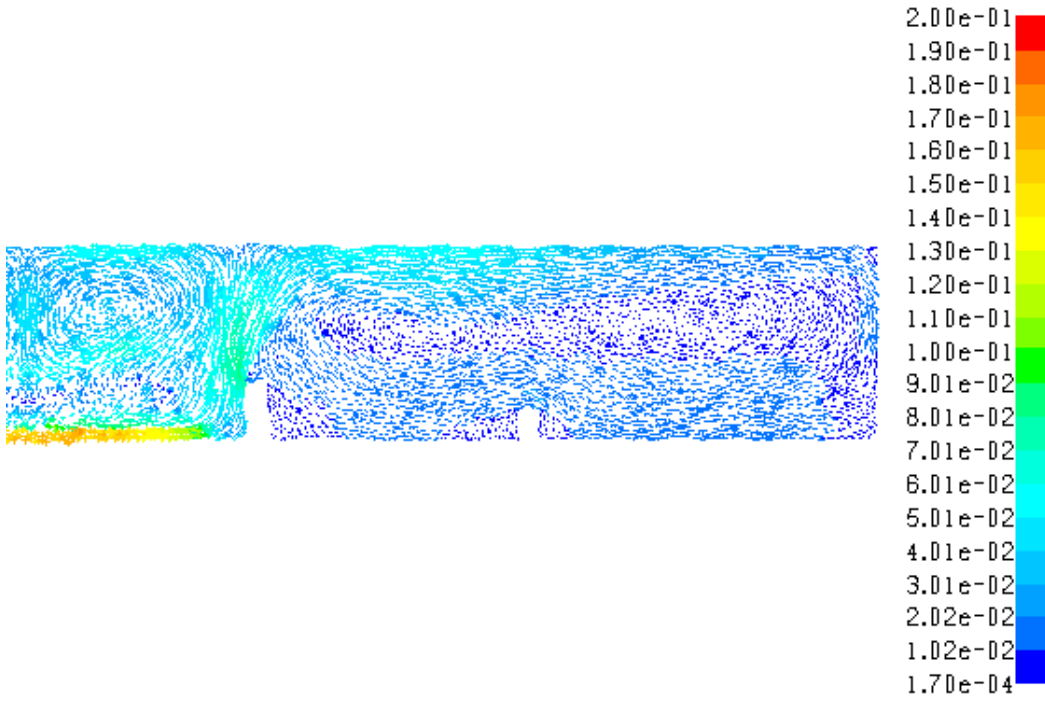


Figure-4.37 Velocity field ($m s^{-1}$) in the tundish of design 11.

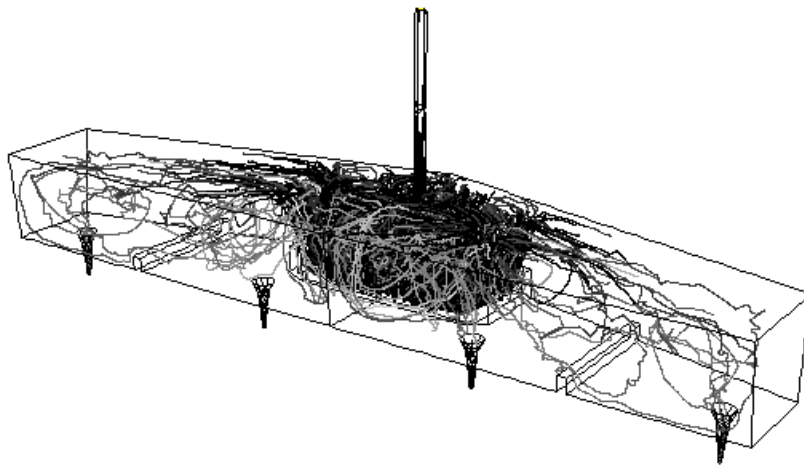


Figure-4.38 Inclusion ($50-200\mu m$) trajectories in the tundish of design 11.

(j) Design 12

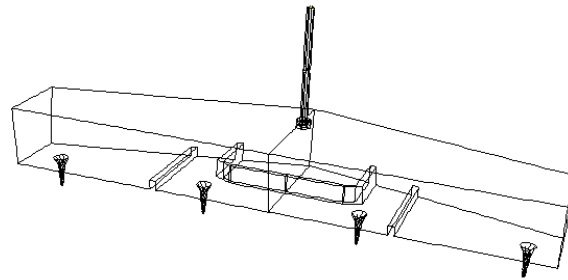


Figure-4.39 Tundish of design 12

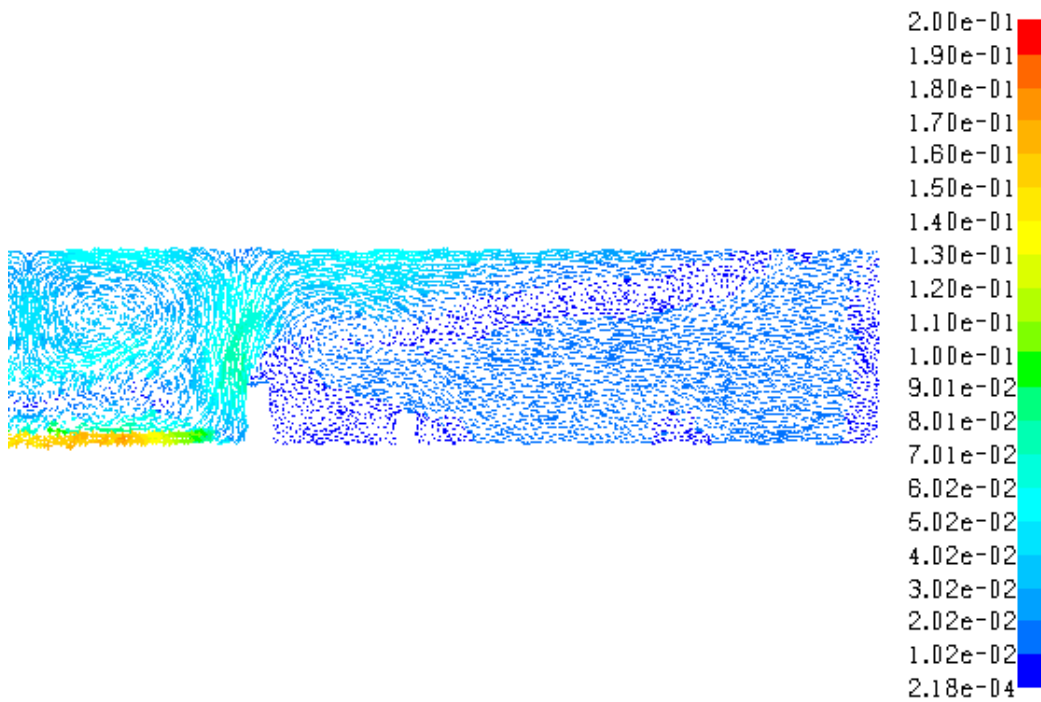


Figure-4.40 Velocity field ($m s^{-1}$) in the tundish of design 12.

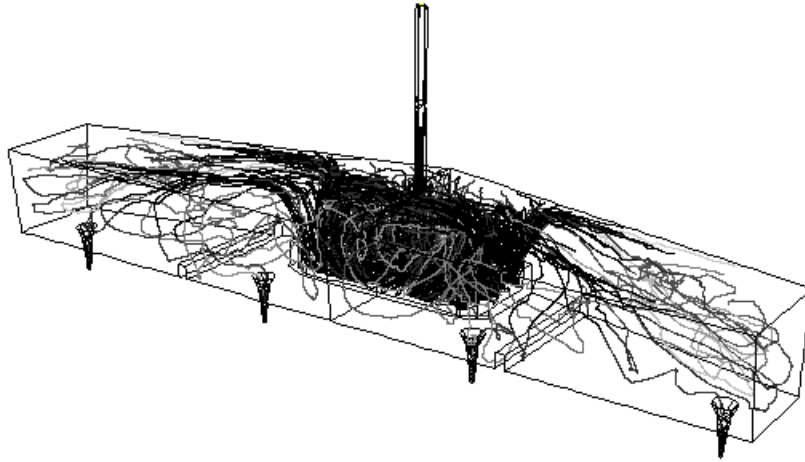


Figure-4.41 Inclusion (50-200 μ m) trajectories in the tundish of design 12.

Here, the low dam was brought closer to the inner SEN. This again caused more inclusions to cluster near the inner strand and pass through the inner SEN. Also as it was a very low dam, and closer to the inner SEN, it was not efficient in floating up the inclusions before they reach the outer strand. So the idea of placing a dam of any height near the inner SEN, was not good at all. It always degraded the steel quality in the inner strands.

(k) Design 13

The 0.08m dam was now placed at a distance of 1m from the pad. The low dam did not facilitate inclusion float out as usual.

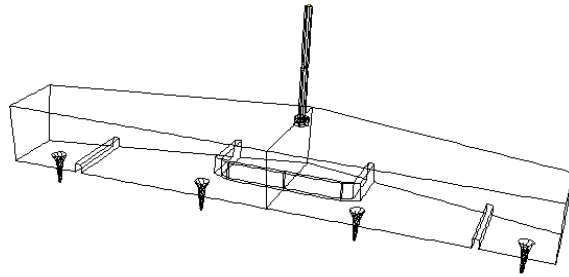


Figure-4.42 Tundish of design 13

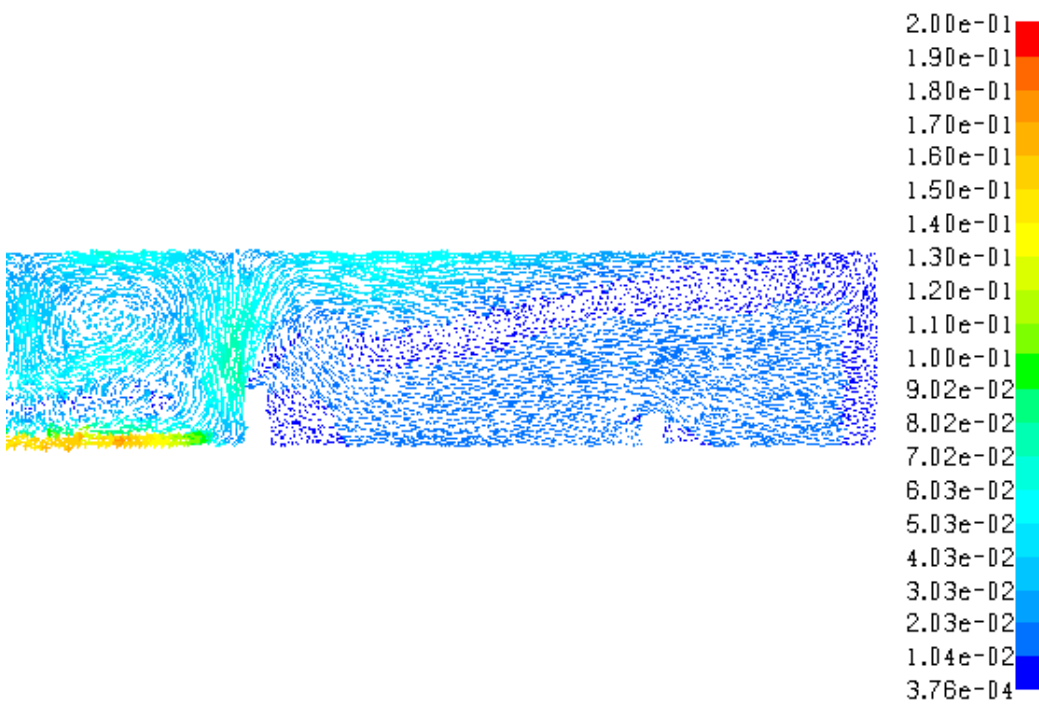


Figure-4.43 Velocity field ($m s^{-1}$) in the tundish of design 13.

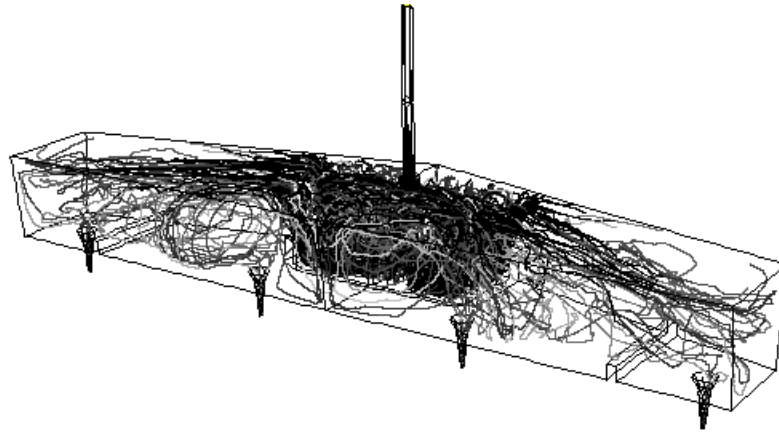


Figure-4.44 Inclusion (50-200 μ m) trajectories in the tundish of design 13.

(I) Design 14

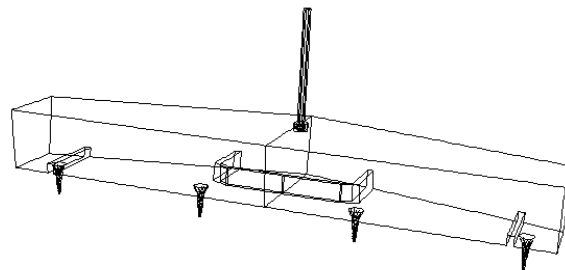


Figure-4.45 Tundish of design 14

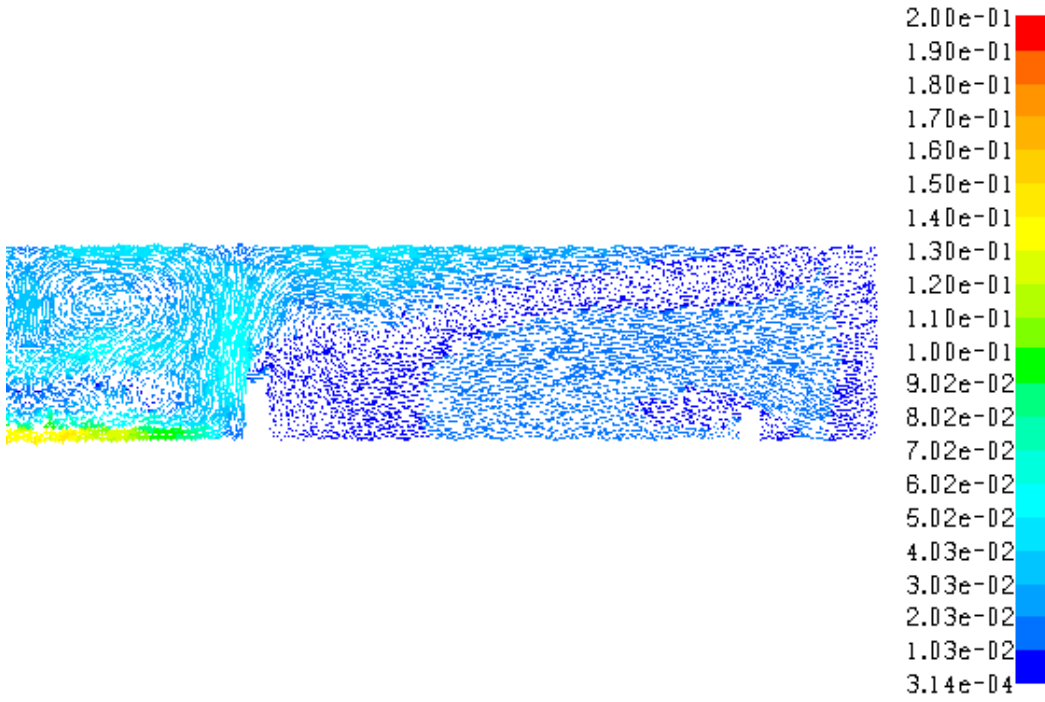


Figure-4.46 Velocity field ($m\ s^{-1}$) in the tundish of design 14.

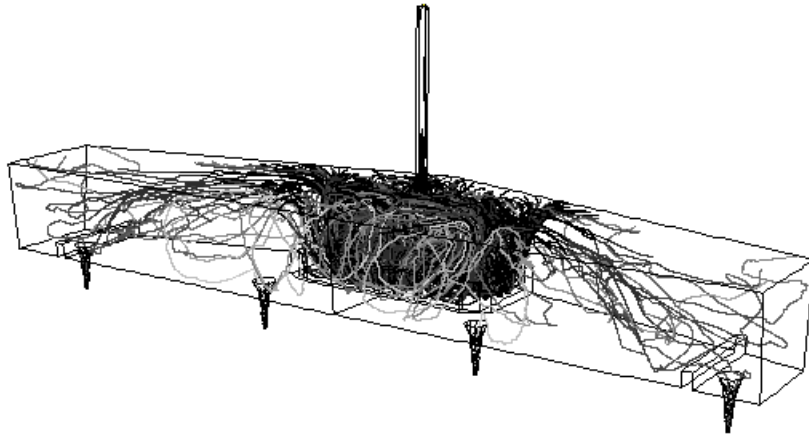


Figure-4.47 Inclusion (50-200 μm) trajectories in the tundish of design 14.

The dam was now placed adjacent to the outer strands. The inclusions were allowed to flow all the way towards the outer SEN as opposed to the fact, when the dam was closer to the inner SEN. As soon as the inclusions reached near the outer SEN, the low dam helped to change their direction upwards, and thus inclusion content of the liquid steel coming out of the outer strands was less.

Figure 48 (a) and (b) below shows the RRI% values for the tundish fitted with the standard impact pad and a 0.08m high dam.

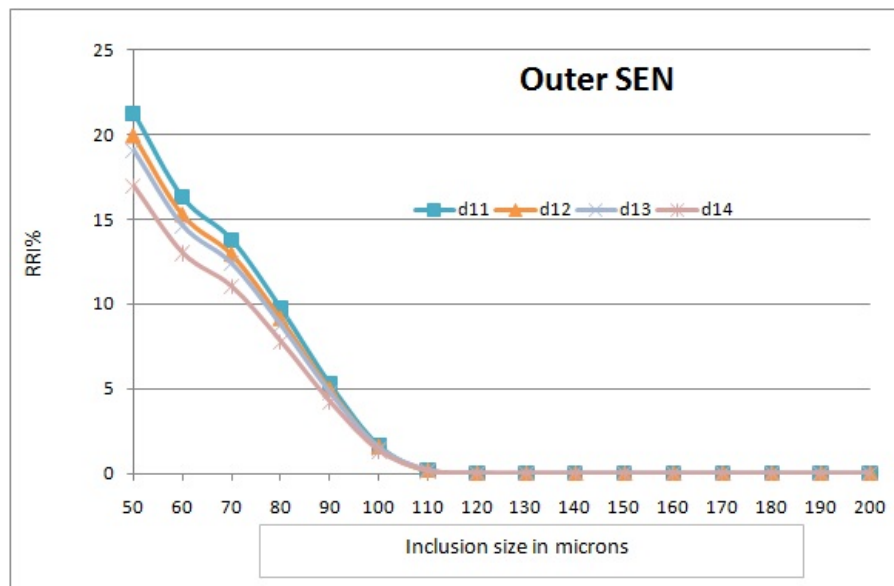


Figure- 4.48(a) Showing RRI% for d11, d12, d13 and d14 in the outer SEN

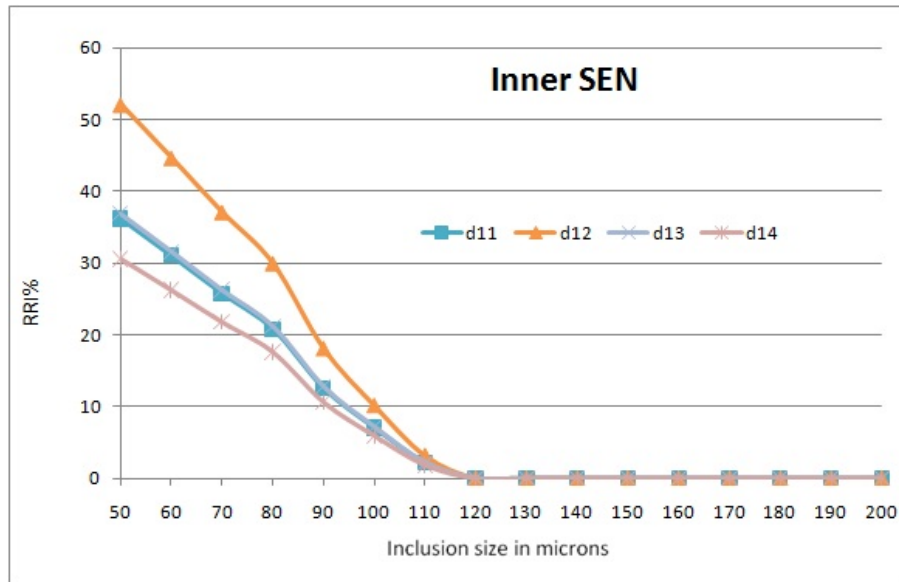


Figure- 4.48(b) Showing RRI% for d11, d12, d13 and d14 in the inner SEN

From the above results, it is clear that placing the dam closer to the inner SEN (d12) was not good in terms of inclusion content of the liquid coming out of the inner strand. When the low 0.08m dam was placed closest to the outer SEN (d14), best results in terms of steel cleanliness was obtained for both the inner and outer SENs.

The discussions in section 4.4.1 are now summarized. For some cases, using a dam in conjunction with the standard impact pad increased the inclusion removal efficiency of the tundish. However, this was highly dependent on the height and position of the dam. When a high dam of 0.254m was used, placing it at a distance of 1m from the impact pad (d5) yielded best results. When lower dams of height 0.152m or 0.08m was used, placing it at a distance of 1.26m

from the impact pad, i.e. just adjacent to the outer SENs (d10, and d14) yielded best results. Positioning of the dam closer to the inner SEN always degraded the steel quality in the inner strand for all heights of the dam.

4.4.2 Effect of different sizes of the impact pad on fluid flow and inclusion removal

The inhibition of turbulence in the jet entry zone is very important and ‘turbostops’ and ‘impact pads’ have been widely used by steel plants. The size and proper positioning of them is very important. The standard impact pad used at the RTIT/QIT plant also helps in cleaning the steel by removing inclusions in addition to inhibiting the turbulence in the entry zone. The size of the impact pad was varied and its effect on inclusion removal was studied. A schematic diagram of the impact pad is given for each tundish design, along with the flow field and inclusion trajectories. Here, the velocity field was examined on a vertical plane through the ladle shroud.

(a) Design 15

In design 15, the height of the pad was increased to 0.3m. All the other dimensions were same as the standard impact pad. There was a big recirculation formed inside the pad region, and it helped to drag all inclusions upwards. Since the pad was higher, the flow was

such that inclusion float out was enhanced and this is also evident in Figure 4.51 where the inclusion trajectories are presented.

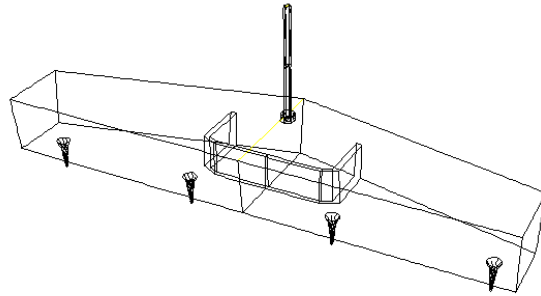


Figure-4.49 Tundish of design 15 (0.3 m high impact pad)

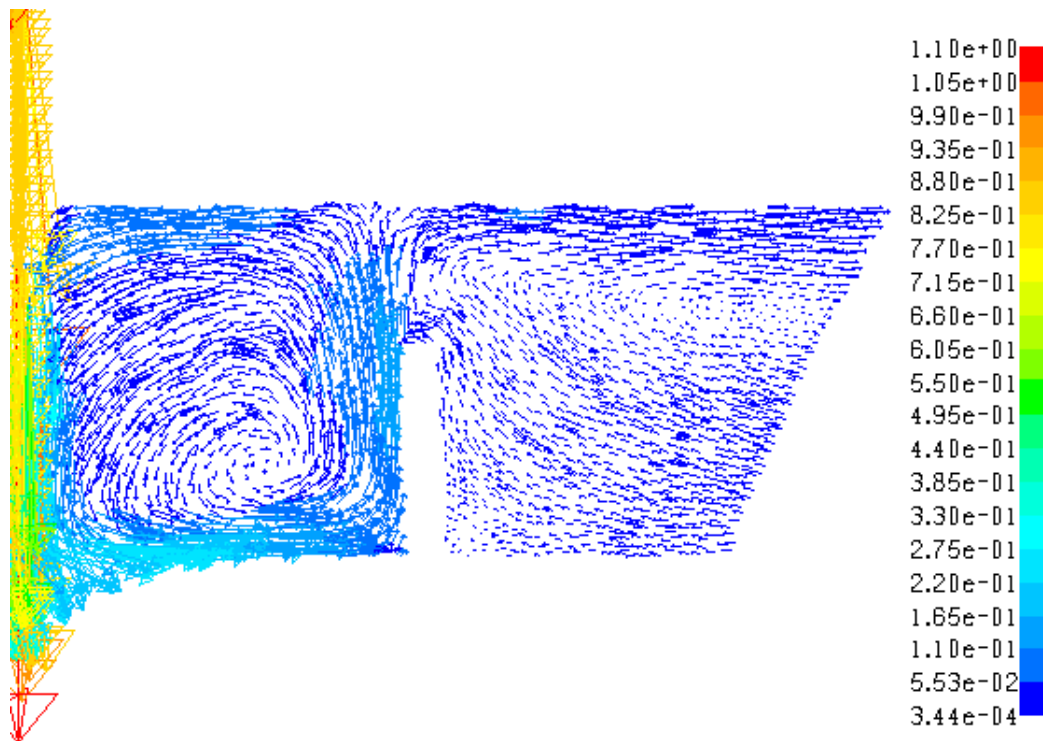


Figure-4.50 Velocity field ($m s^{-1}$) in the tundish of design 15

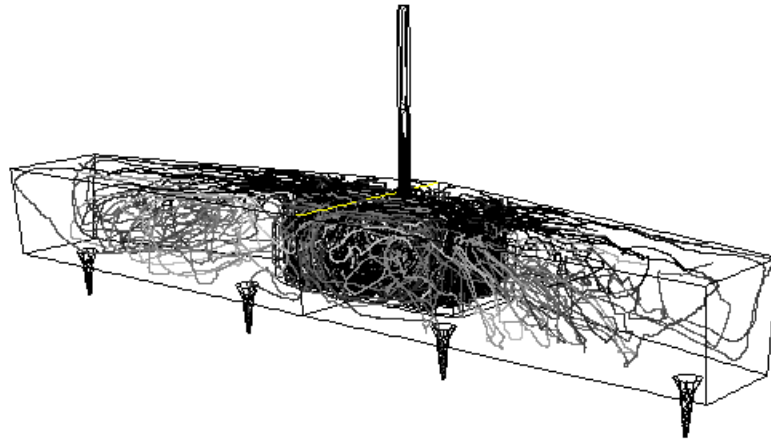


Figure-4.51 Inclusion (50-200 μ m) trajectories in the tundish of design 15.

(b) Design 16

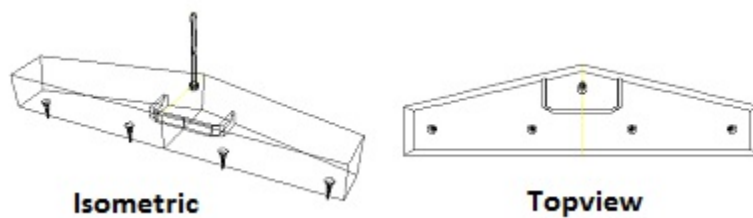


Figure-4.52 Tundish of design 16

Here, the impact pad was reduced in length and width, but the height was the same as the standard impact pad. The recirculation formed

within the pad region was much smaller here, and so inclusion floatation was not expected to be high here. When the inclusion trajectories are examined in Figure 4.54, it is clearly seen that some inclusions are back flowing and are entrained in the inner SENs. So the inclusion content of the liquid coming from the inner SENs will be very high.

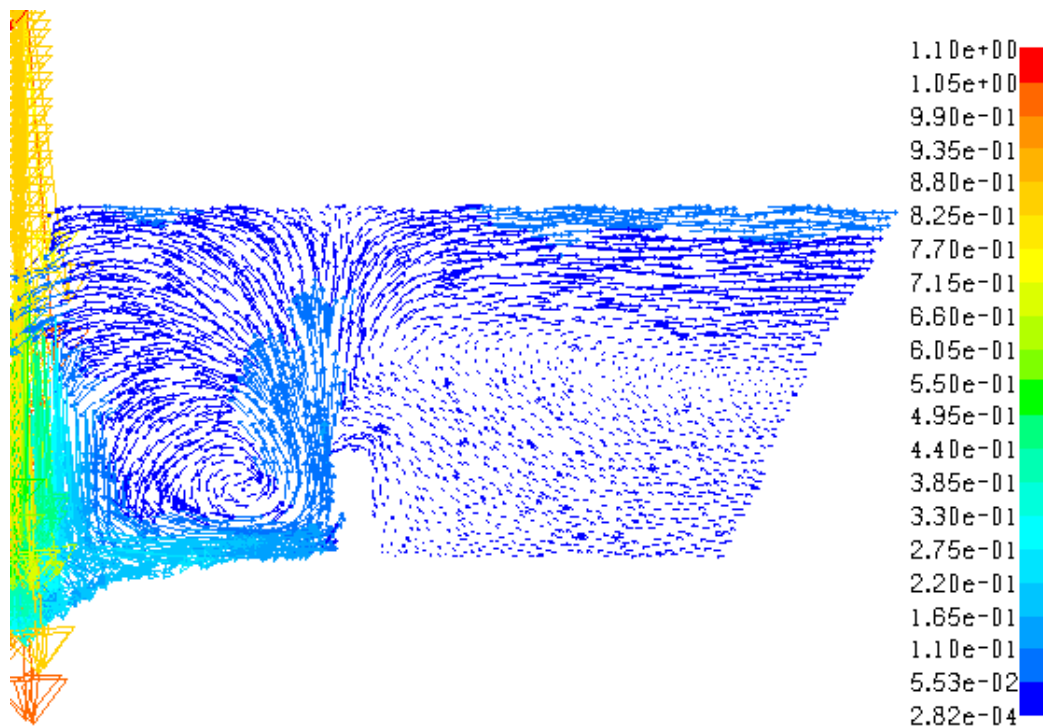


Figure-4.53 Velocity field ($m\ s^{-1}$) in the tundish of design 16

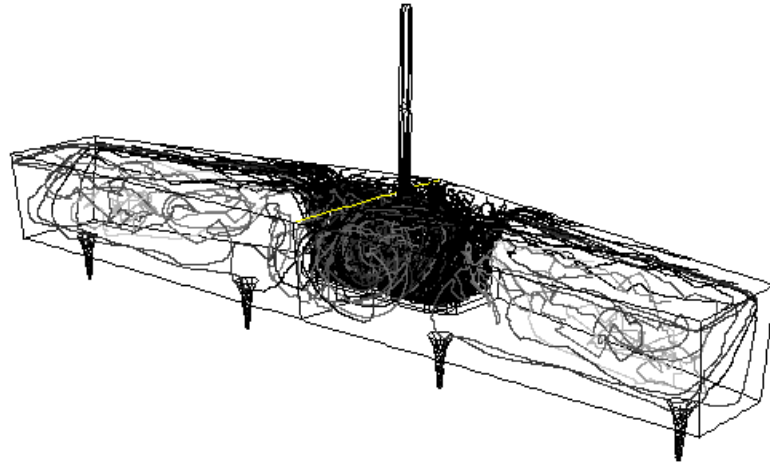


Figure-4.54 Inclusion (50-200 μ m) trajectories in the tundish of design 16.

(c) Design 17

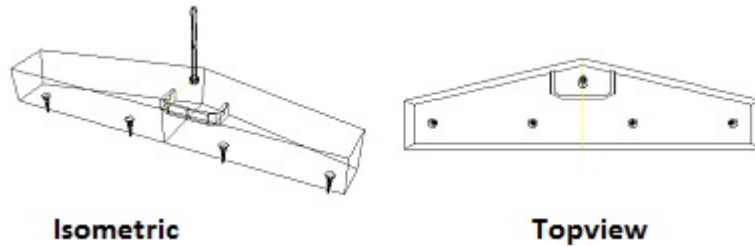


Figure-4.55 Tundish of design 17

In design 17, the size of the impact pad was even smaller than that in design 16. From the flow field (Figure- 4.56) and inclusion trajectories (Figure- 4.57), it is clear that a smaller impact pad is not a good solution to remove inclusions.

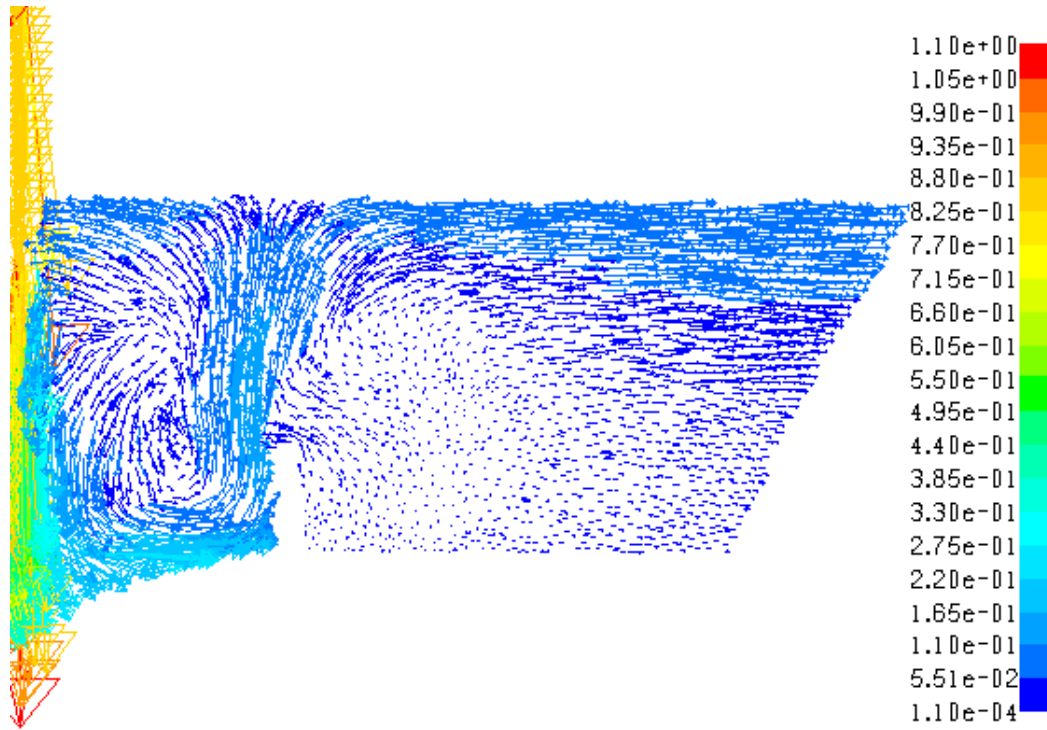


Figure-4.56 Velocity field ($m s^{-1}$) in the tundish of design 17

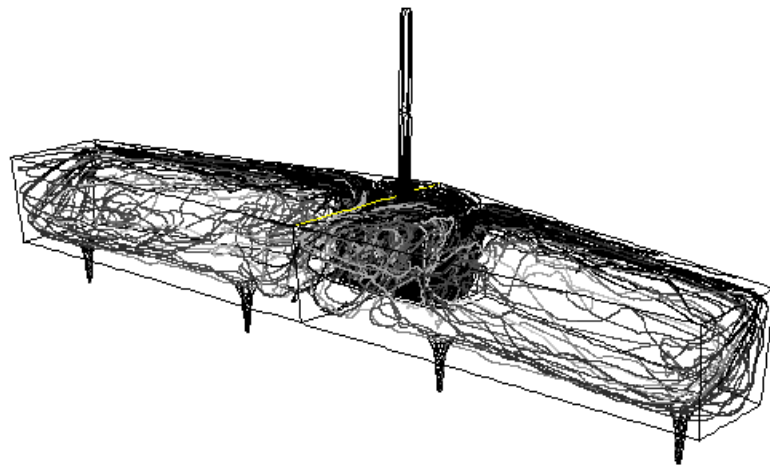


Figure-4.57 Inclusion ($50-200\mu m$) trajectories in the tundish of design 17.

(d) Design 18

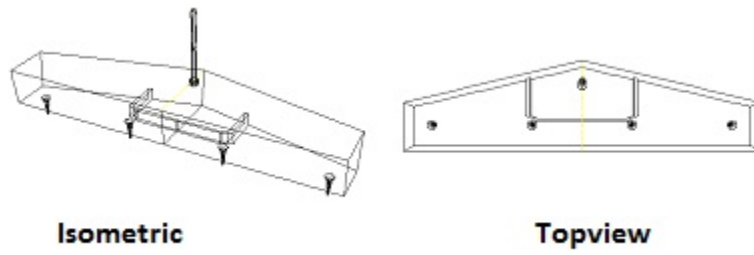


Figure-4.58 Tundish of design 18

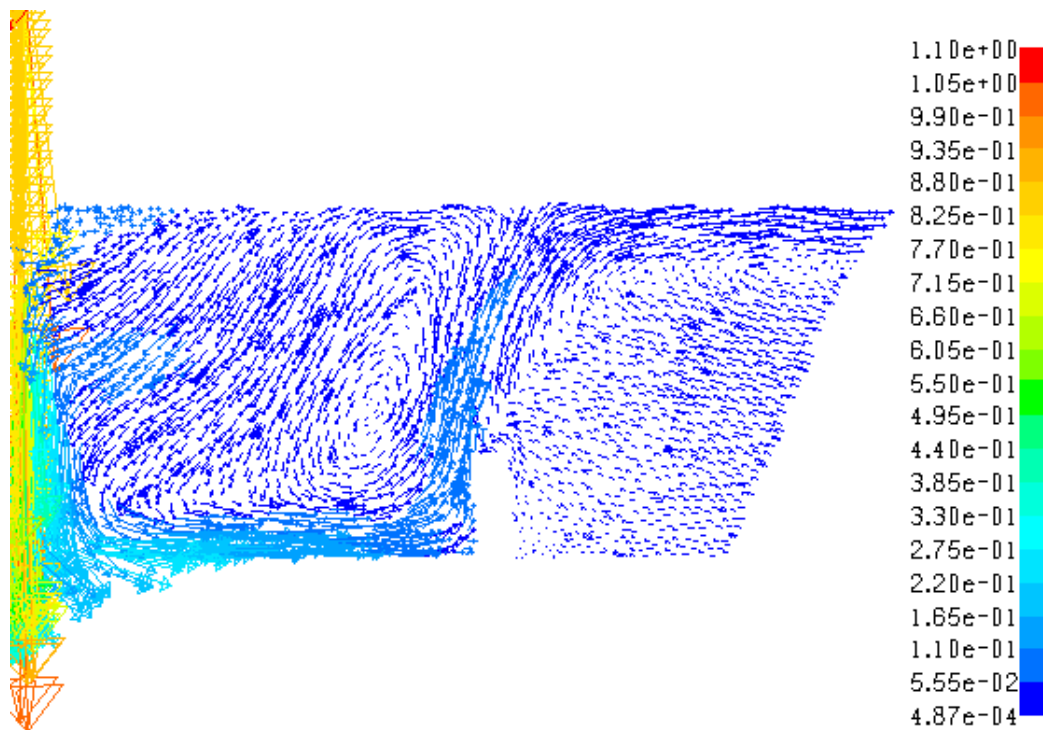


Figure-4.59 Velocity field ($m\ s^{-1}$) in the tundish of design 18

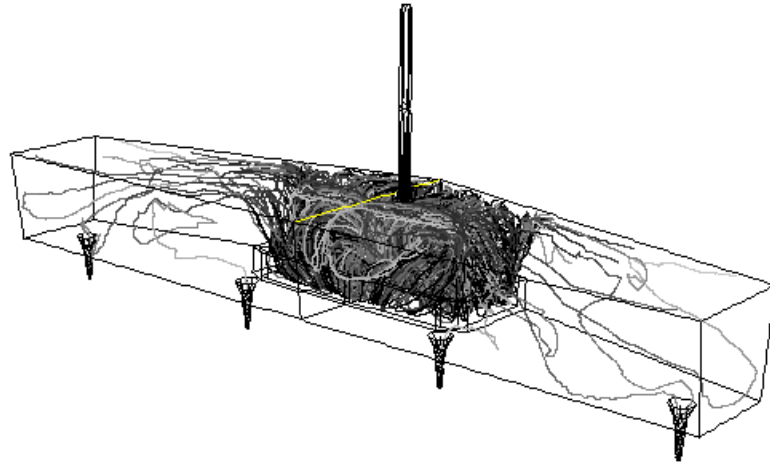


Figure-4.60 Inclusion (50-200 μ m) trajectories in the tundish of design 18.

In design 18, the size of the impact pad was increased and is now bigger than the standard impact pad. This was the largest impact pad that could be placed in the tundish. Due to large size of the pad, the shape of the recirculation in the pad region was changed. However, this did not affect the upward direction of the flow, and inclusion floatation was not hampered as seen in Figure- 4.60. Now it is of great interest to see which impact pad of d2, d15, d16, d17, and d18, dissipates the maximum amount of turbulence in the jet entry zone. Figure- 4.61 below shows the TKE contours for the five impact pads considered. It is observed that the smaller impact pads, d16 and d17, could not inhibit the turbulence in the jet entry zone as

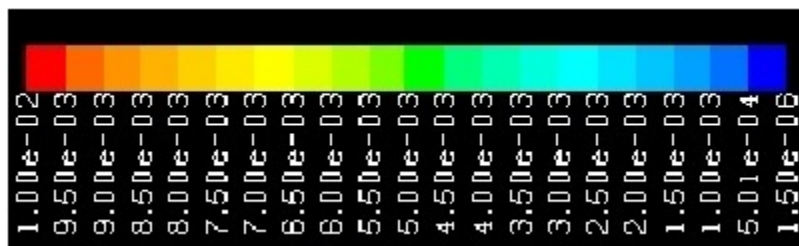
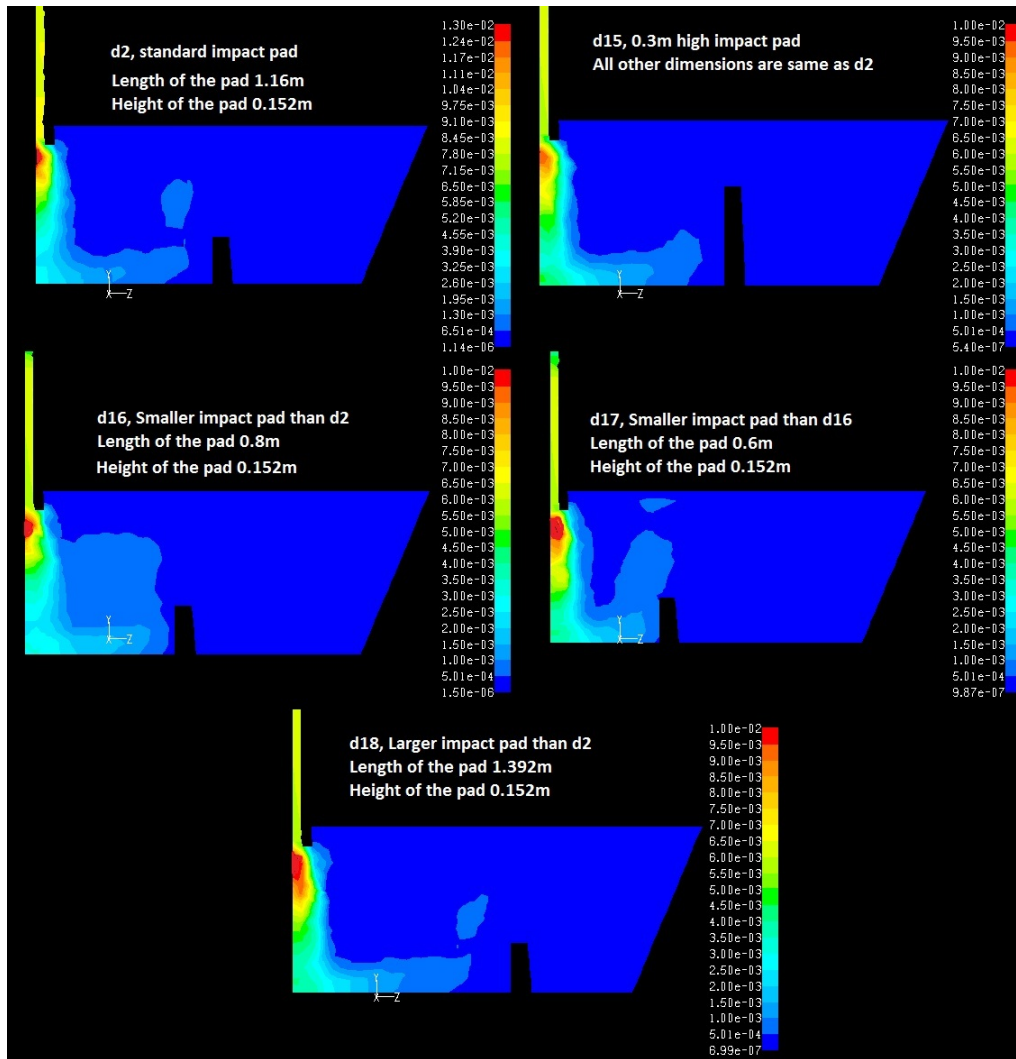


Figure- 4.61 TKE contours (m^2/s^2) in the jet entry region with different sizes of the impact pad.

compared to the other impact pads. There was not much difference between d2 and d18, but d15 i.e. the high impact pad was the best

in terms of turbulence inhibition. Figure 4.62 below shows the RRI values for all the impact pads. It is clear that the smaller impact pads (d16 and d17) were not good in terms of inclusion removal. The standard impact pad (d2) and the larger impact pad (d18) behaved similarly. So the size of the impact pad matters and standard impact pad currently used at QIT was well designed. However, when the height of the standard impact pad was increased to 0.3m from 0.152m (d15), inclusion removal was enhanced and is evident from the RRI calculations. For both the inner and outer SENs, the higher impact pad (d15) outperforms the other impact pads d2, d16, d17, and d18.

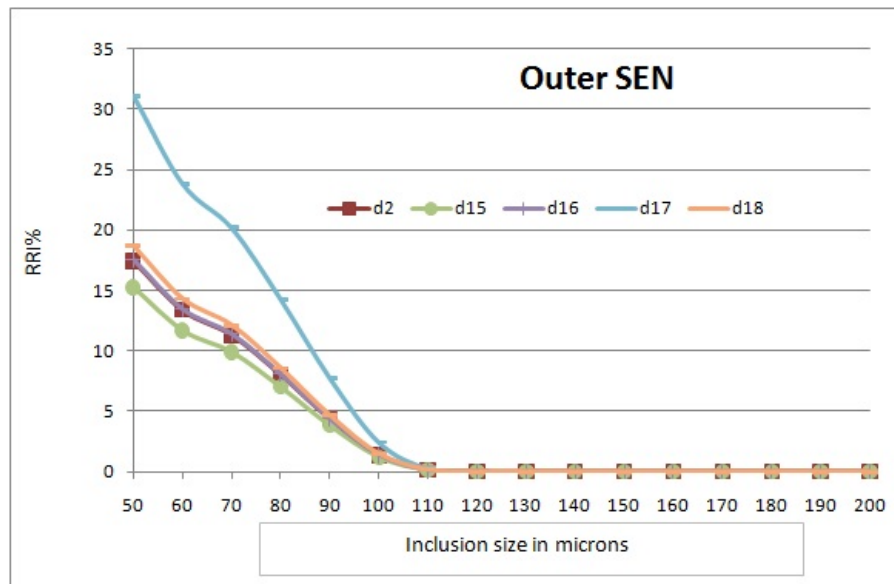


Figure- 4.62(a) Showing RRI% for d2, d15, d16, d17 and d18 in the outer SEN

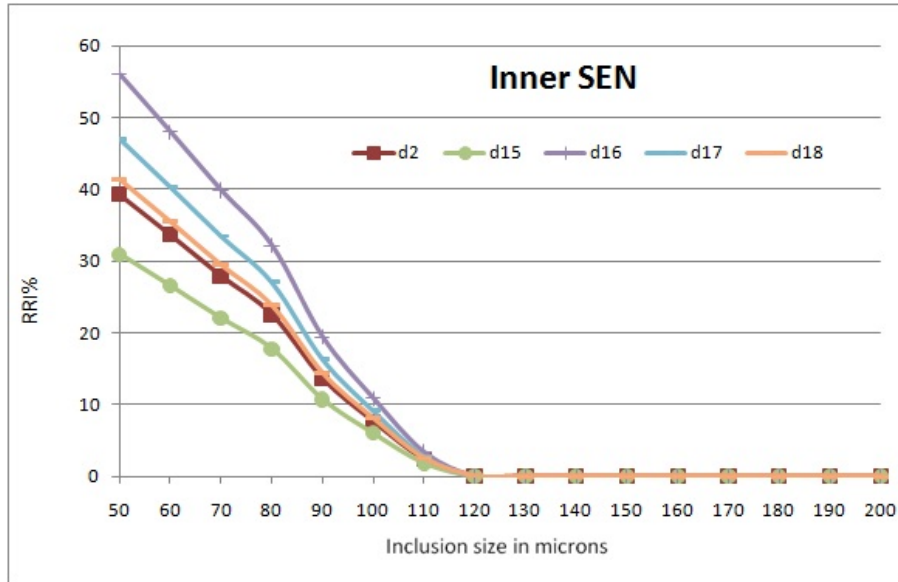


Figure- 4.62(b) Showing RRI% for d2, d15, d16, d17 and d18 in the inner SEN

4.4.3 Comparative values of (RRI) for all 18 designs

In the previous sections, eighteen different arrangements of flow furniture have been evaluated and now it is very important to know which arrangement is the best in terms of inclusion removal. Figure 4.63 below shows the RRI values for all the eighteen designs of the tundish. For the outer SEN, d5 had the lowest value of RRI, while for the inner SEN d15 had the lowest value of RRI. Now considering both the inner and outer SENs together, the higher impact pad (d15) yielded good results. So, the tundish performance will be better, if the height of the standard impact pad is increased to 0.3m from the existing 0.152m. It is also a good point that just by increasing the height of the pad, the inclusion content of the steel can be reduced,

and use of extra dams in between the inner and outer SEN is not required.

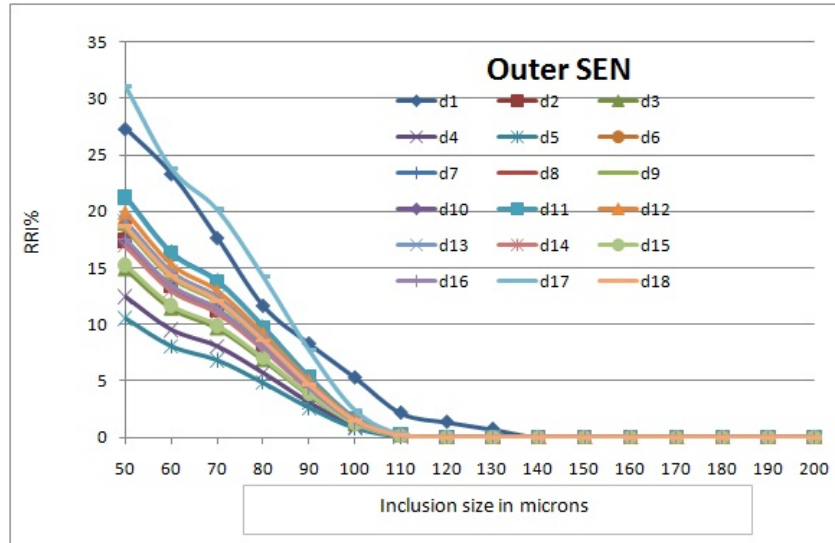


Figure- 4.63 (a) RRI for all eighteen tundish configurations in the outer SEN

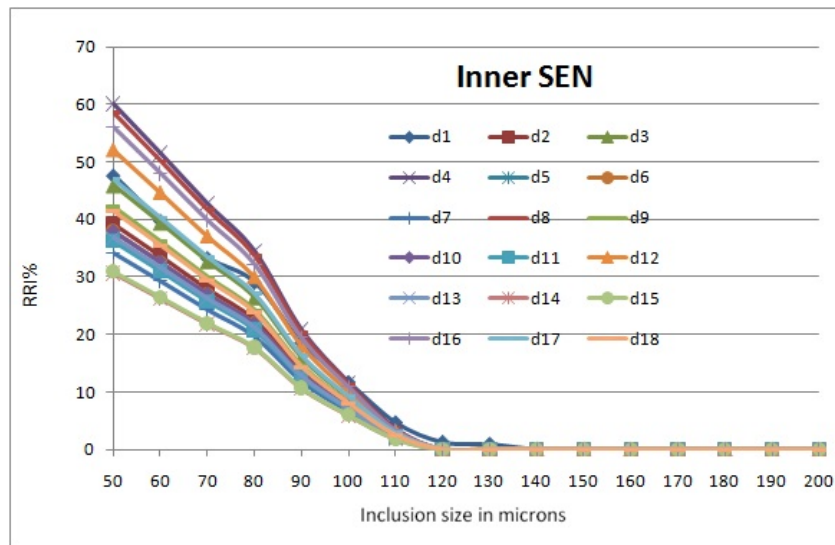


Figure- 4.63 (b) RRI for all eighteen tundish configurations in the inner SEN

4.4.4 Validation of mathematical prediction with water LiMCA studies

At the MMPC water modelling laboratory, the aqueous particle sensor (APS) or the water LiMCA was used to measure the RRI values for a couple of tundish configurations¹⁰⁰. Hollow glass microspheres of size range 50 -150 microns were injected through the shroud and RRI was evaluated for the bare tundish and that with the standard impact pad. Figure 4.64 below shows the experimentally measure RRI values and comparison with the numerical predictions.

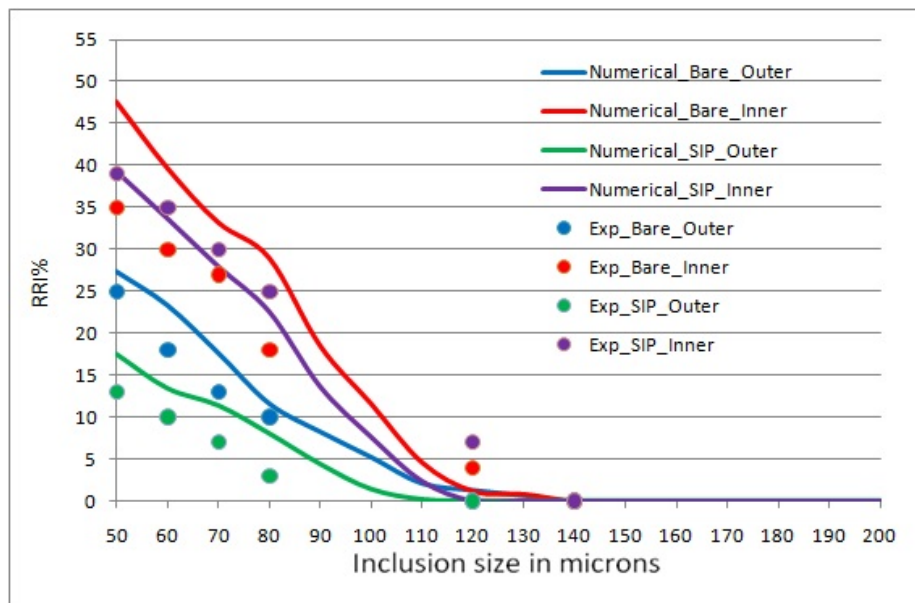


Figure- 4.64 Showing experimentally measured and numerically predicted RRI values for the bare tundish and the tundish with SIP

The numerical model tends to slightly over predict the RRI values in all cases, but the trends are pretty similar for both tundish

configurations. The small variations are because of the fact that, the numerical calculations are based on the RANS equations along with the k - ϵ turbulence model and discrete random walk model. Also, certain assumptions are taken into consideration like; inclusions are elastically colliding with the tundish walls, inclusions are completely trapped in the top surface of the tundish and finally, collisions between the inclusions are neglected. However, in reality may be some of these assumptions are not true and hence; there is a deviation in the results. Considering 3D turbulent flow, these deviations will always be present between the physical and mathematical models. However, the 3D mathematical model gives the exact trend of the RRI versus inclusion size range and can be used for comparative analyses. When there are eighteen designs of the tundish and RRI needs to be evaluated, this mathematical model is quite robust and does a decent job.

4.5 Importance of dimensionless numbers and the Guthrie Number (Gu)

Dimensionless numbers are very important in process modelling and can be defined according to our convenience. For example, the Reynolds number is a ratio of inertial forces to viscous forces. However, it can also be defined as a ratio of two characteristic time scales.

$$Re = \rho LV / \mu \quad [\text{Eq. 4.1}]$$

$$\text{or, } Re = LV / \nu \quad [\text{Eq. 4.2}]$$

$$\text{or, } Re = L^2 V / \nu L \quad [\text{Eq. 4.3}]$$

$$\text{or, } Re = \frac{V}{L} \frac{L^2}{\nu} \quad [\text{Eq. 4.4}]$$

$$\text{or, } Re = \frac{\frac{L^2}{\nu}}{L/V} \quad [\text{Eq. 4.5}]$$

If the last of the above equations is critically examined, $\frac{L^2}{\nu}$ represents a characteristic time scale for momentum transfer. If a dimensional analysis is done, it will be seen that $\frac{L^2}{\nu}$ has units of $[\text{m}^2/(\text{m}^2/\text{s})]$ i.e. seconds, which is clearly a unit of time. Similarly, $\frac{L}{V}$ is the characteristic time scale of advection, and has units of $[\text{m}/(\text{m}/\text{s})]$ i.e. seconds. So, in a dynamic sense,

$$Re = \frac{\tau_{\text{momentum}}}{\tau_{\text{advection}}} \quad [\text{Eq. 4.6}]$$

Now, let us re-consider the Prandtl Number.

$$Pr = \frac{\nu}{\alpha} = \frac{L^2/\alpha}{L^2/\nu} \equiv \frac{\tau_{\text{heat}}}{\tau_{\text{momentum}}} \quad [\text{Eq. 4.7}]$$

So, in a dynamic sense, the Pr becomes a ratio of the time scale for heat transfer to the time scale of momentum transfer.

Now let us re-examine the Schimdt Number.

$$Sc = \frac{v}{D} = \frac{L^2/D}{L^2/\nu} \equiv \frac{\tau_{mass}}{\tau_{momentum}} \quad [\text{Eq. 4.8}]$$

Finally, the Froude Number;

$$Fr = \frac{v^2}{gL} = \frac{v}{g} \frac{v}{L} = \frac{v}{\frac{L}{v}} \equiv \frac{\tau_{gravitational}}{\tau_{advection}} \quad [\text{Eq. 4.9}]$$

Although, Residual Ratio of Inclusions (RRI) is a good indicator of steel cleanliness in terms of its inclusion content, it was thought that the liquid melt quality can also be represented in the form of a dimensionless number. Professor Roderick Guthrie contributed immensely to the field of process metallurgy for the last forty years and so this dimensionless number was named in his honour.

It is clearly seen that all the dimensionless numbers can be defined as the ratio of two time scales. Following this approach, the Guthrie Number (Gu) is defined as

$$Gu = \frac{\tau_{residence}}{\tau_{inclusion\ float\ out}} \quad [\text{Eq. 4.10}]$$

The inclusion float out time is defined as the time the inclusion takes to rise up to the upper surface of the steel. Assuming immediate absorption within the upper “slag” phase, this float out time would be synonymous with the inclusion removal time. As such, the lesser the inclusion float out time, the better is the steel quality in the mould.

Also, it is generally recognised that the larger the residence time of fluid within a tundish, the more the inclusions will float out. Here, residence time is referred to as the Nominal residence time, i.e.

$$\frac{\text{Volume of the tundish}}{\text{Inflow rate of the liquid}}$$

So in a sense, a larger Gu Number indicates a better tundish operation, in that it is an indication that most of the inclusions will float out before entering the moulds. In other words a higher Gu means a lower Residual Ratio of Inclusions, or RRI. The definition of RRI is given in the subsequent section on mathematical modelling. Now if there is a larger tundish by volume, it will have a much higher nominal residence time and so it is better for inclusion removal, all the other things being similar. So it is good to have a very large tundish for better inclusion removal, and this is indeed a current trend in large steel companies. Figure-4.65 shows the variation of Gu^{-1} with the nominal residence time of a tundish, assuming all other parameters (viz. inclusion float out time and liquid inflow rate) remain constant. Here the inclusion float out time is assumed to be unity. This does not affect the nature of the plot and is only a scaling factor.

When different types of inclusions are considered, the Gu similarity criterion will help us model them more easily. An average float out time of all the inclusions can be considered and then divide it by the

residence time of the particular tundish. This makes more sense because then the predictions from the water model will be more general and it also does not require that the inclusions be in the Stokes velocity regime.

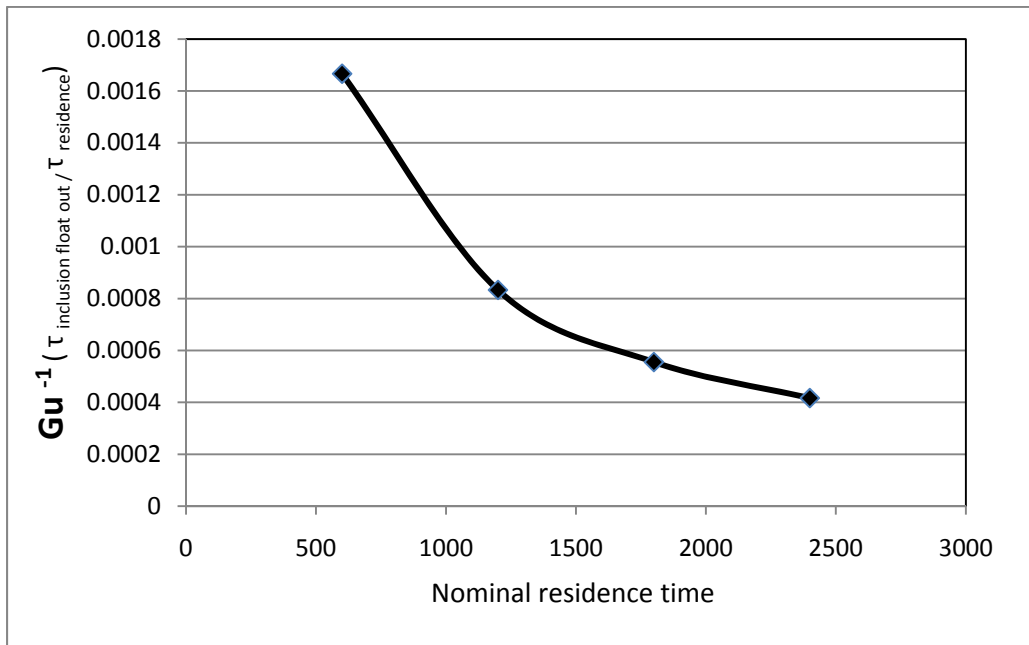


Figure- 4.65 Variation of Gu as a function of nominal residence time

Mathematical modelling was performed for a four strand billet caster tundish, to see the relation between Gu and Residual Ratio of Inclusions (RRI) and also the variation of Gu with inclusion size range. ANSYS 12 was used to perform all mathematical simulations. Systems of hollow glass microspheres in water, alumina inclusions in steel and silica inclusions in steel were considered in the size range of 50-300 microns. The tundish was same for all three cases and hence when evaluating Gu, the nominal residence times were

the same for all three cases. Along with the standard k- ϵ turbulence model, the discrete phase model (DPM) was used where inclusions were tracked in a Lagrangian frame.

An average float out time of 10^6 inclusions of each size range (namely, 50,150 and 300 μm) was evaluated using the mathematical model. Three types of inclusions were considered viz. hollow glass microspheres in water, alumina inclusions in liquid steel and silica inclusions in liquid steel. The properties are listed in Table 4.2 and 4.3.

Type of Inclusion	Size Range (μm)	Density (Kgm^{-3})
Glass microspheres in water	50-300	400
Alumina	50-300	3100
Silica	50-300	2600

Table-4.2 Size range and density of different inclusions

Material	Density (Kgm^{-3})
Liquid Steel at 1600 ⁰ C	7000
Water at 25 ⁰ C	1000

Table- 4.3 Densities of liquid steel and water

The volume of the tundish used in the present calculation is around 1.714 m³. The inflow rate of water is 170 lpm i.e. 0.17 m³ (min)⁻¹. So the nominal residence time,

$$t_N = \frac{1.714}{0.17} = 10 \text{ minutes} = 600 \text{ s} \quad [\text{Eq. 4.11}]$$

The Guthrie number was evaluated using the average float out times and the nominal residence time of the tundish considered. The results are shown in Table 4.4.

Type of inclusion	Size(μm)	T _{inclusion float out} (s)	T _{residence} (s)	Guthrie Number (Gu)	RRI(%)
Glass in water	50	20.15	600	29.77	85
Glass in water	150	17.16	600	34.97	70
Glass in water	300	13.76	600	43.57	48
Alumina in Liquid Steel	50	21.15	600	28.36	83
Alumina in Liquid Steel	150	17.96	600	33.39	68
Alumina in Liquid Steel	300	14.65	600	40.95	48
Silica in Liquid Steel	50	22.13	600	27.11	82
Silica in Liquid Steel	150	18.96	600	31.64	68
Silica in Liquid Steel	300	14.98	600	40.02	46

Table-4.4 Values of inclusion float out times and Gu for different types and size range of inclusions

It is seen that a higher G_u corresponds to a lower RRI (Figure-4.66). Here, RRI refers to the total number of inclusions coming out of all four strands.

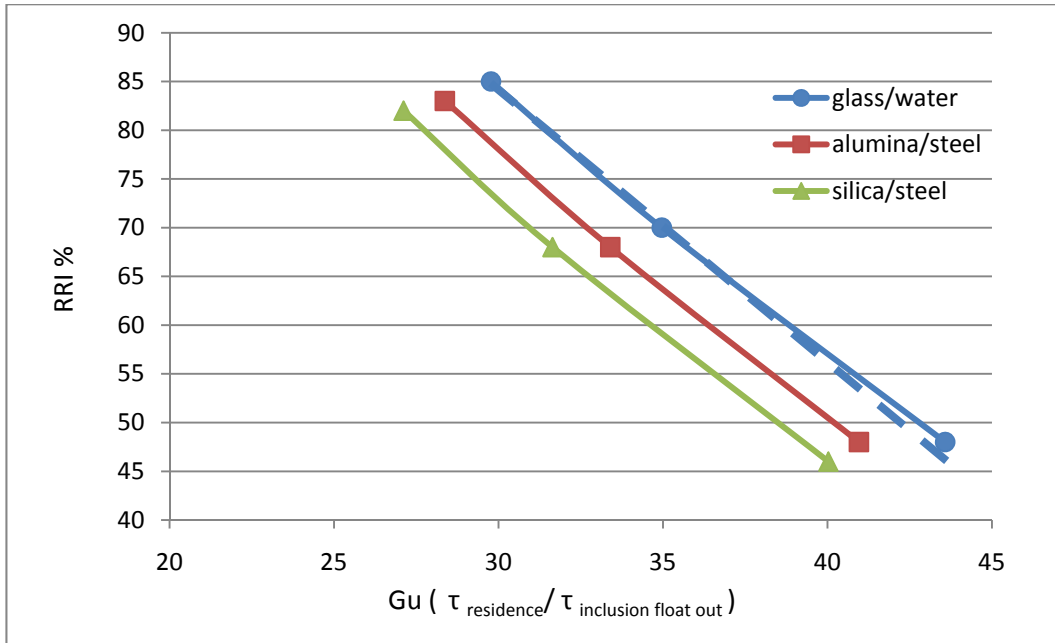


Figure-4.66 Residual Ratio of Inclusions as a function of Guthrie number (G_u)

Similarly with an increasing size of inclusions, the G_u number increases (Figure-4.67). There is a small deviation in the trend for the 300 μ m glass spheres in water. This deviation is because the inclusion float out time is 13.768 seconds. Had the inclusion float out time been 14 seconds, it would be a perfect straight line as the other systems and is represented by the bold dashed line on the graphs. So basically, this is not a big deviation. One important observation is that all three systems behave similarly. So the G_u number can be an

efficient similarity criteria for modelling inclusion removal in different tundishes.

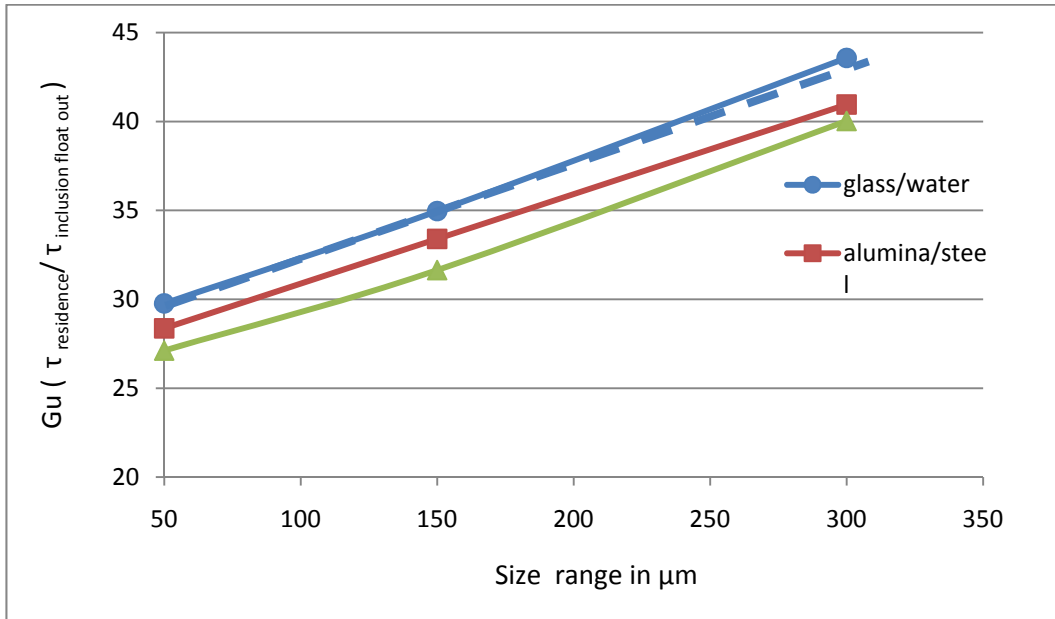


Figure-4.67 Guthrie number (Gu) as a function of inclusion size

5.0 Inert Gas Shrouding During Melt Transfer from the Ladle to the Tundish

5.1 Introduction

The injection of argon gas into the ladle shroud and Submerged Entry Nozzles (SEN's) is a common practice in continuous casting. The primary objective is to prevent the melt stream from re-oxidation due to aspiration of ambient air. H.B. Kim¹⁰¹ in 1998 in his M. Eng thesis at McGill University, discussed in detail about air aspirations in ladle shrouds. The benefits resulting from shrouding the melt

stream are manifold. There is a definite reduction in the oxygen content in the bath, a lesser number of oxide inclusions, a decrease in nozzle clogging frequency, an improvement in surface quality of slabs and billets, and a reduction of melt temperature loss from ladle to tundish⁷. Despite these benefits, too much of argon gas should be avoided, as it forms an exposed eye of steel around the ladle shroud by sweeping off the protective layer of tundish slag. In early work, D. Bolger et al¹⁰² identified the transitions between bubbly flow, churn-turbulent, and separated flows, as the gas flow injected into the ladle shroud is gradually increased. That work was in relation to the development of a slag detector system for slag carry-over from a ladle into a tundish. The optimal argon flow rate depends on casting speed, tundish level and nozzle bore diameter¹⁰³. G.M.Evans et al.¹⁰⁴, mentioned that for applications like SEN's, too much gas injection results in a transition from the bubbly flow regime to the churn-turbulent regime, and that is highly undesirable. Thus, it is essential to have a scientific understanding of the gas shrouding phenomenon, so that it becomes easier to optimize the process. Bai and Thomas^{105, 106} studied turbulent flow of liquid steel and argon gas bubbles in a slide gate tundish nozzle during the transfer of liquid steel from tundish to mould. They developed an Eulerian multiphase mathematical model using the finite difference program CFX and studied 3D turbulent flow of liquid steel and gas bubbles. The multi-fluid Eulerian multiphase model of

CFX¹⁰⁷ was used to simulate the time averaged flow of argon bubbles within the liquid steel. In CFX modelling, each phase has its own set of continuity and momentum equations. Coupling is achieved through an empirical interphase drag between liquid steel and argon bubbles. The model predictions agreed both quantitatively and qualitatively with measurements conducted using PIV on a 0.4-scale water model. G. M. Evans et al¹⁰⁴ studied the flow characteristics of a down flowing gas-liquid column incorporating a submerged entry porous nozzle system. They developed the model based on the one-dimensional drift flux analysis and critical Weber number for stable bubble size. The model was used to predict the bubble size and gas void fraction as a function of the gas and liquid flow velocities within the bubbly flow regime. It could also be used to predict the gas and liquid flow conditions at which the transition from bubbly to churn-turbulent flow occurs. Li Tao et al.¹⁰⁸ developed a mathematical model to study inclusion removal by injecting gas into the ladle shroud. They reported that the greater the number of bubbles generated, the better this was for maximum removal of inclusions. Zhang et al.¹⁰⁹ reported on the effect of nozzle diameter on bubble sizes formed in a water model. The finer the injection nozzle, the smaller are the bubbles formed. Hae-Geon Lee and co-workers^{110,111,112} investigated the removal of inclusions from “liquid steel” using “fine” gas bubbles in a water model. The bubbles were created by injecting air into a model ladle shroud, immediately below

the slide gate. They reported that the governing factor is one of wettability, as quantified by the contact angle of the inclusion with the water, the larger the contact angle, the higher was the efficiency. They discussed bubble formation and dispersion in the model ladle shroud, and mentioned that bubbles in the size range 0.5-1 mm can be formed in water. However, no exact measurement of bubble size is given in their work, nor has there been any comparison to bubbles formed in steel melts. Koria and Srivastava¹¹³ investigated the residence time distribution of steel melts associated with an argon shrouded stream of water pouring in a water model tundish. In the model, the air shrouded water stream entered the tundish and flow patterns and RTD's were studied using the impulse response technique. They concluded that the mean residence time depends on shroud diameter, air rate and submergence depth of the shroud. From the above discussions, it is clear that many researchers have studied the injection of gas in tundish nozzles, inclusion removal by gas shrouding, etc., but no one has reported on the trajectory of these bubbles within a water model tundish, or how they affect the liquid flow field within the model tundish. Similarly, the formation of an exposed 'eye' of hot steel and/or slag, due to gas injection through the shroud has not been considered in any of the work mentioned above. Chattopadhyay et al.¹¹⁴ have reported on the effect of inert gas shrouding on fluid flow within the tundish, and associated slag movements. For this, they used a 2D mathematical

model. However, a 2D numerical model has definite drawbacks versus a 3D model, especially when modelling a three dimensional delta-shaped tundish. Similarly, turbulence is three dimensional. Perhaps the only advantages are the shorter computational times, and its relative ease. For the present computations, the ANSYS 12.0 package was used to develop the 3D mathematical model, and the results were compared with water model experiments, using a **full-scale** delta shaped tundish, and a third scale equivalent.

5.2 Experimental and mathematical modelling procedures

In the physical modeling research, a full-scale water model and its one third scale equivalent was used to simulate the gas-shrouding process. Liquid steel was replaced by its low-temperature aqueous analogue (water), while argon was substituted by compressed air. A schematic diagram of our system is given in Figure 5.1 below. The square tank above the tundish was used to provide the 3-m head pressure of water, and was used to control the inflow rate of water into the tundish. A flow rate of $0.17 \text{ m}^3/\text{min}$ was maintained through the ladle shroud, so as to maintain a steady-state height of 500 mm of water within the tundish. The immersion depth of the ladle shroud was 60 mm. Compressed air was injected from just below the slide gate, at volumetric flow rates ranging between 2 and 10 pct of water entry flows. The flow rate of air was controlled with the help of a flow meter (Cole Palmer Instrument Company, Barrington, IL).

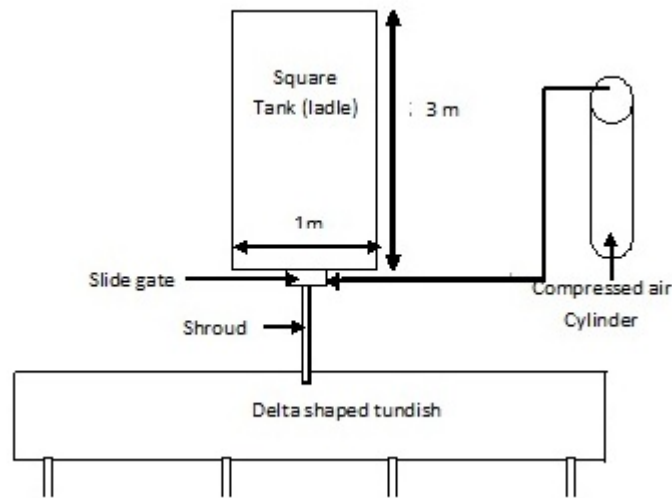


Figure- 5.1 Schematic diagram of the experimental setup.

The upper slag phase was simulated using white coloured polyethylene beads (density = 920 kg m^{-3} , diameter = 2.5mm to 3mm) that were poured uniformly over the free surface of water in the tundish, prior to the experiment. The thickness of the polyethylene bead layer in the vicinity of the ladle shroud was $0.02\text{m} \pm 0.002\text{m}$. For the one third scale model, a flow rate $0.01\text{m}^3/\text{min}$ was maintained from the inflow, so as to obtain a steady state height of 167mm, based on Froude ($\frac{U^2}{gL}$) similitude. A 0.01m thick layer of mineral oil (density= 870 kg m^{-3} , viscosity = 0.017 Pa.s) was used to simulate the slag phase in the small scale model. High Definition video photography was used to visualize bubble tracks, together with slag layer movements and disruptions. Neither flow modifiers nor flow control devices were used for any experiments described in this Chapter.

The mathematical model of the two phase gas/liquid flows in the ladle shroud was based on the following assumptions:

- (1) The liquid passing down the shroud (water) is an incompressible, Newtonian fluid.
- (2) The two phase flow within the shroud is predominantly bubbly; discrete bubbles are formed at the entry location, which then are evenly distributed as they move down the shroud, in conjunction with the down-flowing water. This assumption of bubbly flow holds true because the volume fraction of gas in the shroud was not greater than 10%. Above that, gas curtains are formed instead of gas bubbles and hence the discrete phase approach is incorrect.

The standard k - ϵ model of Launder and Spalding⁷⁹ was used, coupled with the discrete phase model. These models are explained in great detail in Chapter 3. Two-way turbulence coupling was used to capture the effects of the discrete phase on the primary liquid phase. In the two way turbulence coupling, as the trajectory of a particle is computed, a track of the momentum gained or lost by the particle stream that follows that trajectory is kept, and these quantities are then incorporated in the subsequent continuous phase calculations. Thus, while the continuous phase always impacts the discrete phase, we can also incorporate the effect of the discrete phase trajectories on the continuum phase. This two-way coupling is accomplished by alternately solving the discrete and continuous

phase equations, until the solutions in both phases have stopped changing⁸³.

As noted, the present calculations were carried out using the ANSYS FLUENT 12.0. The drawing of the system and meshing were performed using GAMBIT 2.4.6. Calculations were performed in one half of the tundish, assuming a vertical symmetry plane between the two sides of the tundish, and ignoring any potential large scale transient turbulent motions. This was done to save on computational time. All velocity components were set to zero at the walls by using the no-slip boundary condition. At the free surface of the liquid, the shear stress was set as zero. The primary fluid was taken to be water and the discrete phase material was set as air.

In the numerical modeling, the steady flow field solution was first obtained in the absence of any gas injection. After obtaining the steady state velocity field, gas injection was started under transient conditions, using a time step size of 1 millisecond (10^{-3} s).

During the initial steady state calculations, the SIMPLE^{81,82} algorithm, along with a first order upwind scheme for momentum, k , and ϵ equations, was used. Default values of the under relaxation factor were used i.e. unity for body forces, density and turbulent viscosity; 0.8 for the k and ϵ equations; 0.7 for the momentum equation. For pressure, the standard scheme was used, with an

under relaxation of 0.3. After obtaining the steady state velocity field, the inert gas injection was started, at which point the under relaxation factors for k and ε were changed to 0.5. For the unsteady simulations the PISO algorithm was used for pressure-velocity coupling and the second order upwind scheme was used momentum, k , and ε equations and PRESTO for pressure.

For tracking the upper slag phase, the VOF multiphase model was used. The VOF model is also explained in Chapter 3. The primary phase was considered as water and mineral oil was taken as the secondary phase.

5.3 Results and discussion

5.3.1 Bubble trajectories in the tundish

The 3D numerical model proved very effective in predicting bubble trajectories within the tundish. The gas flow rate was varied from 4% to 10% of the volumetric flow rate of water. The bubble tracks in the full scale tundish for 6% gas flow are shown in Figure 5.2. As seen, at first the bubbles come down the ladle shroud together with the liquid and touch the base of the tundish. Then, due to their buoyancy, they rise almost straight back up to the surface, forming a bubble plume within the tundish around the ladle shroud. These rising bubbles disrupt the protective slag phase (polyethylene

particles or mineral oil), creating a reverse flow, and forming an exposed 'eye' of water (steel).

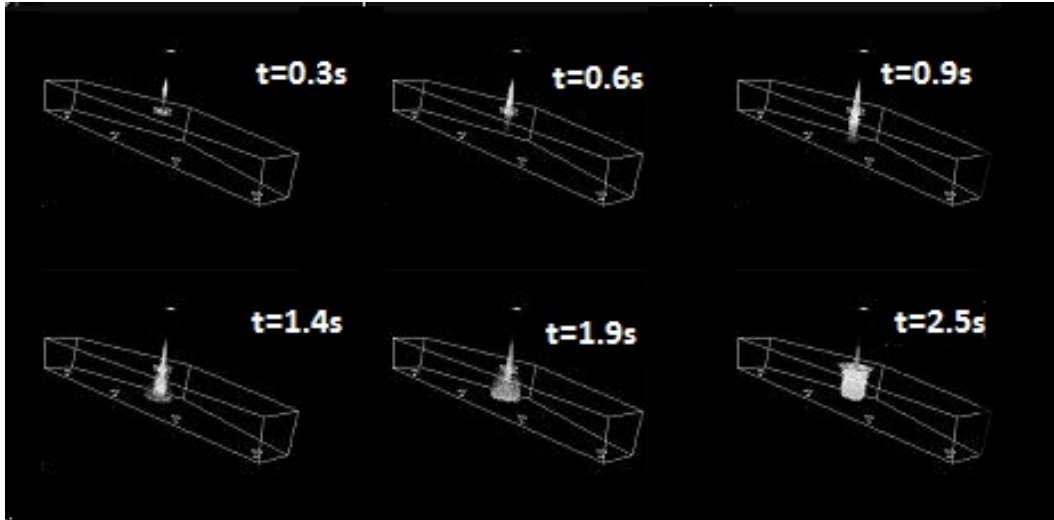


Figure-5.2 Numerically predicted temporal evolution of the bubble plume for gas injection at 6% of water entry flows in the full scale tundish.

Figure 5.3 shows the temporal evolution of the bubble tracks with 10% gas injection. Here, the greater initial gas flow rate, and the larger buoyancy of the forming column, prevents the initial bubbles from reaching the bottom of the tundish. Also, once steady state conditions are reached, the area over which the bubbles spread out around the shroud is very large, as compared to that for 6%. This is due to the overall buoyancy force, which for 10% gas injection is almost double that of 6%.

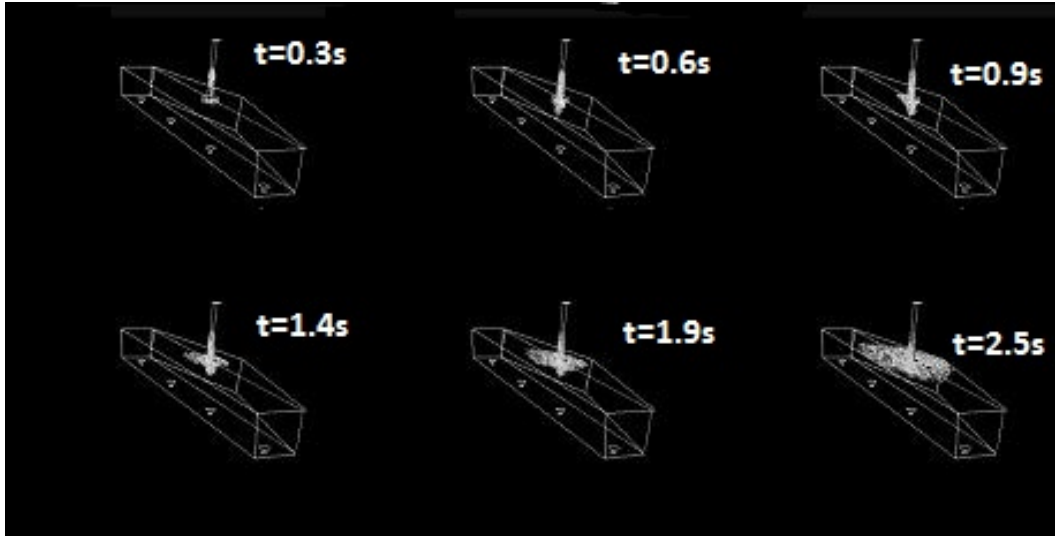


Figure-5.3 Numerically predicted temporal evolution of the bubble plume for gas injection at 10% of water entry flows in the full scale tundish.

When the mathematical modelling results are compared with the physical modelling results, the same trend was observed. These are shown in Figures 5.4 and 5.5.

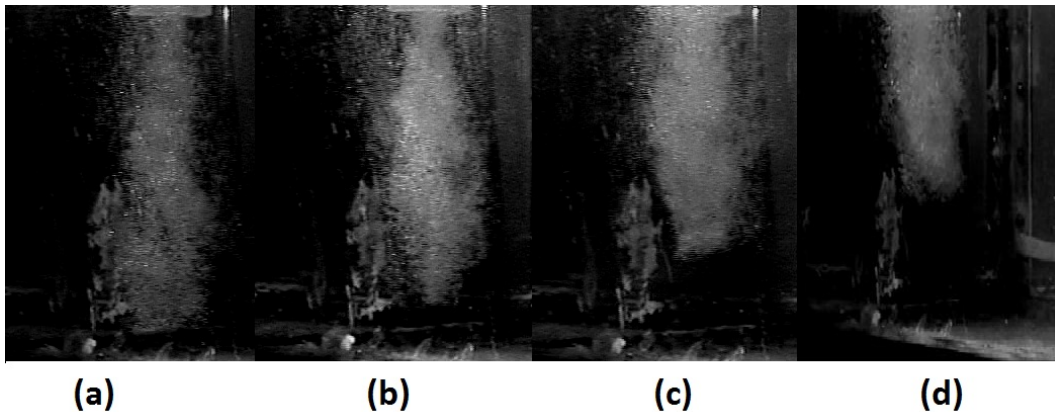


Figure-5.4 Bubble plume in the full scale water model for gas injection at (a)4% (b)6% (c)8% (d)10% of water entry flows.

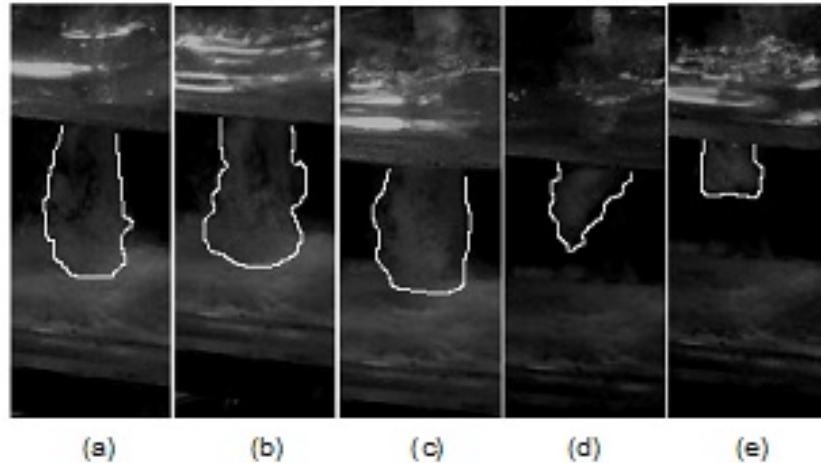


Figure-5.5 Bubble plume in the one third scale water model for gas injection at (a) 2% (b) 4% (c) 6% (d) 8% (e) 10%, of water entry flows.

The depth of penetration of the bubble column varies with the volume fraction of gas injected. This was measured from the full scale water model experiments and compared with those predicted from the mathematical model. The percentage error was also calculated and was found to be within +15%. Figure 5.6 shows the numerically predicted maximum depths of penetration of the bubble column (in the full scale tundish), which decreases as the amount of gas injected in the entering liquid is increased. The corresponding experimental and computed penetration values, as a function of the percentage of gas blown, are given in Table -5.1. As seen, the model tends to slightly over-predict the degree of penetration.

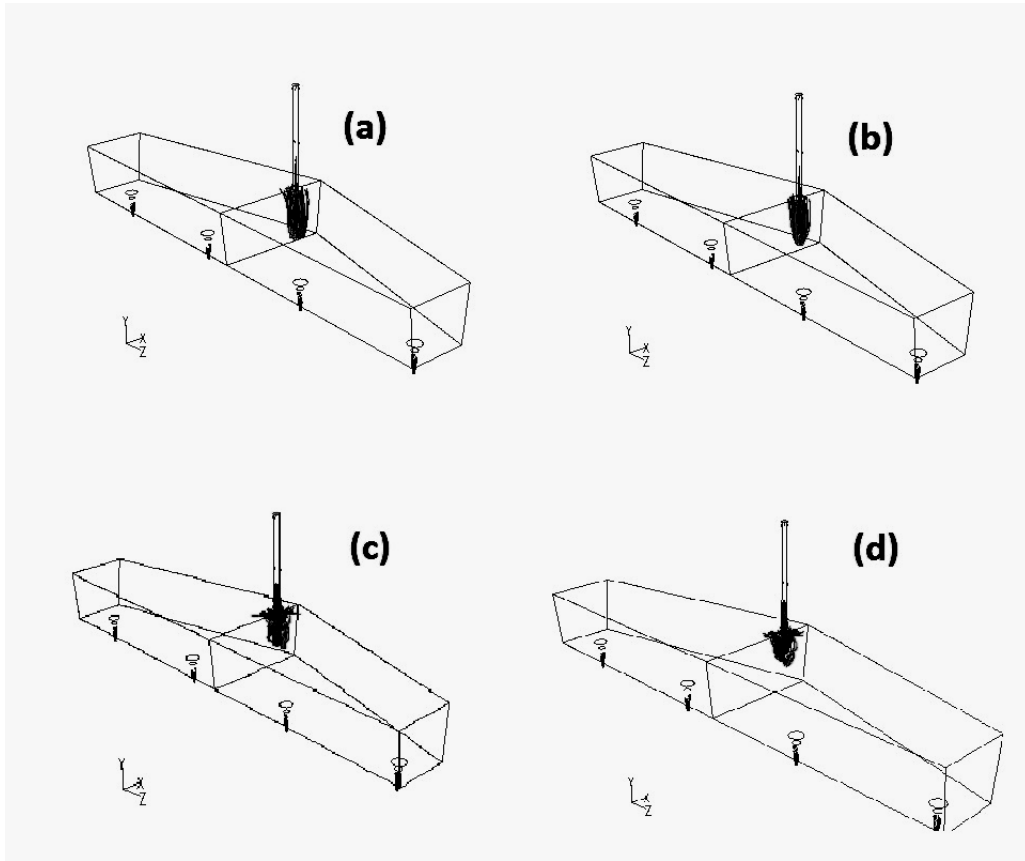


Figure-5.6 Numerically predicted penetration depth of the bubble column in the full scale water model for gas injection at (a)4% (b)6% (c)8% (d)10% of water entry flows.

Volume fraction of gas injected	Experimentally measured penetration depth of the bubble column from the free surface of the tundish (m)	Numerically predicted penetration depth of the bubble column from the free surface of the tundish (m)	Percentage Error
4%	0.5	0.5	0%
6%	0.416	0.433	+4.09%
8%	0.324	0.355	+9.57%
10%	0.267	0.294	+10.11%

Table-5.1 Depth of penetration of the bubble column from the free surface of the tundish.

Another interesting observation was made from this 3D model. The trajectories of micro bubbles in the size range 150-500 μ m are totally different from those of the 3-5 mm diameter gas bubbles. Since micro bubbles have much lower buoyancy forces compared to 3-5mm sized bubbles in steel, they tend to be in the Stokesian flow regime, with the bubbles fully entrained within the entering flow of liquid. They therefore spread out within the tundish with the liquid (Fig -5.7), rather than decoupling to form a rising bubble column. This was not reported by previous researchers. It is probable that this bubble spreading phenomenon could be very beneficial for removing smaller inclusions from steel baths, so as to produce super clean steel.

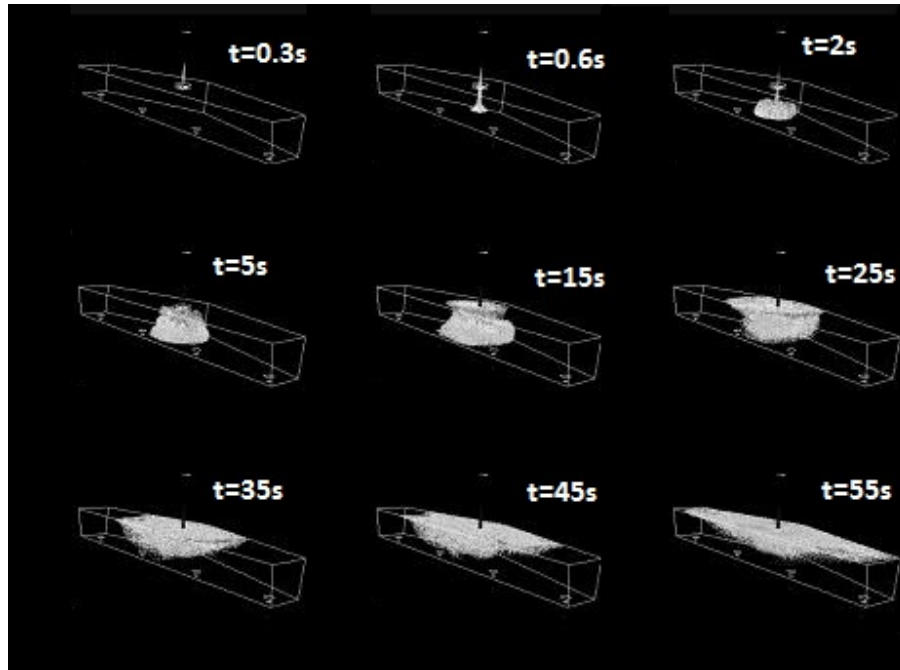


Figure-5.7 Predicted bubble trajectories when micro bubbles of size 150-400 μ m are formed in a tundish.

The fluid flow modifications were validated with some water model experiments, in which surfactants were injected simultaneously with compressed air into the ladle shroud, thereby generating 0.05-0.3 mm micro – bubbles. The trajectories of these micro-bubbles were similar to our numerical predictions (Fig-5.8), and are quite different from the larger bubbles that are normally associated with gas bubbling in steelmaking operations. For these, the high surface tensions and non-wetting properties make the stability of injected micro-bubbles most unlikely.

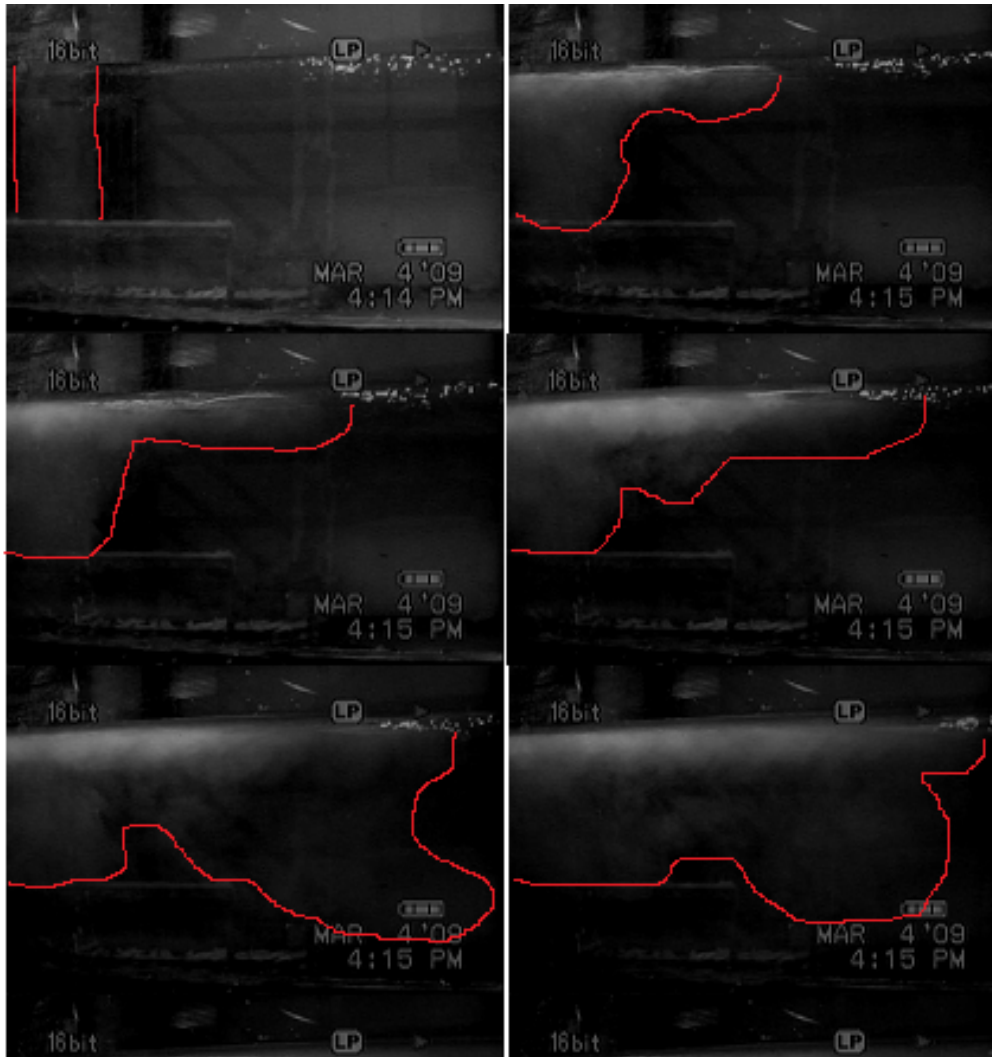


Figure-5.8 Experimentally observed micro bubble cloud movement in the full scale water model tundish.

5.3.2 Fluid flow patterns in the tundish

The flow fields predicted from this 3D numerical model are next considered. Figure 5.9 shows the flow field at the top surface of the tundish with different amounts of gas injected. It is clearly seen that the fluid vectors are pointing away from the shroud and thus reversed flows are formed which tend to push the slag layer away

from the shroud. The higher the amount of gas injected, the stronger are these reverse flows.

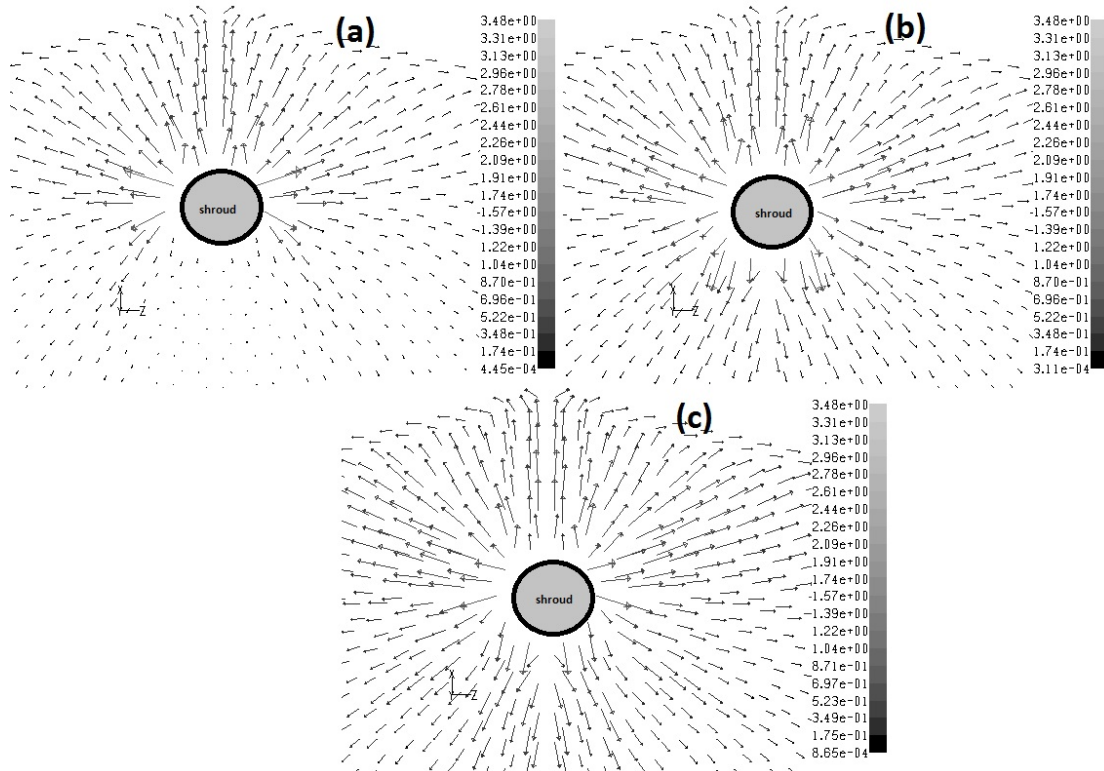


Figure-5.9 Predicted flow field (ms^{-1}) on the surface of the tundish (around the ladle shroud) with gas shrouding at (a)4% (b) 6% (c) 10%, of water entry flows.

This fact was also validated with 2D PIV experiments in the full scale water model. Reverse flows were detected on a plane just beside the ladle shroud and these are shown in Figure-5.10.

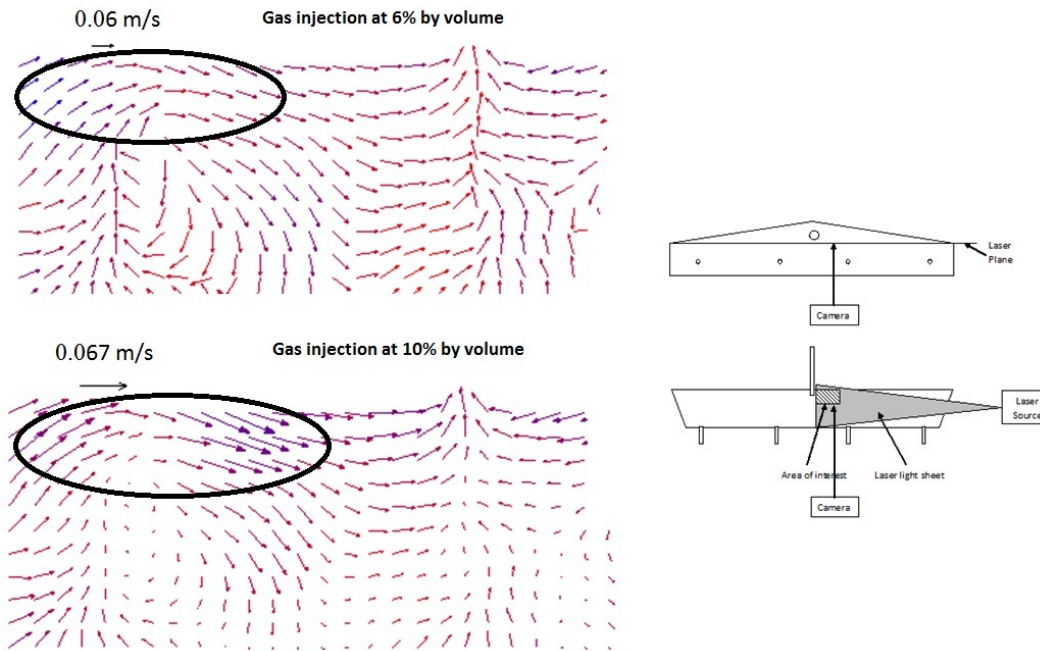


Figure-5.10 Velocity field (ms^{-1}) on a plane just beside the shroud measured by 2D PIV

Figure 5.11 shows the numerically predicted flow fields around the ladle shroud on the surface of the tundish without any gas injection. It is seen that the vectors now point towards the shroud and thus prevents the formation of an “eye” around it.

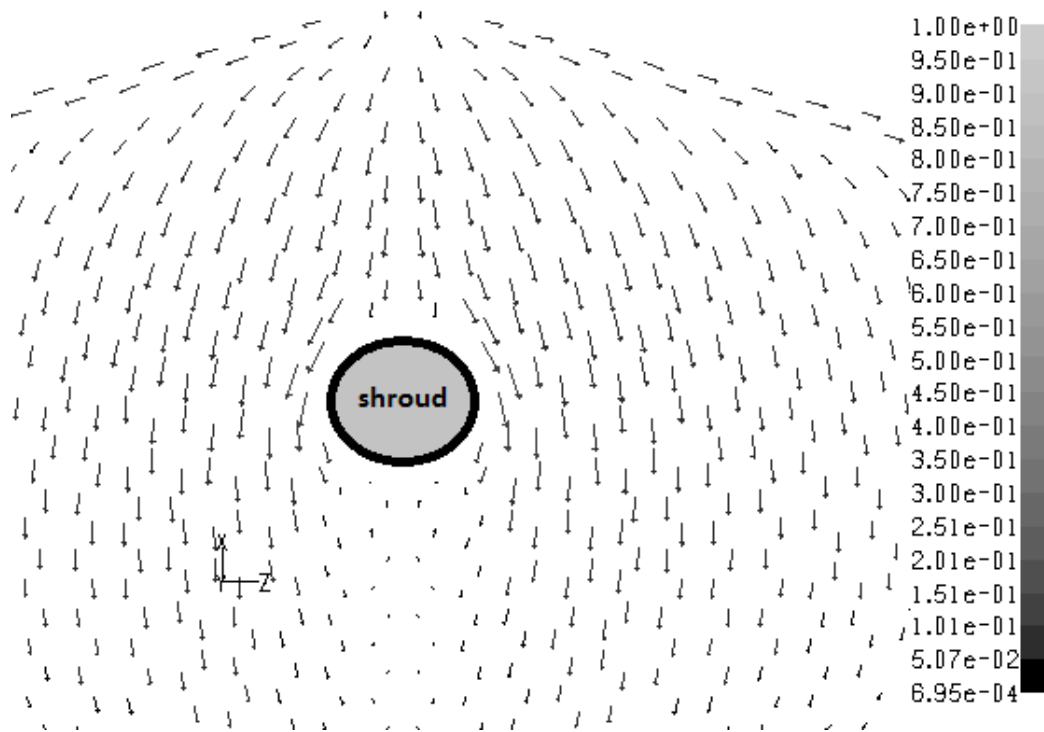
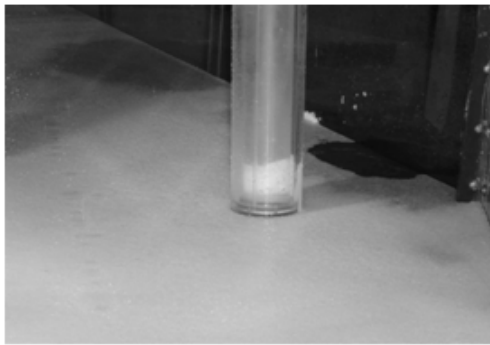


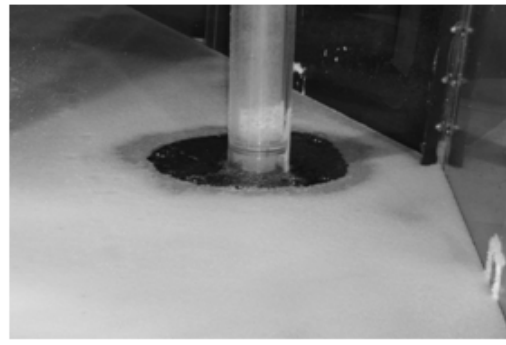
Figure-5.11 Predicted flow field (ms^{-1}) on the exposed liquid surface of the tundish (around the ladle shroud) without gas shrouding (no reverse surface flows).

The area of the exposed “eye” varies with gas flow rate, and slag thickness, and this is shown in Figures 5.12 and 5.13. Figure 5.12 represents full scale water modelling with polyethylene beads as the slag phase, whereas Figure-5.13 represents one third scale water modelling with mineral oil as the slag phase. It is interesting to note that both systems behave similarly. Initially, without gas injection, the simulated slag phase (polyethylene beads or mineral oil) completely covers the water in the tundish. Then with increasing gas flow rate, the size of the exposed eye increases, and then when gas

flow is stopped, they are restored back to their original positions. For low gas flow rates, the reverse flows are not so strong and hence the area of the exposed eye is small. For high gas flow rates, there are stronger reverse flows and so the area of the exposed eye is greater.



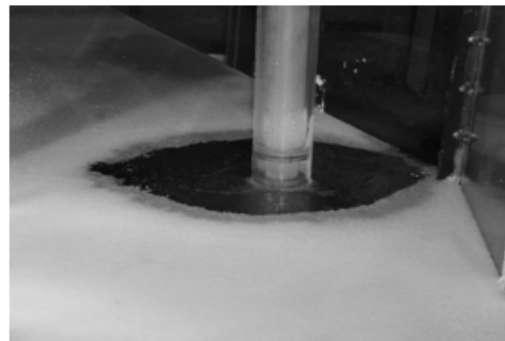
0% volume fraction of gas



2% volume fraction of gas



4% volume fraction of gas



6% volume fraction of gas

Figure-5.12 Showing exposed 'eye' around the shroud in the full scale water model due to inert gas shrouding

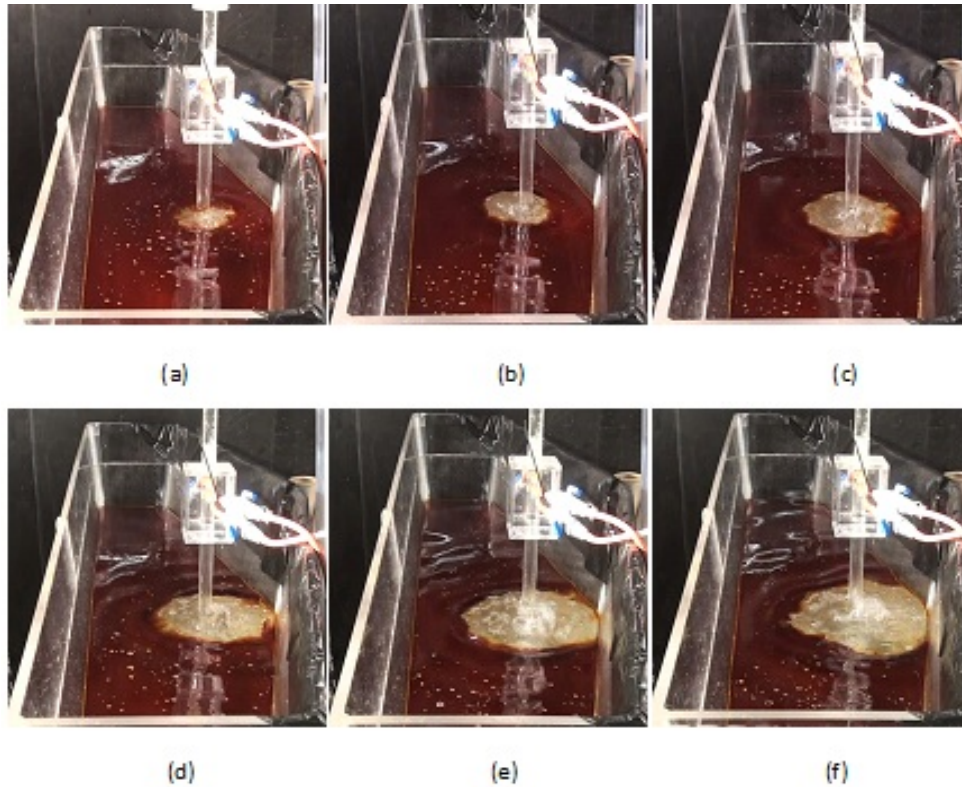


Figure-5.13 Showing exposed 'eye' around the shroud in the one third scale water model for gas injection at (a) 2% (b) 4% (c) 6% (d) 8% (e) 10% (f) 12%, of water entry flows.

The size of the exposed 'eye' was measured from the full scale water model and was compared with that predicted numerically. To measure the area of the exposed 'eye' from the numerical model, regions of high surface velocity were identified and the radius of the 'eye' was calculated indirectly. For this, the edge of the 'eye' was assumed to be located where the velocity was ten times higher than the rest of the tundish (Figure-5.14). The area over which this high velocity region extends should correspond to the area of an exposed

'eye', depending on slag thickness. The values of the average radius of the exposed 'eye' are given in Table-5. 2 along with the percentage errors. The error was always less than +15%.

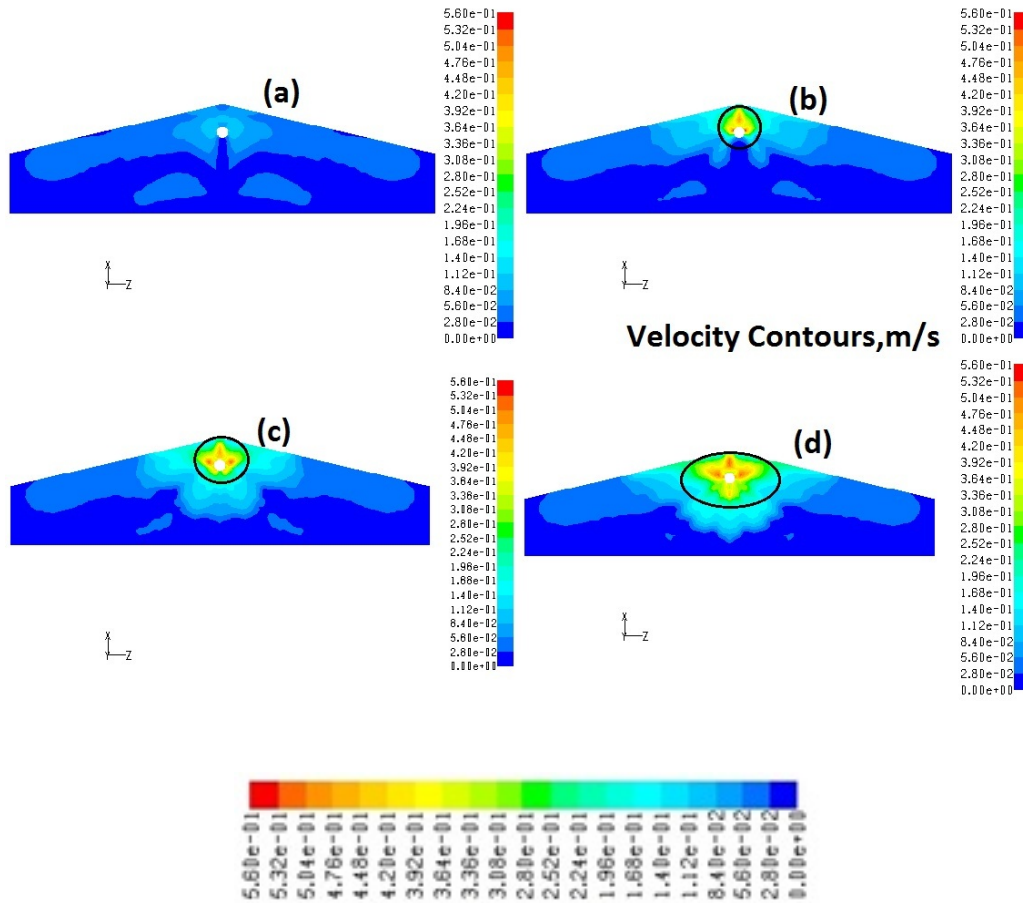


Figure-5.14 Numerically predicted velocity contours (ms^{-1}) on the surface of the tundish for gas injection at (a) 0% (b) 4% (c) 6% (d) 10%, of water entry flows

Volume fraction of gas injected	Experimentally measured average slag 'eye' radius (m)	Numerically predicted average slag 'eye' radius(m)	Percentage Error
4%	0.227	0.255	+12.55%
6%	0.3063	0.323	+5.45%
10%	0.43	0.474	+10.23%

Table-5.2 Average radius of the slag 'eye' measured from the full scale model.

This amount of error can be tolerated, considering the randomness of turbulent flows. So without going into an actual multiphase model, an estimation of the 'eye' diameter could be obtained.

5.3.3 Modelling of the exposed 'eye' using the multiphase VOF model

Modelling of the slag eye due to inert gas purging in steel ladles has been an active area of research for the last few years. Krishnapisharody and Irons¹¹⁵ performed water model experiments to study the formation of spouts on the bath surface in gas stirred ladle systems. The experimental data was used to correlate, the spout dimensions to the operating variables, namely, the gas flow rate and heights of water and oil layers. Non dimensional

representations of the spout height revealed that factors such as the diameter of the ladle, size, and type of gas injector and physical properties of the gas-liquid system did not play any major role in the spout formation. Krishnapisharody and Irons^{116,117} also developed mathematical models to estimate slag eye size in gas stirred ladle systems. Their model computed the eye size from the primary operating variables of the ladle and proved to be reliable in a variety of multi-phase systems. Baokuan et al.¹¹⁸ developed a three phase mathematical model to study the formation of exposed eyes in gas stirred ladle systems. Multiphase Volume of Fluid (VOF) method was used to simulate the behaviour of the slag layer. Numerical simulation was conducted to clarify the transient phenomena of gas injection into the molten steel. When argon gas was injected into the molten steel in a ladle, the gas rising passage was formed near the plug, and then bubbles were created in the molten steel. The rising gas bubbles impinged on the slag intermittently and broke the slag layer to create the slag eye. Simultaneously, the wave at the slag-steel interface was formed and the wave frequency increased with the increase of argon gas flow rate for one off-centered plug case. Their modeling simulations showed that the diameter of slag eye changed from 0.43 to 0.81 m when the flow rate of argon gas was varied from 100 to 300 NL/min for a 220 ton ladle. The relationship between non-dimensional areas of slag eye and the modified Froude number was in good agreement with the experimental data reported

in the literature. At the same total gas flow rate of 300 NL/min, the two-plugs generated two eyes with the diameters of around 0.6 m. Since the significant deformation of slag layer occurred during gas stirring operation, the thickness of slag became thin near the slag eye and thick near the ladle wall, respectively. The downward flow velocity of steel at the slag eye periphery might be affected significantly by flow rate of Ar gas. Therefore, when the downward flow velocity would be larger, the more emulsification of slag could be expected. Peranandhanthan and Mazumdar¹¹⁹ performed physical modelling to estimate the slag eye area in bottom purged ladles. They concluded that the slag eye area increased as the gas flow rate and depth of bulk liquid were increased. On the contrary, the size of the exposed eye decreased with increasing thickness of the upper buoyant phase. Physical properties of the slag phase affected the area of the 'eye'. They developed a new simple correlation (which included three Froude number, Reynolds number and density ratio) which could effectively predict the slag eye area in both aqueous and industrial scale ladle systems under a wide range of operating variables and upper slag phases. Mazumdar and Guthrie¹²⁰ reported on the input energy dissipation by an upper buoyant phase in gas stirred ladle systems. They mentioned that several factors like thickness of the slag layer and its properties like viscosity and density, has an important effect on the exposed eye area. A thicker slag phase would result in the formation of a smaller

exposed 'eye' and so is the case with a highly viscous slag phase. A highly viscous slag phase would tend to dissipate more energy due to frictional effects and viscous dissipation within, resulting in a smaller slag eye opening. Llanos et al.¹²¹ developed a three dimensional three phase mathematical model to study the fluid dynamics in slag covered gas stirred ladles. Four cases were considered using one and two argon injection inlets with different configuration, where the multiphase steel/slag/argon system was simulated numerically in Three-dimensional transient conditions and a water/oil/air system for the physical model was considered. The Volume of Fluid (VOF) model was employed to simulate the interaction between the phases considering the surface tensions. The simulation results were evaluated using a fluid dynamic analysis of the systems and by a numerical prediction of three important operational parameters, namely, mixing time, lining refractory wear and slag opening. The implementation of two argon inlets did not reduce the mixing time; however, the slag layer opening was decreased by 30%, and the refractory wear in terms of the skin friction coefficient value was also decreased by 63 %. A good agreement was obtained between the physical and mathematical modelling results, where the VOF model showed to be a powerful tool to simulate ladle gas stirring operations. From the above discussions it is clear that a lot of researchers have modelled exposed eyes in gas stirred ladle systems, but none of them ever

tried to simulate it in a tundish. As seen in the previous section, the injection of inert gas into the shroud results in the formation of an exposed 'eye' around the ladle shroud, and this is primarily caused because of reversed flows created on the bath surface. Also, when bubble trajectories were examined it was clear that a bubble column was formed just beneath the ladle shroud, within the tundish. However, this bubble column was not a conical plume, as in the case of bottom purged ladles. Most of the researchers, who performed mathematical modelling, used three phase (VOF) mathematical models to simulate the formation of the 'eye'. In this study, the formation of the 'eye' was modelled by using the discrete phase model and a two phase VOF model in synergy along with the $k-\epsilon$ turbulence model. Review of the literature reveals that, this approach has never been used before to simulate the exposed 'eye'. The Volume of Fluid (VOF) approach is discussed in detail in Chapter 3. Very fine mesh was necessary to obtain higher accuracy of the results. Considering this fact, the one third scale tundish was chosen to develop this model. Around three million eight hundred thousand (3.8×10^6) tetrahedral cells were generated inside the domain and this was the maximum that could be done with the computers available. In this model, the phenomena considered were, fluid flow, turbulence, discrete phase motion and multiphase flow. Also, to efficiently track the formation of the exposed 'eye' a very small time step of 10^{-5} s was used and this was the maximum

allowed. Increasing the time step any further, resulted in divergence of the solutions because of increased Courant number. The maximum Courant number during the solutions was 0.33. From the above discussions it is very clear that the simulations for the exposed 'eye' would require long computational times. Each simulation took around 40-45 days in order to simulate 6-7 seconds on a computer incorporating 8 processors and 16 GB of RAM. Gas injections of 2%, 4% and 6% by volume through the ladle shroud were considered, and were modelled as discrete gas bubbles using the discrete phase model. For the VOF model, the primary phase was taken as water and the secondary phase was taken as mineral oil (density= 870kg m^{-3} , viscosity = $0.017\text{ Pa}\cdot\text{s}$ and interfacial tension = 0.0425 Nm^{-1}). In reality, a third phase of air is present on the top of the slag, but it could not be considered here, because then the simulations were out of range of the memory available. Another interesting observation was that whenever the volume fraction of injected gas was set as 8% and higher, the computations exceeded memory after a very short period of time. The probable reason for this may be attributed to the fact that for 8-10% gas injection more bubbles need to be tracked as opposed to that for 6% and lower. So for tracking this extra amount of bubbles, some computational memory was used and this caused the overall solution to be out of memory.

In the physical model, it was seen that after the start of the gas injection, the exposed 'eye' was formed in about 2 seconds and the size of the 'eye' became stable after around 6-8 seconds. So for the mathematical model, for all the three gas flow cases, the simulations were done for 6 seconds. Figure- 5.15 below shows the exposed 'eye' formed in the tundish for gas injections varying between 2-6% by volume after 6 seconds of gas injection. The red region represents mineral oil and the blue region is water. It is clearly seen that as the volume fraction of gas is increased, the area of the exposed 'eye' increases. The average radius of this 'eye' was measured and compared with that measured from the experiments in the one third scale tundish. The percentage error was reported and it was found that the errors are well below 10%. The mathematical model always over predicted the 'eye' radius. This error will be always present because in reality, there is an upper phase of air and the free surface fluctuates. Finally, if the mesh size can be reduced further, maybe higher accuracy will be achieved.

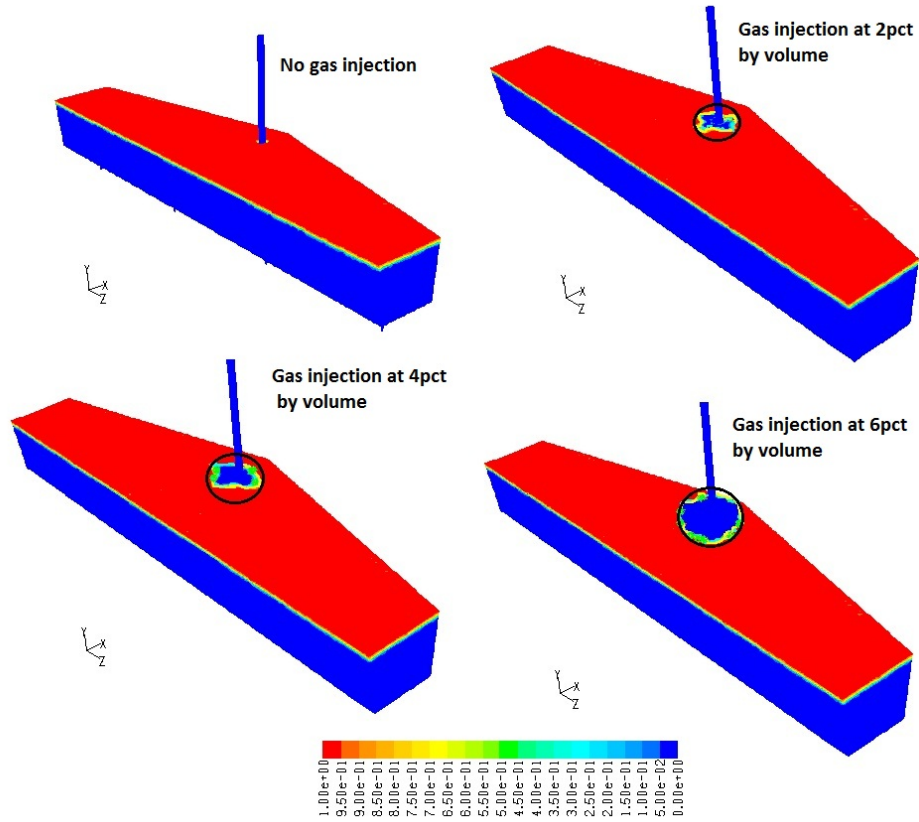


Figure-5.15 Predicted contours of the second phase (mineral oil) in the tundish after 6 seconds of gas injection

Volume fraction of gas injected	Experimentally measured average slag 'eye' radius (m)	Numerically predicted average slag 'eye' radius(m)	Percentage Error
2%	0.0527	0.0563	+6.83%
4%	0.0845	0.0913	+8.05%
6%	0.1266	0.1317	+4.02%

Table-5.3 Average radius of the slag 'eye' measured from the one third scale model.

It should be also noted that the shape of the eye is circular, but never a perfect circle and this was evident in both the physical and mathematical model. Figures 5.16 a, b, and c shows the temporal evolution of the exposed 'eye' for 4% gas injection by volume. The shape of the 'eye' changed with time and is evident in Figure 5.16. This phenomenon was captured because of the very small time step used during the simulations. The exposed 'eye' formed after about 0.5 seconds of gas injection. The area of the 'eye' increased with time and became prominent at $t=1s$. After $t=6s$, the area of the 'eye' became stable and continued to remain so till $t=11s$. However, the shape of the 'eye' kept changing and this is quite normal when gas bubbles are displacing a liquid phase. The bubble plume always oscillates with time and hence the mineral oil layer also keeps on displacing.

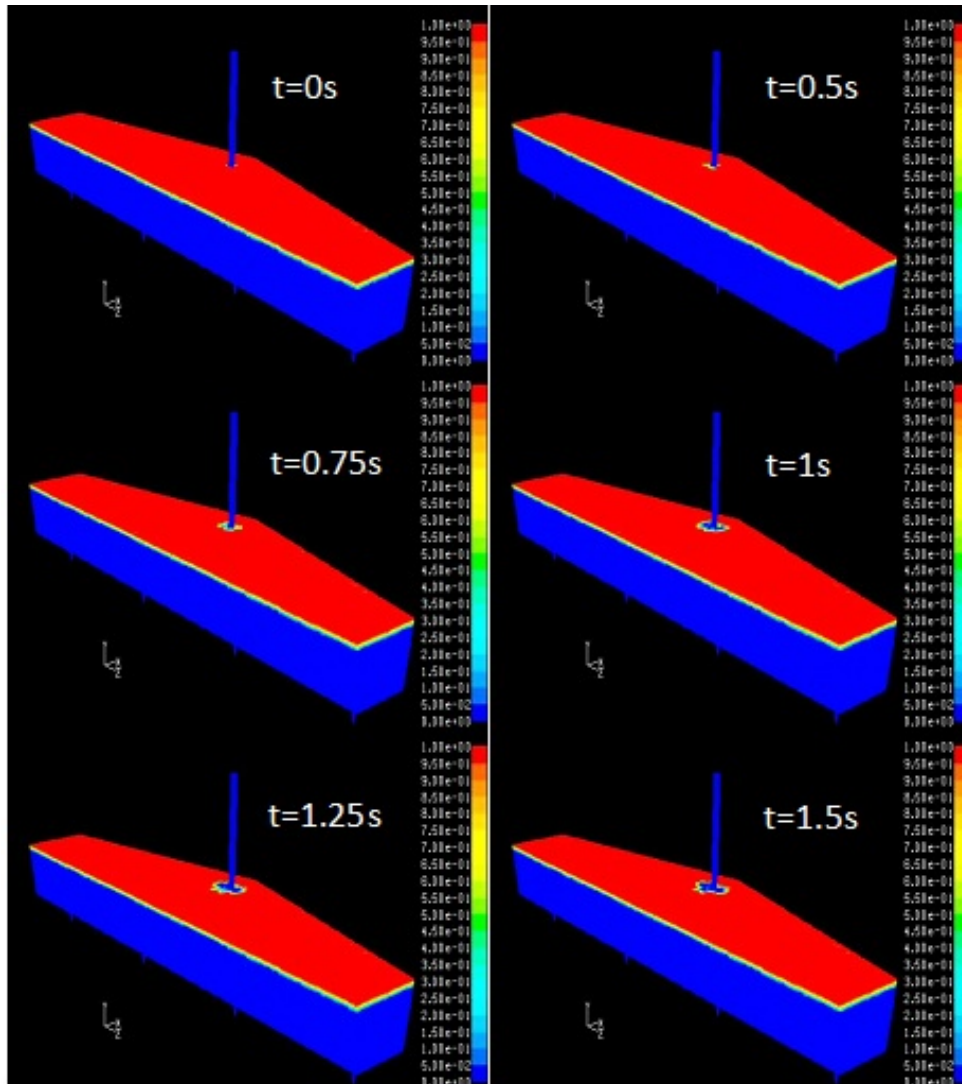


Figure- 5.16(a) Temporal evolution of the exposed 'eye' due to gas injection at 4% of water entry flows.

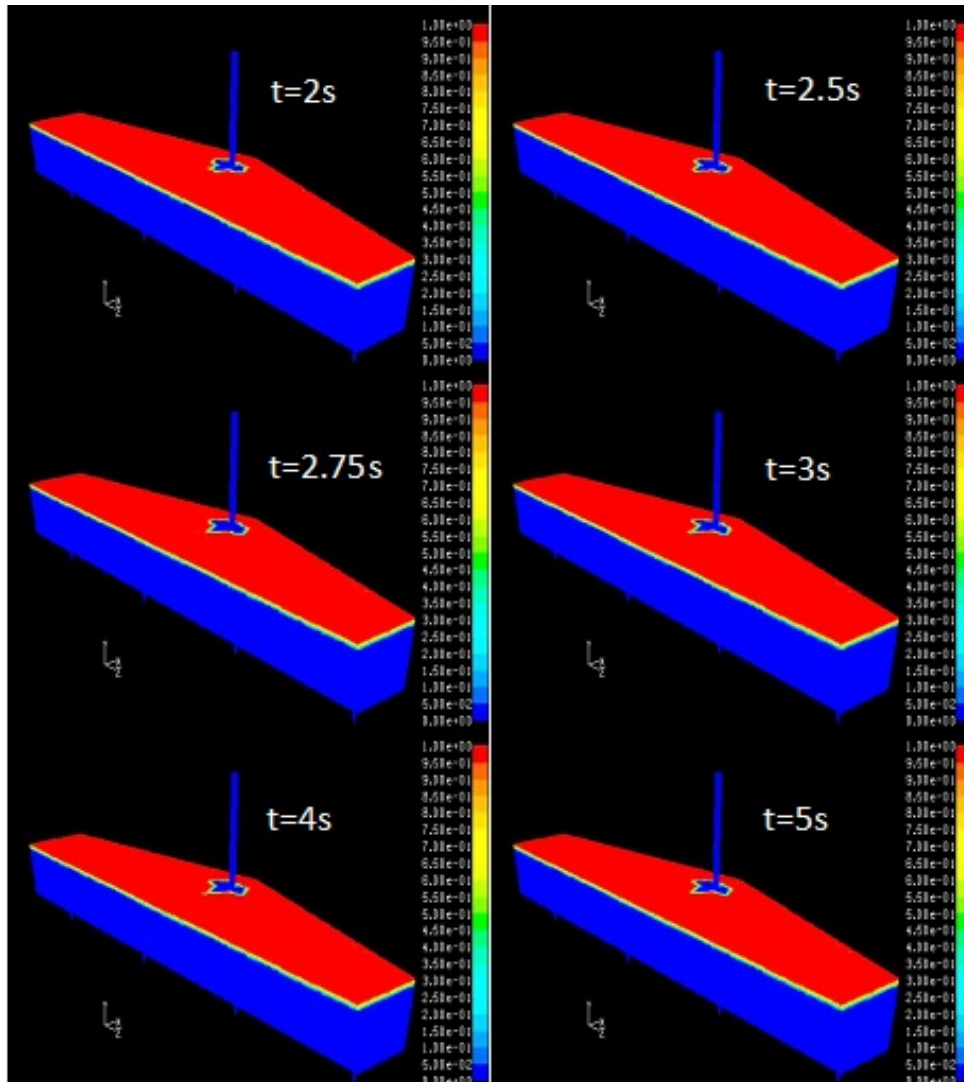


Figure- 5.16 (b) Temporal evolution of the exposed 'eye' due to gas injection at 4% of water entry flows

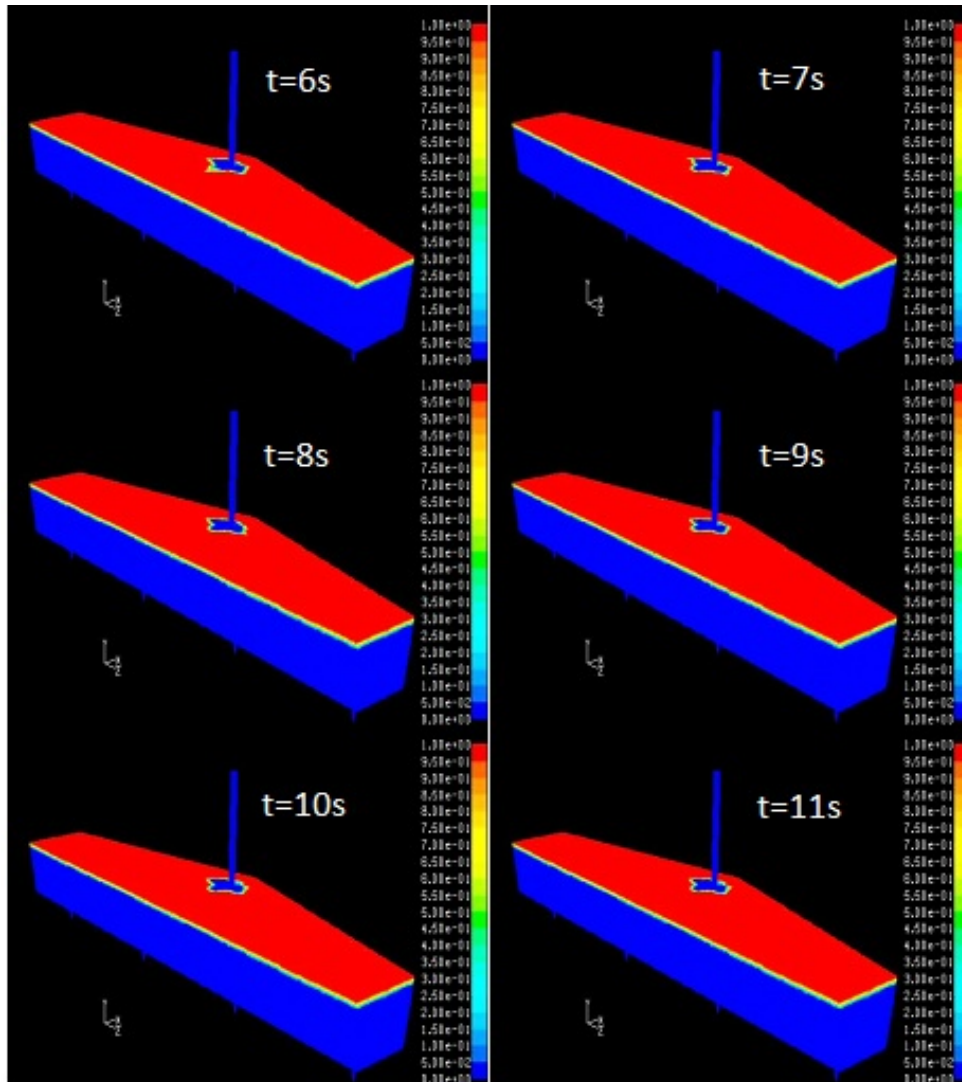


Figure- 5.16 (c) Temporal evolution of the exposed 'eye' due to gas injection at 4% of water entry flows

5.3.4 Effect of inert gas shrouding on residence time distribution

It is already seen that inert gas shrouding, considerably affects the fluid flow behaviour in the tundish. It would be very interesting to know the effect of inert gas injection on residence time distribution in the tundish. Residence time distribution studies were done for two conditions viz. gas injection at 6% and 10% of water entry flows and then compared with the RTD when no gas was injected. 1(N) NaCl solution was prepared and 60 ml of it was pushed through a syringe for each experiment in the one third scale water model tundish. Conductivity meter probes were fixed at the outlets of the tundish, and the change in conductivity was monitored with time. The conductivity meters were connected to a computer through a data acquisition system and the data was recorded in a file. Experiments were done in one half of the four strand delta shaped tundish, assuming perfect symmetry. The nominal residence time of the one third scale tundish was 355 seconds. The dimensionless concentration $C(\theta)$ was plotted against the dimensionless time(θ) as usually done for a tundish and these procedures are explained in detail in the literature⁷. The results were represented in two figures, one for the outer SEN and the other for the inner SEN. Figure 5.17 (a) below shows the RTD curves for the inner SEN. The behaviour of the RTD curve totally changed when inert gas was injected. The

bubble plume formed just below the shroud, resulted in a well mixed zone in the inner SEN region and this was reflected in the RTD curve. The peak value of $C(\theta)$ got lowered with increased amount of injected gas. For all three cases the curves did not extend beyond $\theta=2$.

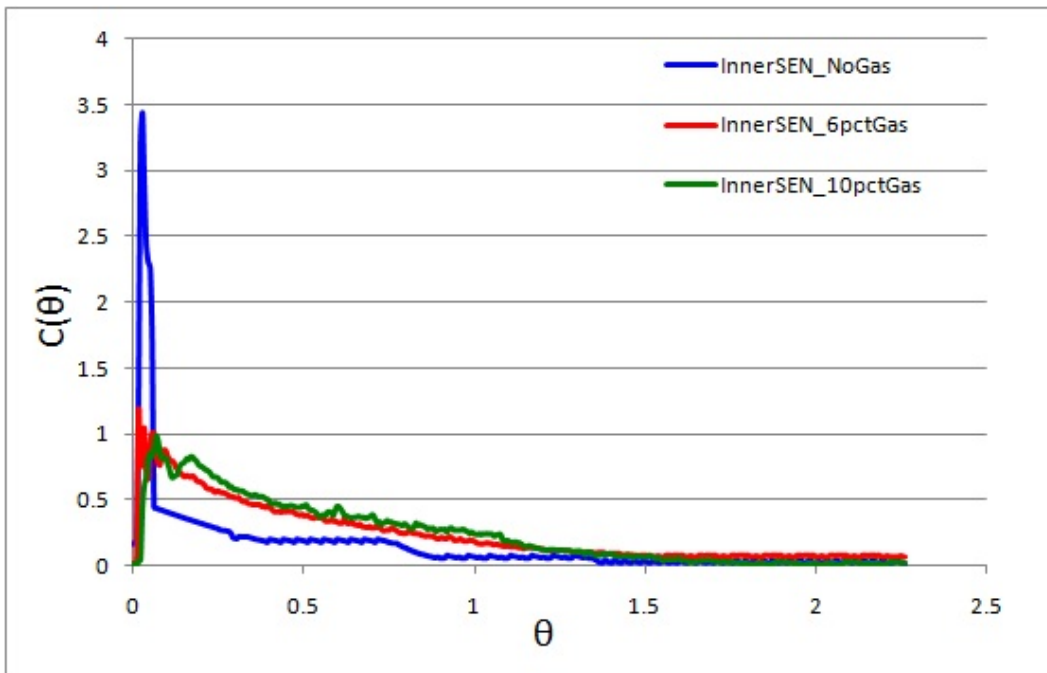


Figure-5.17 (a) Residence time distributions for the inner SEN

Figure 5.17 (b) shows the RTD curves for the outer SENs. As the tracer took longer time to reach outer SEN, the peaks were formed at a higher value of θ . Here, also as the amount of gas injected was increased, the value of $C(\theta)$ got lowered. Multiple peaks were observed for all the three RTD curves and this is normal for the bare tundish. It indicates that a lot of short-circuiting flows are present in

the tundish. The fraction of dead volume was always very low for all three cases, as the curves did not go beyond $\theta=2$.

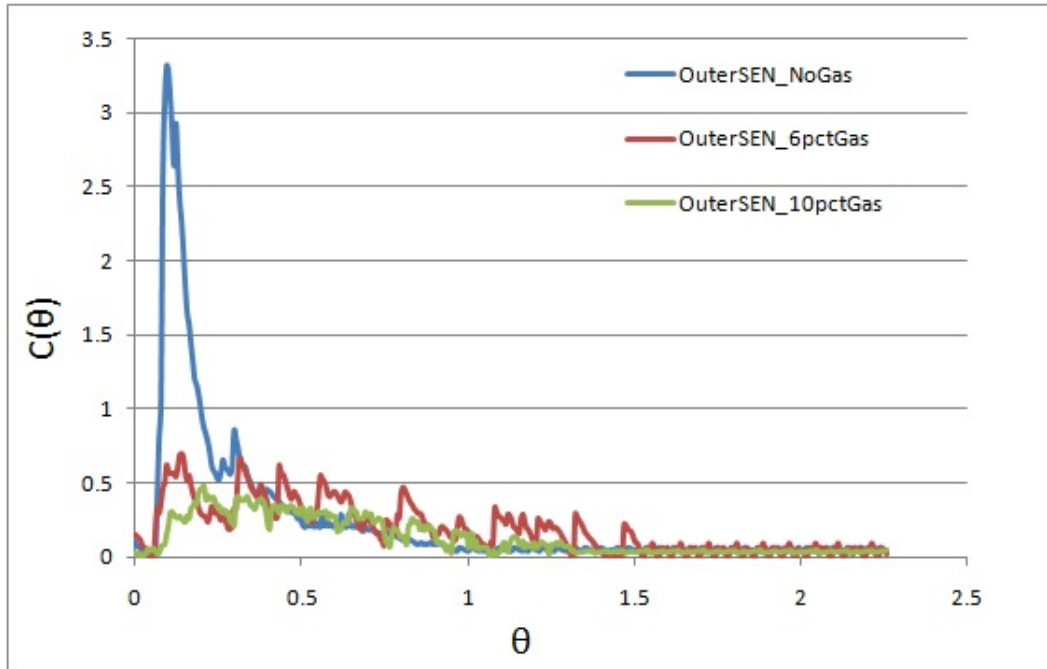


Figure-5.17 (b) Residence time distributions for the Outer SEN

Now let us conclude what has been discussed in Chapter 5. The present 3D numerical model could efficiently predict bubble tracks and flow fields in the tundish, and was validated with water model experiments. In terms of quantitative measurements, the mathematical model was quite robust and the error with respect to experimental measurements is less than 15 percent in all cases. The 3D model took into account the delta shape of the tundish, and gave a better picture of the bubble tracks as compared to the previous 2D model. The spread of the bubble column could be correlated to the area of the exposed eye, using the 3D model. The simple single

phase mathematical model as well as the multiphase model developed using the VOF method were efficient in measuring the exposed 'eye' size, the later being more realistic. While it is very true that the amount of shroud gas should be optimised it is very difficult in practise. From the results, it was seen that at high gas flow rates, the area of the exposed eye was more and so are the chances of greater re-oxidation. Also, higher gas flow rates will increase slag-metal interactions and the slag droplets thereby formed may become entrained into the final product, by passing through the SEN's. An optimum amount of 6% gas by volume injected would be good for plant operations, because the bubble column does not spread too much, and the area of the exposed eye is smaller.

Inert gas injection completely changed the residence time distribution in the tundish. The formation of the bubble column created a mixed zone in the tundish, and it was evident in the RTD curves.

Finally, as micro bubbles could be a very efficient means to cleanse the steel of smaller inclusions (<50 μ m approx.) during tundish operations, their generation in a real steelmaking tundish, represents a difficult, but rewarding, challenge to steelmakers.

6.0 Effect of Ladle Shroud Misalignment on Liquid Metal Quality

6.1 Introduction

The improvement of liquid steel quality during continuous casting operations has been the major goal for steelmakers. Much information on steel quality issues has been archived over the last four decades. Most of the researchers reported on the importance of the tundish shape, size, and use of flow control devices in improving liquid steel quality. However, concerning the entrainment of tundish slag, a very important phenomenon during ladle changes, this has not been considered in most cases. Henrik Solhed et al^{122,123} included slag entrainment in their work, but the majority of the work to date has been done at the McGill Metals Processing Centre by R. I. L. Guthrie and co workers^{124,125}. During melt transfer from ladle to tundish a refractory ladle shroud is used and this is detached and reattached during each ladle change operation. Due to this detaching and reattaching for numerous times, there is a high probability that the nozzle gets mis-aligned by a small angle (5-6 degrees) in any direction. This small bias can affect the output steel quality coming out from a multi-strand tundish. The liquid steel coming out from one of the strands can be dirtier than the other. Chattopadhyay et al¹²⁶ did some preliminary work to study the effect of ladle shroud mis-alignment on steel quality. They used a 2D mathematical model, coupled with full scale water model

experiments. Slag entrainment was used as a parameter to evaluate liquid metal quality during a ladle change operation. They also discussed some remedial measures that should be followed in equivalent steel plant operations. However, the authors felt that there was scope to study this phenomenon in greater detail, using a 3D mathematical model and full scale and one third scale water model tundish experiments. In the present 3D numerical model, the shroud was biased in all possible lateral directions by 4-5 degrees off the vertical. Similarly, the 3D mathematical model was used to predict inclusion trajectories under biased shroud conditions. In the one third scale model, tracer dispersion studies were performed, and filmed with high definition cameras, in order to study the effects of the bias.

6.2 Experimental and mathematical modelling procedures

Physical modelling was performed using a full-scale water model of a twelve tonne, delta shaped, four strand tundish, and its third scale equivalent. The slag phase was simulated by using a 0.02 ± 0.002 m thick layer of polyethylene beads of density ~ 920 kg/m³. A water inflow rate of 0.17 m³ per minute was used to maintain a steady state height of 500mm of water from the inner base of the tundish. The ladle change operation was simulated by stopping the flow of water passing through the shroud for three minutes while the tundish drained, and then fully opening the slide gate to achieve a refilling

rate of around 0.4-0.5 m³ per minute, in order to regain the height of 500mm above the tundish floor, as quickly as possible. During this operation, owing to the high degree of turbulence generated by the plunging free jet of liquid from the ladle, the slag layer adjacent to the entry region is severely disrupted. Many “slag droplets” are entrained within the “steel”, and many of these can then pass through each strand. By counting the numbers of slag beads collected in each strand, the relative performances of the exit strands were assessed, using the full scale water model tundish. Seven slag entrainment experiments were performed for each tundish configuration and the average was taken. Table 6.1 shows an example of a data set of seven experiments performed, and the average and standard deviation reported for slag entrainment tests in a full scale water model tundish fitted with the standard impact pad.

Exp	SEN 1	SEN 2	SEN 3	SEN 4
1	10	6	7	14
2	14	6	4	15
3	3	3	1	6
4	10	3	4	17
5	7	4	3	9
6	8	6	5	12
7	13	7	6	10
Average	9	5	4	12
Stdev	3.73	1.63	1.97	3.80

Table-1 Number of slag beads collected during a ladle change in the full scale water model tundish fitted with the standard impact pad.

As mentioned, the ladle shroud was purposefully biased by 4-5 degrees off the vertical and this is shown schematically in Figure-6.1.

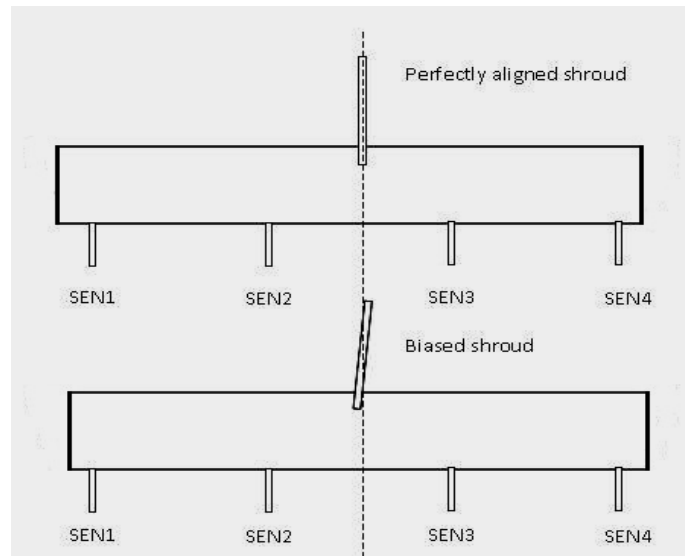


Figure-6.1 Schematic representation of a mis-aligned shroud

The shroud was biased towards SENS 1 and 2. In the small scale water model, mineral oil was used to simulate the slag layer. A red tracer was injected and its mixing behaviour was studied under the biased shroud conditions.

For mathematical modelling the domain of calculation was drawn using GAMBIT 2.4.6, as shown in Figure 6.2. The shroud was biased by 5 degrees off the vertical in the longitudinal and transverse planes, as shown clearly in Figure 6.2. The ladle shroud was not submerged, as in real life plant practise, during a ladle change operation.

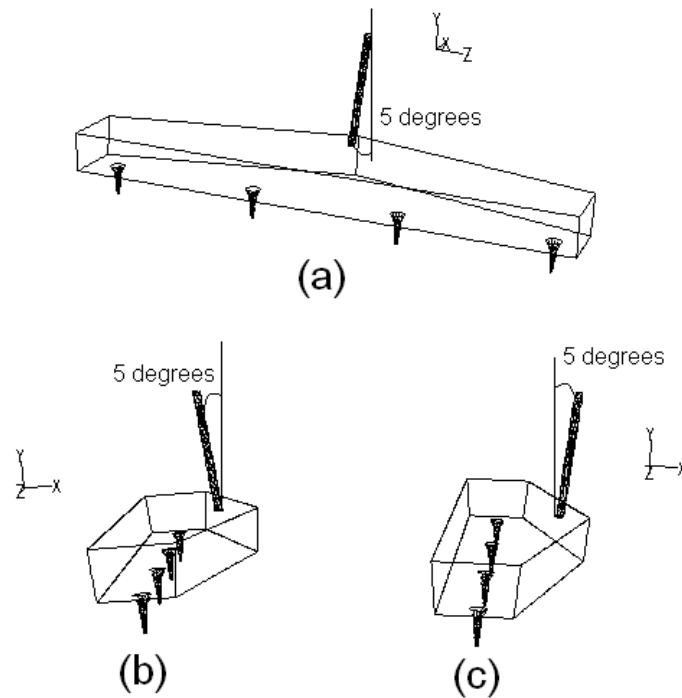


Figure-6.2 Tundish with a biased shroud drawn in GAMBIT 2.4.6 (a) 5° in YZ plane (b) -5° in XY plane (c) 5° in XY plane

The simulations were carried out using ANSYS 12.0. The fluid (water) in the tundish and shroud were considered as Newtonian and incompressible. The standard k - ϵ turbulence model of Launder and Spalding⁷⁹ was used, where k is the kinetic energy of turbulence per unit mass and, ϵ is the rate of turbulence energy dissipation. The velocity inlet boundary condition was used for the inlet, and outflow boundary conditions were used for the outlets. The top surface was set as a free surface, and all other surfaces were walls with the no-slip condition. To model the non-submerged shroud, which occurs

during refilling of the tundish, the "Zero Shear Stress" wall boundary condition was used on the exposed part of the jet, between the ladle shroud and the free surface of the tundish. Steady state simulations were done for all cases. The SIMPLE^{81,82} algorithm was used for pressure-velocity coupling and the first order upwind scheme was used for momentum, k , and ϵ equations.

6.3 Results and discussion

6.3.1 Slag entrainment

Slag entrainment tests were carried out in the full-scale water model tundish. Two tundish configurations were considered, viz. the bare tundish, and the tundish with the standard impact pad. The location and geometry of the standard impact pad are given in Chapter 4. Figure- 6.3 shows the amounts of "slag" entrained in each SEN during a ladle change operation using a perfectly aligned shroud. Symmetry can be clearly seen in the amounts of slag particles entrained in individual strands on either side of the shroud. For the bare tundish (Figure-6.3a) there are many more slag particles reporting to the inner strands as compared to the outer ones. For the impact pad arrangement (Figure-6.3b), there were more slag particles reporting to the outer strands as compared to the inner strands. These trends are perfectly normal, because with the use of an impact pad, there is a recirculation in the inner strand zone and

slag particles are carried upwards. As such, the amount of slag entering the inner SENs is much less compared to the outer SENs.

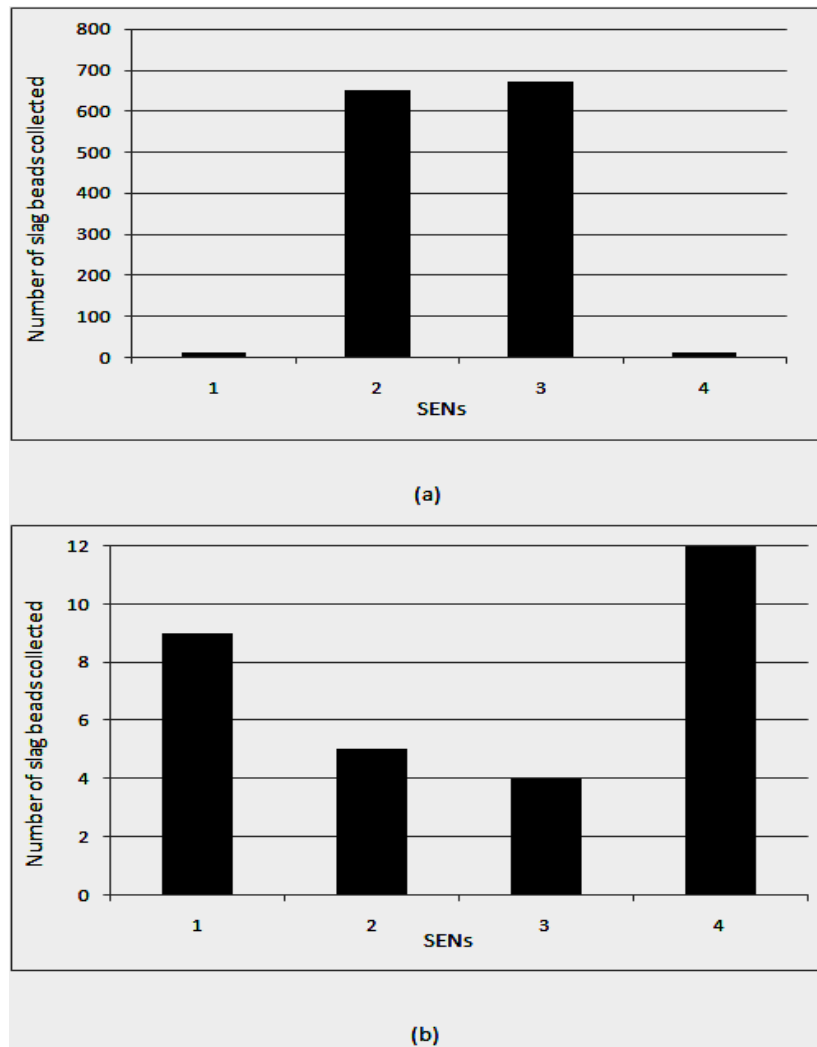


Figure-6.3 Number of slag beads collected in each SEN of the tundish with a perfectly aligned shroud (a) bare tundish (b) impact pad arrangement

If the y axes of the plots are examined carefully, it is seen that for the tundish fitted with the impact pad, the number of beads collected was much less (60 times) than those collected in a bare tundish. The

number of beads collected does not correspond to a specific weight of slag entrained in the real plant, but indicates relative amounts of slag entrained in each strand and follows the same trend as those happening in the plant, where measurements are far more difficult. The results of slag entrainment with a biased shroud are shown in Figure-6.4.

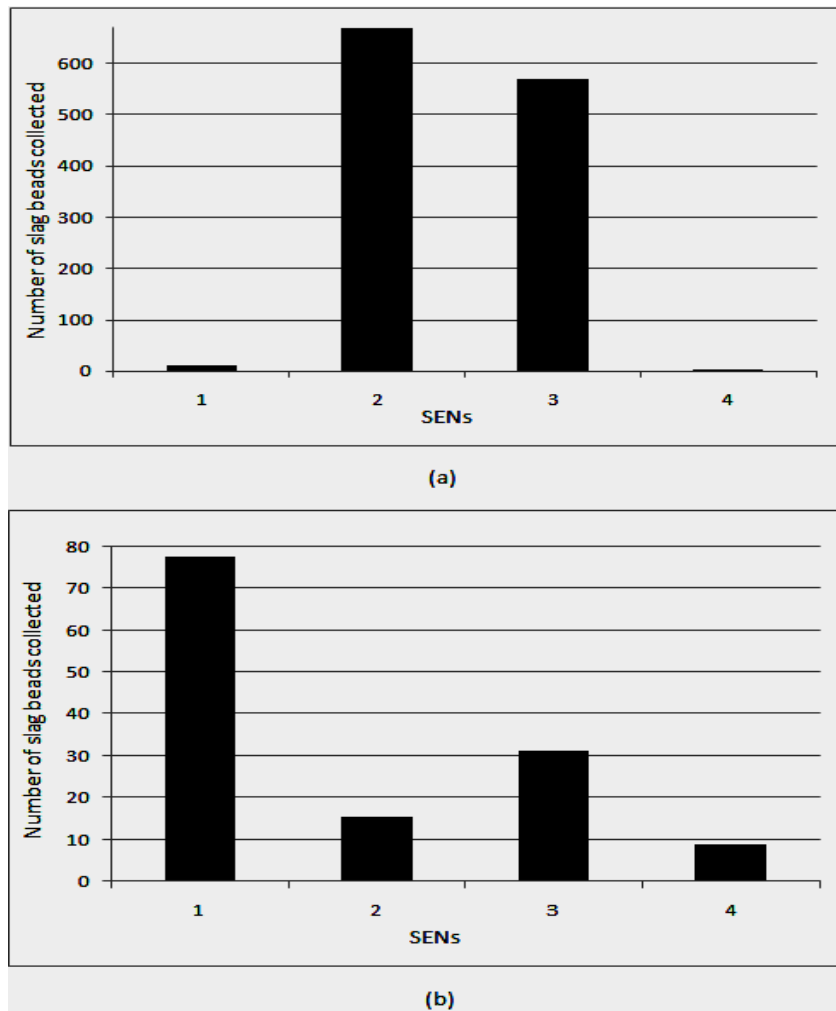


Figure-6.4 Number of slag beads collected in each SEN of the tundish with a biased shroud (a) bare tundish (b) impact pad arrangement

For the bare tundish (Figure -6.4a), the effect of the bias is not clearly seen, because of the high amounts of beads entrained in the inner strands. However, if carefully observed, there are more slag particles reporting to SEN 1 than to SEN 4, and also more to SEN 2 than to SEN 3. In other words, for both the inner and outer strands, more slag is entrained in the SENs in the direction of the bias. For the impact pad arrangement (Figure 6.4b), it is clearly seen that much more slag is entrained in SEN 1 compared to SENs 2, 3, and 4. From the above results, it can be inferred that there must be biased flows to one side of the tundish i.e. towards SENs 1 and 2 and this causes more slag entrainment. Just to confirm our observations a new tundish configuration was also examined. 15 inch high dams were placed on both sides of the ladle shroud and slag entrainment tests were performed with a perfectly aligned shroud and a biased shroud. The results are shown in Figure- 6.5. In Figure 6.5 (a) it is seen that the number of slag beads entrained are similar on either half of the tundish. However, as soon as the shroud was biased by 5 degrees towards SEN 1 and 2, much more slag entrained in SEN 2. This is shown in Figure 6.5 (b).

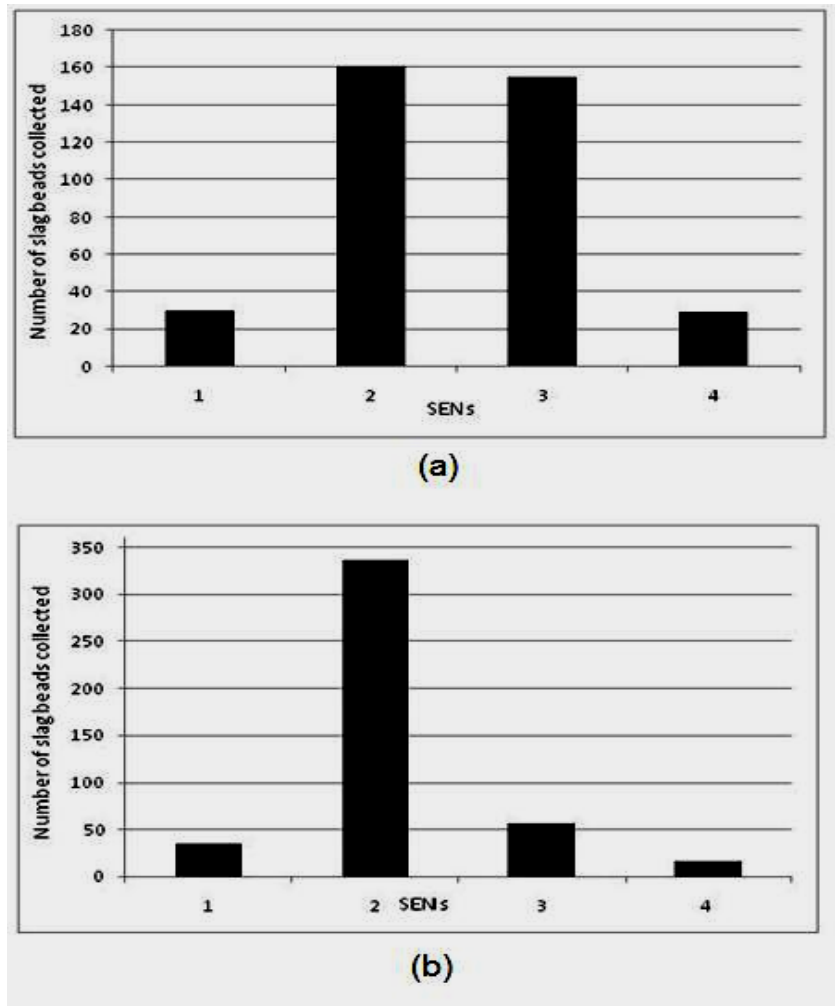


Figure-6.5 Number of slag beads collected in each SEN of the tundish fitted with 15 inch dams on both sides of the ladle shroud (a) perfectly aligned shroud (b) biased shroud.

6.3.2 Tracer Dispersion and 'Exposed Eye'

In the one third scale water model tundish, the shroud was biased by 4-5 degrees off the vertical towards SENs 3 and 4 as shown in Figure 6.6.

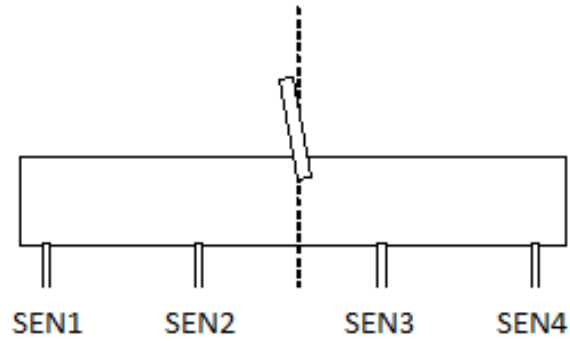


Figure-6.6 Schematic representation of a biased shroud (-5° in YZ plane)

A red dye was injected through the biased shroud at steady state, to observe the mixing behaviour. It was seen that the dye mixes faster in one half of the tundish i.e. in the direction of the bias. However, when the bias was eliminated and then the dye injected, symmetrical mixing patterns are observed. These are shown in Figures 6.7a and 6.7b respectively.

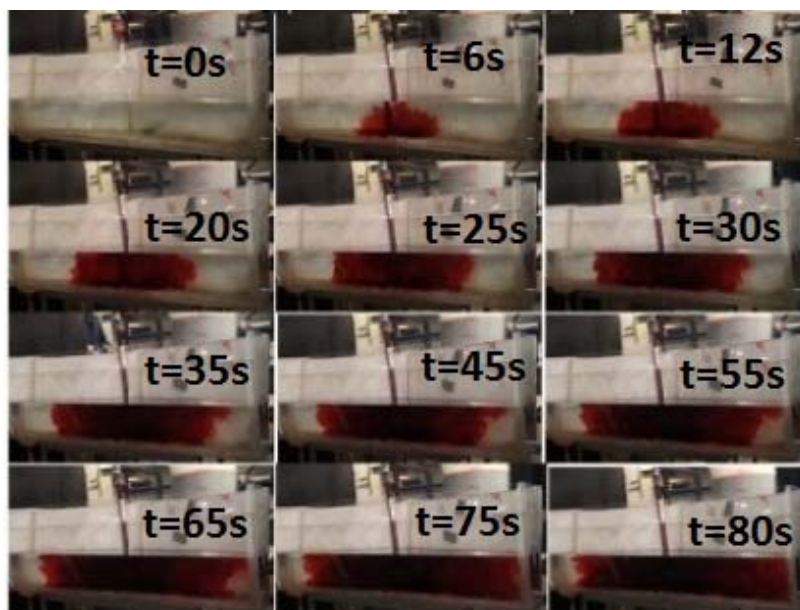


Figure-6.7(a) Tracer dispersion under a biased shroud condition



Figure-6.7(b) Tracer dispersion under an aligned shroud condition

Compressed air was injected through the biased shroud at volumetric flow rates of 4-10pct of the water entry flows and the movements of the slag layer were recorded. Mineral oil was used to simulate the slag phase. Figure 6.8a shows the shape of the ‘exposed eye’ with a mis-aligned shroud. The ‘eye’ is not concentric with the shroud; rather it is more towards the direction of the bias. However, when the shroud is perfectly aligned and the experiment is repeated, it can be seen that the exposed ‘eye’ is now concentric (Figure 6.8b). All these observations correspond to the fact that there are biased flows in one half of the tundish, as a result of a slight mis-alignment of the shroud.

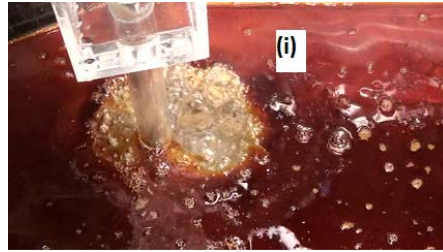


Figure-6.8(a) Exposed 'eye' with a biased shroud (i) 4% (ii) 6% gas injection by volume

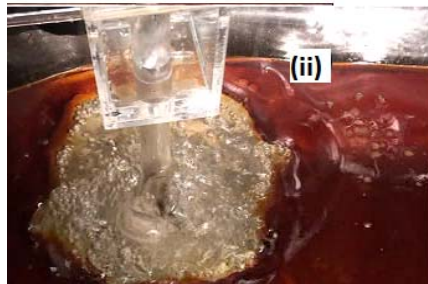
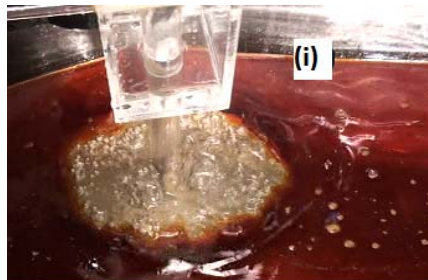


Figure-6.8(b) Exposed 'eye' with a perfectly aligned shroud (i) 4% (ii) 6% gas injection by volume

6.3.3 Bubble and Inclusion Trajectories

The 3D mathematical model along with the DPM was used to predict bubble tracks and inclusion trajectories within the tundish with a biased shroud. Figure 6.9 (a and b) shows predicted inclusion trajectories within the tundish. It is clearly seen that inclusions spread much more to one half of the tundish in the direction of the bias.

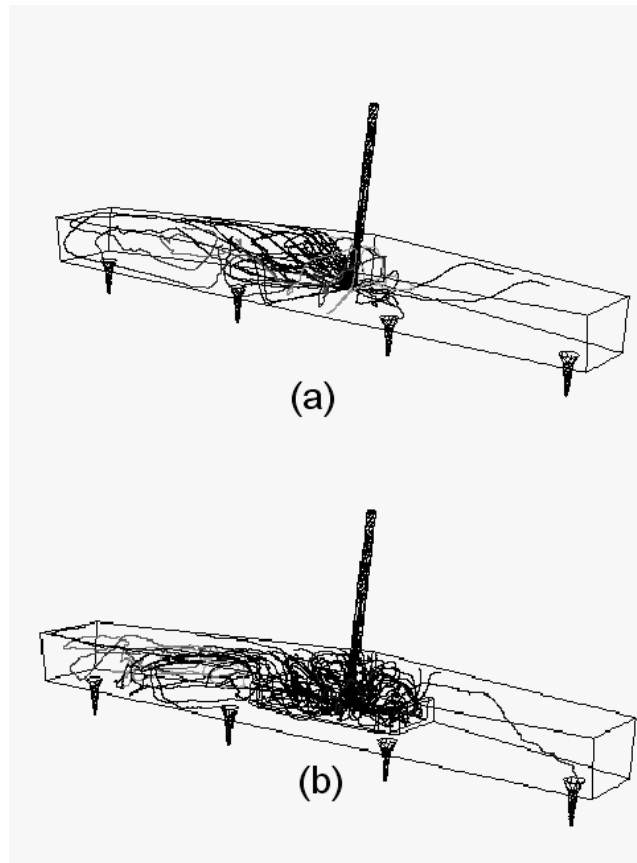


Figure-6.9 Numerically predicted inclusion trajectories within the tundish with a biased ladle shroud (a) bare tundish (b) impact pad arrangement

For the bubbles, a similar argument applies, as represented in Figure-6.10. The bubble column becomes biased, and the bubbles rise up in one half of the tundish. This also explains the fact that the 'exposed eye' of slag is formed on one side of the shroud, as observed in our physical model experiments. However, when simulations were done using a perfectly aligned shroud, then the bubble column was concentric with the shroud, as represented in Figure 6.11.

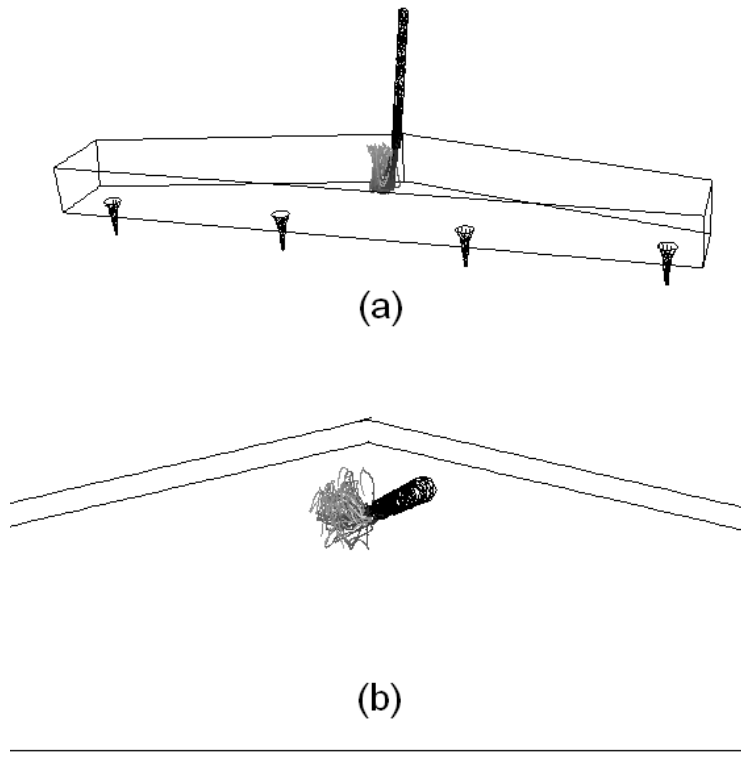


Figure-6.10 Bubble tracks in the tundish with a biased shroud shown in (a) isometric view (b) top view

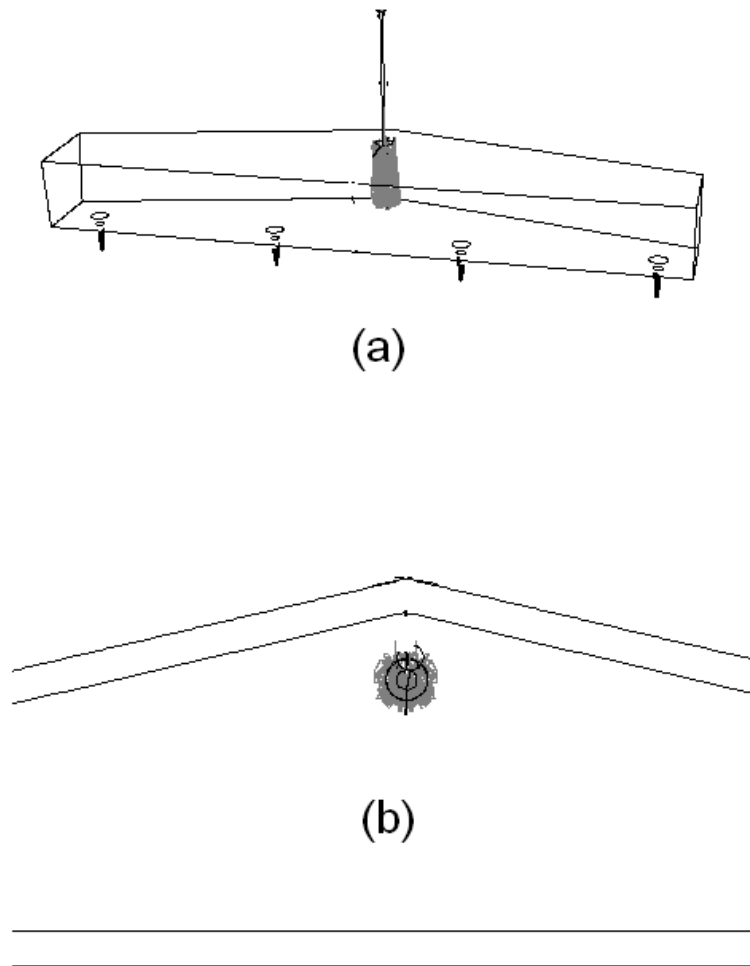


Figure-6.11 Bubble tracks in the tundish with a perfectly aligned shown in (a) isometric view (b) top view

6.3.4 Contours of turbulent kinetic energy

Given all these observations, it is believed that any slight misalignment of a ladle shroud definitely affects the flow within the tundish, and that the amount of turbulence is dissimilar in either half of the tundish. Turbulent Kinetic Energy (TKE) is a good measure of

turbulence, and so using the 3D mathematical model, contours of TKE were examined within the tundish. First a simulation was performed with a perfectly aligned shroud (submerged and non-submerged) and the results are shown in Figures-6.12 and 6.13.

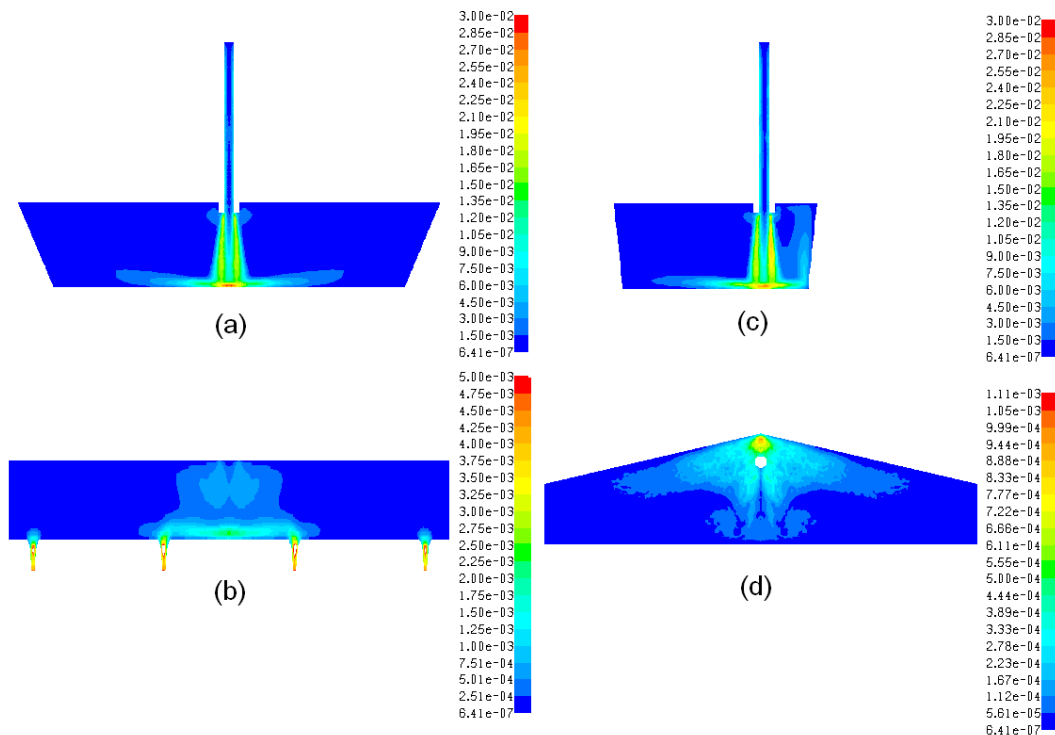


Figure-6.12 TKE contours (m^2s^{-2}) within the tundish with a perfectly aligned submerged shroud (a) plane of the shroud (b) plane of the outlets (c) transverse plane through the centre of the shroud (d) free surface

It is evident that in the non-submerged condition, the turbulence is much higher within the tundish because of the free impinging jet of liquid. However, with a perfectly aligned shroud, the turbulent kinetic energy is similar in both halves of the tundish.

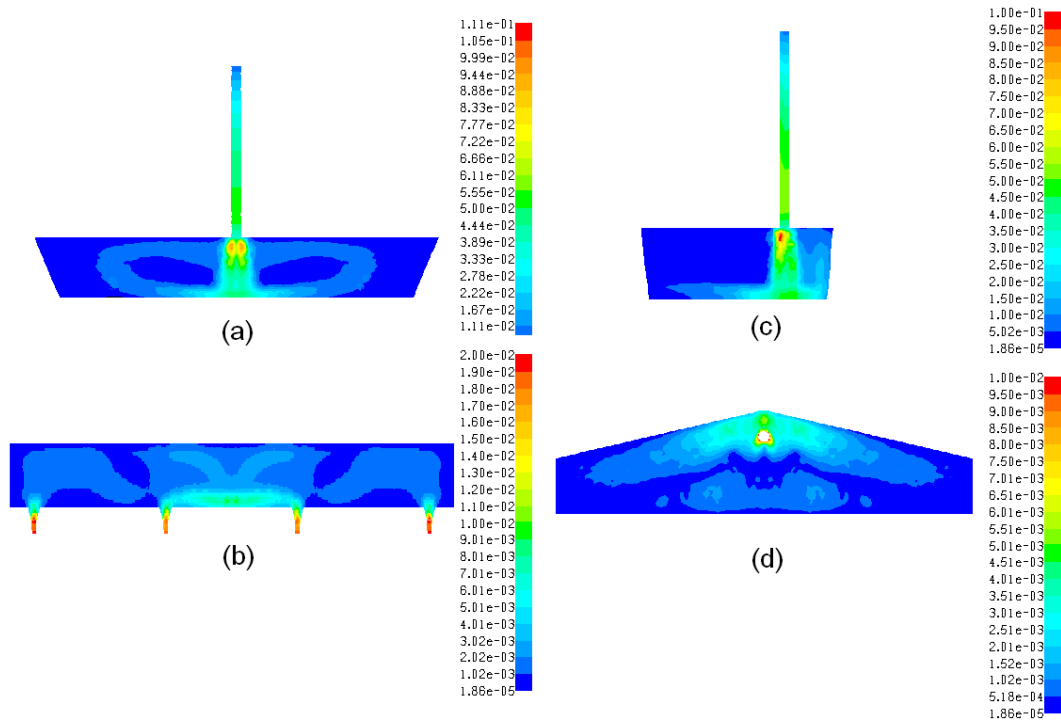


Figure-6.13 TKE contours (m^2s^{-2}) within the tundish with a perfectly aligned non-submerged shroud (a) plane of the shroud (b) plane of the outlets (c) transverse plane through the centre of the shroud (d) free surface

The shroud was then biased in two possible planes and TKE was examined on the free surface, the plane of the shroud and the plane of the outlets. Figure 6.14 represents contours of TKE within the bare tundish with a biased shroud in the YZ (vertical longitudinal) plane. It is clear that there is more TKE in the direction of the bias and the TKE is not distributed uniformly. The same logic applies for the tundish fitted with an impact pad, whose TKE contours are shown in Figure 6.15. As seen, the effect of the bias is quite prominent when the shroud is biased in the YZ plane.

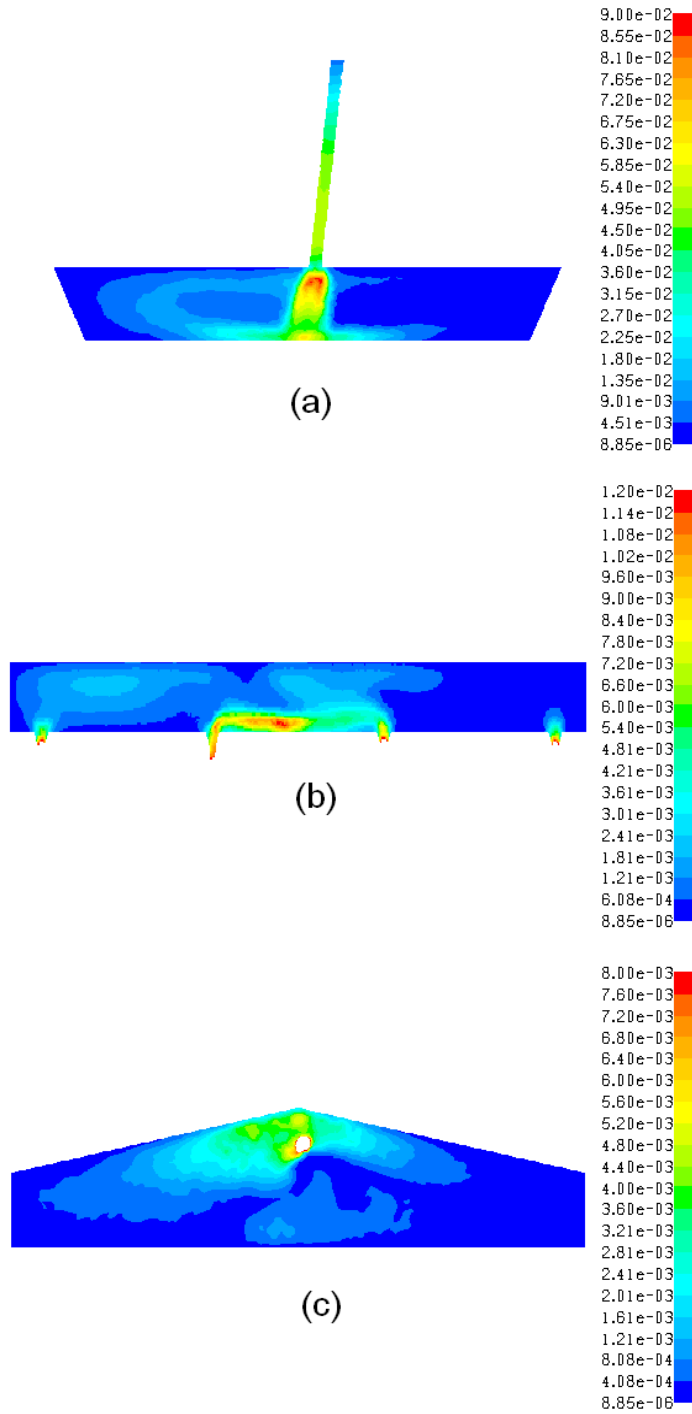


Figure-6.14 TKE contours (m^2s^{-2}) in the bare tundish with a biased non-submerged shroud (a) plane of the shroud (b) plane of the outlets (c) free surface

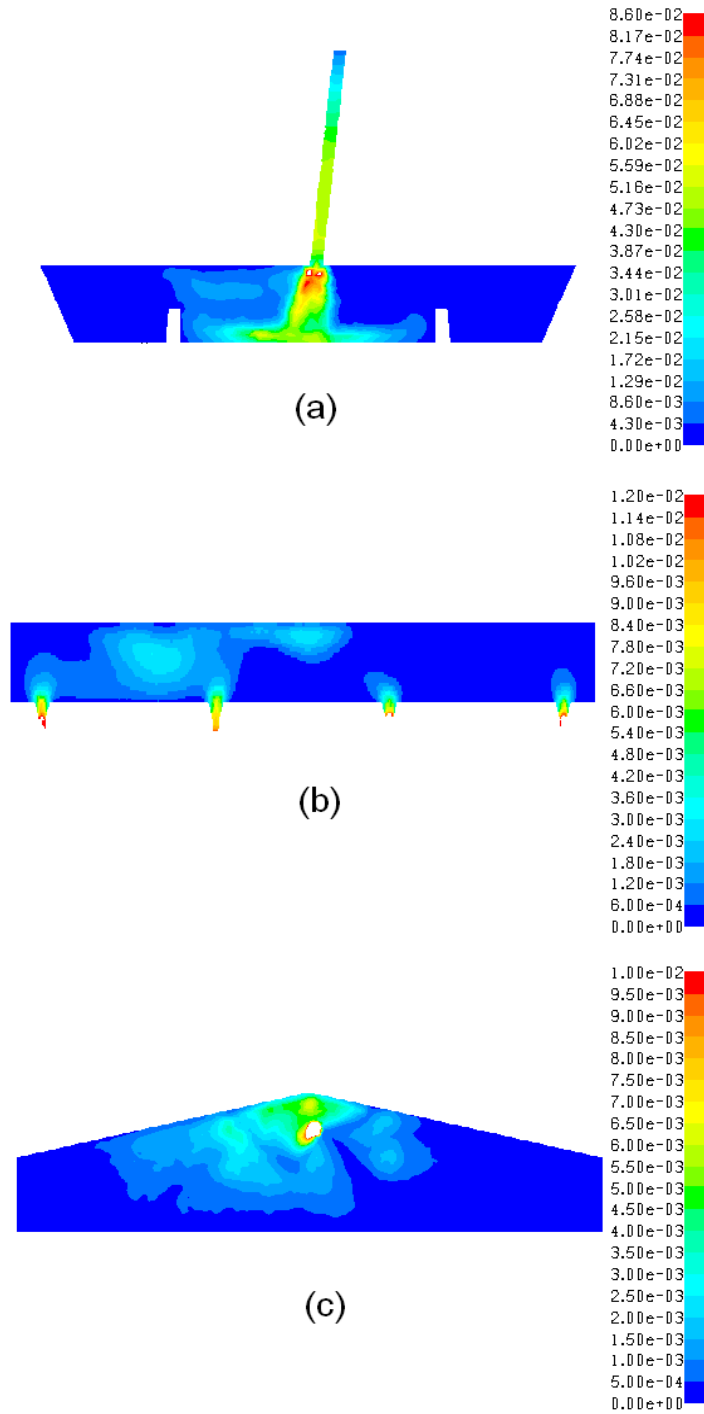


Figure-6.15 TKE contours (m^2s^{-2}) in the tundish fitted with the standard impact pad under a biased non-submerged shroud condition (a) plane of the shroud (b) plane of the outlets (c) free surface

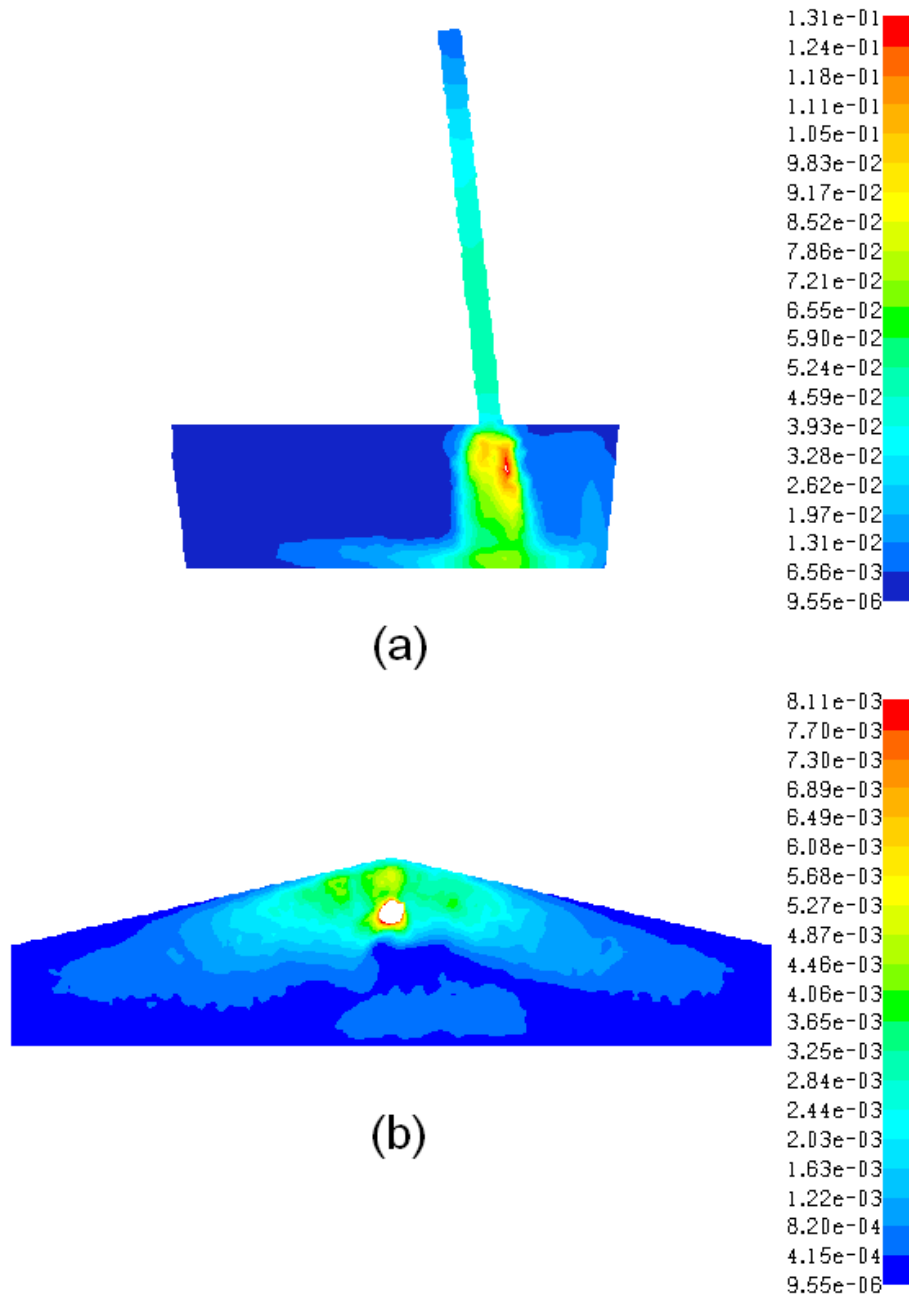


Figure-6.16 TKE contours (m^2s^{-2}) in the bare tundish when the shroud (non-submerged) is biased in the vertical cross-width plane by $+5^\circ$ (a) transverse plane through the centre of the shroud (b) free surface

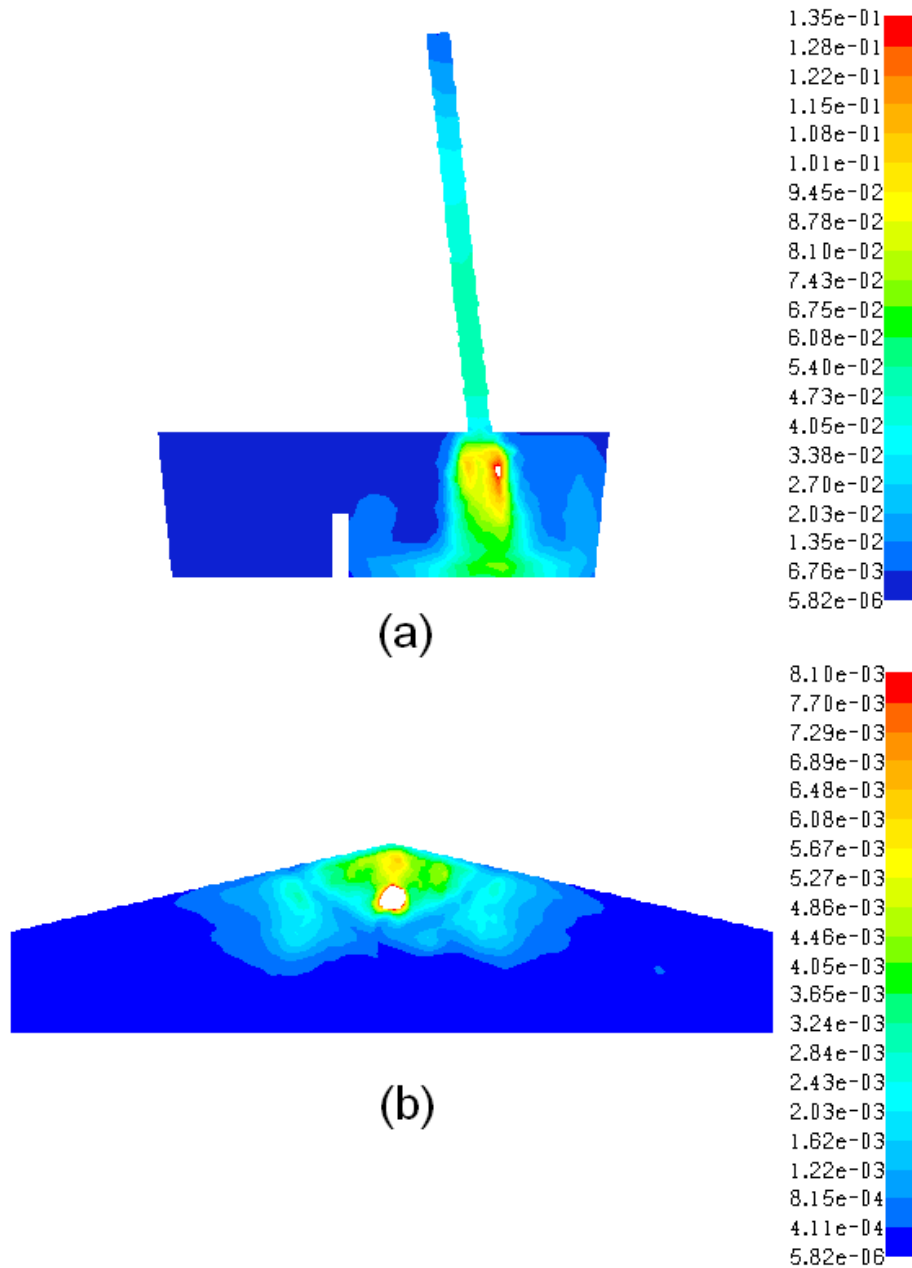


Figure-6.17 TKE contours (m^2s^{-2}) in the tundish with an impact pad when the shroud (non-submerged) is biased in the vertical cross-width plane by $+5^\circ$ (a) transverse plane through the centre of the shroud (b) free surface

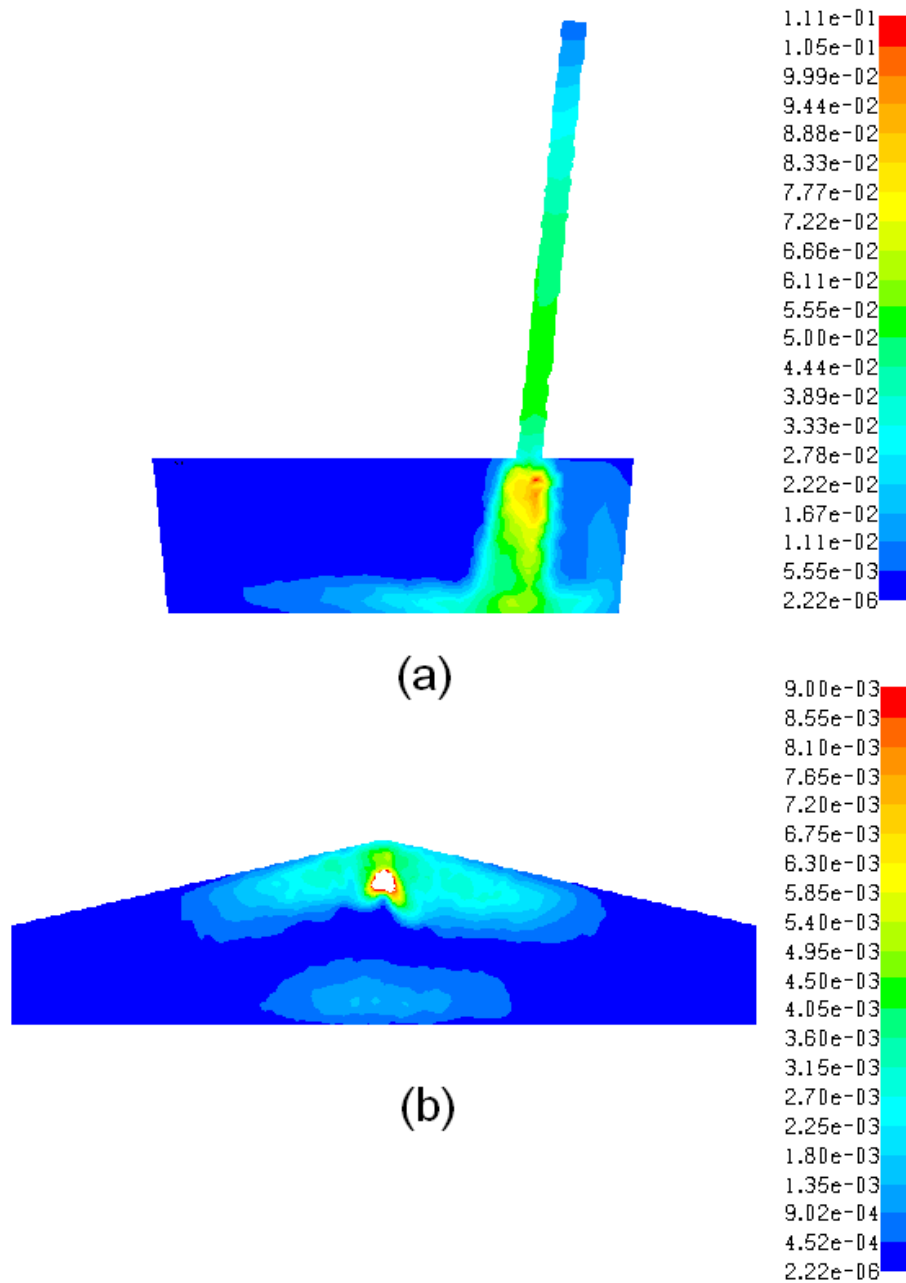


Figure-6.18 TKE contours (m^2s^{-2}) in the bare tundish when the shroud (non-submerged) is biased in the vertical cross-width plane by -5° (a) transverse plane through the centre of the shroud (b) free surface

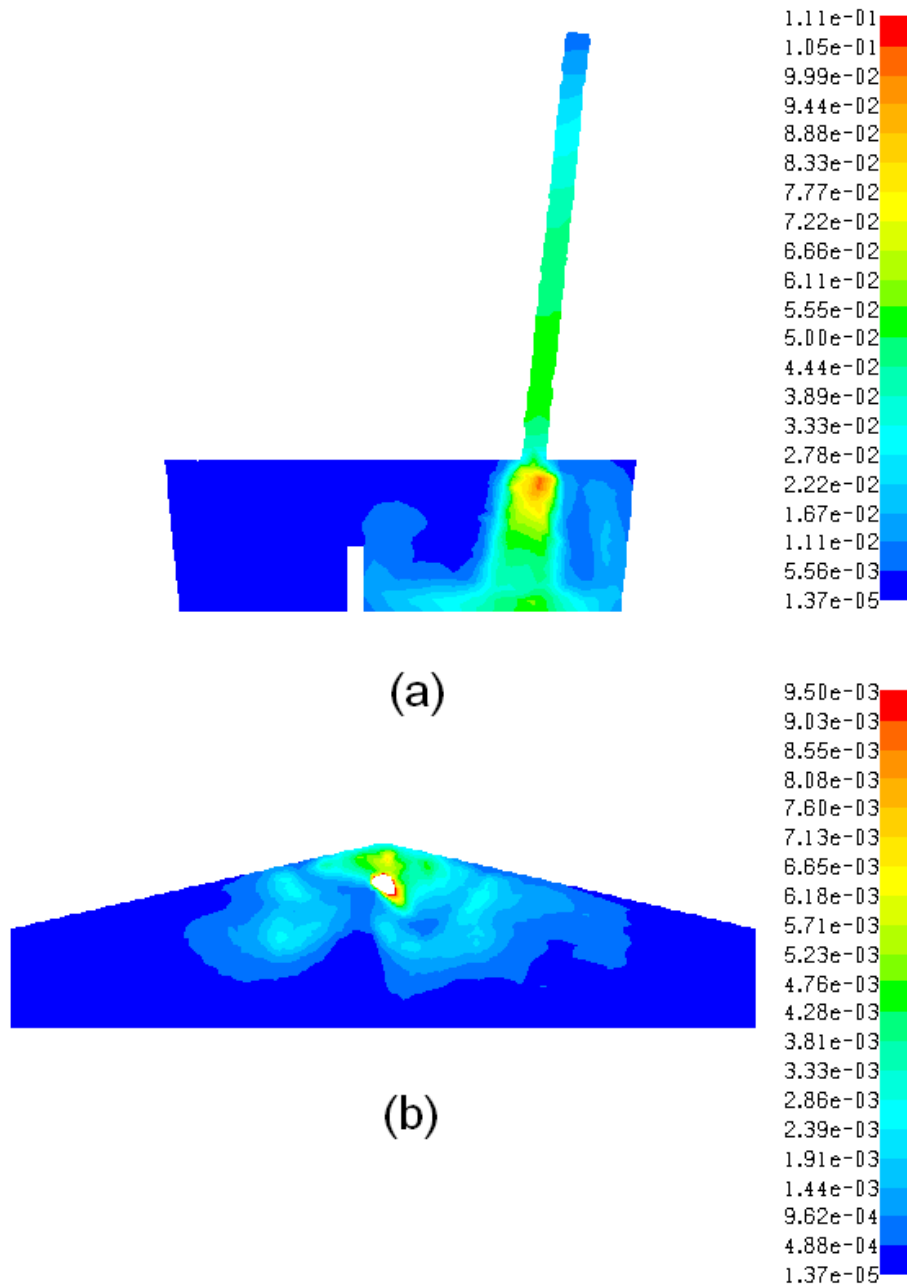


Figure-6.19 TKE contours(m^2s^{-2}) in the tundish with an impact pad when the shroud (non-submerged) is biased in the vertical cross-width plane by -5° (a) transverse plane through the centre of the shroud (b) free surface

Figures 6.16, 6.17, 6.18, and 6.19 above, represent TKE contours within the tundish when the shroud was biased in the XY (vertical cross width) plane. In all cases, the TKE contours are not symmetrical but the effect of the bias is less pronounced. So a small bias along the length of the tundish is far more harmful than a bias across its width. There is more turbulence in the direction of the bias, and hence there is more slag disruption in that region, leading to higher amounts of slag entrainment.

6.3.5 Submerged and non-submerged ladle shroud considerations

In all the above cases, the shroud was not submerged. A simulation was carried out with a biased submerged shroud in the YZ plane. The results are shown in Figures 6.20 and 6.21.

It is clearly seen that the effect of the bias is much less now. Although there is more TKE in the direction of the bias, it is still evenly distributed, as compared to the non-submerged condition. So a ladle change operation with a submerged ladle shroud is preferred, but practical difficulties do not always allow this practice in industry.

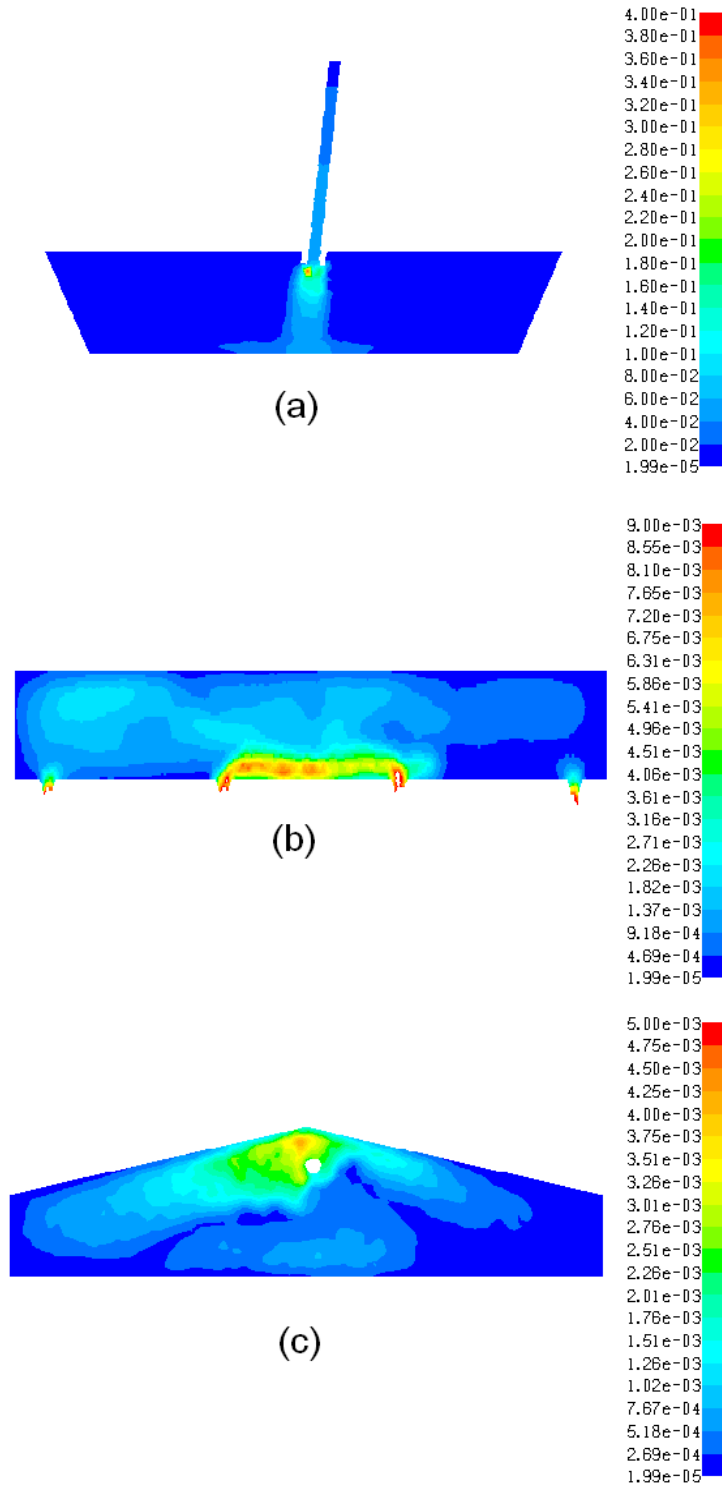


Figure-6.20 TKE contours (m^2s^{-2}) in the bare tundish with a submerged biased shroud (a) plane of the shroud (b) plane of the outlets (c) free surface

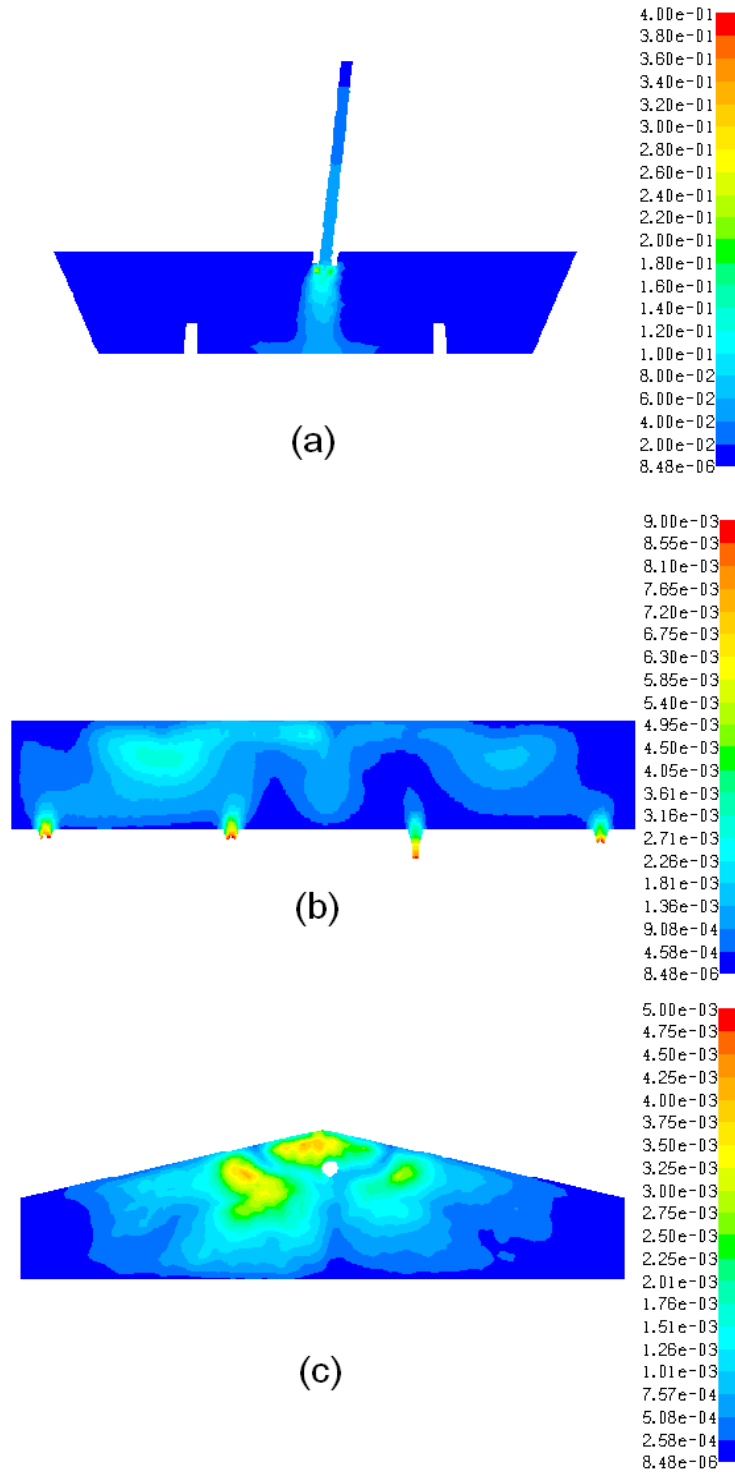


Figure-6.21 TKE contours (m^2s^{-2}) in the tundish with impact pad with a submerged biased shroud (a) plane of the shroud (b) plane of the outlets (c) free surface

6.3.6 Preventive measures recommended in the plant

The above computations revealed that a slight mis-alignment of an un-submerged (exposed) ladle shroud can be catastrophic in terms of liquid metal quality to the strands. Clearly, some preventive measures are called for. From the 3D numerical predictions, it is clear that in the submerged condition, a biased shroud has much less effect on the TKE fields. Furthermore, slag is not entrained when the shroud is submerged. This suggests that opening up a new ladle when the ladle shroud is not submerged in the tundish, should be avoided. That procedure is possible with bell-shaped ladle shrouds which can accommodate gas pockets, but not with the straight nozzles more frequently used in the industry. For these, one opens up a new ladle with the ladle shroud clear of the melt. This precaution avoids exploding ladle shrouds and/or dangerous sub-surface gas explosions. Given that the collector nozzle shroud is reset from one ladle to another, the nozzles are invariably slightly biased (e.g.>90%). So the time period during which the shroud is exposed, and slag is entrained, must be minimised. In this regard, a three plate slide gate shroud is superior to the two plate slide gate system, since the latter precludes lateral movements during operations. Assuming normally designed shrouds with a two-plate system is being used, the first measure is to minimise exposure times prior to re-submergence of the shroud, so as to limit the

amount of slag entrainment. One technique would be to raise the steel level in the tundish above the normal operating height (500mm in the case modelled), a few minutes before the end of a ladle pour. This allows time for the collector nozzle to be de-coupled from the emptied ladle, the turret rotated to the new ladle, and the collector nozzle re-fitted to the collector nozzle of the new ladle with a gasket. This procedure would be carried out such that the level of steel in the tundish would be just below the end of the shroud collector nozzle once ended. As soon as the level of steel within the tundish drops below the end of the ladle shroud, the new ladle should be opened immediately, and the ladle shroud quickly re-submerged. Ladle change times should be reduced from the current 3-4 minutes to 1-2 minutes. This can be done using efficient handling systems which are already used by large steel companies in Asia. Also, proper instrumentation (like laser levels) should be installed in the plant, in order to check the alignment of the shroud during each casting sequence.

Now let us summarize what is discussed in this Chapter. It is very clear that ladle shroud mis-alignments is an important issue and should be given high priority in the industry to maintain steel quality. Ladle change times should be reduced to minimize shroud exposure times and thus try to circumvent the effects of a biased shroud. The physical modelling results correspond very well to our mathematical

predictions. The 3D mathematical model enabled us to visualize bubble tracks and inclusion trajectories within the tundish to predict TKE contours on the free surface, on the plane of the shroud, and on the plane of the outlets. The 3D model also helped us to find the fact that a mis-alignment of the shroud along the length of the tundish is more harmful than a bias along its width. A submerged shroud operation would be better than the non submerged operation during a ladle change, as indicated from the 3D numerical model predictions, but practical difficulties do not normally permit for this.

7.0 Modelling of Non-Isothermal Melt Flows

7.1 Introduction

Conditions in the plant are non-isothermal and that cannot be ignored. The non- isothermal nature of melt flows may be due to energy losses that take place from the top surface and through the side walls and through bottom of the tundish. It is also very much possible that the temperature of the inlet stream into the tundish from the ladle may vary from heat to heat or with teeming time from the same ladle of steel. Thus, there are many situations in actual practise where the temperature of the incoming stream from the ladle is different from that of the molten steel already present in the tundish. It has been shown by Chakraborty and Sahai¹²⁷ , and by Joo and Guthrie¹²⁸, that the fluid flow patterns developed in such cases

are quite different from those obtained under isothermal conditions. Non-isothermal conditions give rise to natural convection and buoyancy driven flows within a tundish that are of a comparable order of magnitude to the inertially-driven components. Thus, it is very useful that water modeling can simulate the non-isothermal aspects of the fluid flow phenomena taking place in a continuous casting tundish. Damle and Sahai¹²⁹ examined the necessary modeling criteria for a non-isothermal tundish system. For non-isothermal flows, it is necessary to satisfy thermal similarity in addition to the geometric and dynamic similarities. Fluid flows and mixing of molten steel in a twin-slab-strand continuous casting tundish were investigated using a mixing model under non isothermal conditions by Alizadeh et al.¹³⁰ This model led to a set of ordinary differential equations that were solved with a Runge-Kutta algorithm. Steady state water modelling tests were carried out under non-isothermal conditions. Experimental data obtained from the water model were used to calibrate the mixing model. As a result of the presence of mixed convection phenomena in the non-isothermal tundish, parts of the primary fluid were mixed in with the warm incoming fluid. Due to the density difference between the two fluids, fluid channelling became evident within the tundish. The volume flow rate of the fluid in the channel was found to depend on the ratio of inertial to buoyancy forces inside the tundish. They mentioned that if Re_T and Tu between two tundishes are identical, (i.e. model and

prototype), then the RTD curves would be in absolute accordance with each other. The mixing model results showed that the total mixed flow volume fraction in the non-isothermal tundish was lower than that for an isothermal one. Sheng and Jonsson¹³¹ in MEFOS, Sweden, reported on convection patterns of liquid steel in the continuous casting tundish under non-isothermal conditions. They concluded that the convection pattern is controlled by a combination of natural convection and forced convection i.e. mixed convection. Some researchers at Baosteel¹³² reported on numerical simulation of coupled fluid flow and heat transfer to enhance their tundish design. They had problems of temperature homogenization in the tundish. However, after doing a thorough investigation of fluid flow, RTD and temperature distributions, under non-isothermal conditions, they were able to solve their problems. R. D. Morales et al¹³³ reported on buoyancy effects on the melt flow pattern in continuous slab casters. Thermal responses of step-input temperatures in steel for different flow rates were predicted. The molten steel velocity profiles were determined for these temperature and flow rate variations. The importance of natural flow convection was established through a dimensionless number given by the ratio Gr/Re^2 . Buoyancy forces proved to be as important as inertial forces, especially in the extremities of the tundish. The simulations indicated that these forces increase the residence time of the molten steel flowing near the slag layer, allowing more time for the non-metallic inclusions to

be captured. They also found that the turbulence inhibiting device helps to redirect the flow towards the top free surface. It was shown that this device helped to decrease turbulence near the entry zone and has a damping effect on the temperature step inputs, allowing for better control of the casting temperature. The traditional flow control devices such as weirs and dams were not as effective as the turbulence inhibitor. Braun et al.¹³⁴ performed transient non-isothermal numerical simulations to investigate the influence of transient boundary conditions at the outlet of the tundish on the flow structure and mixing process of fluid during the casting process. They emphasized that the tundish is a dynamic system, and hence time dependent in nature, because of the presence of transient thermal boundary conditions at all times. A positive thermal gradient is always formed along the length of the tundish until the ladle is completely drained. However, on opening up a new ladle the thermal gradient is reversed. Miki and Thomas¹³⁵ reported on the effects of thermal buoyancy forces which significantly affect the flow pattern and thus influence inclusion separation. Sheng and Jonsson^{136, 137} performed physical and mathematical modelling of non-isothermal fluid flow in continuous casting tundishes. Apart from PIV and mathematical modelling, they performed tracer dispersion studies, to visualize the flow in the physical model. Tracer dispersion studies are more practical over PIV, because in the latter it is often very difficult to see the differences between isothermal and non-isothermal systems. From the above discussions it is clear that, some researchers included non-

isothermal fluid flow models to analyze continuous casting tundishes, but when compared to the number of papers published on fluid flow and turbulence, information published on non-isothermal melt flows is very less. Also another important observation is that, mostly single strand tundishes were considered for modelling non-isothermal fluid flow. Mathematical modelling was the preferred choice for most of the researchers, while only a very few performed physical modelling of non-isothermal tundish systems.

Shamik Ray et al¹³⁸, performed both physical and mathematical modelling work to analyse non-isothermal melt flows in a delta shaped four strand tundish. In his full-scale water modelling experiments as well as mathematical simulations, it was observed that during step inputs of hot water into a relatively cooler liquid in the tundish, the buoyancy driven flows cause the incoming hotter fluid to move above the remaining colder fluid and to move ahead of it. However, in the physical modelling experiments, they were only able to simulate a step input of +3⁰C to +4⁰C. As result of this, not much difference was observed in between the isothermal and non-isothermal conditions.

To carry this work ahead, physical experiments were done in the one third scale water model. Step inputs of 5⁰C, 10⁰C and 15⁰C hotter water were introduced into the tundish through the shroud. Thermal gradients of ten to fifteen degrees had a significant effect on the fluid

flow pattern. Mathematical modelling was also performed and validated with physical experiments.

7.2 Experimental Procedures

Experiments were carried out in the one third scale water model of the delta shaped four strand tundish. Firstly, the bare tundish was considered in all cases in order to capture the effects to buoyancy driven flows alone. Insertion of flow control devices changes the flow pattern significantly, and hence it becomes very difficult to see the effect of the natural convection. However, later on for some experiments, the standard impact pad was introduced into the tundish. The flow rate of water at the inlet of the tundish was maintained at 10.6 lpm to maintain a steady state height of 0.167m. The water temperature was around 23⁰C for all experiments. A hot water tank was placed beside the tundish where the water temperature was maintained at around 50-55⁰C. In order to introduce step inputs of hot water at the inlet, hot water from the tank was allowed to mix with the existing water at the inlet. The flow rate of the hot water from the tank was varied in order to produce step inputs of 5, 10, and 15 degrees resulting in the inlet temperature to be 28⁰C, 33⁰C, and 38⁰C respectively. A red tracer (food colour) was introduced along with the hot water and tracer dispersion studies were done using a high definition video camera. Three k-type thermocouples were placed at the inner strand, outer

strand and the inlet to monitor the variations in temperature. The thermocouples were connected to a computer through a data acquisition system, and the thermal response curves were recorded. During the experiment, after about 60-70 seconds, the tracer mixed uniformly within the tundish resulting in a total red coloured fluid, and the movement of the wave front of the tracer, could not be demarcated any more. So the high definition video photography was done till 70 seconds from the time of injection of the tracer. A schematic diagram of the experimental set up is given in Figure- 7.1 below.

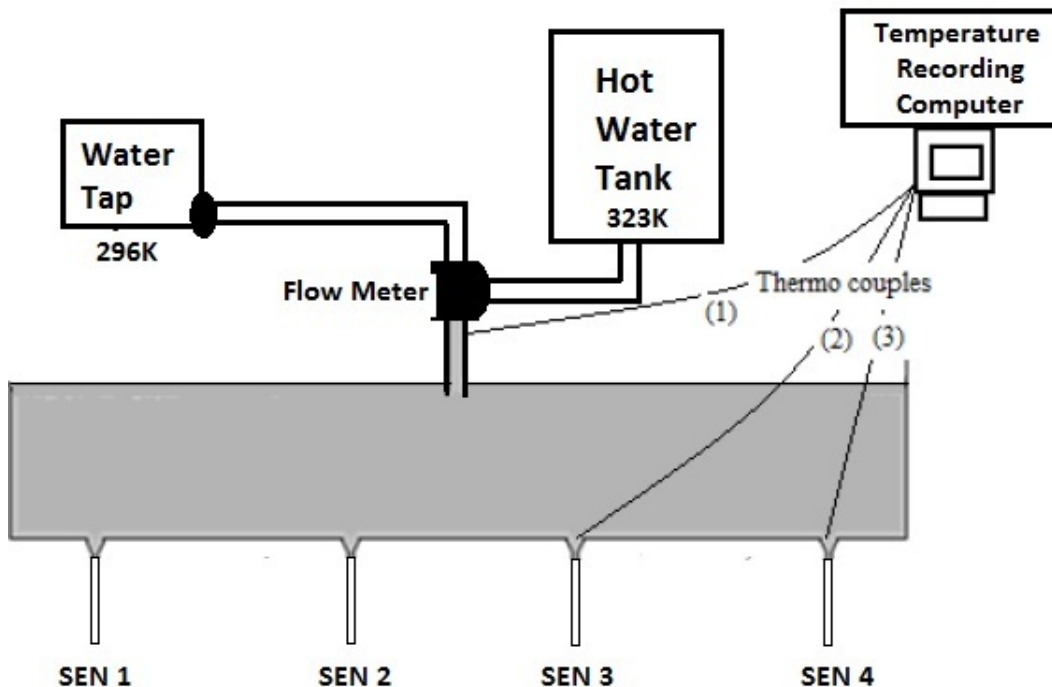


Figure -7.1 Experimental set up for modelling non-isothermal fluid flow in a tundish.

Table 7.1 below shows the properties of water and liquid steel.

Material	Density (ρ) $kg.m^{-3}$	Volumetric expansion coefficient (β) K^{-1}
Water	$654,619 + 2,5446 T - 0,004683 T^2$	$2,95 \times 10^{-4}$
Steel	$7010,0 - 0,833(T - 1808,0)$	$1,27 \times 10^{-4}$

Table-7.1 Properties of water and liquid steel.

The value of the step increase in water temperature was selected by maintaining a similarity criterion, called the Tundish Richardson number (Tu)⁷, similar for the model and the prototype.

$$Tu = \frac{Gr}{Re^2} = \frac{gL\beta\Delta T_0}{U^2} \quad [\text{Eq. 7.1}]$$

The above equation basically represents a ratio of the buoyancy forces to the inertial forces, and this ratio was kept the same for the model and the prototype. Following this similarity criterion, the following relationship is obtained.

$$\Delta T_{water} = \frac{\beta_{steel}}{\beta_{water}} \times \Delta T_{steel} \quad [\text{Eq. 7.2}]$$

So step inputs of 5, 10, and 15 degrees in the water model correspond to a step input of 11.61, 23.23, and 34.84 degrees respectively in liquid steel.

7.3 Numerical modelling procedures

ANSYS 12 was used to perform mathematical modelling of non-isothermal fluid flow in the tundish. The calculations were done in the one-third scale delta shaped tundish and symmetry was assumed in both halves of the tundish. Hence, only one half of the tundish was considered. As the water temperature for most of the experiments was around 23⁰C, the isothermal steady state solution was first computed at T=296K.

In order to simulate the transient, non-isothermal fluid flow, the following equation was considered.

$$\frac{\partial(\rho u_i)}{\partial t} + \frac{\partial(\rho u_i u_j)}{\partial x_j} = \frac{\partial}{\partial x_j} \left[\mu_{eff} \left[\frac{\partial u_i}{\partial x_j} + \frac{\partial u_j}{\partial x_i} \right] \right] - \frac{\partial p}{\partial x_i} - \rho_{ref} \beta \Delta T g_i$$

[Eq. 7.1]

μ_{eff} , the effective viscosity, in equation 7.1 was calculated using the eddy viscosity approach and the standard k- ϵ model. Details of these are already given in Chapter 3 and hence not repeated here. The last term in equation 7.1 accounts for the density differences between the existing fluid in the tundish, and the hotter or cooler incoming fluid from the ladle. Now the last term in equation 7.1 is formulated based on the Boussinesq's approximation. For most natural-convection flows, faster convergence can be achieved with the Boussinesq's model than by setting up the problem with fluid density as a

function of temperature. This model treats density as a constant value in all solved equations, except for the buoyancy term in the momentum equation.

$$(\rho - \rho_{ref})g_i = -\rho_{ref}\beta(\Delta T)g_i \quad [\text{Eq. 7.2}]$$

Here, ρ_{ref} is the reference density of the fluid and β is the thermal expansion coefficient. The Boussinesq's approximation is valid when the temperature changes are small and more specifically when $\beta.\Delta T$ is much less than 1. Now the β for water (or liquid steel) is in the order of 10^{-4} . So even if the ΔT is 15-20 degrees, the $\beta.\Delta T$ is in the order of 10^{-3} which is much less than 1 and hence the Boussinesq's approximation holds good. However, just to confirm, a few simulations were done by putting the density as a function of temperature. It took much longer time to converge (15 hrs), and the results were similar to those obtained by the Boussinesq's approximation (9 hrs). The transient thermal distributions within the tundish were determined by the equation of conservation of energy.

$$\frac{\partial \rho C_p T}{\partial t} + \frac{\partial (\rho C_p T u_j)}{\partial x_j} = \frac{\partial}{\partial x_j} \left(k_{eff} \frac{\partial T}{\partial x_j} \right) \quad [\text{Eq. 7.3}]$$

The temperature field was coupled with the velocity field through the buoyancy term in equation 7.1. For all the simulations the walls and free surface of the tundish was assumed to be adiabatic, i.e. no heat flux through the tundish walls and free surface.

To simulate the tracer dispersion, a scalar transport equation was considered.

$$\frac{\partial \rho \phi_k}{\partial t} + \frac{\partial}{\partial x_i} \left(\rho u_i \phi_k - \Gamma_k \frac{\partial \phi_k}{\partial x_i} \right) = 0$$

[Eq. 7.4]

A user defined scalar was considered at the inlet of the tundish. The diffusivity of the scalar in water was assumed to be very low ($10^{-9} \text{ m}^2\text{s}^{-1}$). The value of the scalar at the inlet was maintained as unity throughout the time of the experiment. The walls and free surface of the tundish were assumed to be impervious to the tracer, i.e. zero flux condition was considered at the walls and free surface for the defined scalar. The movements of the tracer with time were monitored and compared with those obtained from the physical experiments. The tracer dispersion behaviour under isothermal and non-isothermal conditions was also compared.

The number of cells generated in the calculation domain was around 400,000, with finer mesh in the vicinity of the ladle shroud and the walls of the tundish. The initial steady state solution was obtained at $T = 296\text{K}$ (23°C) using the SIMPLE algorithm for pressure-velocity coupling and the first order upwind scheme for momentum, k , ϵ , and energy equations. For subsequent transient simulations, the PISO algorithm was used for pressure-velocity coupling and the second order upwind scheme was employed for momentum, k , ϵ , and energy

equations. A time step size of 10^{-4} s was used for the transient simulations.

7.4 Results and discussions

7.4.1 Mathematical modelling of tracer dispersion for steady state casting operations

Figure- 7.2 below shows the contours of tracer concentration within the bare tundish under isothermal conditions. The colour map in the figures indicate the concentration of the tracer and is the same for each figure, the red colour at the top representing unit concentration at the inlet, and the blue colour at the bottom indicates 1% of the inlet value. The time between each snapshot is 7seconds, and here the contours are shown up to 70 seconds from the time of injection. The wave front of the tracer forms a curvilinear profile at the beginning but eventually gets flat towards the end of the tundish. The interesting observation is that the tracer mixes much faster in the back wall plane close to the shroud as compared to that in the front wall which is further away from the shroud. This occurs because of higher turbulence in the plane near the shroud, and the higher turbulence enhances the mixing. Figure-7.3 represents the contours of tracer concentration within the bare tundish with a step up of 10 degrees. The inlet temperature was now 33⁰C.

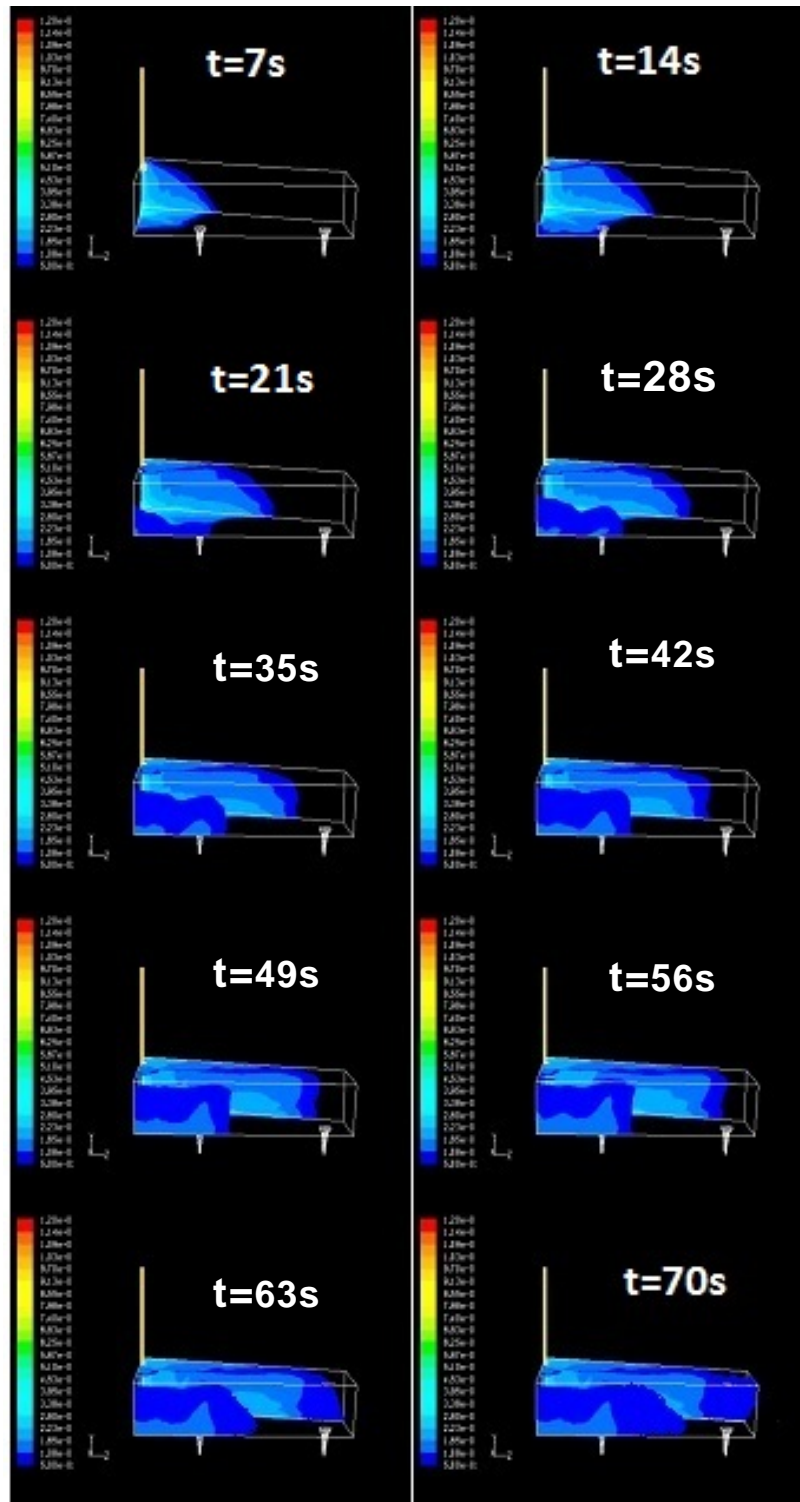


Figure- 7.2 Contours of tracer concentration within the bare tundish, under isothermal conditions. $\Delta t = 7s$.

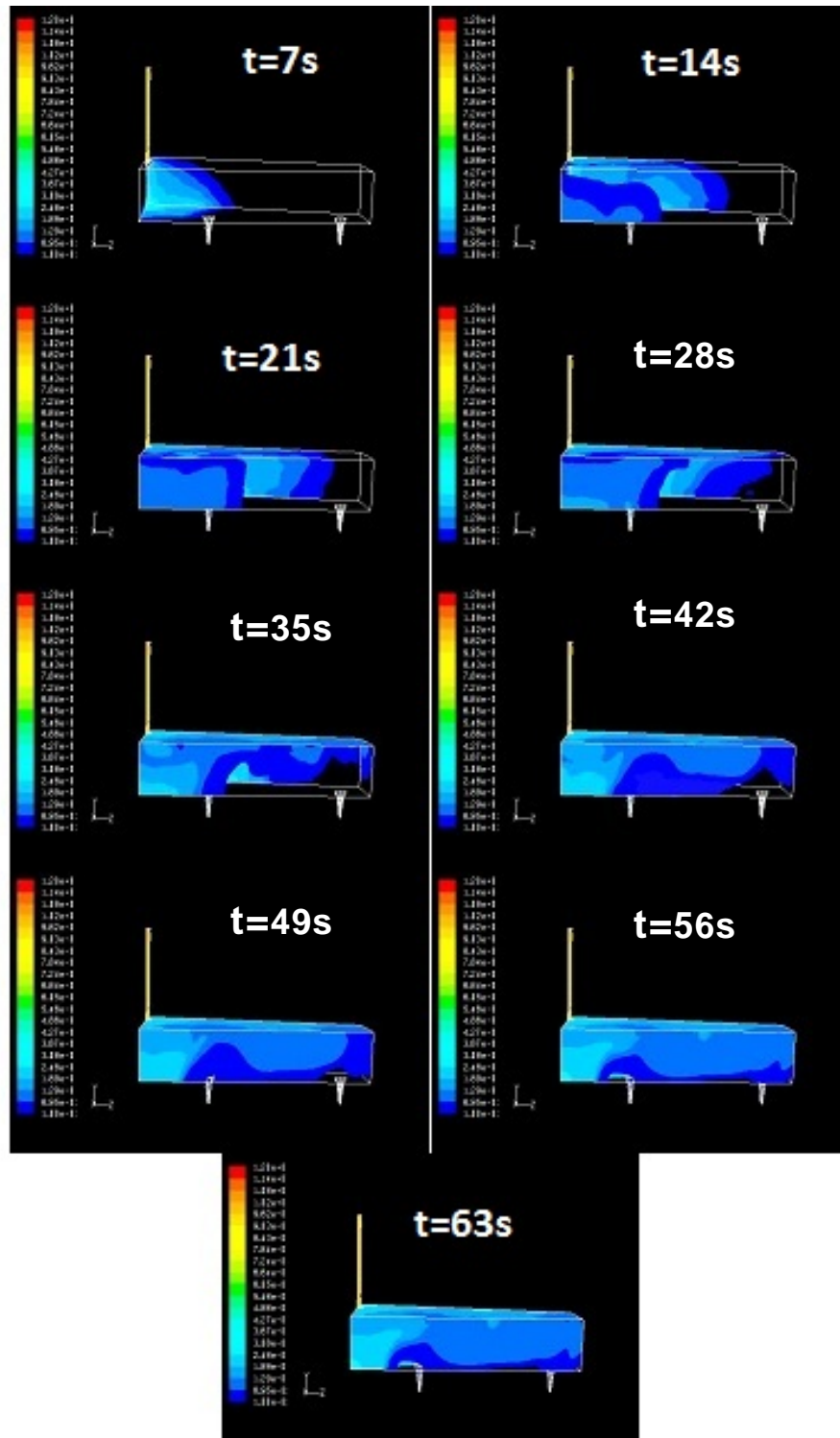


Figure- 7.3 Contours of tracer concentration within the bare tundish, for a step up of 10 degrees. $\Delta t = 7s$.

The dispersion of the tracer is quite similar to the isothermal system at the beginning for the first 14 seconds. After that the dispersion of the tracer totally changes. The wave front starts changing shape, where, the tracer near the top surface of the tundish tends to move faster than that near the bottom. Towards the end of the tundish, at around $t = 28\text{s}$, the tracer is pushed upwards, and then it starts mixing from the top towards the bottom of the tundish. Here also, the tracer mixes much faster near the back wall as opposed to the front wall. The change in behaviour in tracer dispersion can be attributed to the buoyancy forces which come into play due to the non-isothermal conditions. Initially, in the jet entry zone of the tundish, the turbulence is very high, and hence the inertial forces dominate. So the tracer dispersion behaviour is same for both the isothermal and non-isothermal systems. But towards the extremities of the tundish, the turbulence gets significantly lower, and now the buoyancy forces become more significant as opposed to inertial forces. So the mixing pattern of the tracer changes near the ends of the tundish away from the jet entry zone. The hotter water has lower density than the cooler water, and hence moves upwards and pushes the tracer towards the top surface. Now if the thermal gradient is greater than 10 degrees, the effect of buoyancy forces will be even more significant. This is evident in Figure 7.4 below, where there is a step up of 15 degrees.

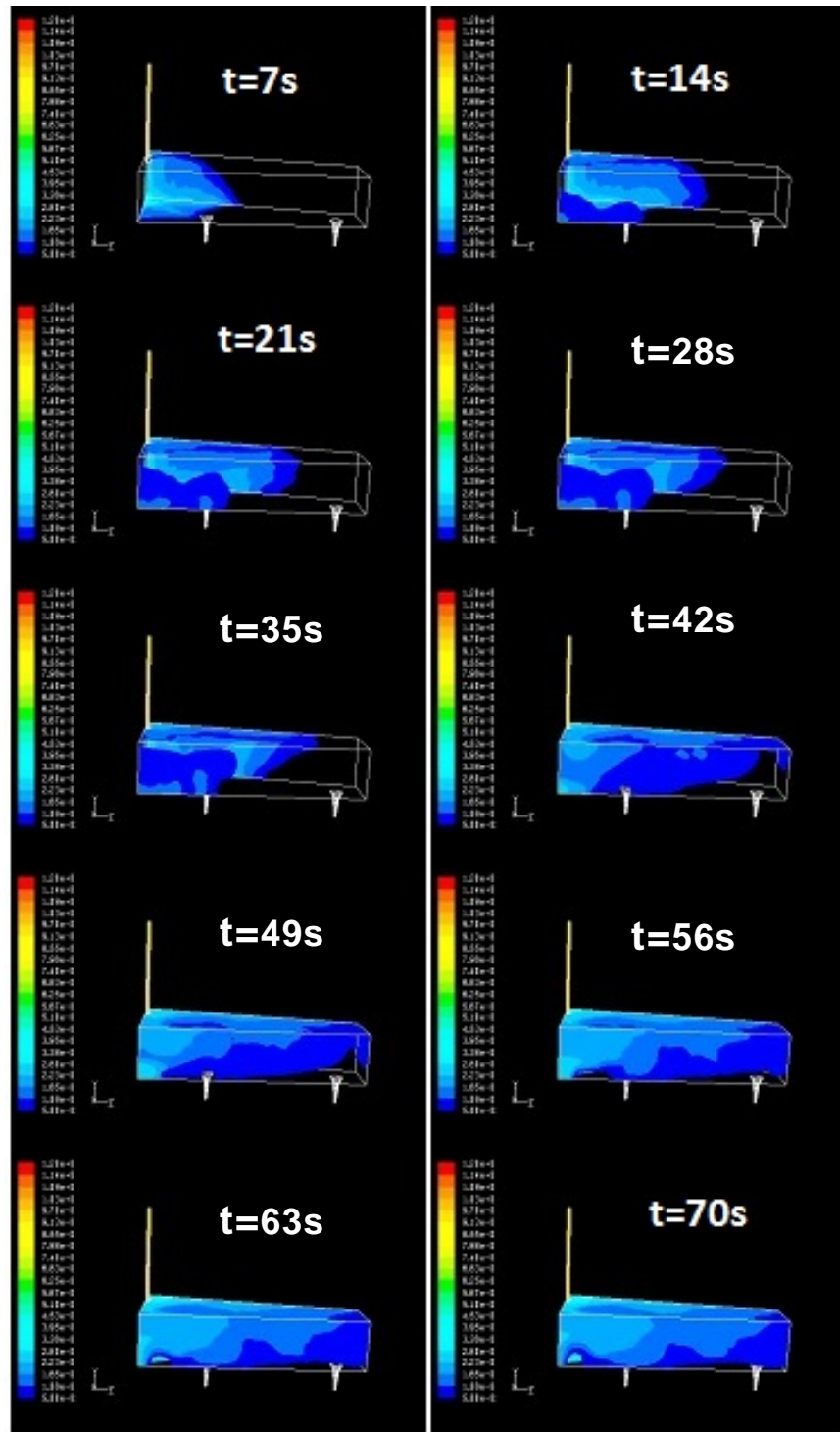


Figure- 7.4 Contours of tracer concentration within the bare tundish, for a step up of 15 degrees. $\Delta t = 7s$.

From the above, results it is clear that the non-isothermal conditions does affect the fluid flow within a tundish. So far only step ups in temperature were considered. However, there could be situations involving a step down in temperature. For example, a new ladle of steel, for some reason can be at a lower temperature than the existing steel in the tundish. Opening up a new ladle like that could result in a step down condition. Figure-7.5 below represents contours of tracer concentration in a tundish, where there is a step down by 15 degrees. The fluid in the tundish was at 38⁰C and cold water was introduced to make the inlet temperature 23⁰C. Here, the mixing behaviour of the tracer changes completely as compared with that to a step up condition. Initially, in the turbulent zone, the wave fronts are quite similar to that for an isothermal system. Towards the ends of the tundish, the buoyancy forces dominate, and now the colder water being heavier, pushes down the existing hotter fluid in the tundish. Now, it would be very interesting to see how the fluid flow pattern changes under non-isothermal conditions. Figures 7.6 (a) to (j) represent the velocity field on a vertical plane through the ladle shroud, at different intervals of time. The velocity fields are given together, for isothermal conditions, step up by 15 degrees and step down by 15 degrees to get a better comparison of the results. A colour map for the velocity fields is given in Figure 7.7.

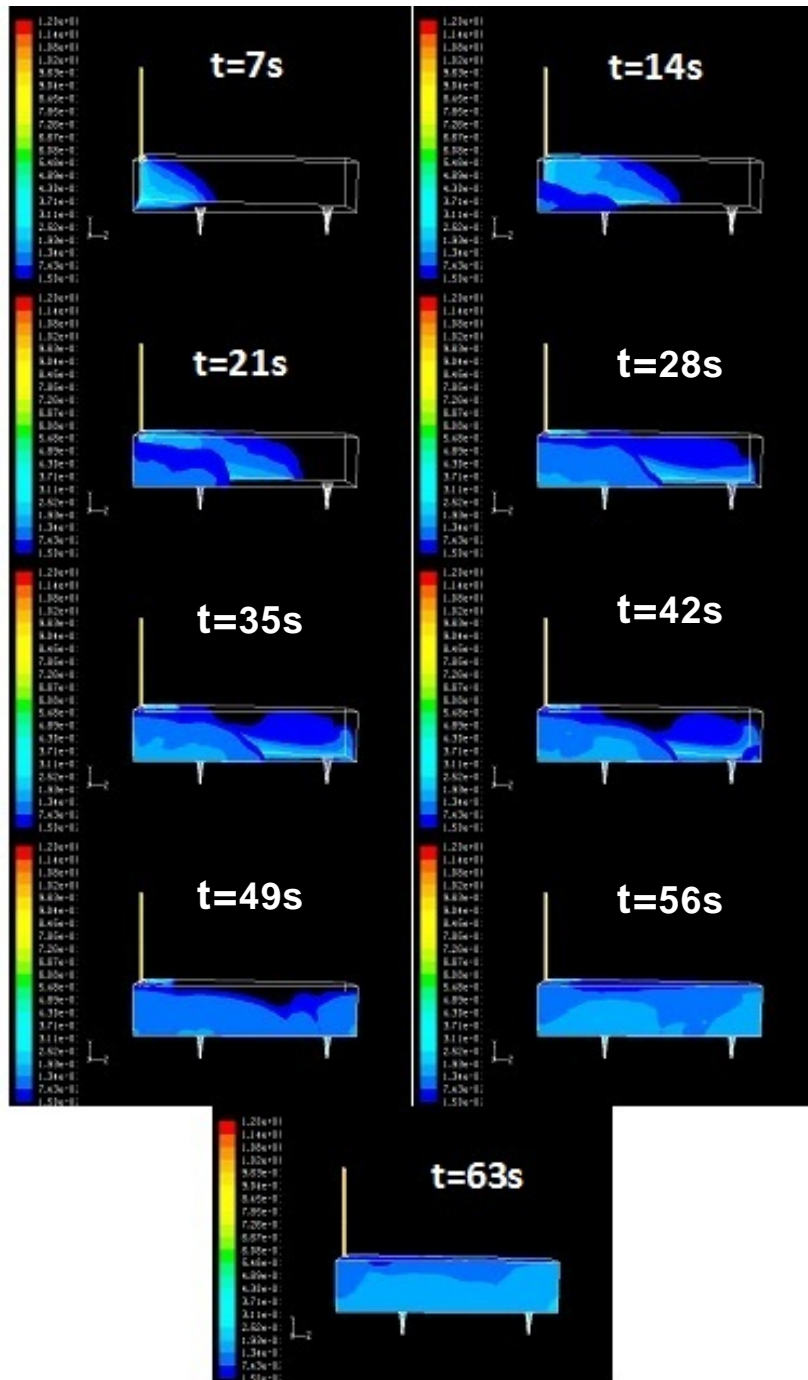


Figure- 7.5 Contours of tracer concentration within the bare tundish, for a step down of 15 degrees. $\Delta t = 7s$.

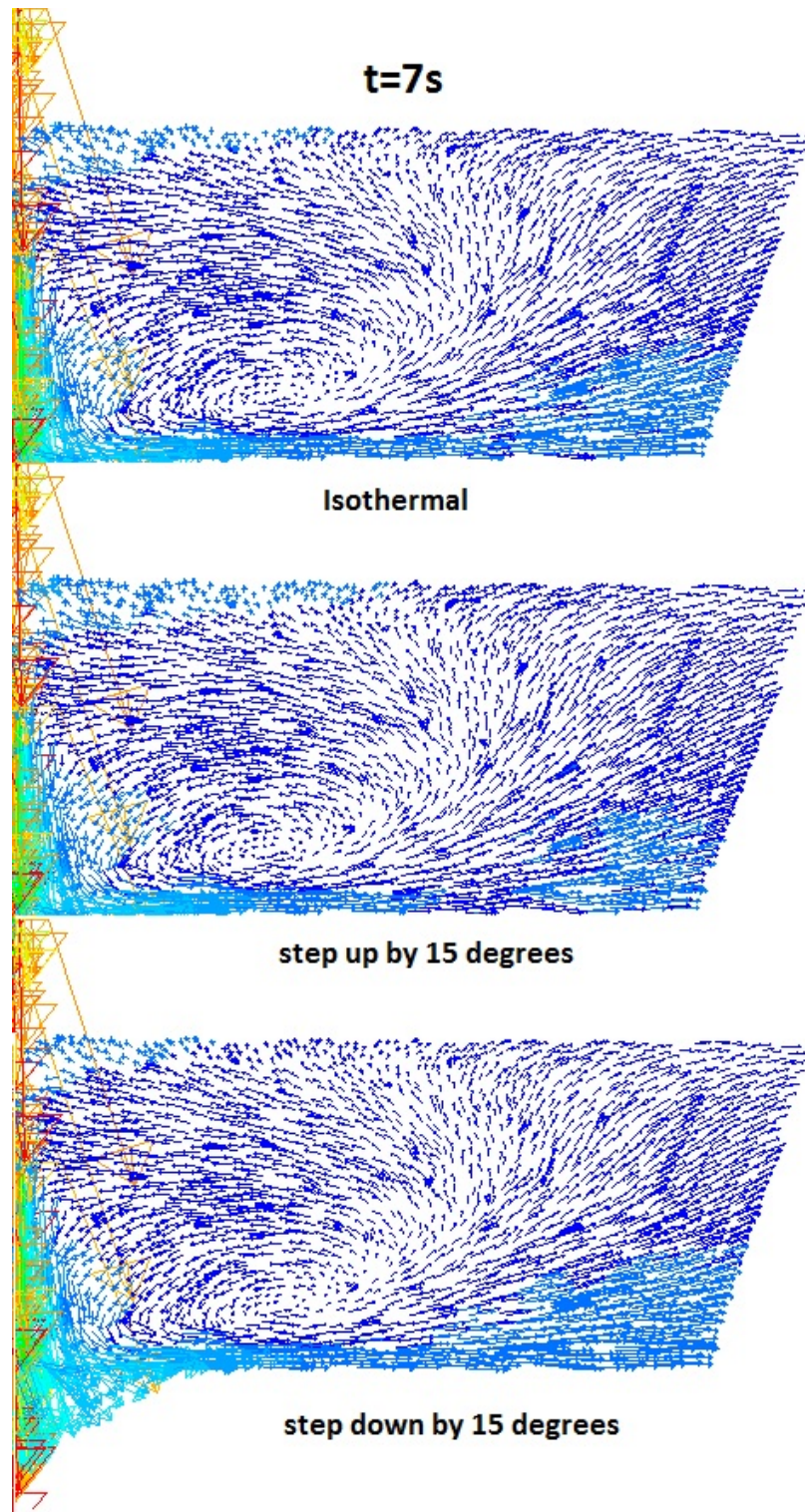


Figure 7.6 (a) Velocity fields under three different conditions at $t=7s$

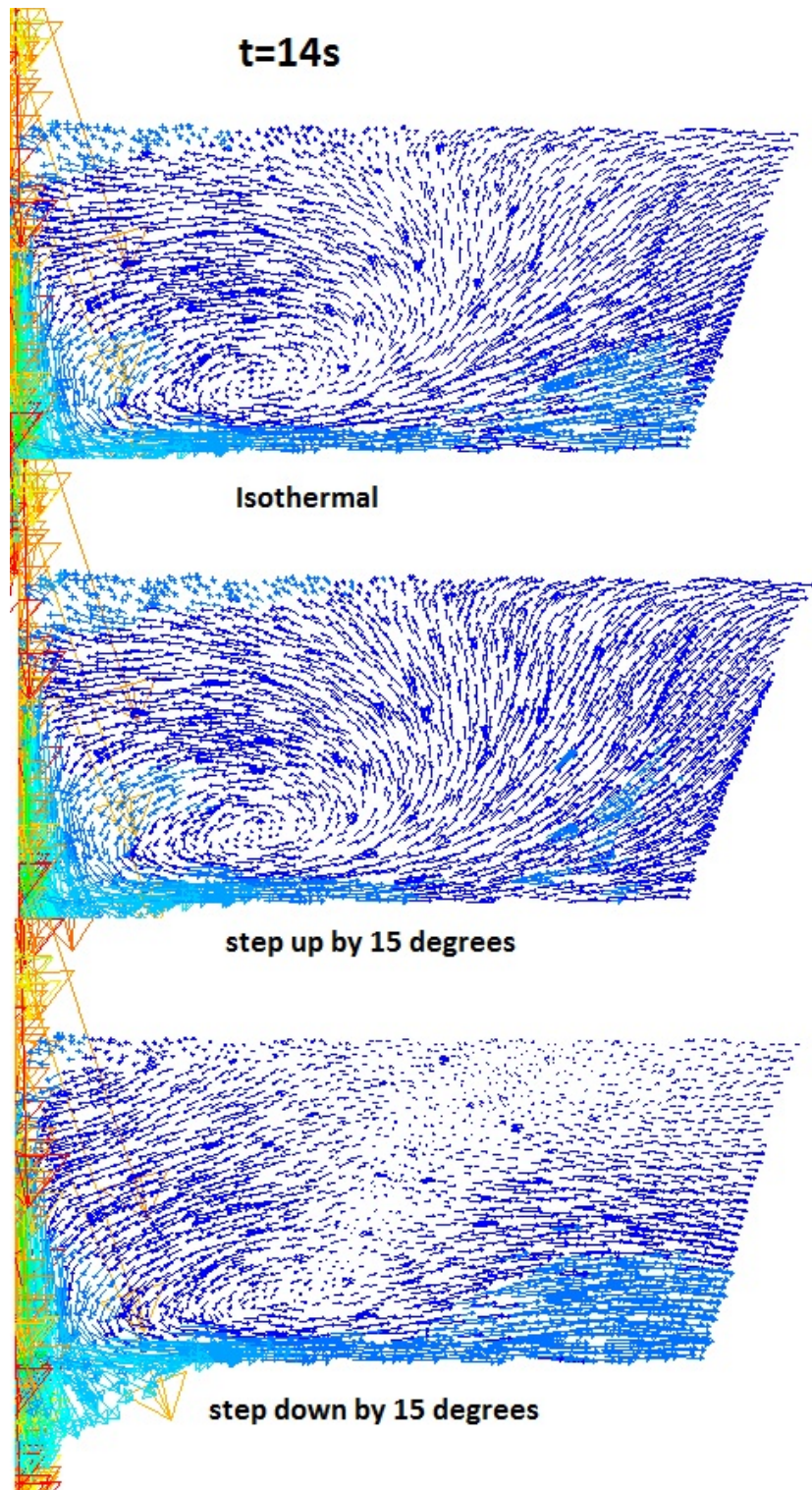


Figure 7.6 (b) Velocity fields under three different conditions at $t=14s$

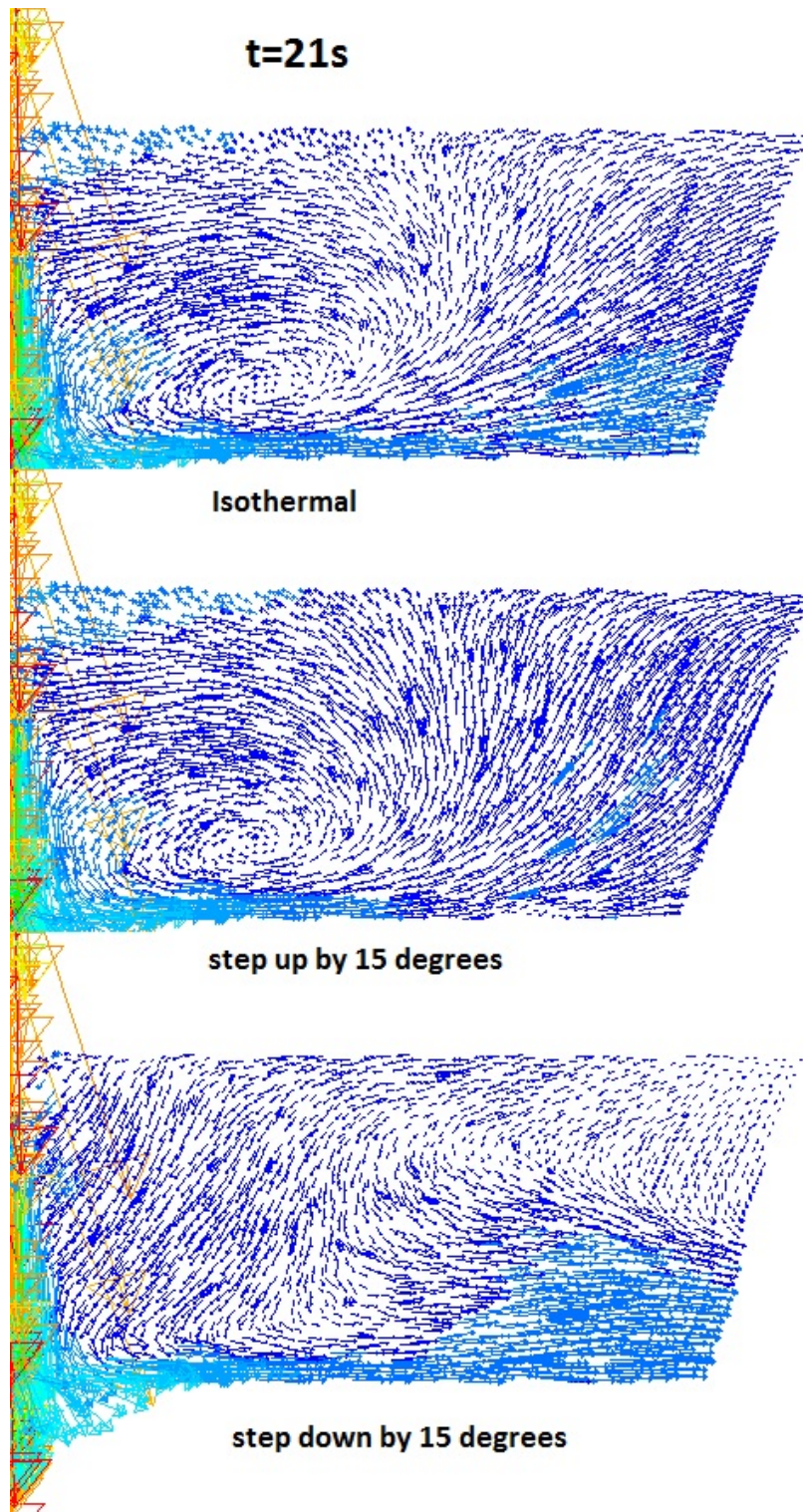


Figure 7.6 (c) Velocity fields under three different conditions at $t=21s$

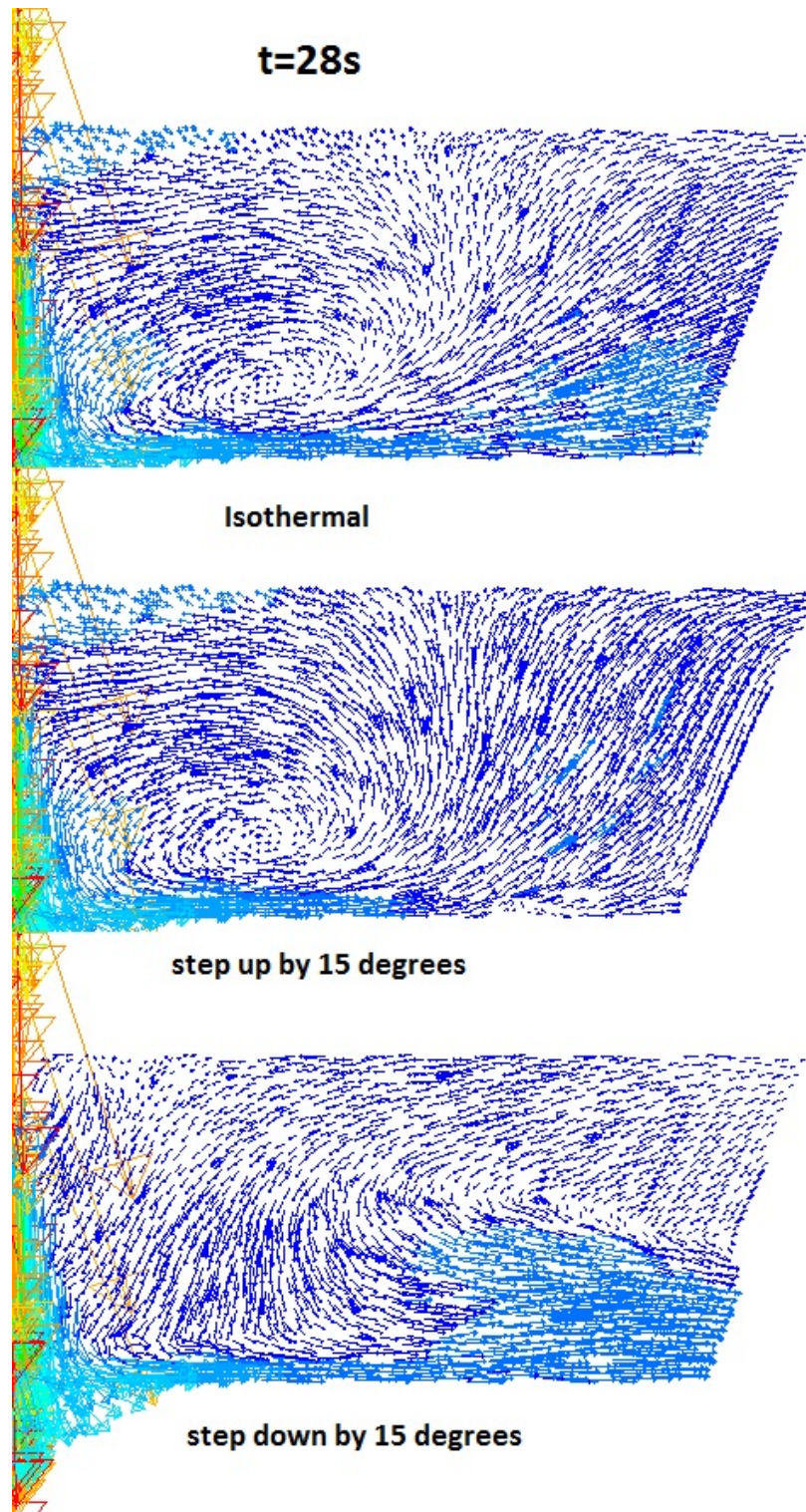


Figure 7.6 (d) Velocity fields under three different conditions at $t=28s$

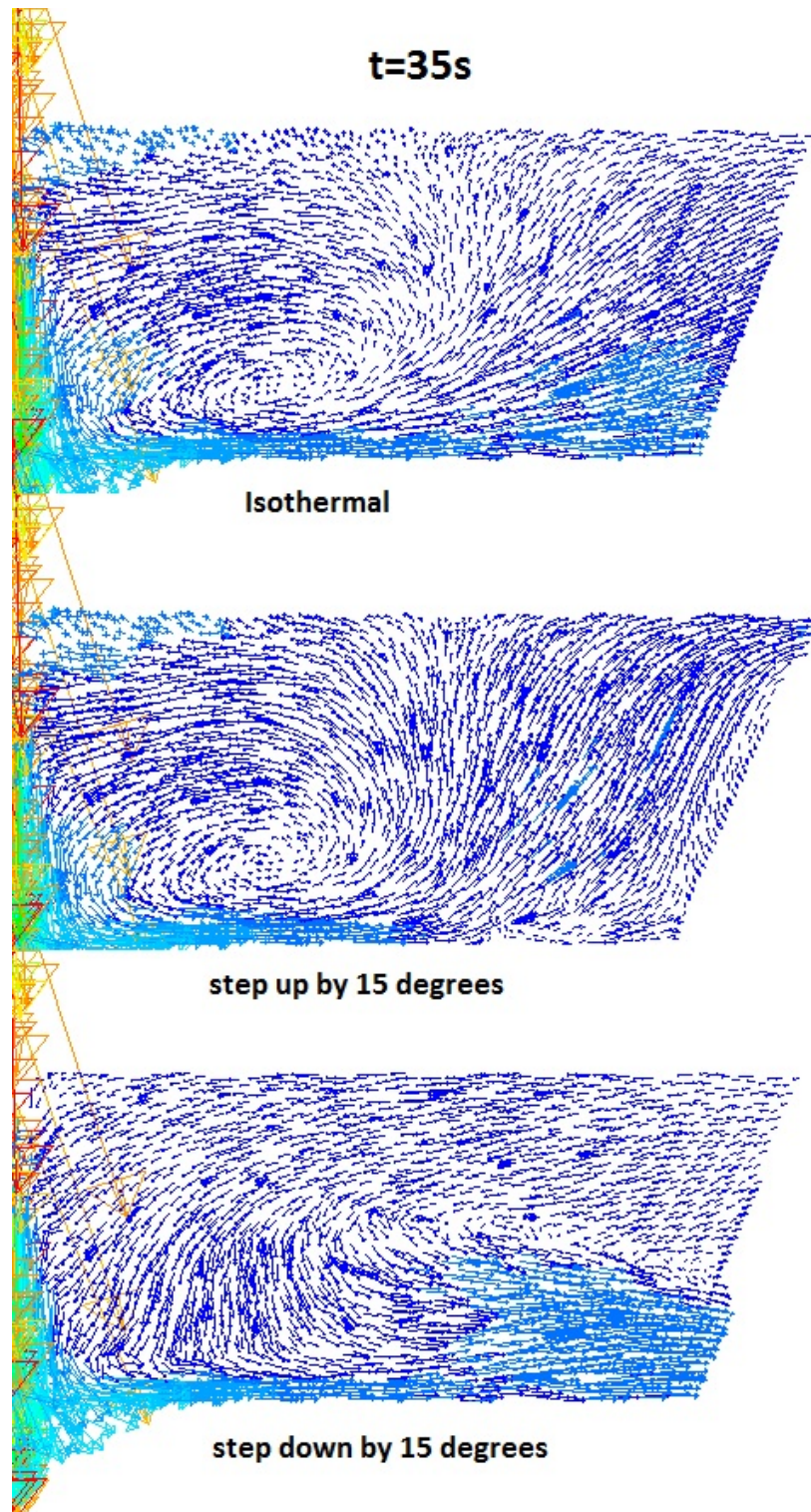


Figure 7.6 (e) Velocity fields under three different conditions at $t=35s$

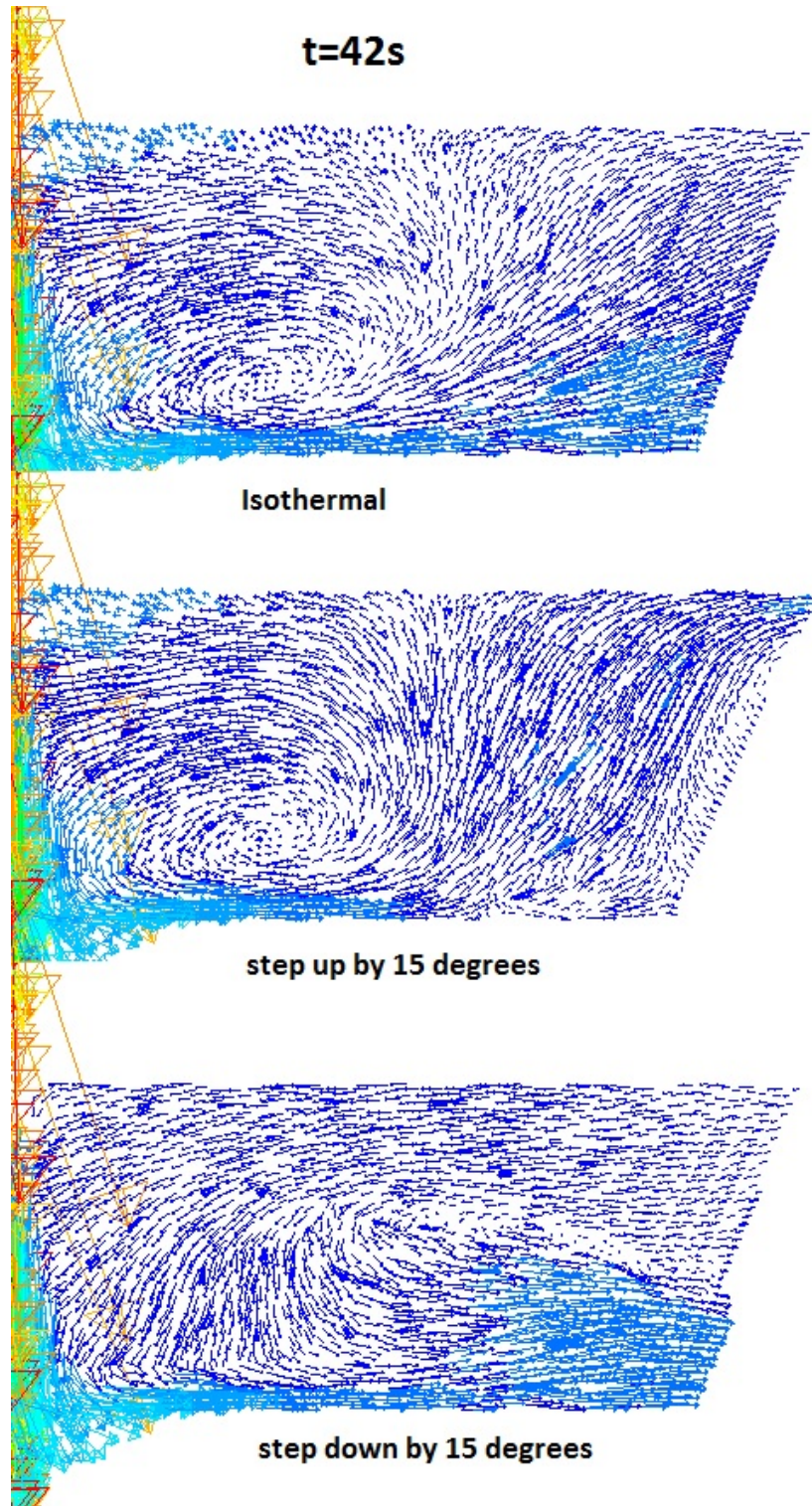


Figure 7.6 (f) Velocity fields under three different conditions at $t=42s$

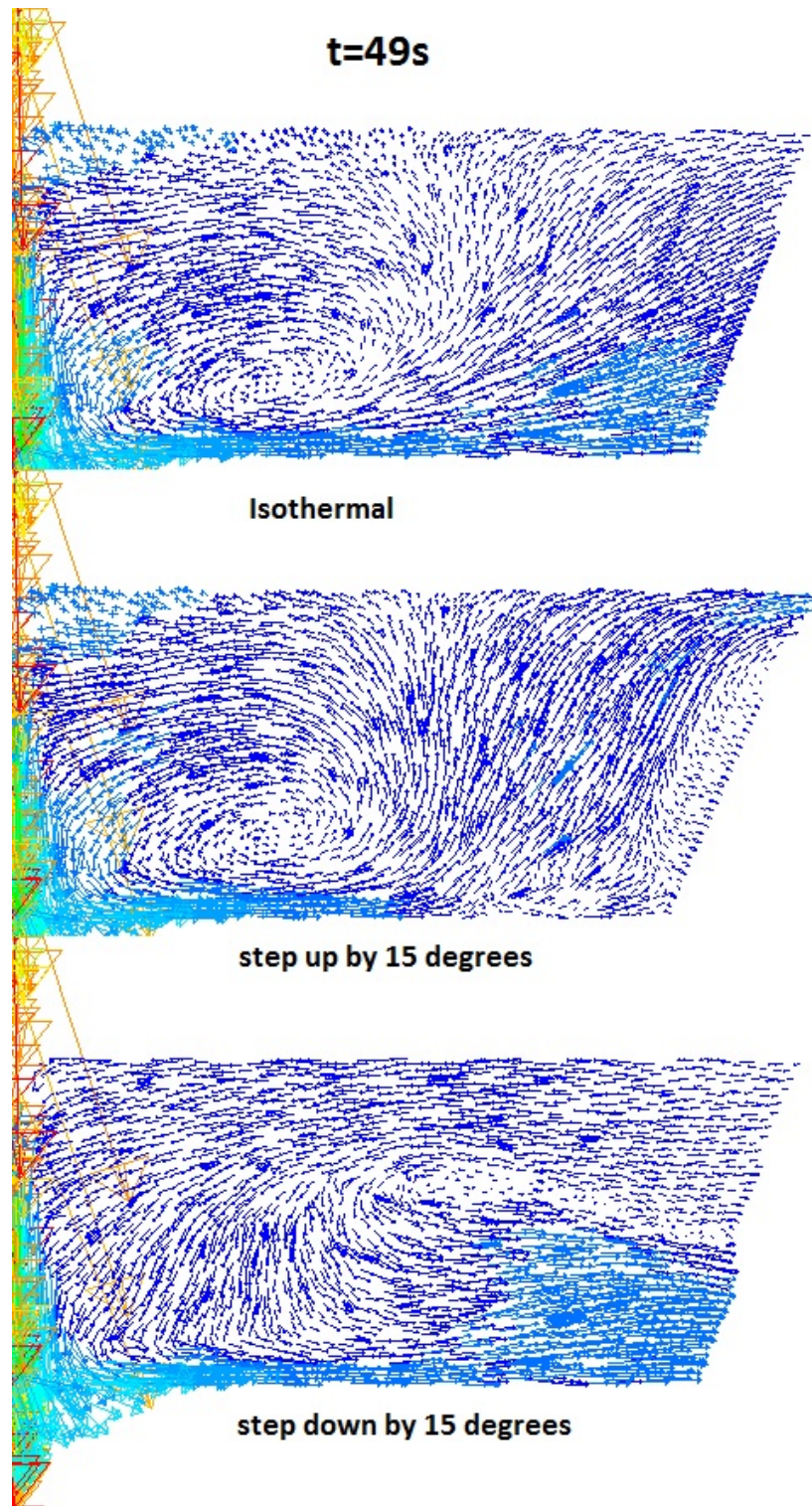


Figure 7.6 (g) Velocity fields under three different conditions at $t=49s$

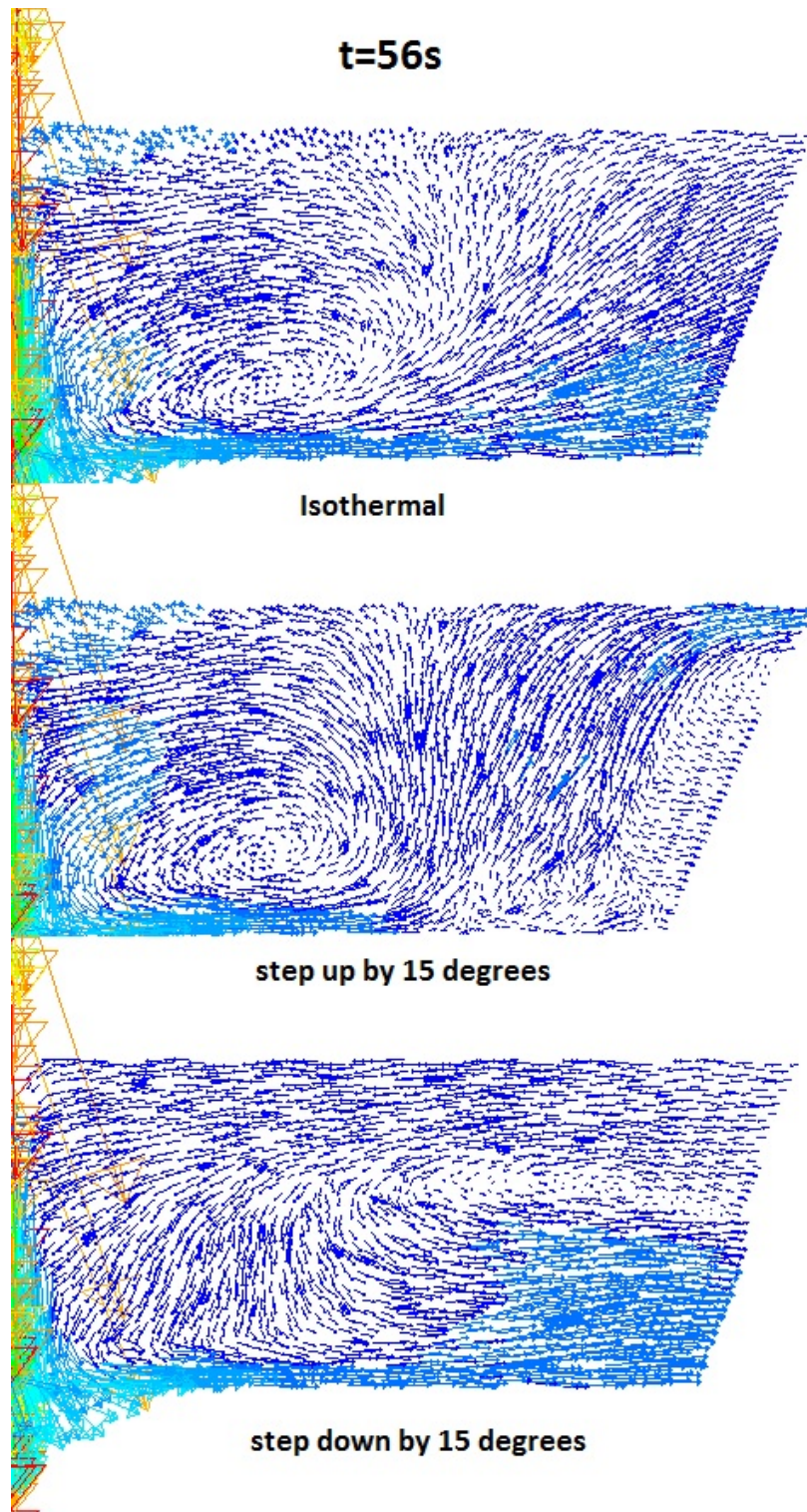


Figure 7.6 (h) Velocity fields under three different conditions at $t=56s$

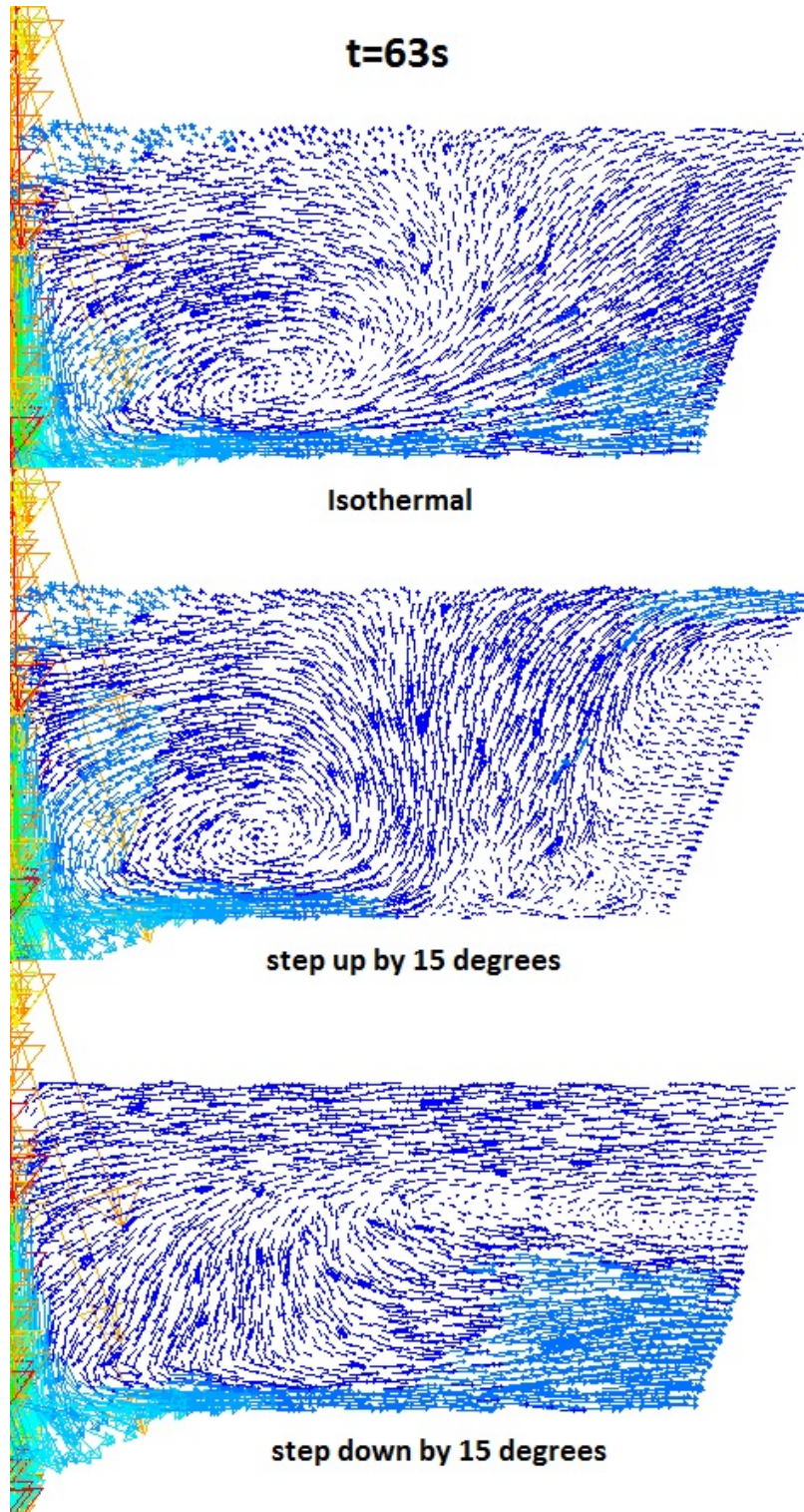


Figure 7.6 (i) Velocity fields under three different conditions at $t=63s$

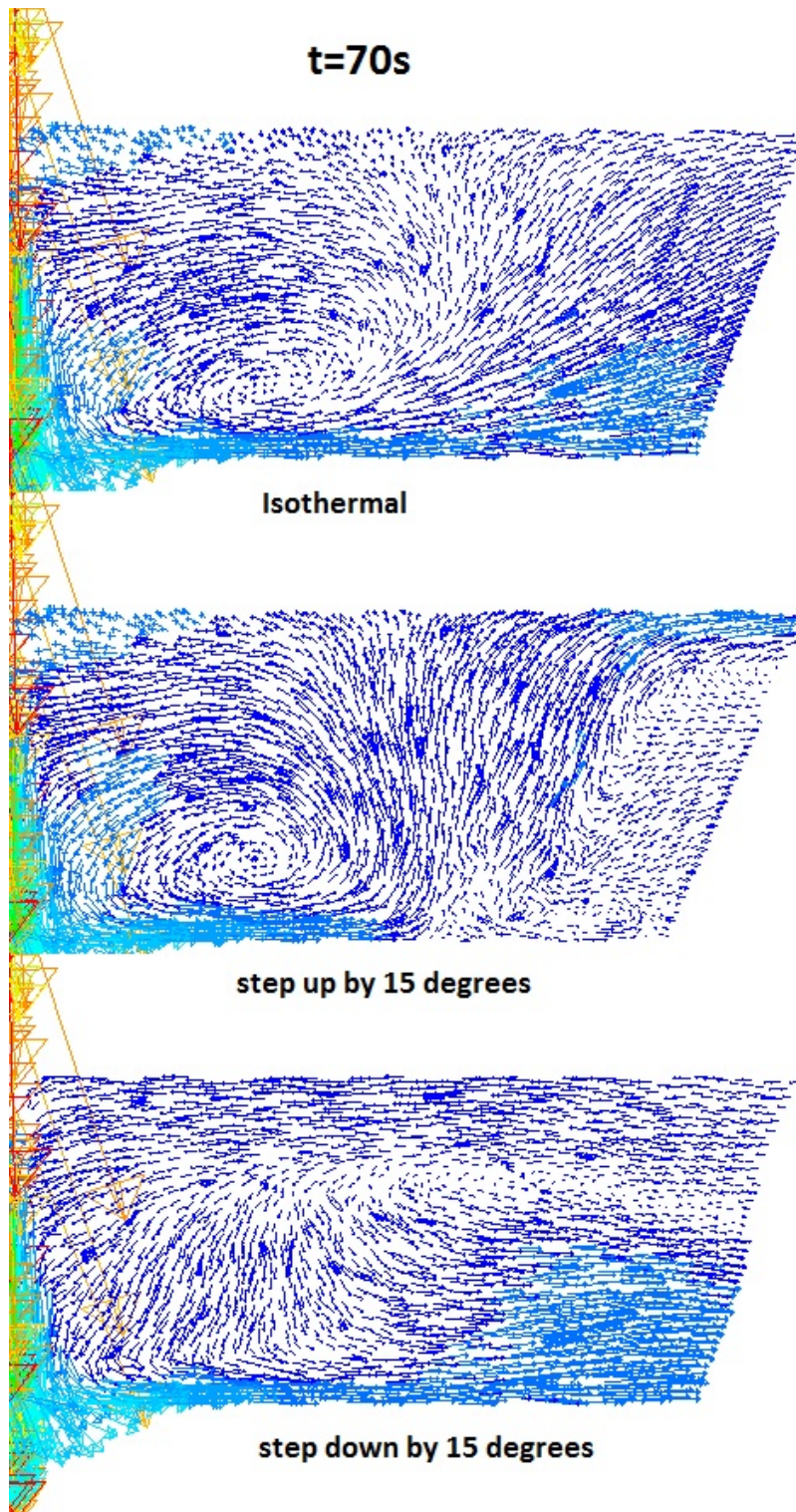


Figure 7.6 (j) Velocity fields under three different conditions at $t=70s$

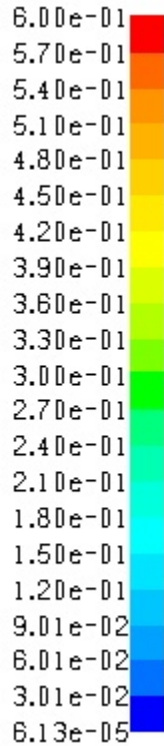


Figure-7.7 Colour map for Figures 7.6 (a) to (j)

Significant differences in the flow pattern can be observed for the isothermal, step up and step down conditions. For the tundish with a step up by 15 degrees, an upward flow is formed away from the jet entry zone, which is responsible for pushing the tracer upwards. This upward flow gets stronger with time. The upward flow could be beneficial in enhancing inclusion separation, as it would carry some inclusions upwards and attach them in the upper slag phase. However, for the tundish with a step down by 15 degrees, a strong downward flow is formed and this results in the tracer being pushed downwards. This downward flow would even worsen the steel cleanliness by dragging more inclusions into the SENs. So, a step

down condition is more harmful than a step up condition and care should be taken in the plant to avoid step down conditions. The bare tundish had been considered so far. In most steel plants, a turbo stop or an impact pad is used just beneath the shroud. At RTIT/QIT, the standard impact is used during most casting sequences. So it would be very interesting to see how flow patterns change under non-isothermal conditions in the tundish fitted with the standard impact pad. Figure 7.8 below shows the tracer dispersion behaviour in the tundish fitted with the standard impact pad under isothermal conditions. The tracer first mixes within the impact pad zone and then starts advancing further. Within the impact pad zone, a recirculation is formed which initially retains the tracer within itself. The tracer moves upwards, because of this recirculation, and then advances towards the ends of the tundish along the top surface. With time the tracer mixes from the upper surface towards the base of the tundish. Figure 7.9 represents the tracer mixing behaviour within the tundish fitted with the standard impact pad for a step up of 10 degrees. Not much difference is observed here, when compared to that under isothermal conditions. The simple reason for this is the presence of the pad. The impact pad already generates a strong recirculation in the jet entry zone and directs the flow upwards. The incoming hot fluid is carried upwards as a result of this recirculation. Now the buoyancy forces become significant towards the ends of the tundish only when the hot fluid being lighter start rising upwards. Since here

the hot fluid is already carried upward because of the impact pad, strong buoyancy forces are not generated towards the extremities of the tundish, and hence there is no difference between isothermal and non-isothermal conditions. This fact is also evident when the step up is even more. Figure 7.10 shows the tracer dispersion behaviour within the tundish fitted with the standard impact pad for a step up of 15 degrees. Figure 7.11 (a) to (i) represent the velocity fields within in the tundish fitted with the standard impact pad. The velocity fields are compared for the isothermal condition and a step up of 15 degrees at different intervals of time. The colour map for figure 7.11 is the given in figure 7.7 above. It is clearly seen, there is not much difference in the flow field under isothermal and non-isothermal conditions. Some minute difference is observed in the recirculation zone within the standard impact pad.

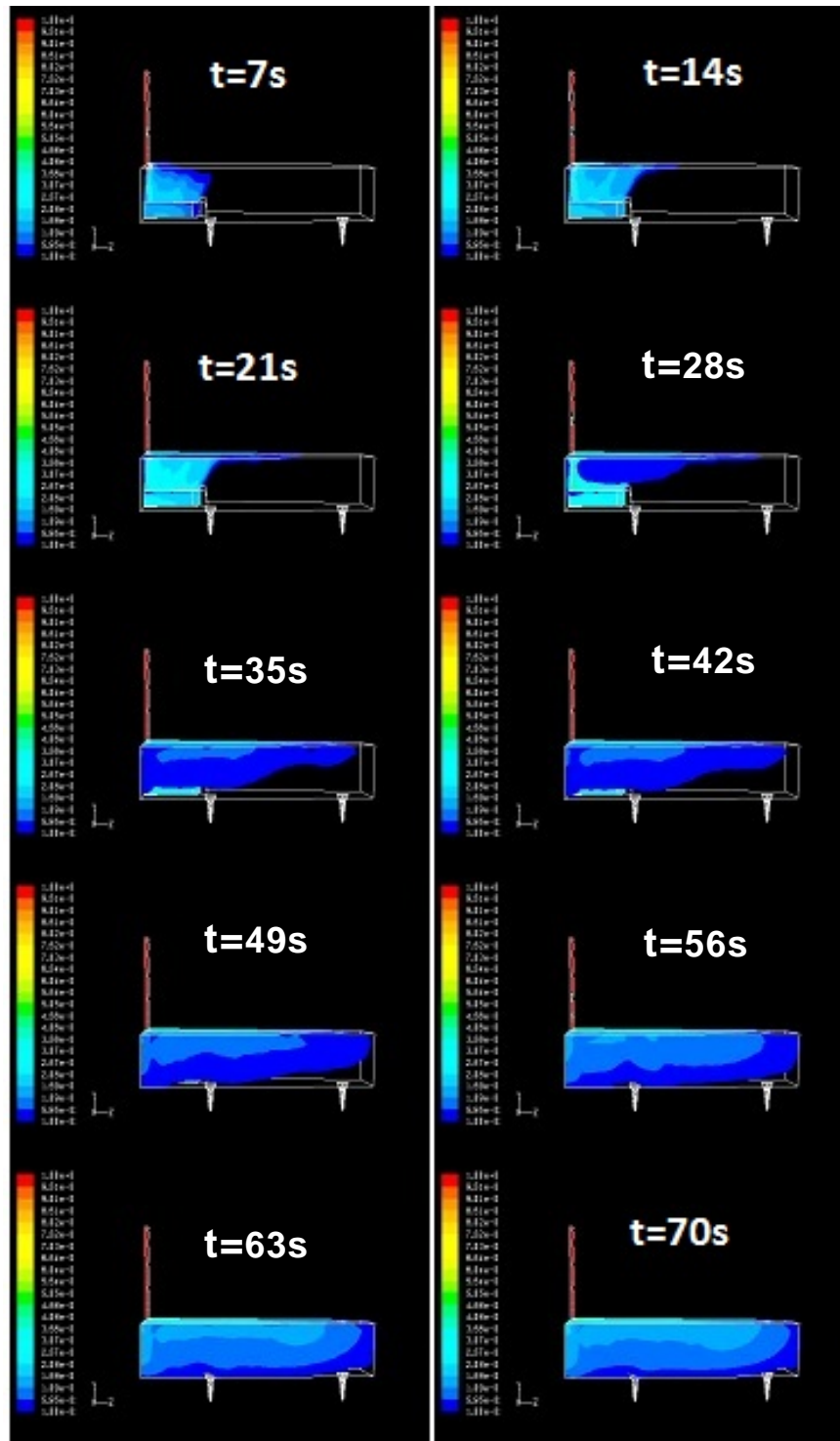


Figure- 7.8 Contours of tracer concentration within the tundish fitted with SIP, under isothermal conditions. $\Delta t = 7s$.

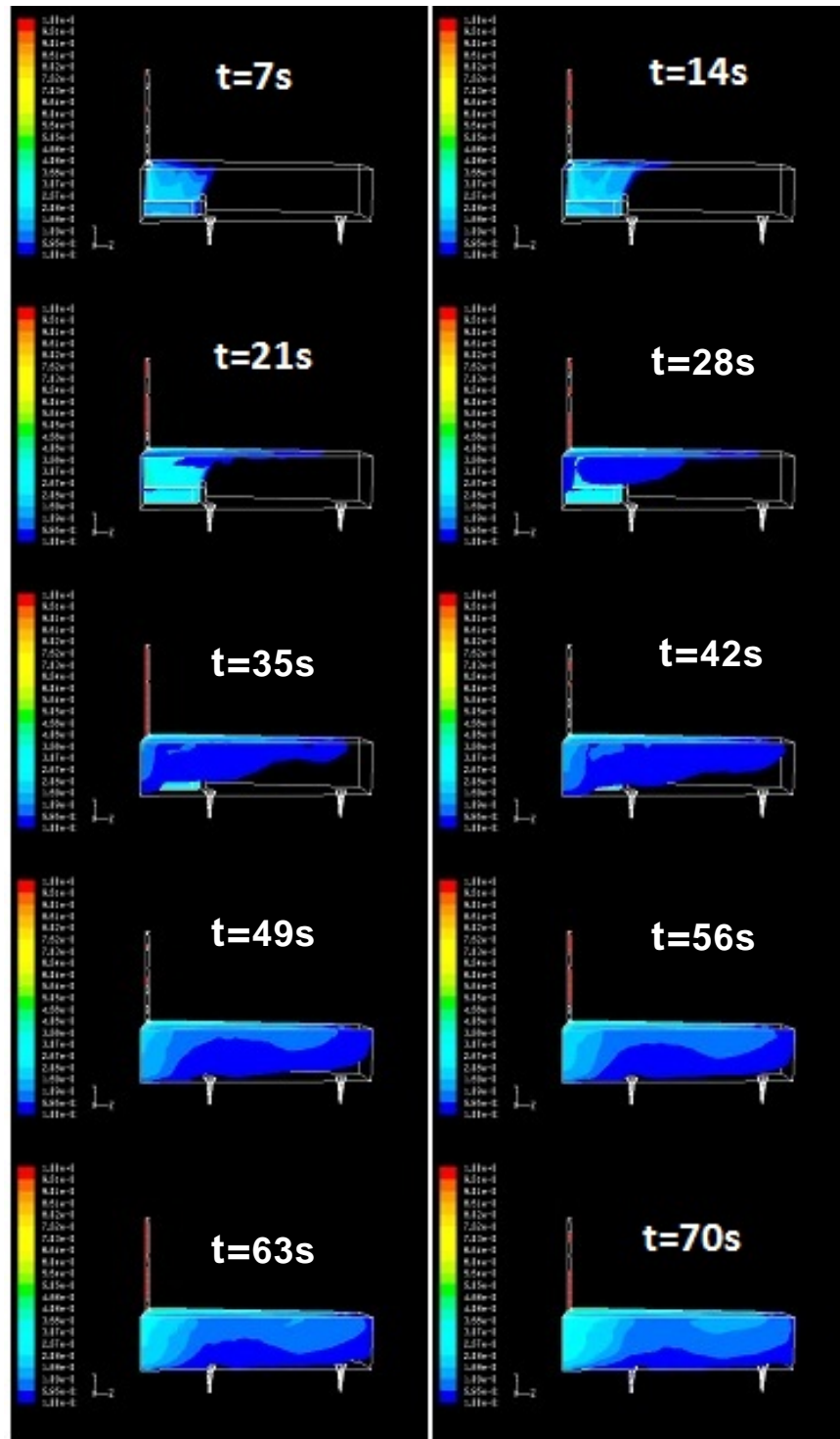


Figure- 7.9 Contours of tracer concentration within the tundish fitted with SIP, for a step up of 10 degrees. $\Delta t = 7s$.

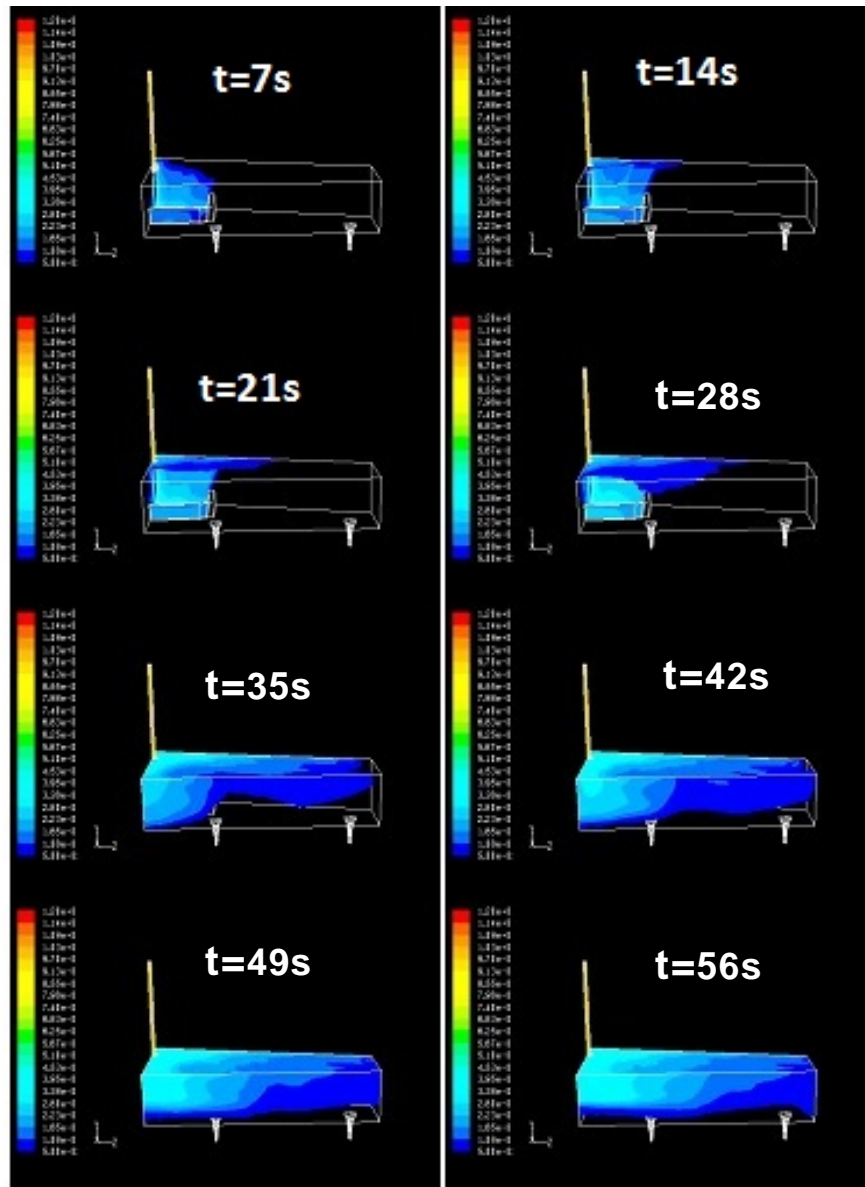


Figure- 7.10 Contours of tracer concentration within the tundish fitted with SIP, for a step up of 15 degrees. $\Delta t = 7s$.

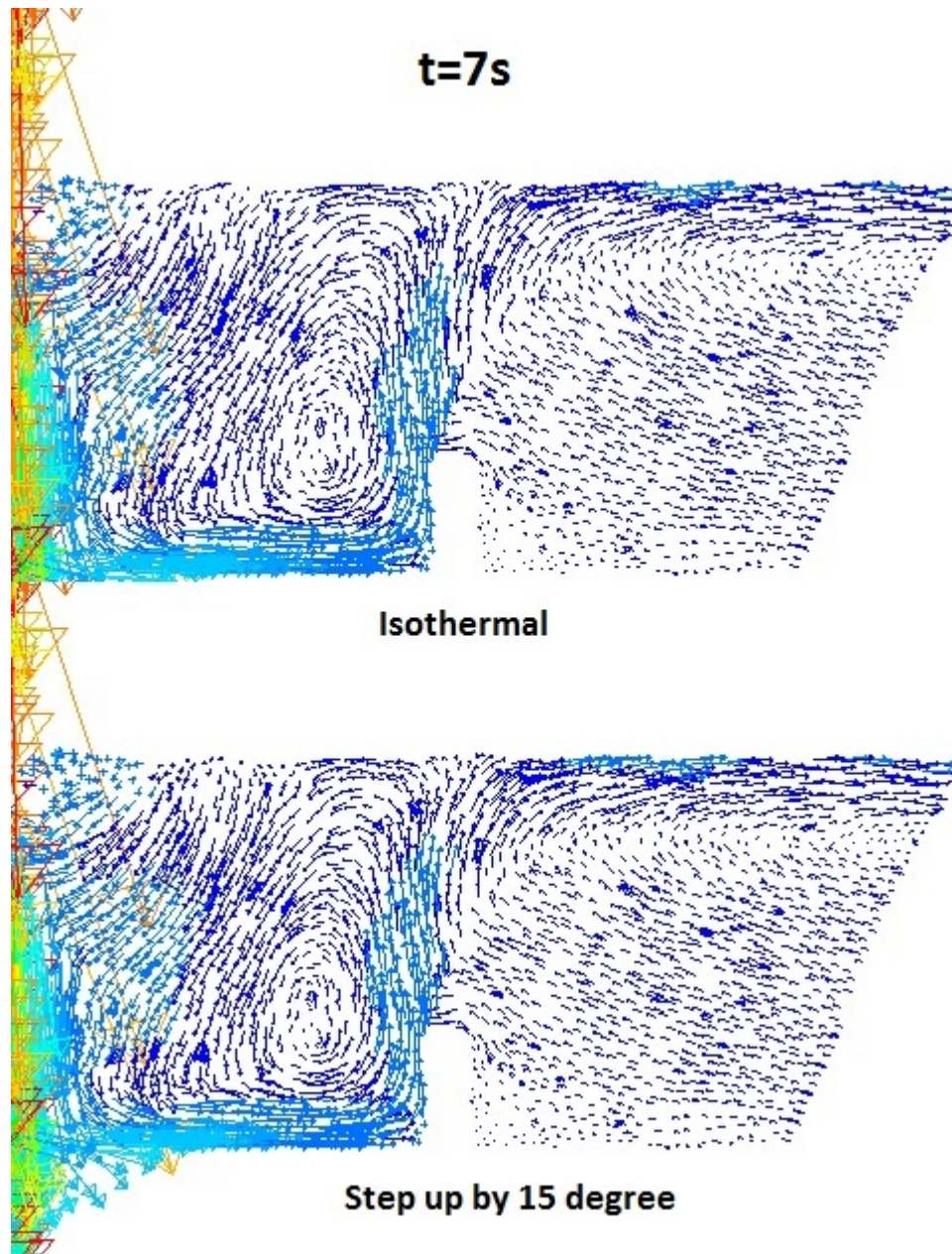


Figure-7.11(a) Velocity fields under different conditions at t=7s

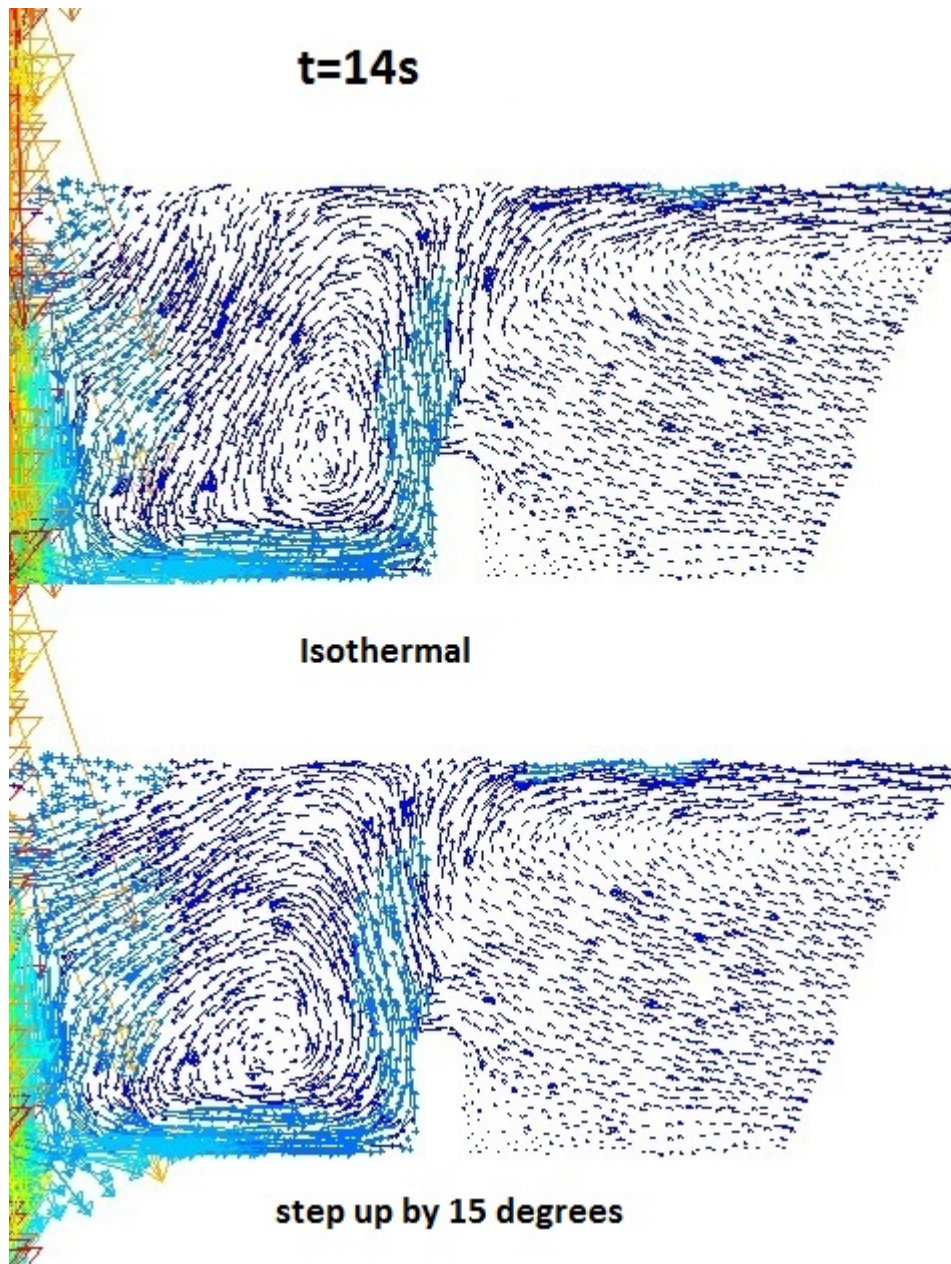


Figure-7.11(b) Velocity fields under different conditions at $t=14s$

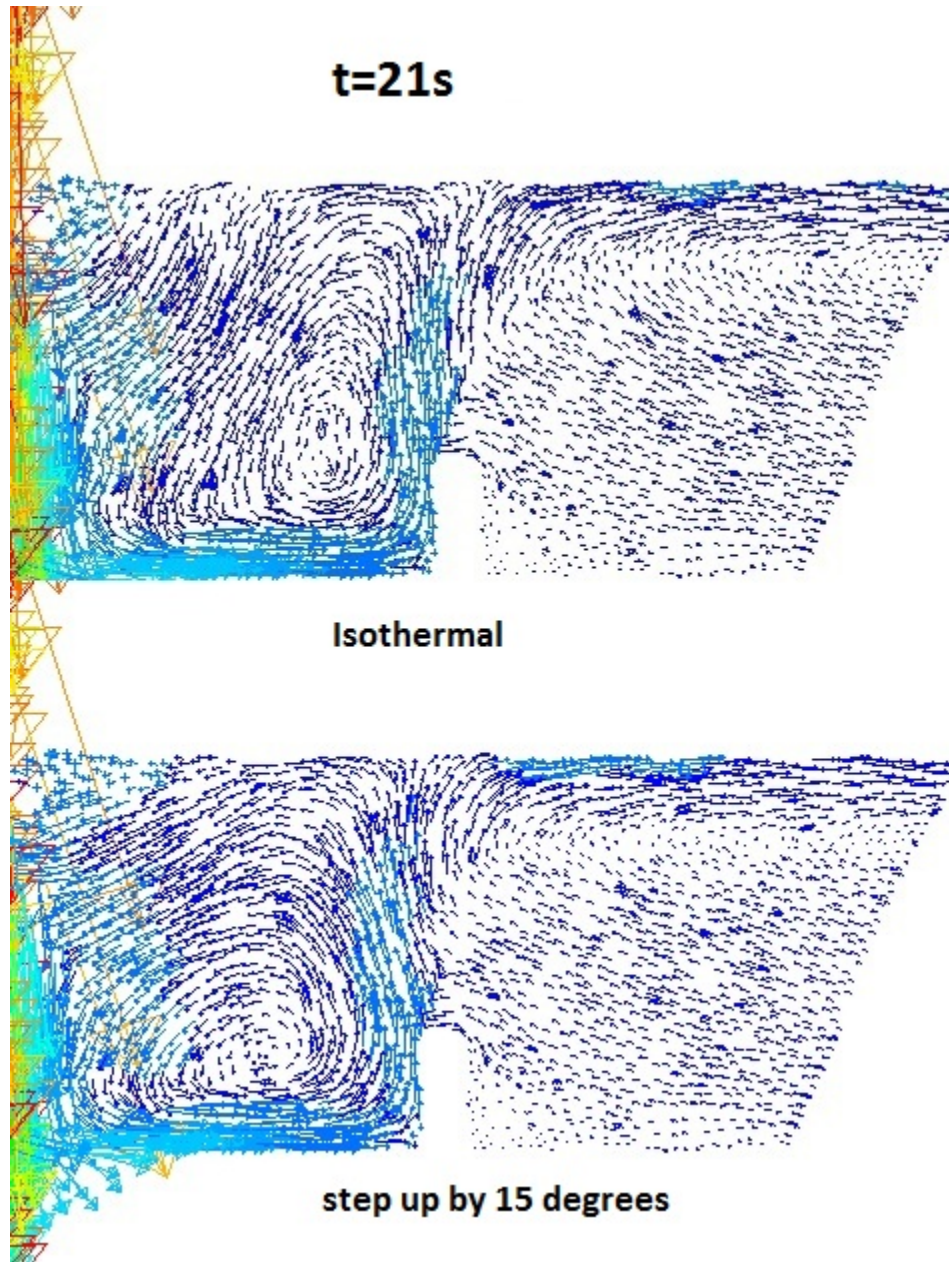


Figure-7.11(c) Velocity fields under different conditions at $t=21s$

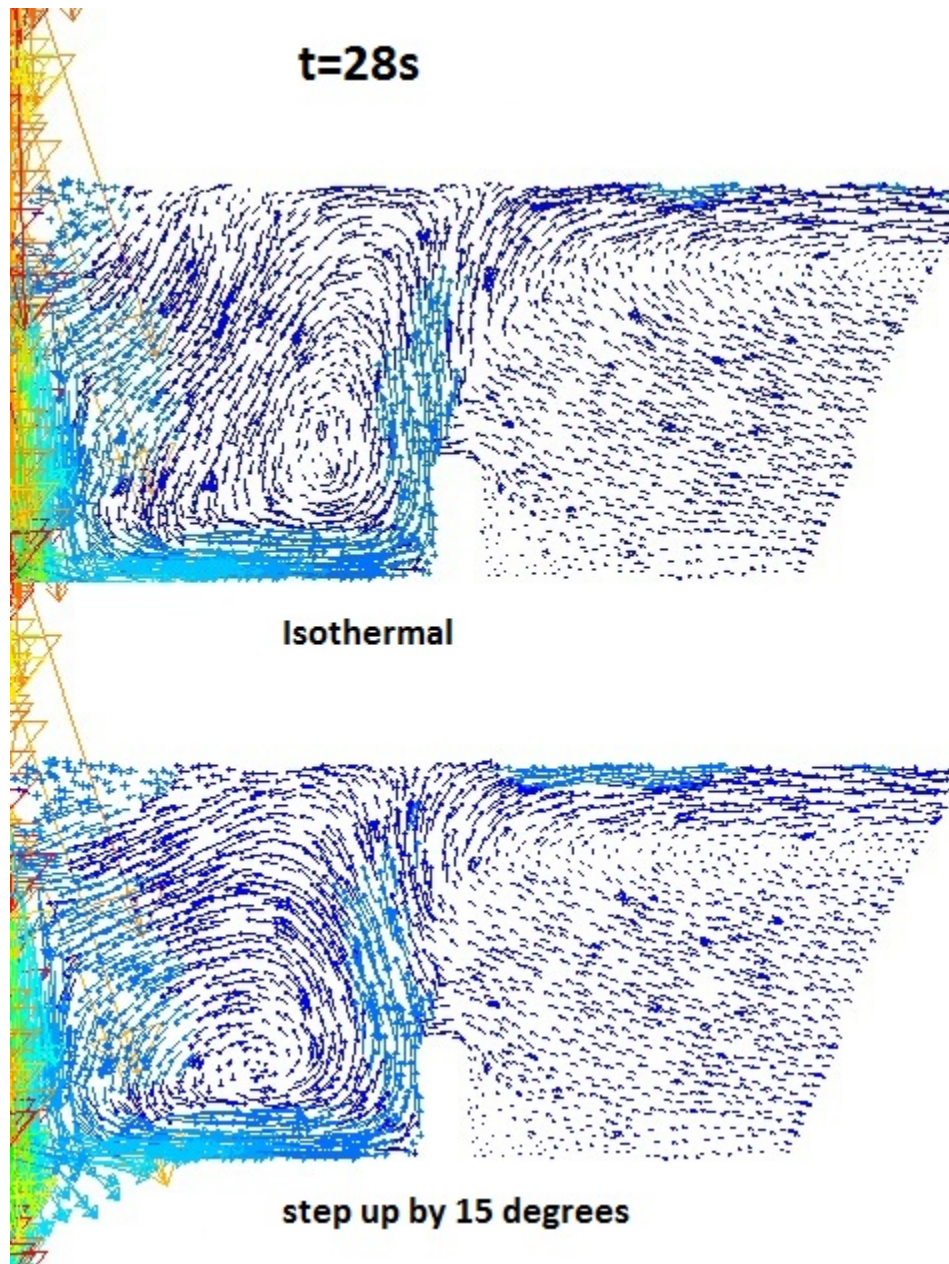


Figure-7.11(d) Velocity fields under different conditions at $t=28s$

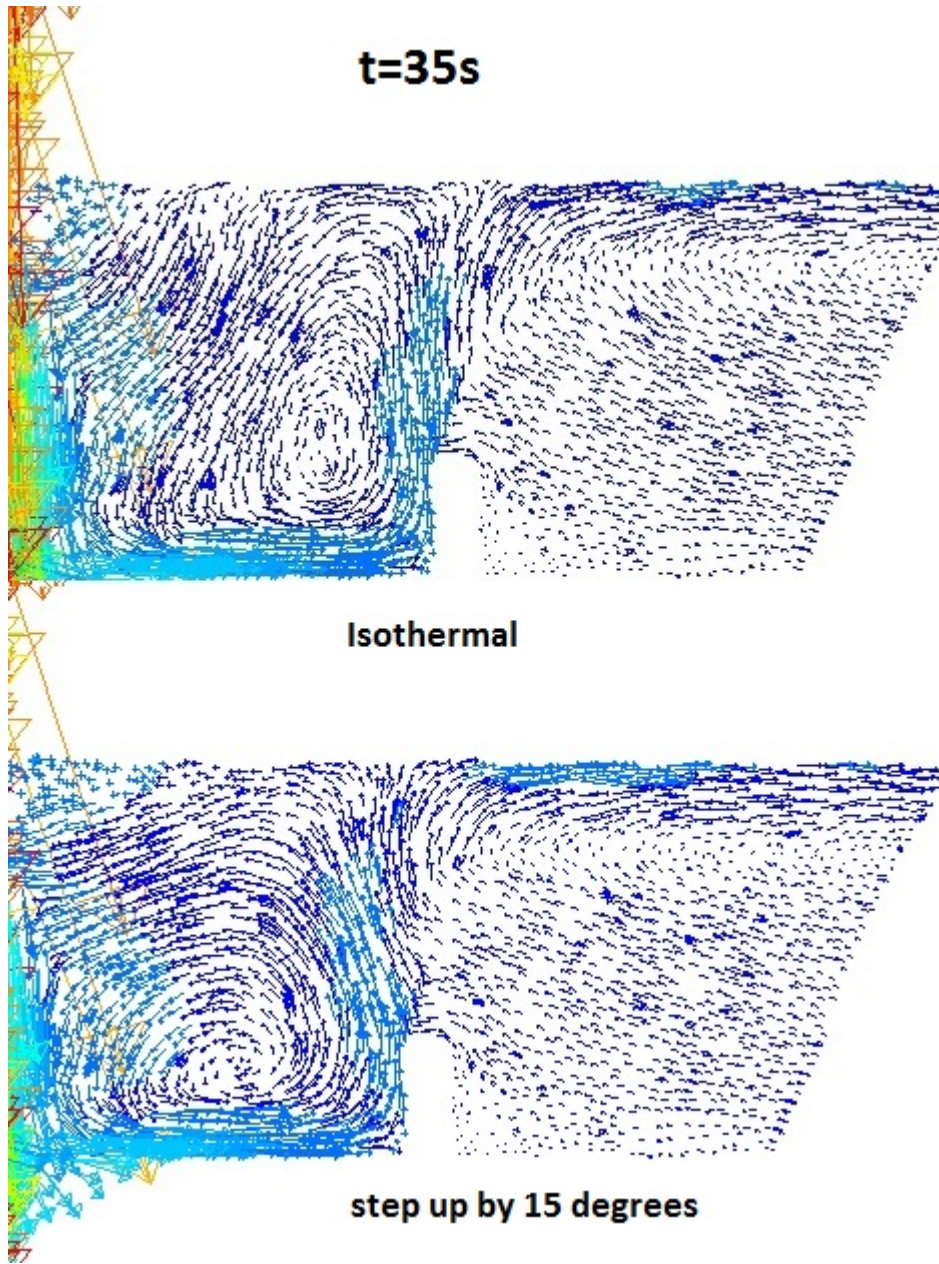


Figure-7.11(e) Velocity fields under different conditions at t=35s

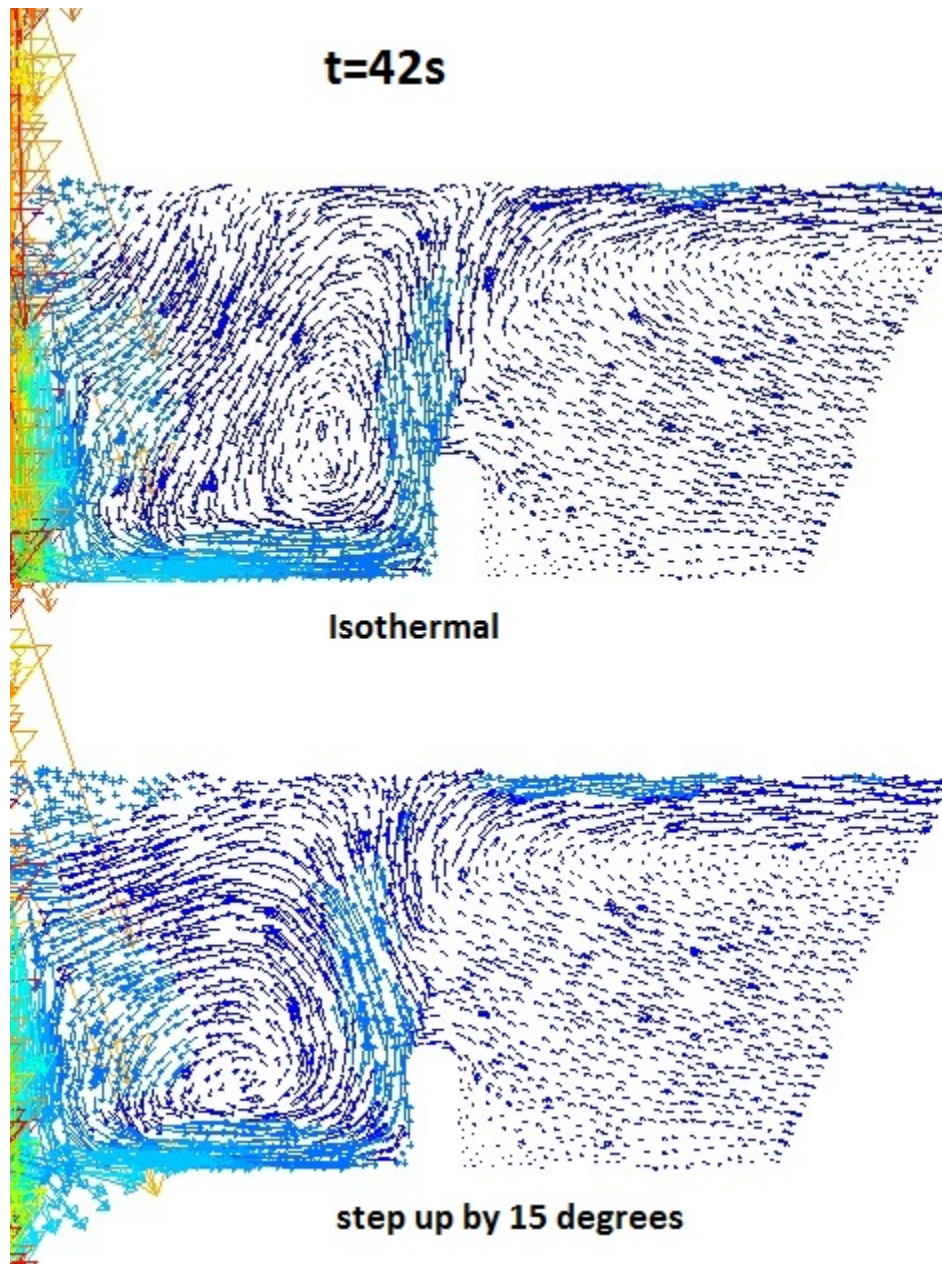


Figure-7.11(f) Velocity fields under different conditions at t=42s

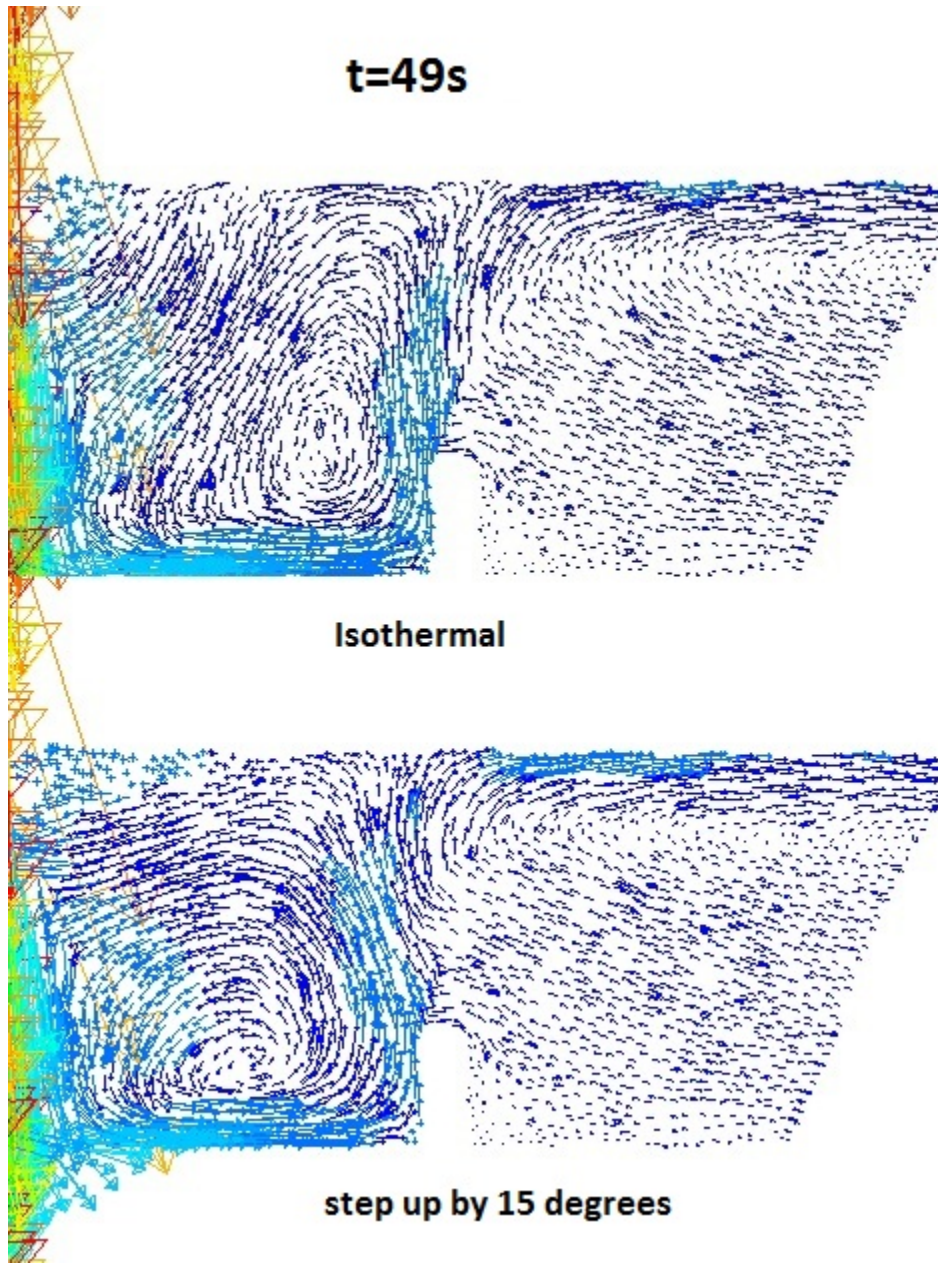


Figure-7.11(g) Velocity fields under different conditions at $t=49s$

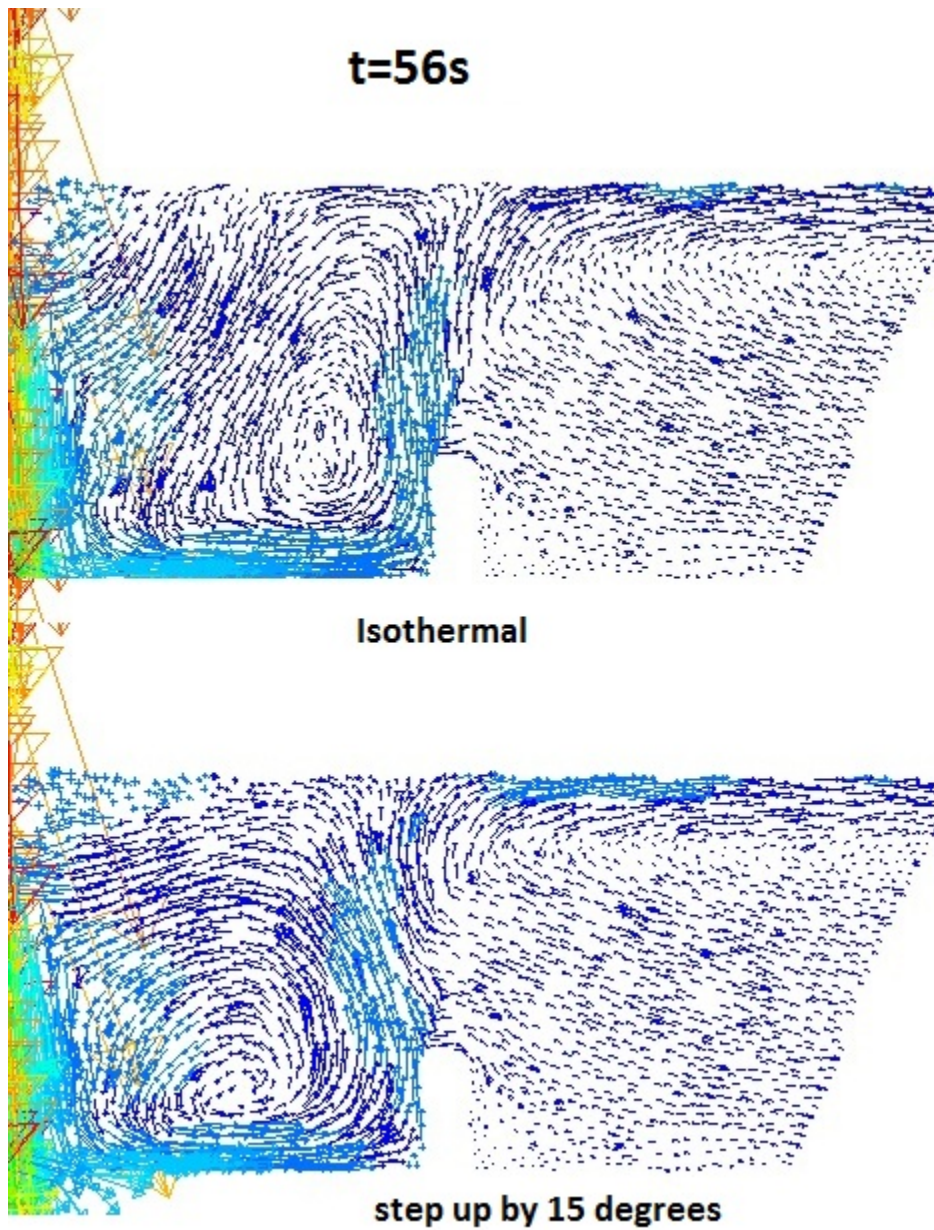


Figure-7.11(h) Velocity fields under different conditions at t=56s

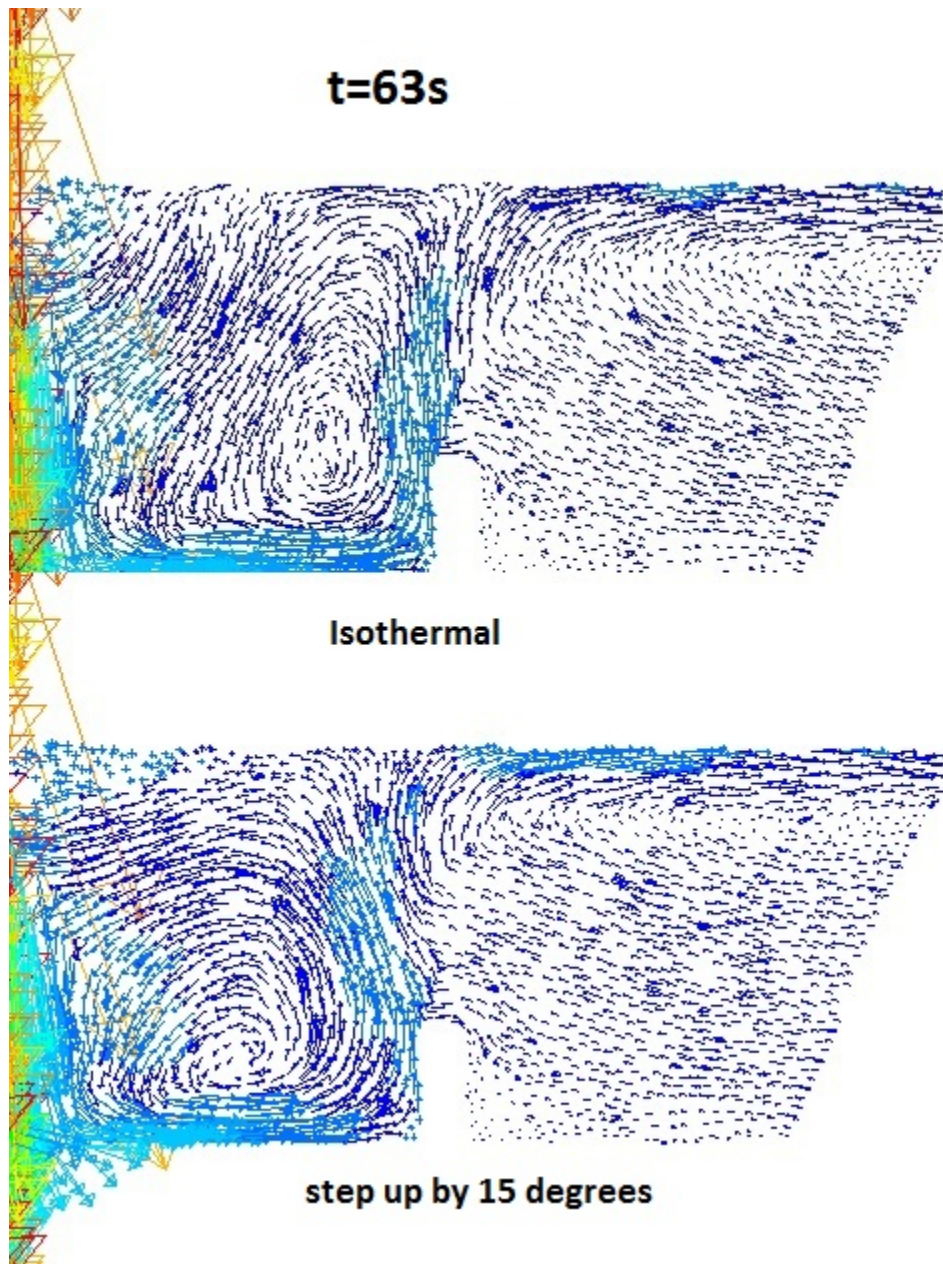


Figure-7.11(i) Velocity fields under different conditions at $t=63s$

7.4.2 Physical modelling of tracer dispersion for steady state casting operations

Physical modelling of non-isothermal fluid flow was carried out in the one third scale water model tundish. For physical modelling, tracer dispersion experiments were done to visualize the effects of step up conditions on fluid flow. Unlike the mathematical model where the step inputs were 10 and 15 degrees, for the physical model step inputs of 5, 10 and 15 degrees have been studied. Figure 7.12 shows the tracer dispersion behaviour under isothermal conditions for a bare tundish. The experiments were performed for 60-70 seconds as after that it was difficult to see any tracer movements inside the tundish. The wave front first forms a curvilinear profile and then slowly flattens towards the end of the tundish. Figure-7.13 shows the tracer mixing patterns within the bare tundish with a step up of 5 degrees. When figures 7.12 and 7.13 are compared, it is clearly seen that towards the extremities of the tundish the tracer mixing patterns are different. In figure 7.13, the presence of buoyancy forces are evident near the end of the tundish, and these are responsible for pushing up the tracer. So even, a 5 degree step up in temperature affects the flow. Figures 7.14 and 7.15 represent the tracer dispersion behaviour for a step up of 10 and 15 degrees respectively. Owing to the higher thermal gradients, buoyancy forces are more severe here and are reflected in the tracer mixing pattern.

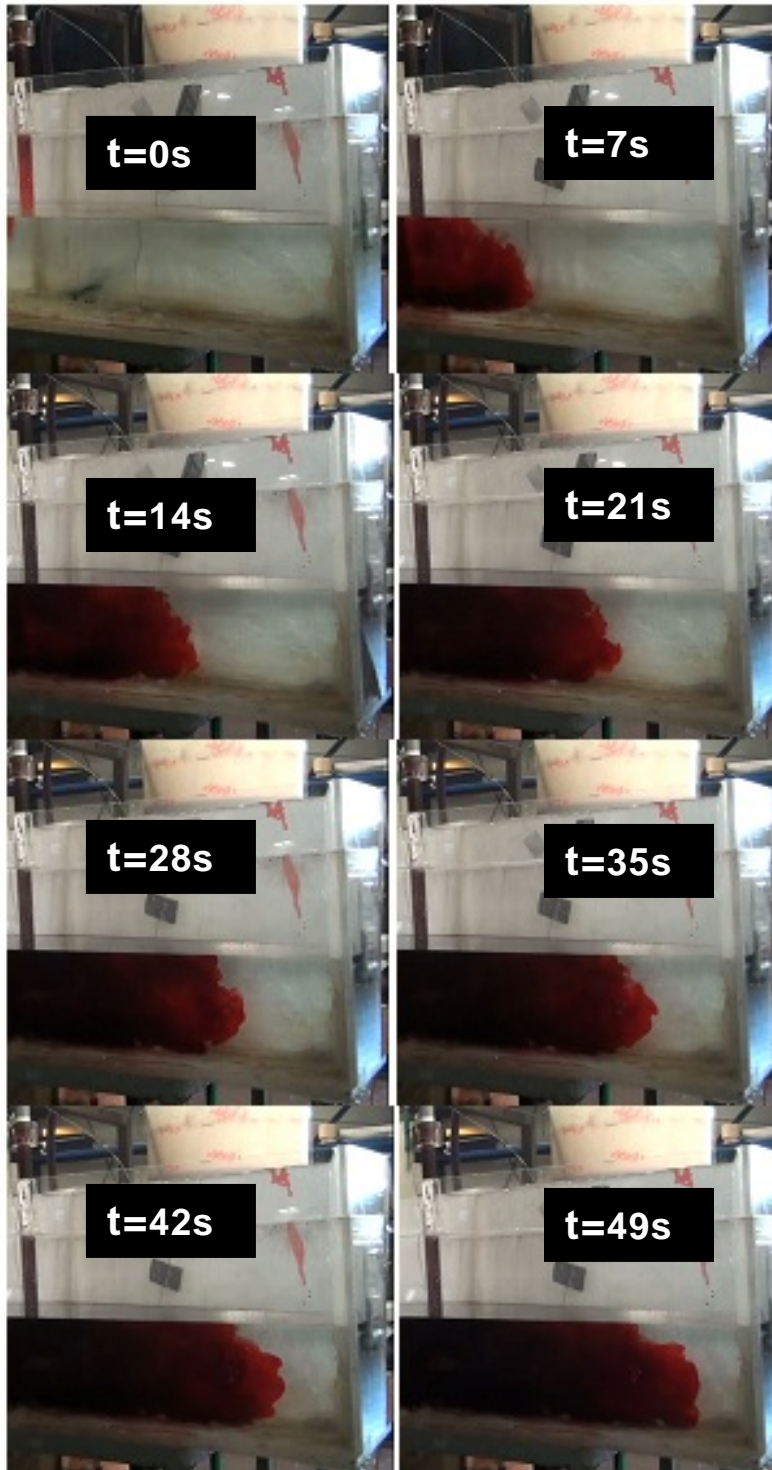


Figure-7.12(a) Tracer dispersion under isothermal conditions in a bare tundish. $\Delta t = 7s$

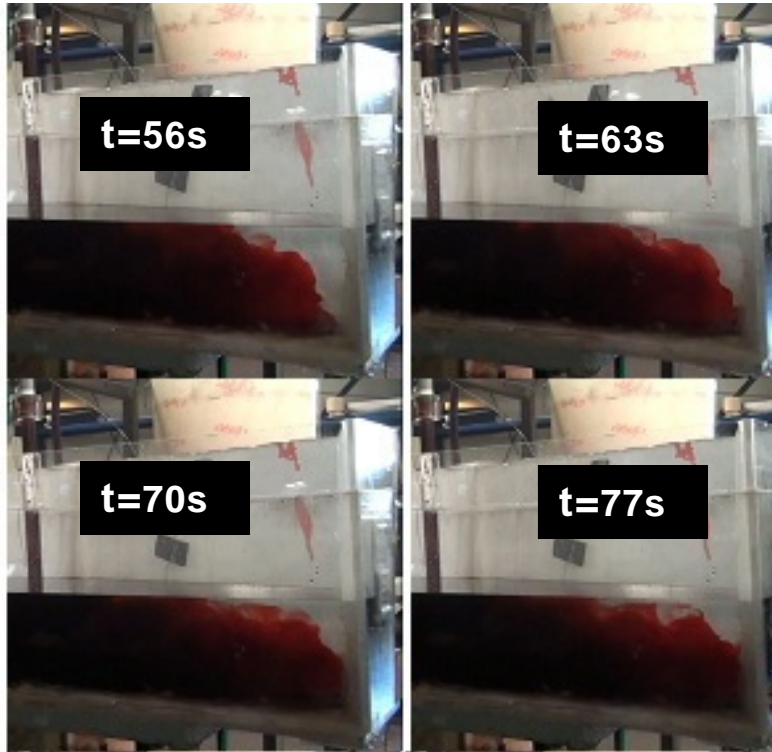


Figure-7.12(b) Tracer dispersion under isothermal conditions in a bare tundish. $\Delta t = 7s$

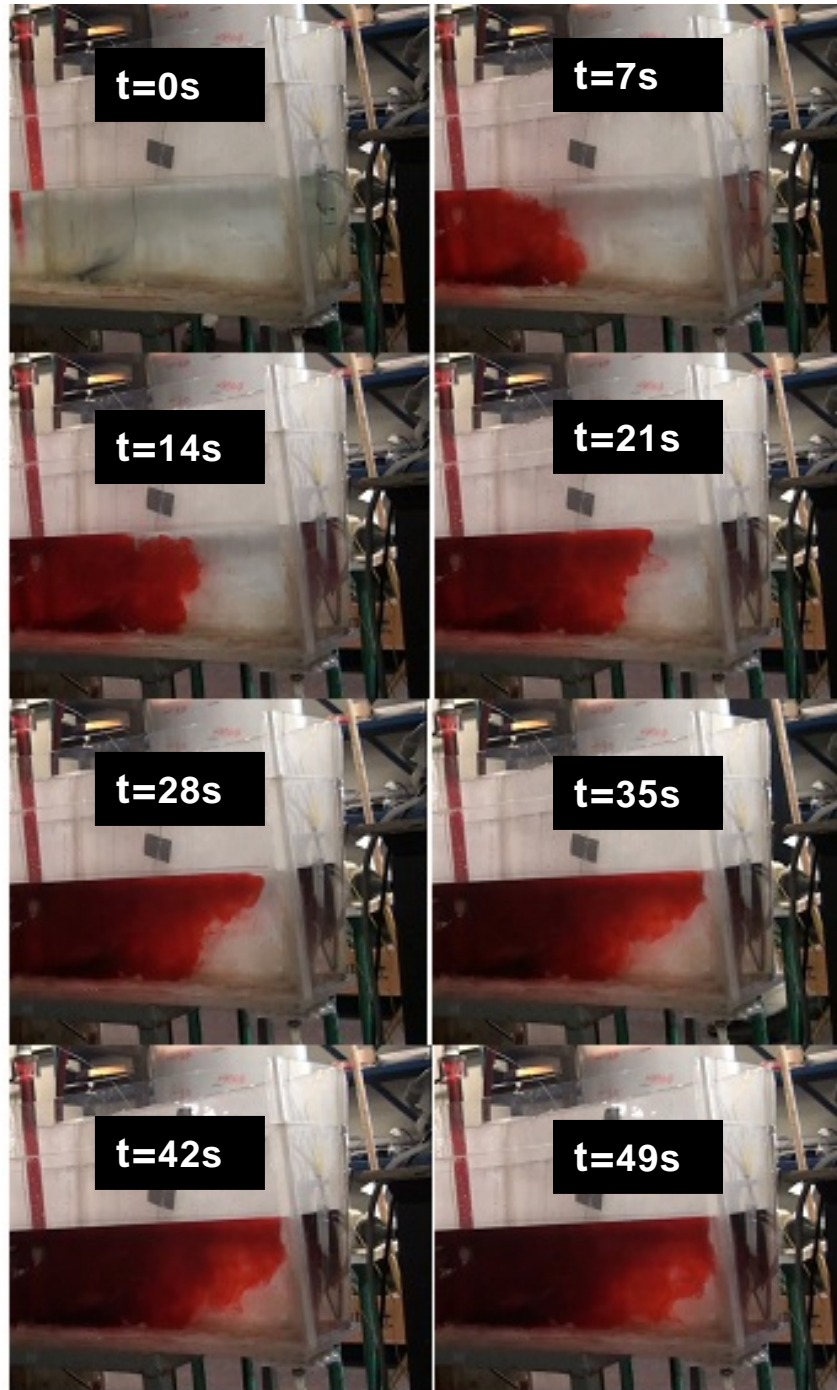


Figure-7.13(a) Tracer dispersion in a bare tundish for a step up by 5 degrees. $\Delta t=7s$

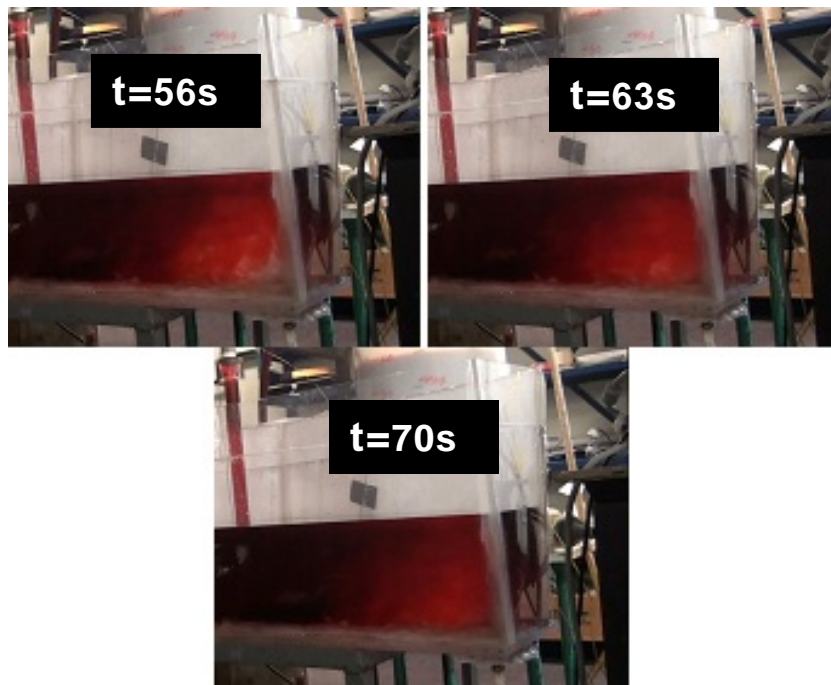


Figure-7.13(b) Tracer dispersion in a bare tundish for a step up by 5 degrees. $\Delta t = 7s$

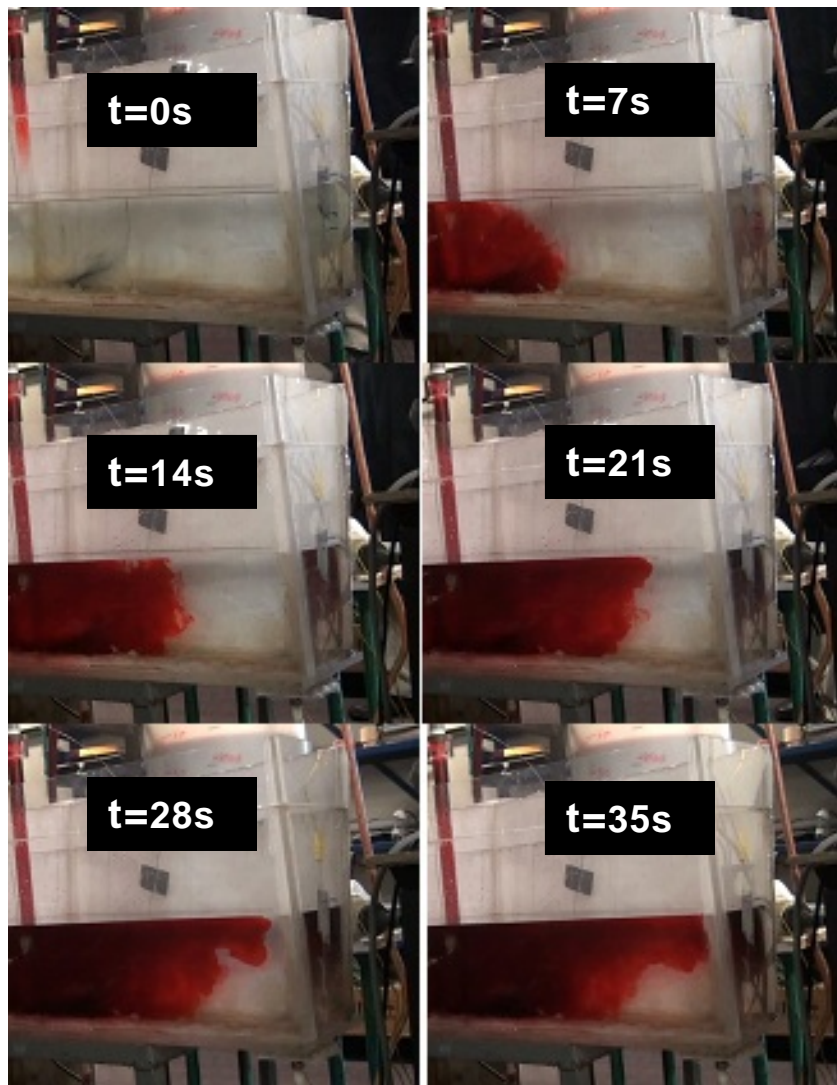


Figure-7.14 (a) Tracer dispersion in a bare tundish for a step up by 10 degrees. $\Delta t = 7s$

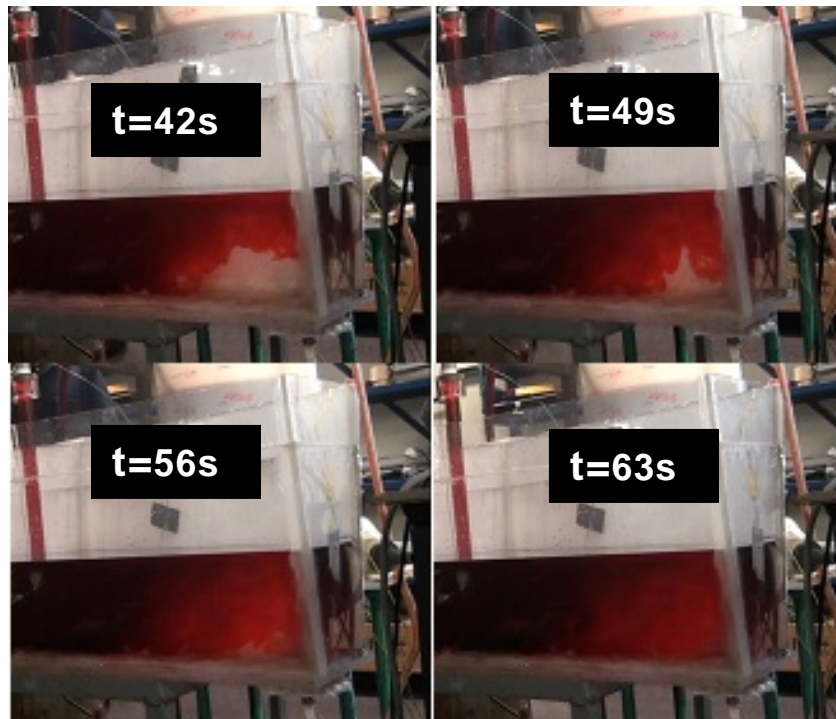


Figure-7.14 (b) Tracer dispersion in a bare tundish for a step up by 10 degrees. $\Delta t = 7s$

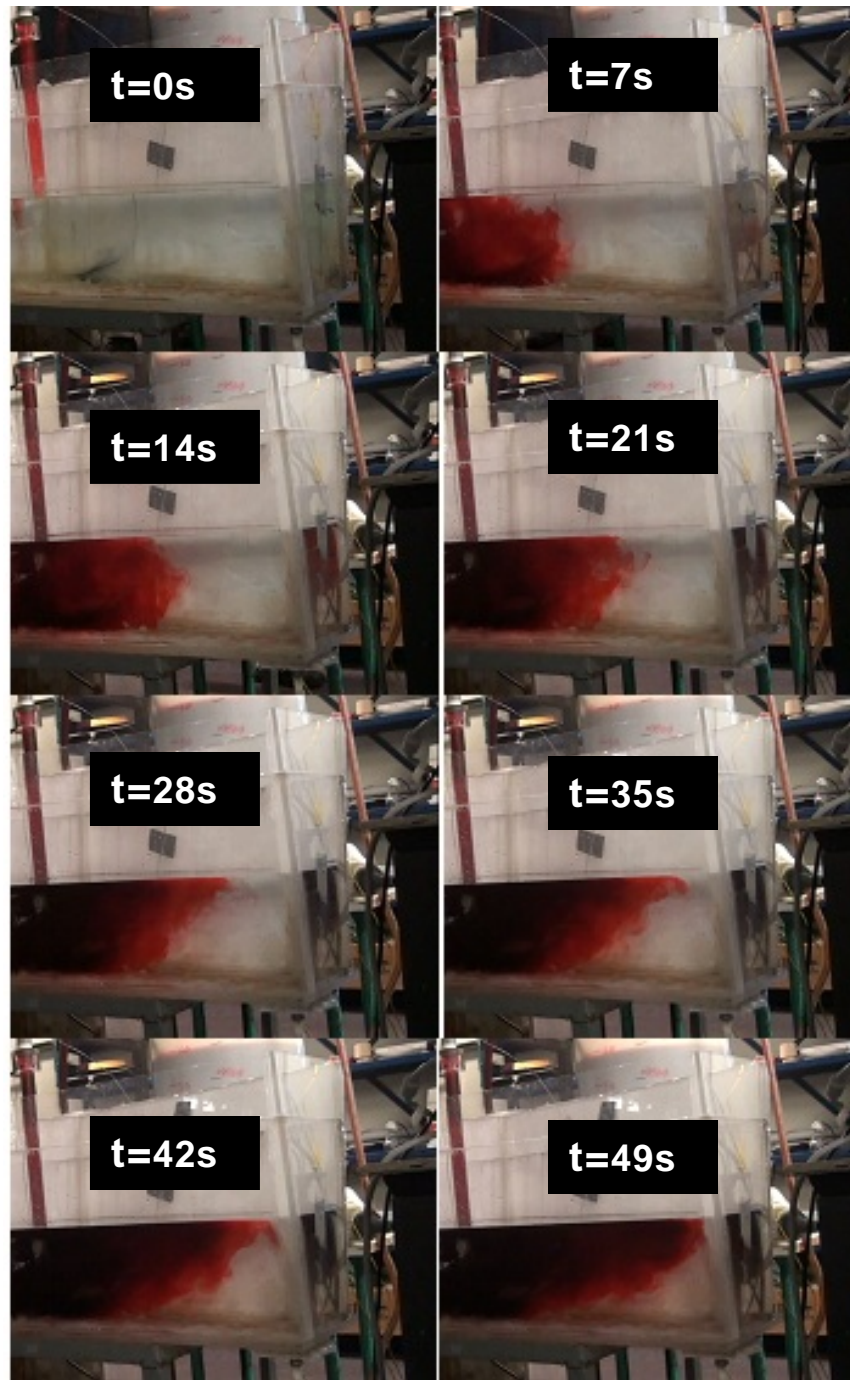


Figure-7.15 (a) Tracer dispersion in a bare tundish for a step up by 15 degrees. $\Delta t = 7s$

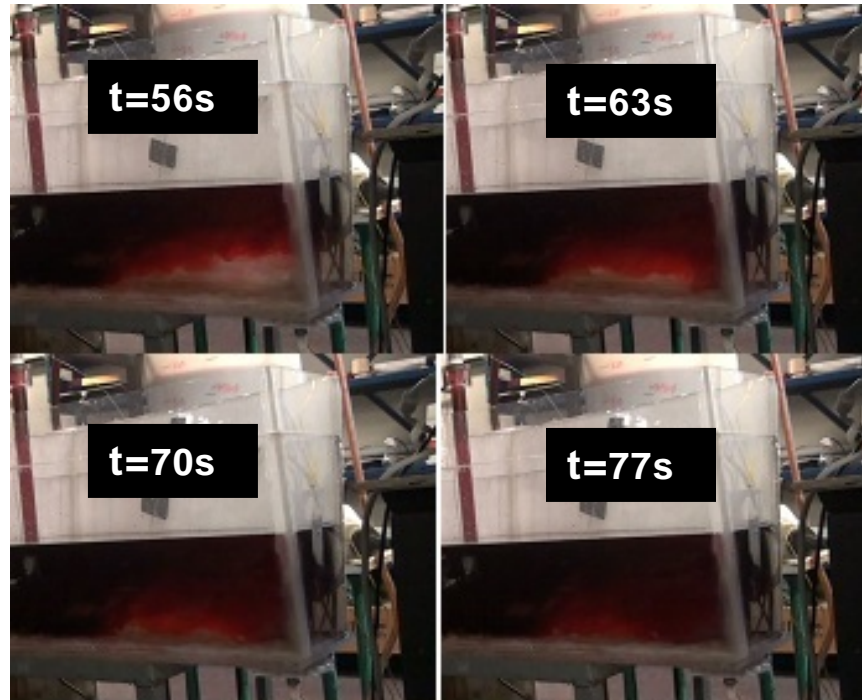


Figure-7.15 (b) Tracer dispersion in a bare tundish for a step up by 15 degrees. $\Delta t = 7s$

In the jet entry zone, near the shroud, the turbulence is very high, and hence inertial forces are significant. Towards the end of the tundish, the turbulence is dissipated, and so the buoyancy forces become dominant over inertial forces. For this reason for all the step up conditions of 5, 10, and 15 degrees, the difference in tracer mixing behaviour is evident near the extremity of the tundish. Now it would be interesting to see, how the flow patterns are affected by these step ups of 5, 10, and 15 degrees in the tundish when it has the standard impact pad. Figure 7.16 below shows the tracer dispersion behaviour in the tundish with the SIP, with a step input of 5 degrees.

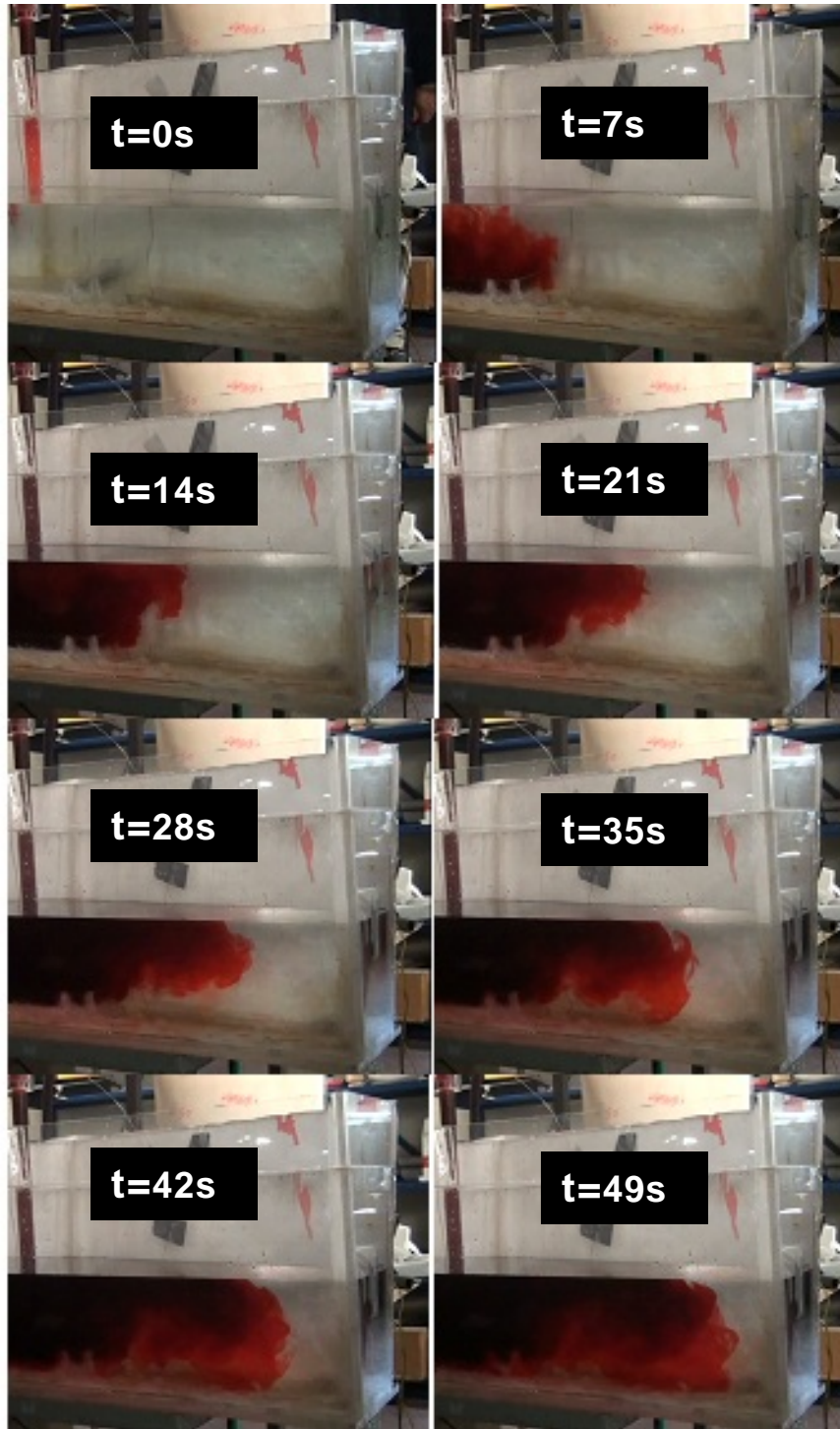


Figure-7.16 (a) Tracer dispersion in the tundish with SIP for a step up by 5 degrees. $\Delta t=7s$

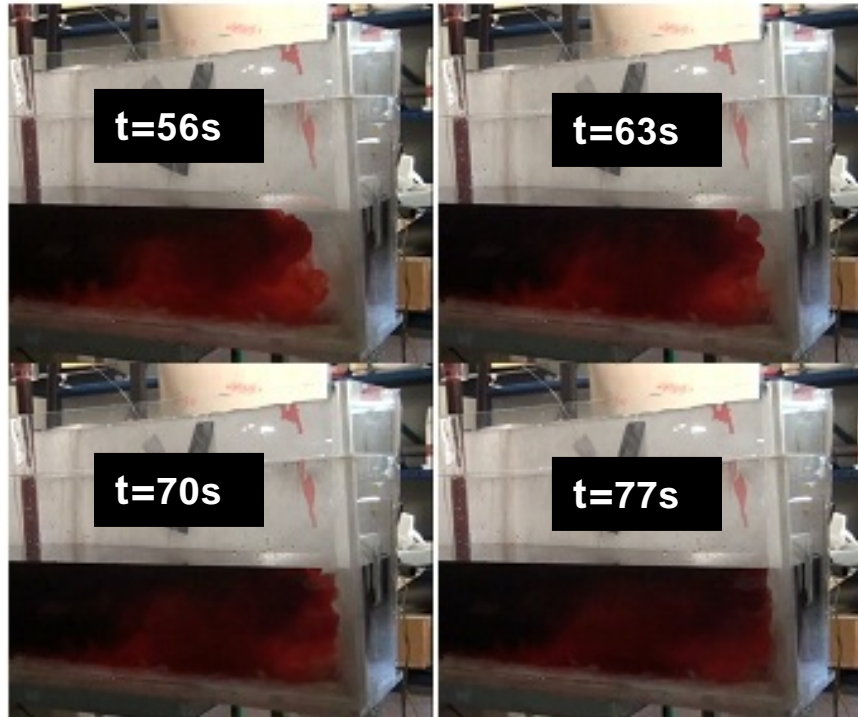


Figure-7.16 (b) Tracer dispersion in the tundish with SIP for a step up by 5 degrees. $\Delta t=7s$

Here, the tracer first mixes within the impact pad and then disperses further. The tracer moves upwards, due to the recirculation generated inside the pad, and then slowly disperses toward the end of the tundish. During its course, it mixes from the top surface towards the base of the tundish. Figure 7.17 and 7.18 shows the tracer dispersion behaviour, within the tundish with the standard impact pad for step ups of 10 and 15 degrees.

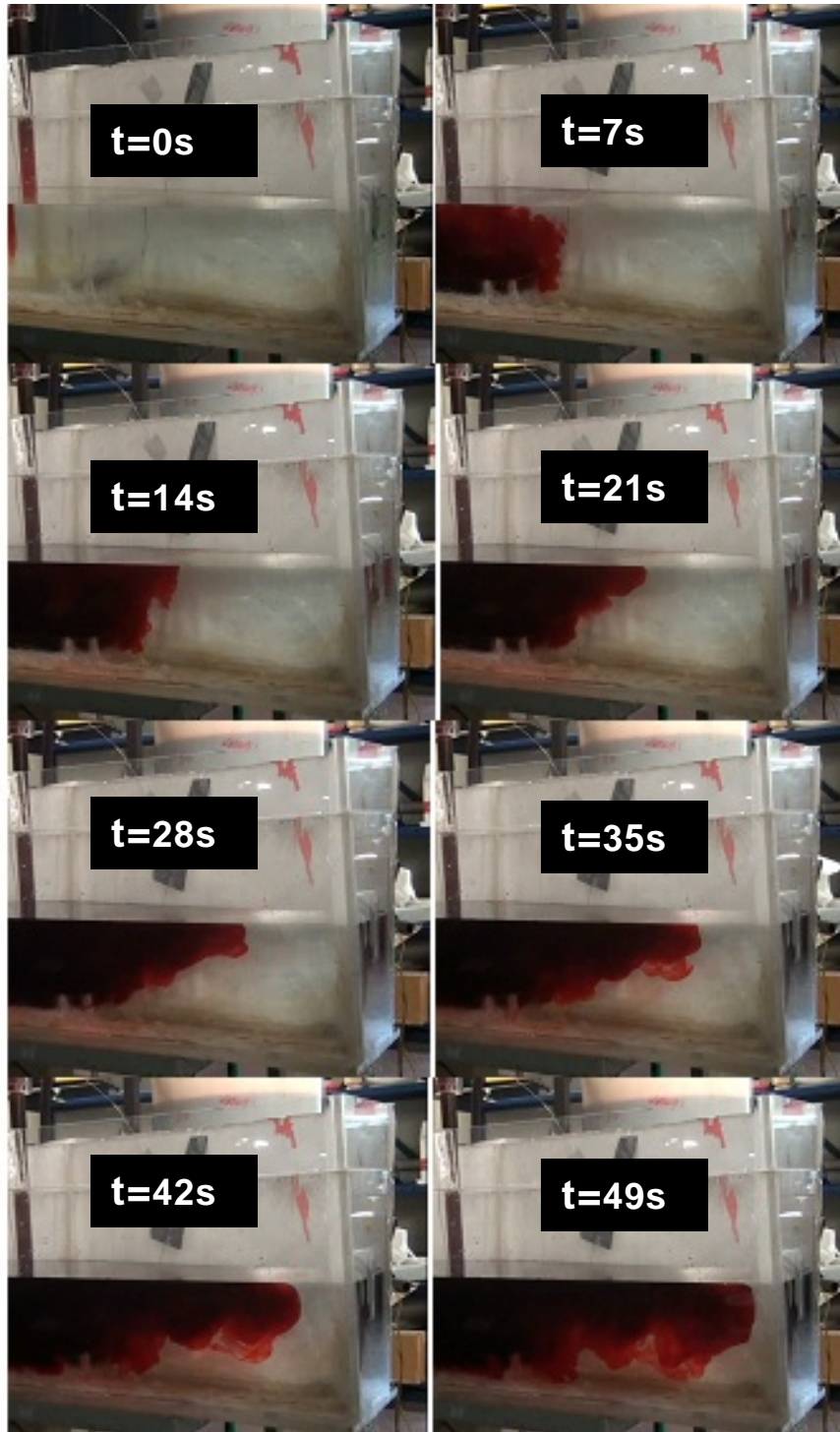


Figure-7.17(a) Tracer dispersion in the tundish with SIP for a step up by 10 degrees. $\Delta t=7s$

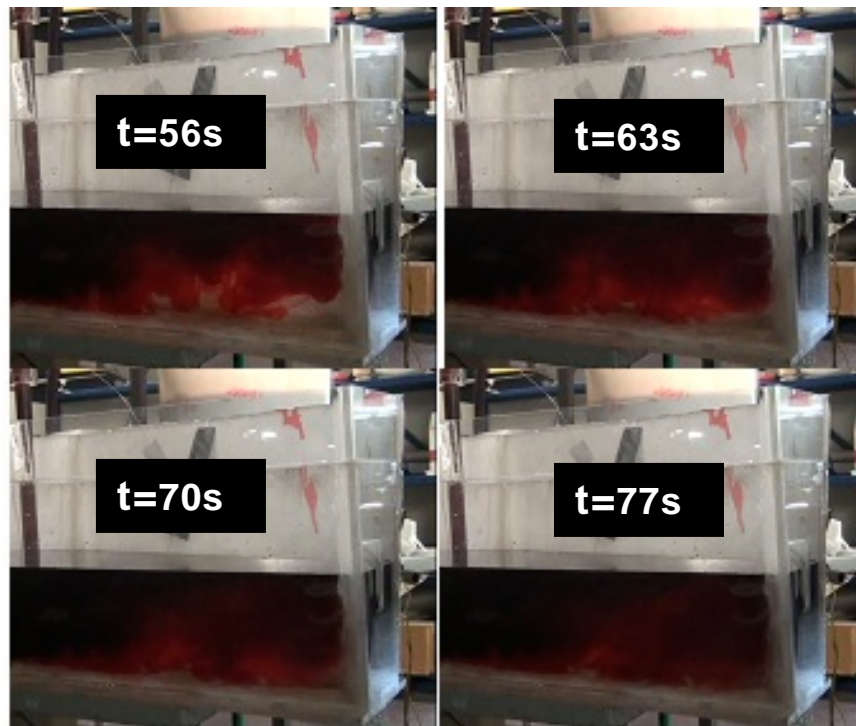


Figure-7.17(b) Tracer dispersion in the tundish with SIP for a step up by 10 degrees. $\Delta t=7s$

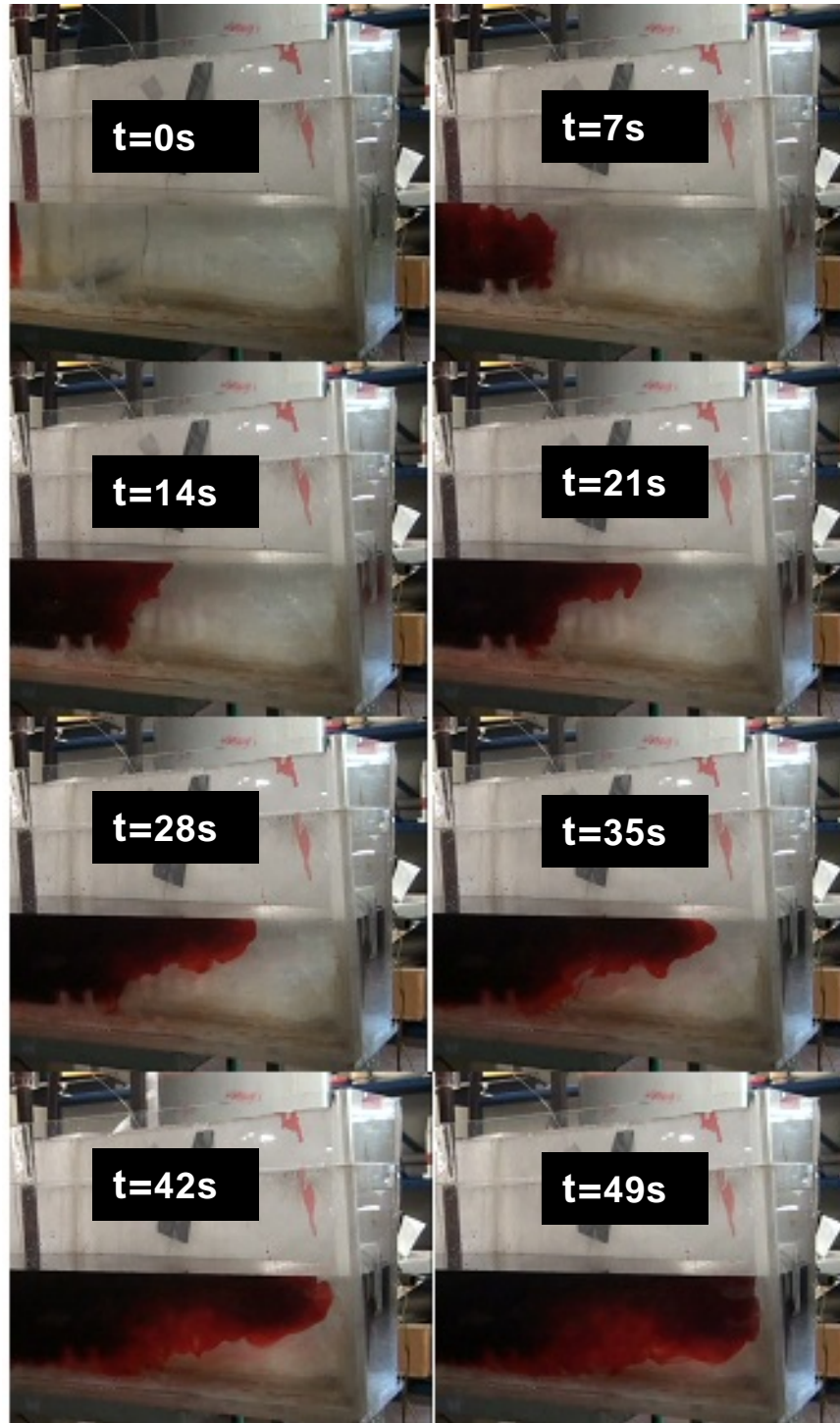


Figure-7.18(a) Tracer dispersion in the tundish with SIP for a step up by 15 degrees. $\Delta t=7s$

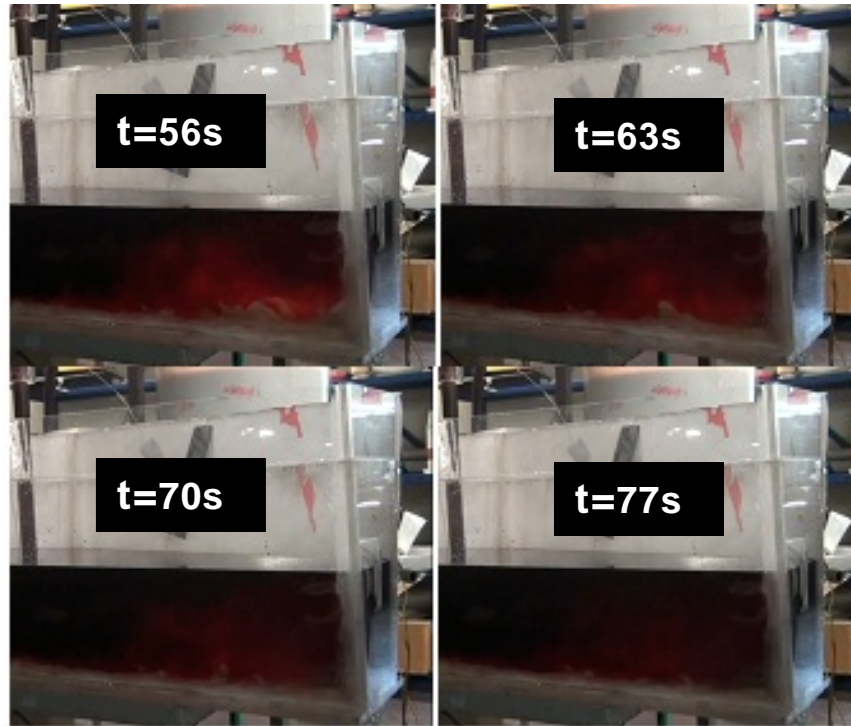


Figure-7.18(b) Tracer dispersion in the tundish with SIP for a step up by 15 degrees. $\Delta t=7s$

When Figures 7.16, 7.17 and 7.18 are critically examined it is clear that the difference in the flow pattern is not significant for step inputs of 5, 10 and 15 degrees. Higher temperature difference (15degrees) should have a significant effect on the flow pattern as opposed to a lower temperature difference (5 degrees) as seen before for the bare tundish. Now the presence of the impact pad mitigates the effect of the non-isothermal condition. The simple reason is that the recirculation present in the impact pad region carries the incoming hot fluid upwards. As a result, there is much less effect of the natural convection towards the ends of the tundish. So even, higher thermal

gradients do not cause a significant change in the flow pattern, with the presence of the impact pad.

To summarize, during steady state casting operations, step inputs of hotter fluid affects the flow pattern within the bare tundish. The higher the thermal gradient, the more is the effect of the buoyancy force. The buoyancy forces become dominant towards the extremities of the tundish and this is accordance with the results published in the literature. However, presence of an impact pad changes the scenario. The recirculation created because of the presence of the impact pad, carries the incoming lighter hot fluid upwards thereby removing the effects of the natural convection towards the ends of the tundish.

7.4.3 Validation of the mathematical model against experimental results

In the previous two sections physical and mathematical modelling has been performed to study the effects of non-isothermal conditions on melt flow in a tundish. It is highly necessary to validate the mathematical models with corresponding experiments. In this section validation of the results is performed. For validation, the tracer dispersion behaviour is compared for several cases under different conditions.

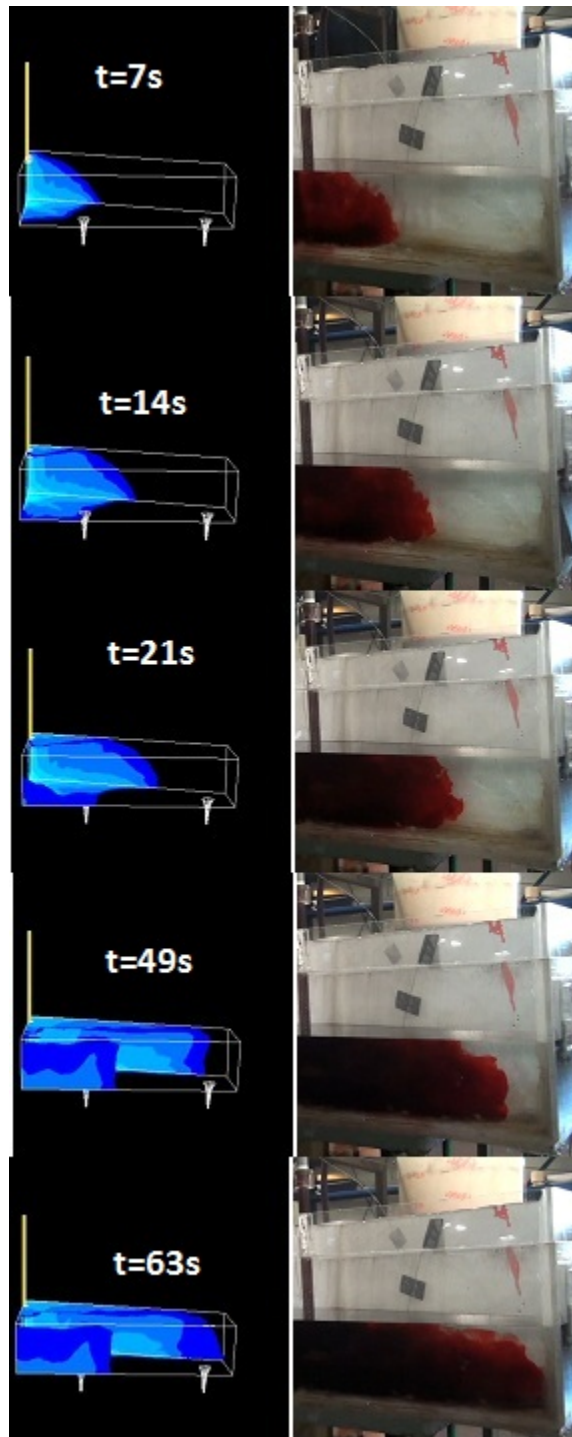


Figure-7.19 Validation of results under isothermal conditions in the bare tundish.

Figure-7.19 above compares the numerically predicted and experimentally observed tracer dispersion behaviour in the bare tundish under isothermal conditions. The profiles of the wave fronts are pretty similar. Figures 7.20 and 7.21 below show the comparison between the numerically predicted and experimentally observed tracer mixing patterns in the bare tundish for step up inputs of 10 and 15 degrees respectively. Here, also the mixing patterns predicted by the mathematical model are very similar to those obtained in the experiments. The minor differences can be attributed to the highly statistical nature of turbulent flow. Also, using another turbulence model or DNS may perhaps eliminate the minor, local, differences in the mixing patterns. Use of even finer mesh may help the purpose as well. However, the results are very similar and the mathematical model is robust. Figure 7.22 shows the comparison between the numerically predicted and experimentally observed tracer mixing patterns in the tundish fitted with the standard impact pad for a step up of 15 degrees. The numerical predictions are in good agreement with physical experiments.

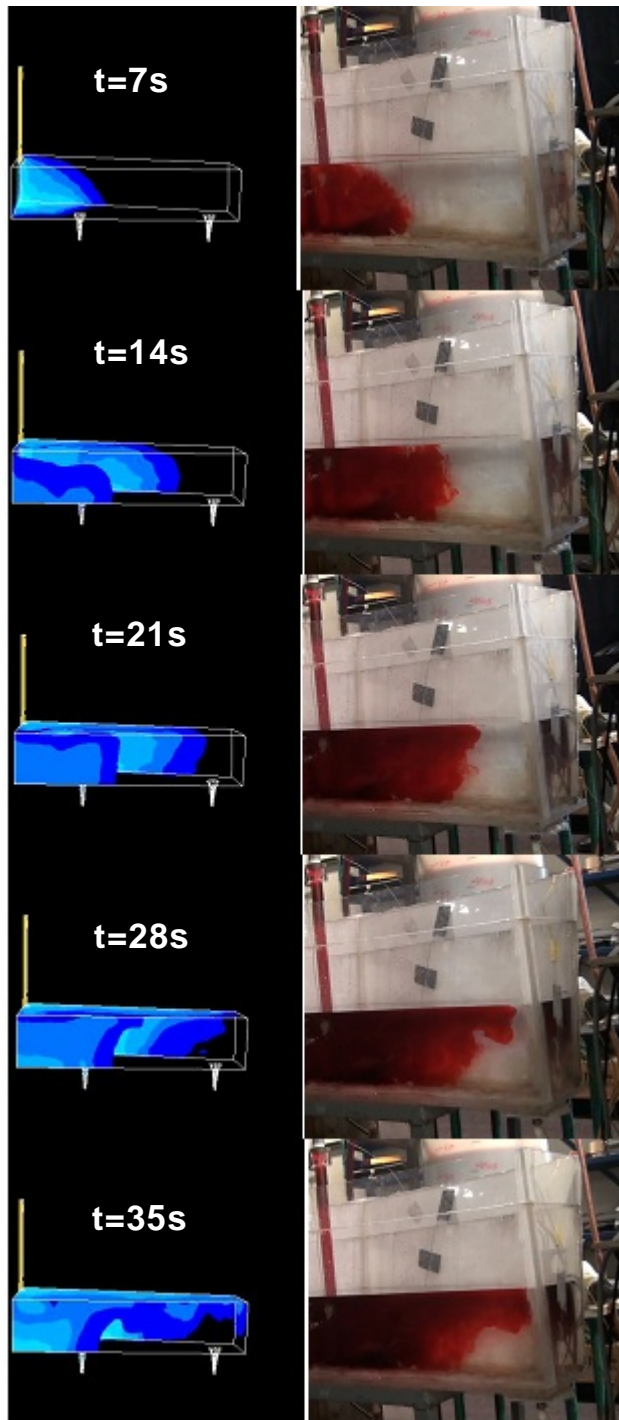


Figure-7.20 (a) Validation of results under non- isothermal conditions in the bare tundish for a step up by 10 degrees. $\Delta t = 7s$

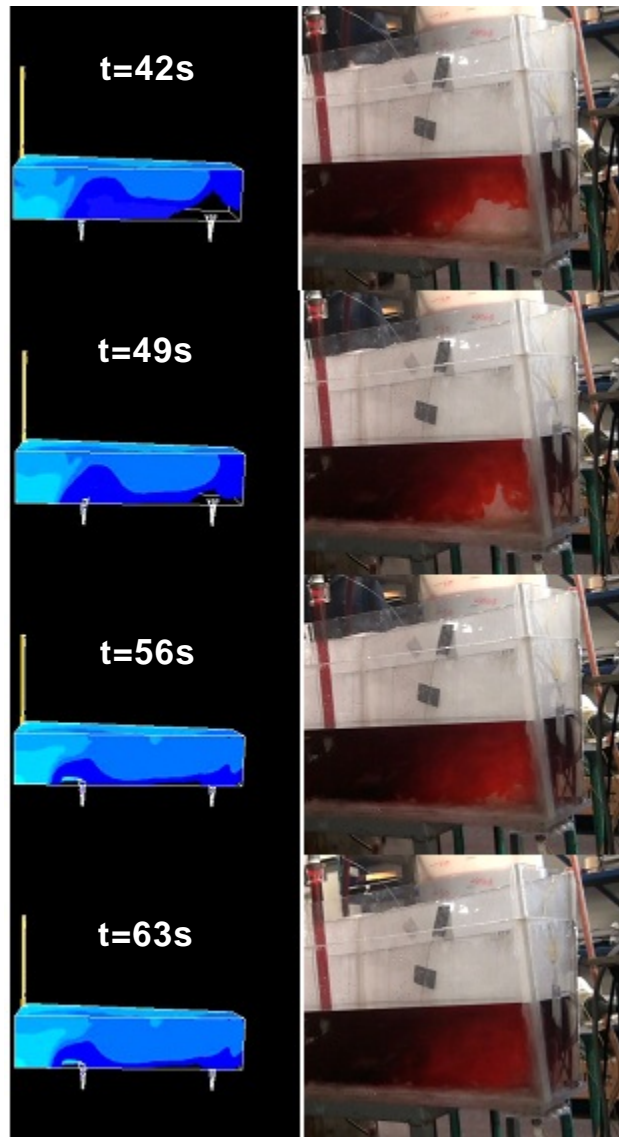


Figure-7.20 (b) Validation of results under non- isothermal conditions in the bare tundish for a step up by 10 degrees. $\Delta t = 7s$

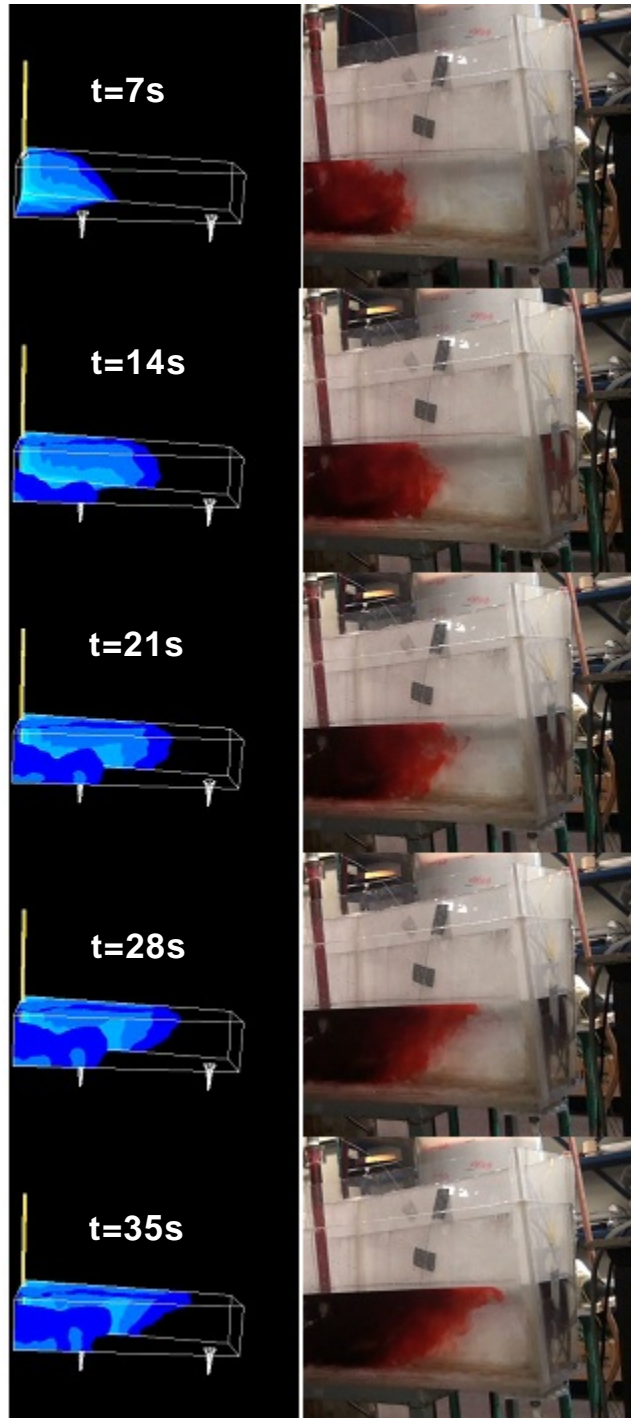


Figure-7.21 (a) Validation of results under non- isothermal conditions
in the bare tundish for a step up by 15 degrees. $\Delta t = 7s$

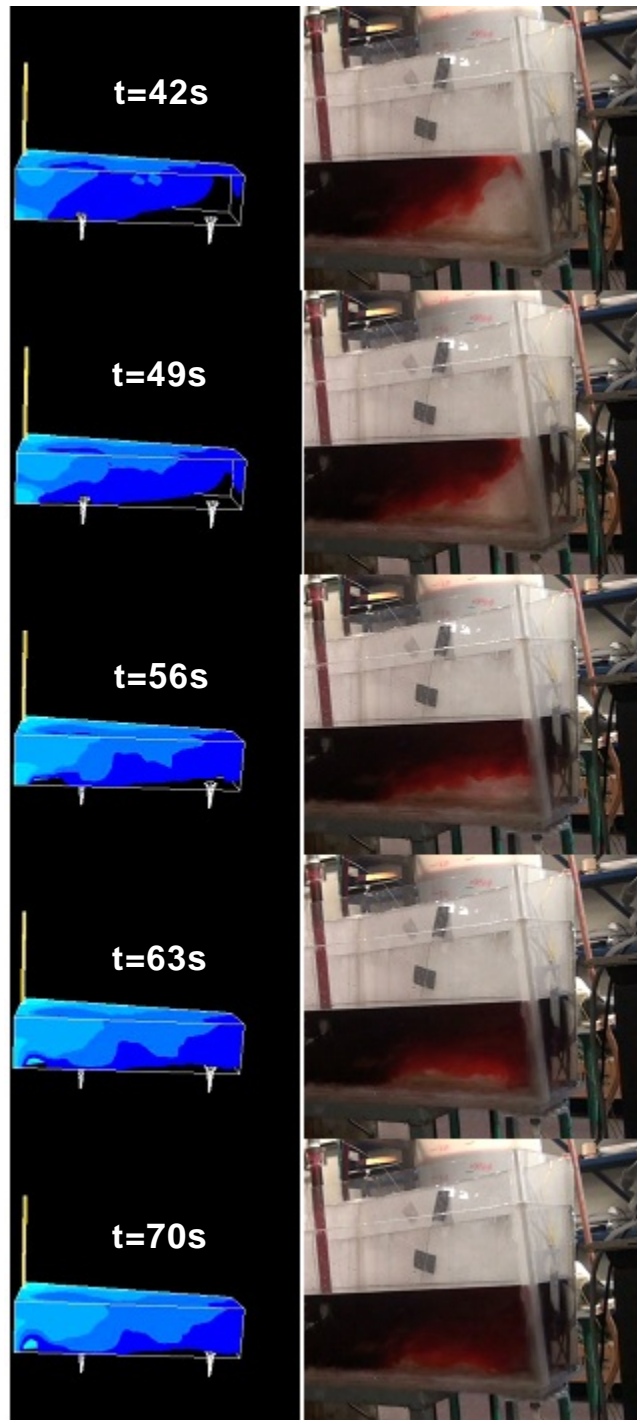


Figure-7.21 (b) Validation of results under non- isothermal conditions in the bare tundish for a step up by 15 degrees. $\Delta t = 7s$

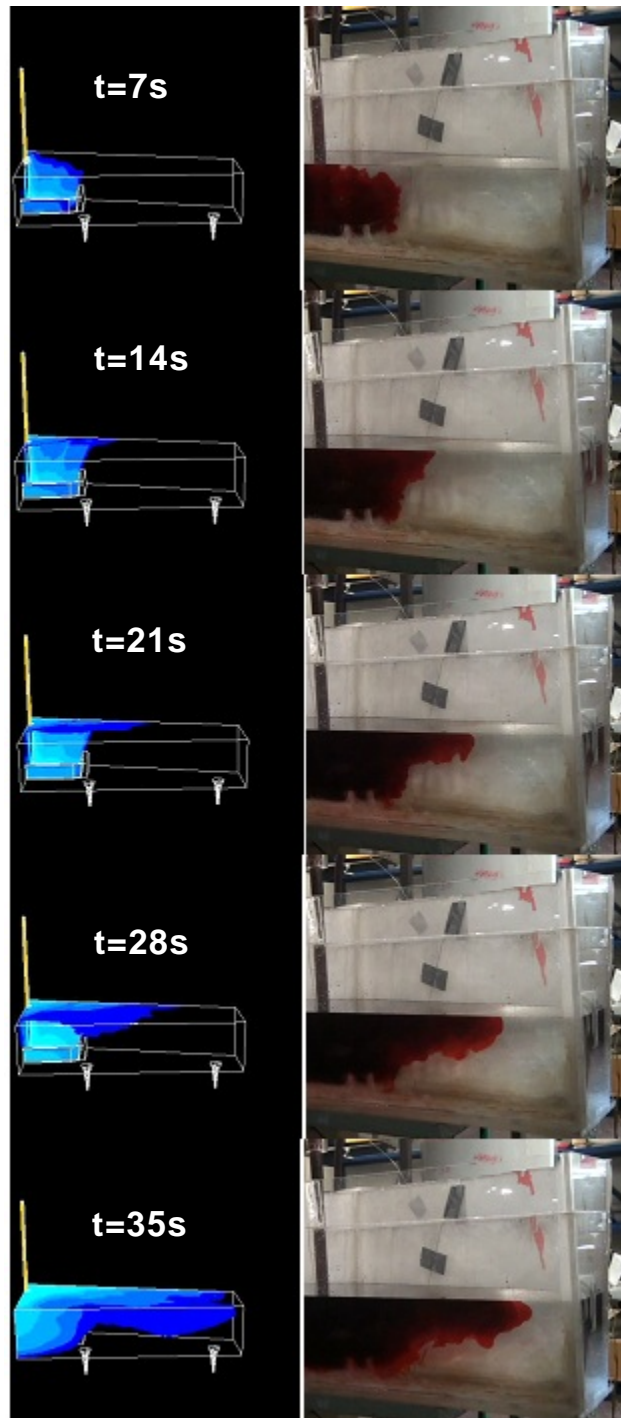


Figure-7.22 (a) Validation of results under non- isothermal conditions in the tundish with SIP for a step up by 15 degrees. $\Delta t = 7s$

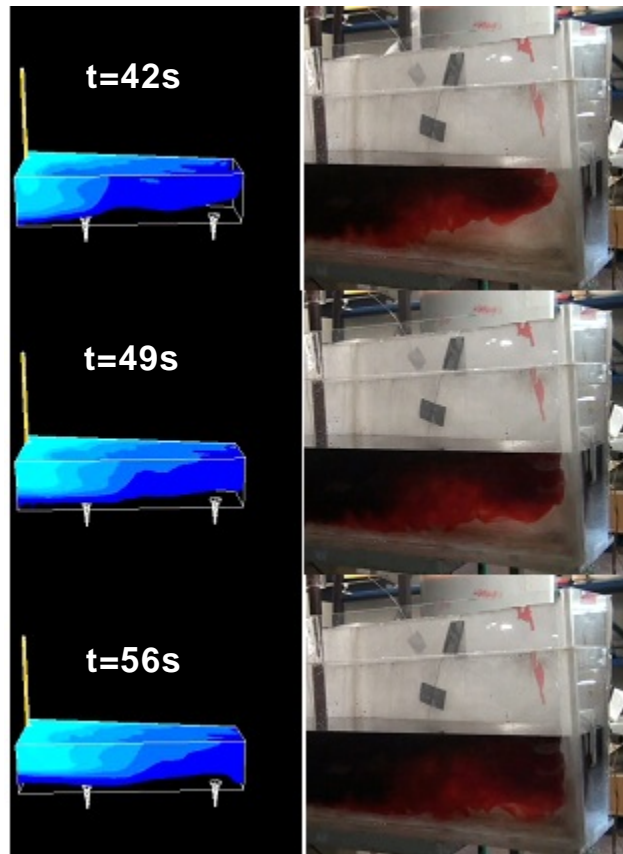


Figure-7.22 (b) Validation of results under non- isothermal conditions in the tundish with SIP for a step up by 15 degrees. $\Delta t = 7s$

In another method of validation, the thermal response curves for a couple of cases have been compared. They are presented in Figures 7.23 and 7.24 below. The numerically predicted thermal response curves for both the cases are pretty similar to that obtained from experimental measurements. In the experiments, thermocouples were used and so fluctuations are visible in the results. Fluctuations are always inherent in thermocouple data. The small variations may be attributed to minute experimental errors and choice of the turbulence model.

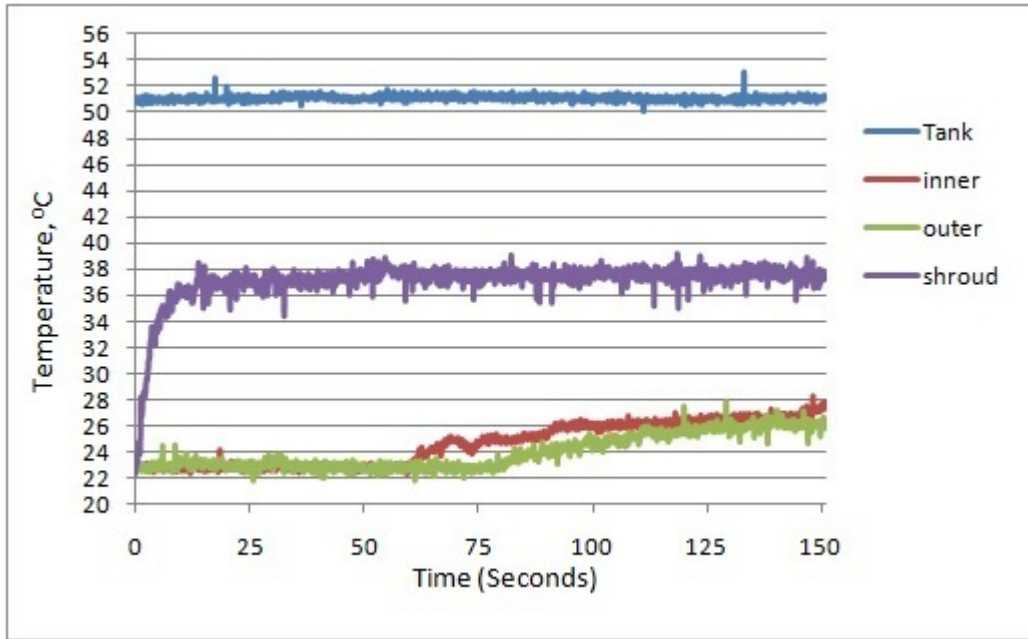


Figure-7.23 (a) Experimentally measured thermal response curve for a step up of 15 degrees in the bare tundish

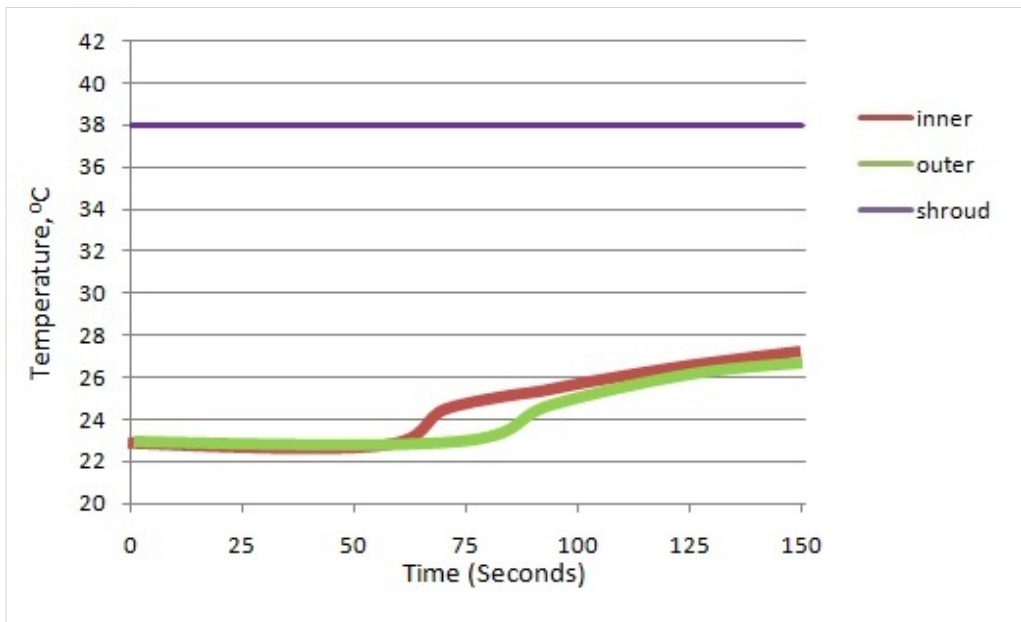


Figure-7.23 (b) Numerically predicted thermal response curve for a step up of 15 degrees in the bare tundish

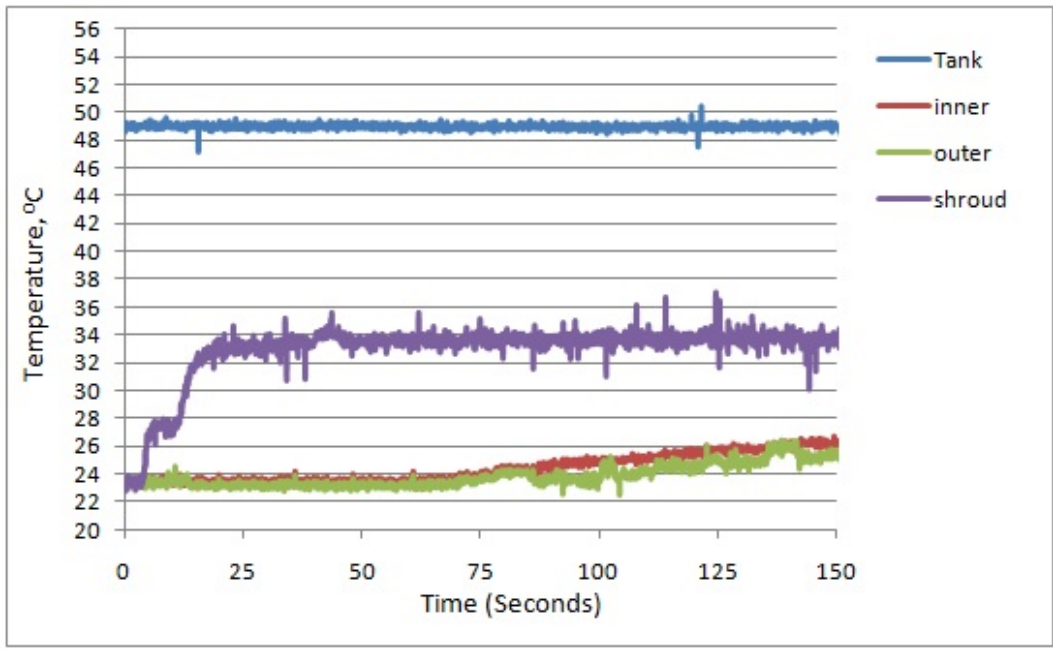


Figure-7.24 (a) Experimentally measured thermal response curve for a step up of 10 degrees in the bare tundish

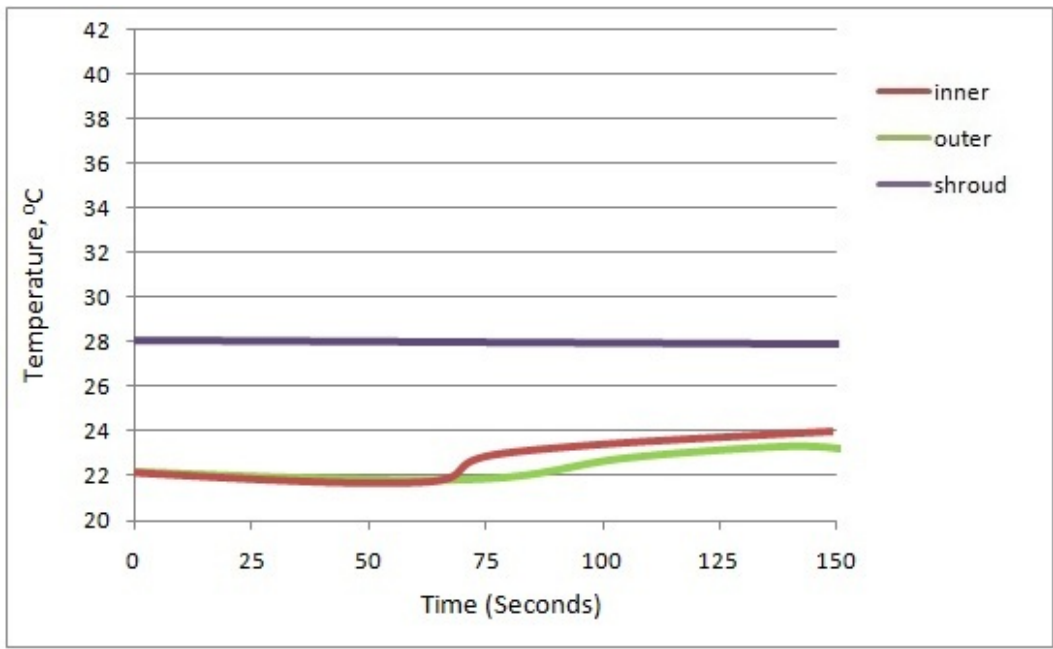


Figure-7.24 (b) Experimentally measured thermal response curve for a step up of 10 degrees in the bare tundish

7.4.4 Physical modelling of tracer dispersion during ladle change operations

In all the above sections, the effect of non-isothermal conditions have been studied under steady state casting operations, i.e. when the liquid level in the tundish is constant. For steady state casting, under non-isothermal conditions the flow pattern was affected towards the ends of the tundish, because of less turbulence and dominant buoyancy forces. However, during a ladle change operation, the new ladle is opened up within 2-3 minutes after the old ladle was removed. During this period, the level drops in the tundish, and in order to regain the operating level quickly, the new ladle is opened up at a flow rate which is almost three times the flow rate at steady state. Owing to this higher refilling rate, the turbulence is much higher, and may be high enough till the extremities of the tundish, as opposed to that under steady state condition. It would be very interesting to see the effect of thermal gradients on melt flow in the tundish during ladle change operations. As during refilling the turbulence is very high, the tracer tends to mix faster and so the snap shots of tracer dispersion were taken at intervals of 3s instead of 7s. Figure 7.25 below shows the tracer mixing patterns in the bare tundish during a ladle change under isothermal conditions. The tracer mixes into the whole tundish in 40s during a ladle change as opposed to 63s under steady state conditions.

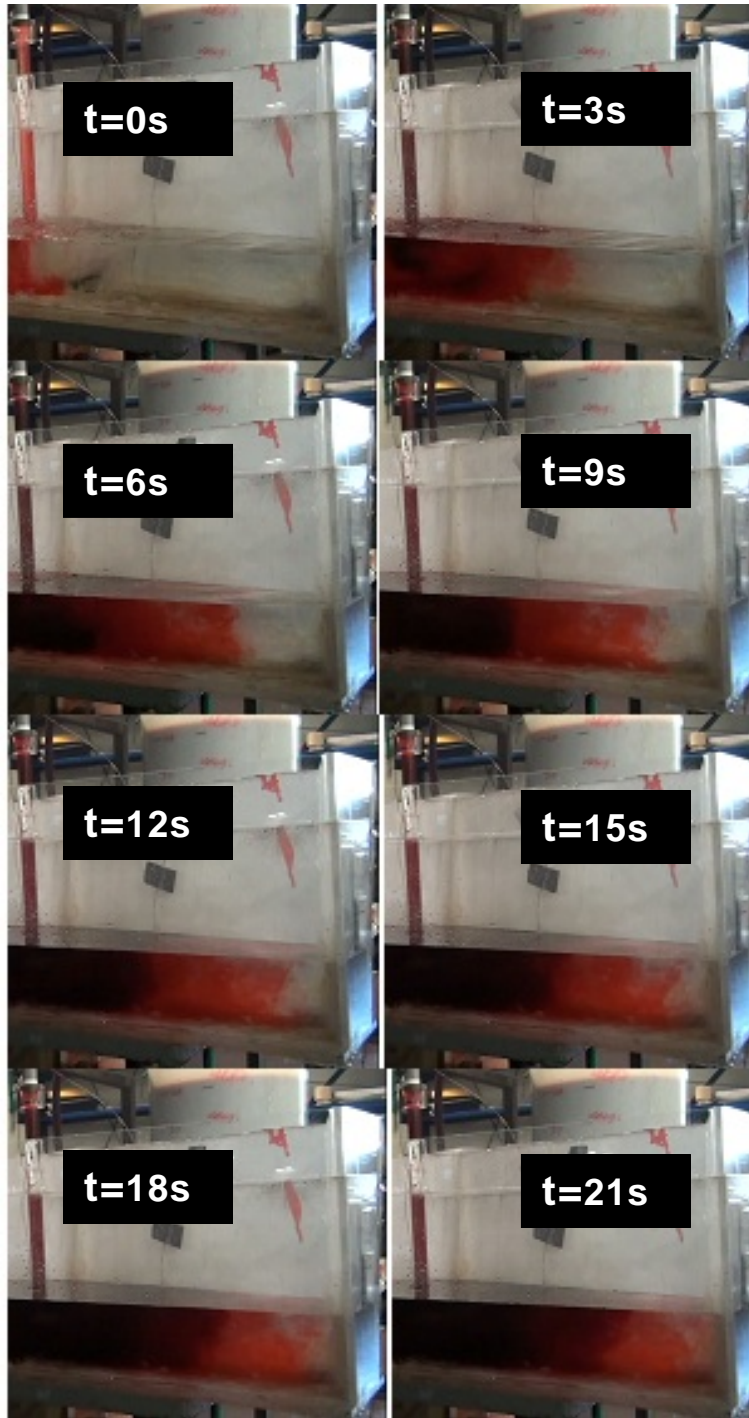


Figure-7.25 (a) Tracer dispersion during a ladle change in the bare tundish under isothermal conditions. $\Delta t = 3s$

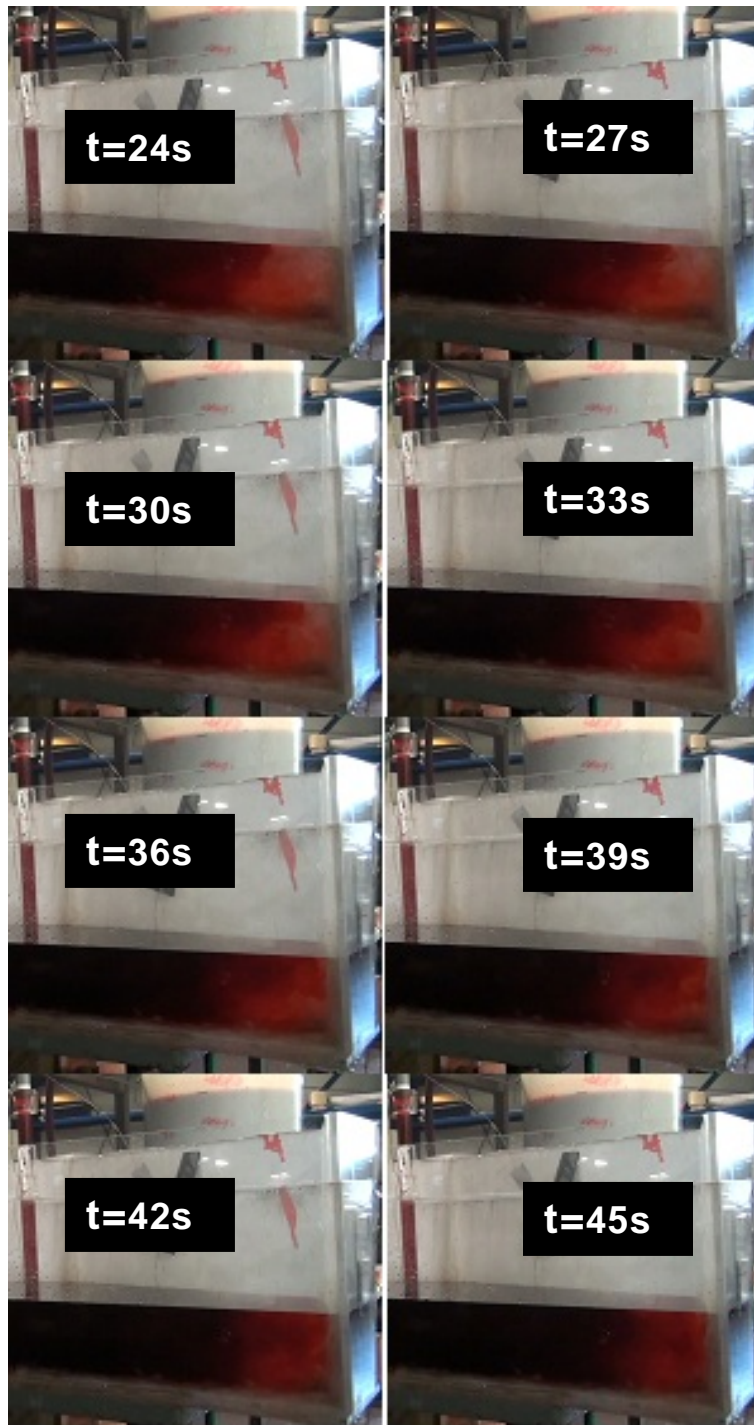


Figure-7.25 (b) Tracer dispersion during a ladle change in the bare tundish under isothermal conditions. $\Delta t = 3s$

Figure 7.26 below represents the tracer dispersion behaviour in the bare tundish during a ladle change operation for a step up of 5 degrees.

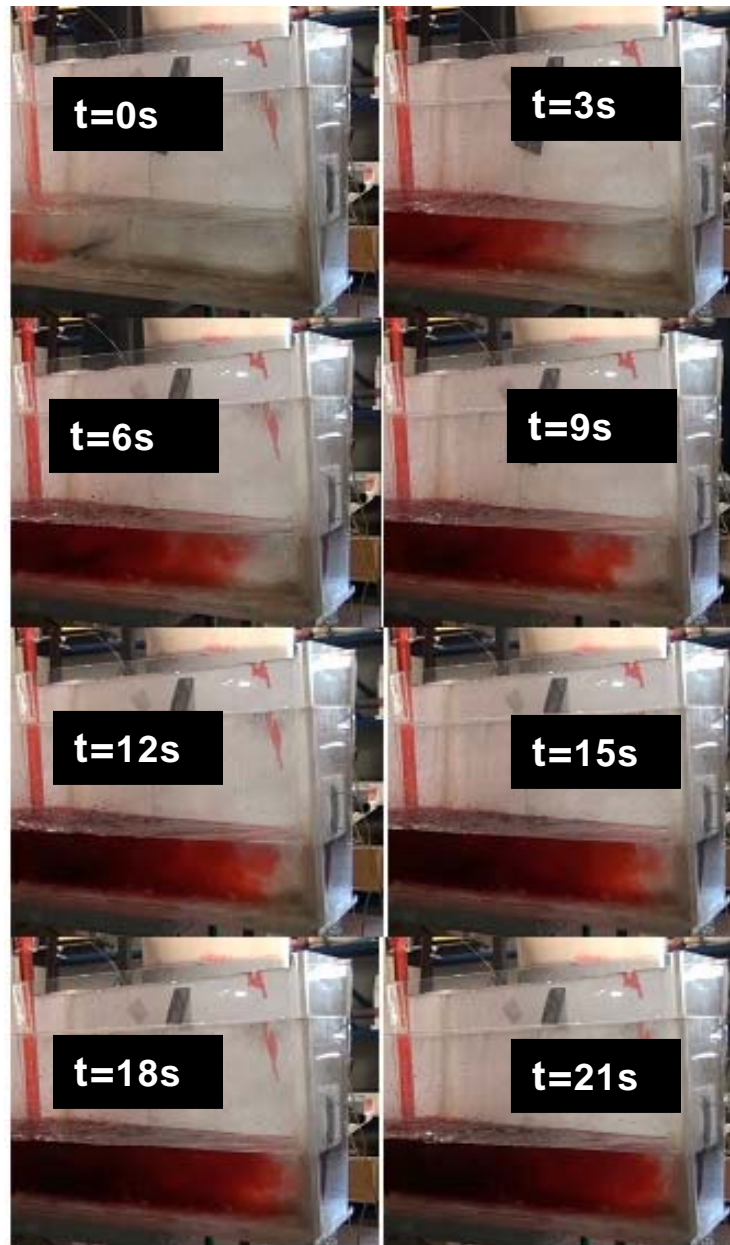


Figure-7.26(a) Tracer dispersion during a ladle change in the bare tundish for a step up of 5 degrees. $\Delta t = 3s$

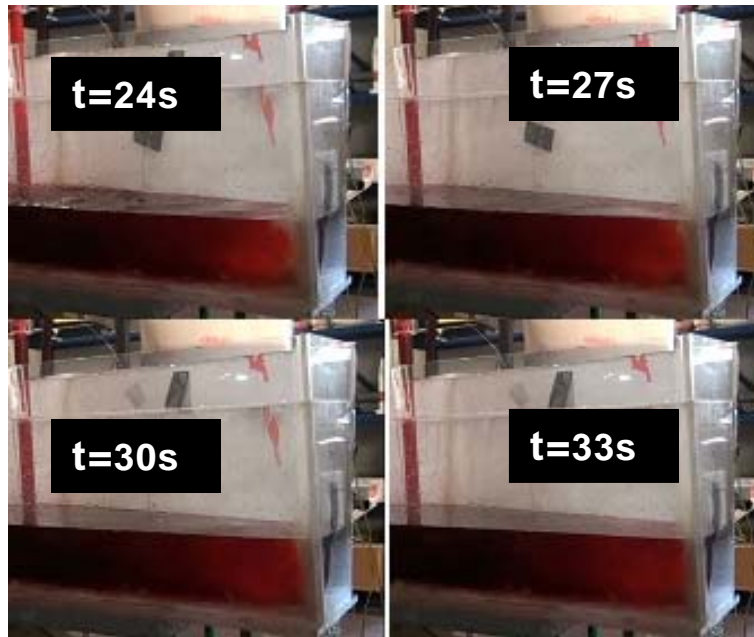


Figure-7.26(b) Tracer dispersion during a ladle change in the bare tundish for a step up of 5 degrees. $\Delta t = 3s$

On comparing Figures 7.25 and 7.26, it is seen, that there is no difference in the tracer mixing patterns during a ladle change operation. This is because; a step up of 5 degrees at the inlet is not enough to produce significantly strong natural convection at the ends of the tundish which would be able to dominate over the existing higher turbulence prevailing due to the ladle change. However, increasing this thermal step up may influence the flow. Figures 7.27 and 7.28 below represent the tracer dispersion behaviour, during a ladle change operation, in a bare tundish, for step inputs of 10 and 15 degrees respectively.

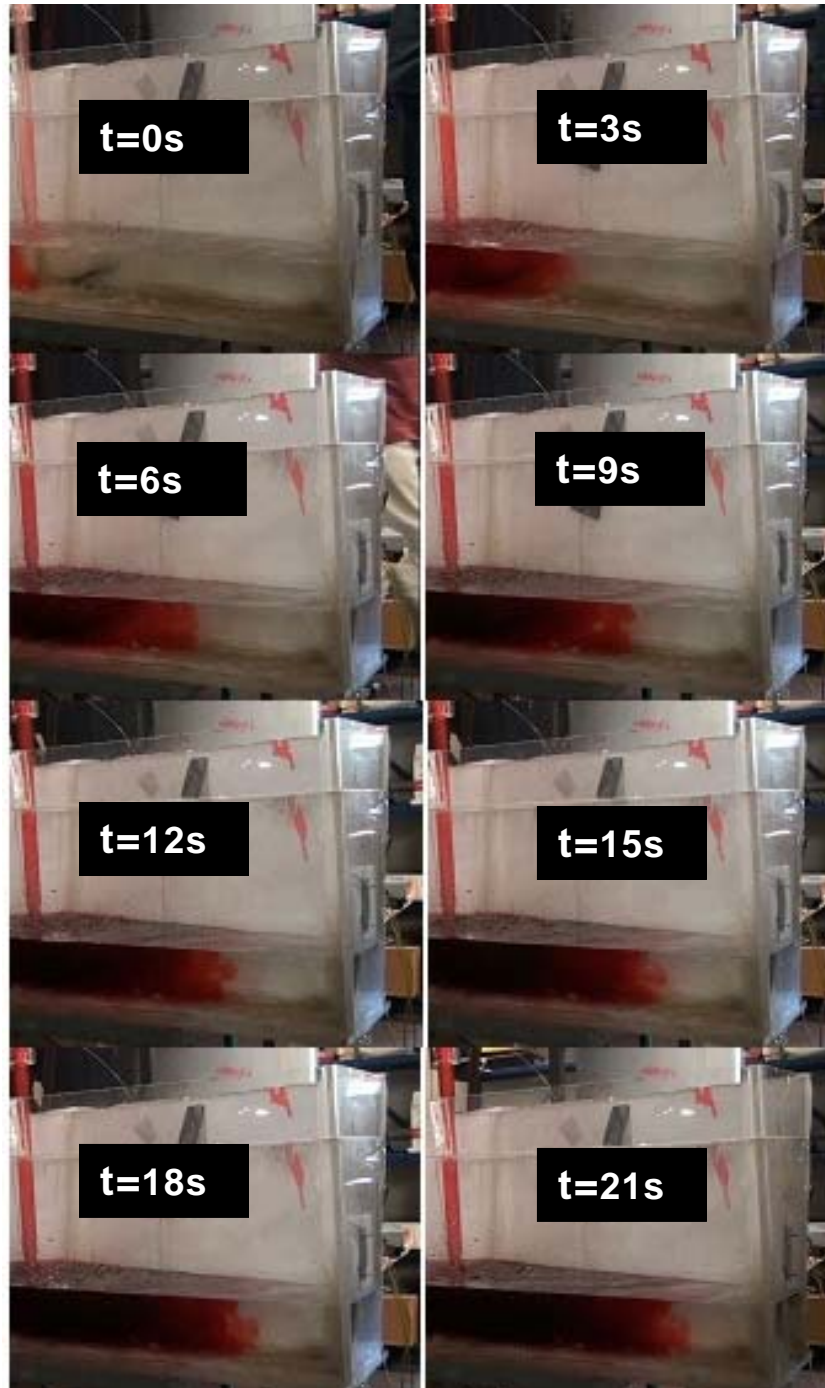


Figure-7.27(a) Tracer dispersion during a ladle change in the bare tundish for a step up of 10 degrees. $\Delta t = 3s$

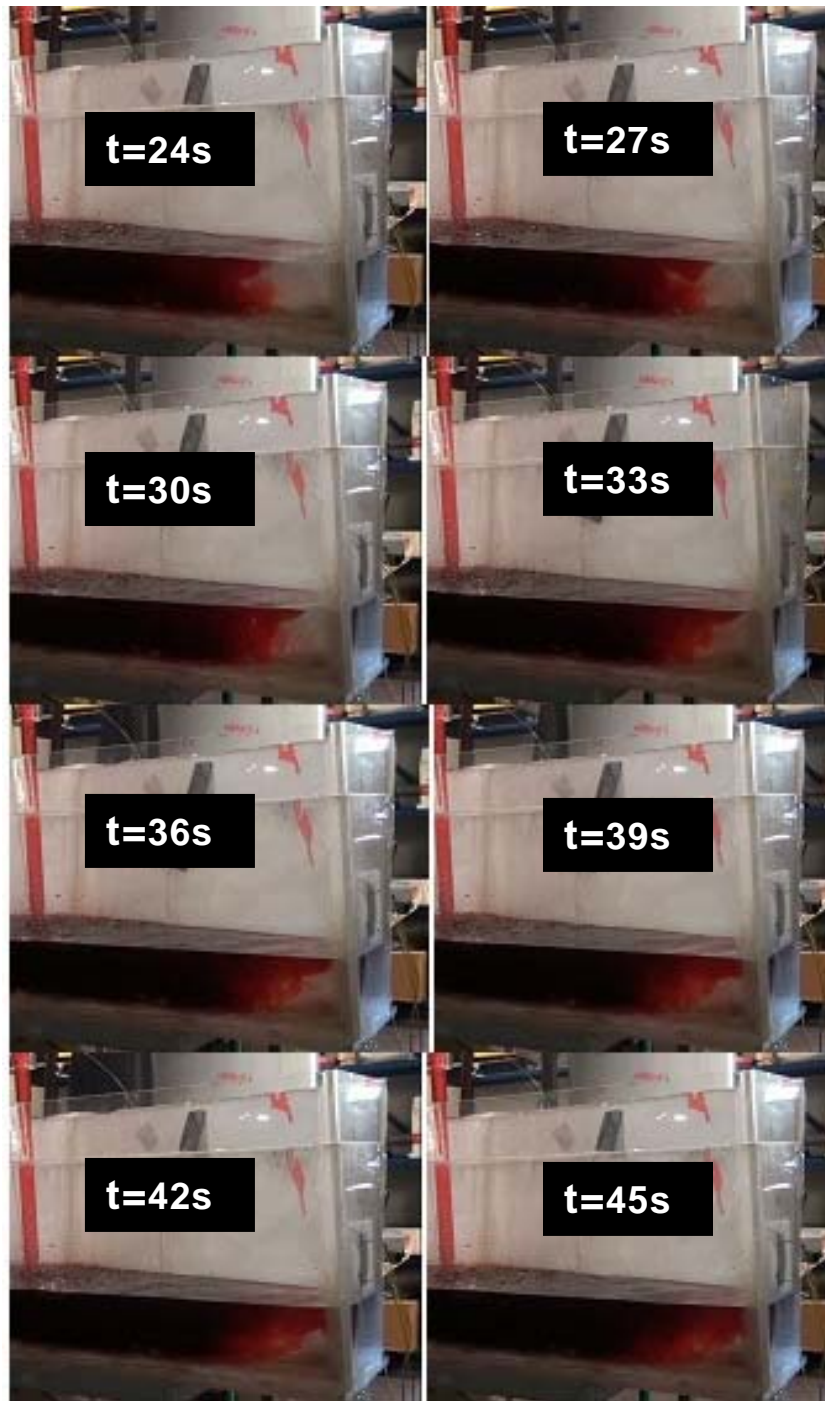


Figure-7.27(b) Tracer dispersion during a ladle change in the bare tundish for a step up of 10 degrees. $\Delta t = 3s$

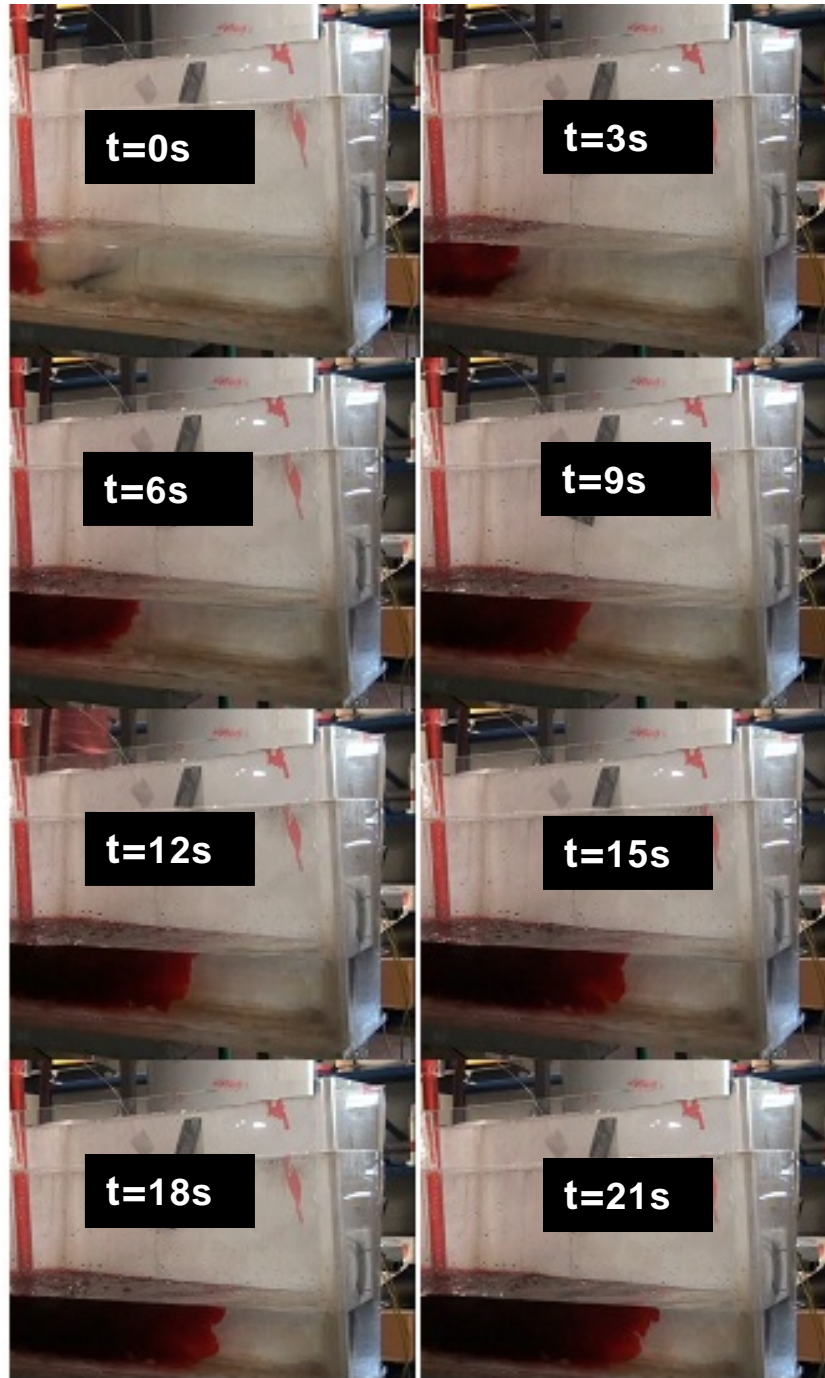


Figure-7.28(a) Tracer dispersion during a ladle change in the bare tundish for a step up of 15 degrees. $\Delta t = 3s$

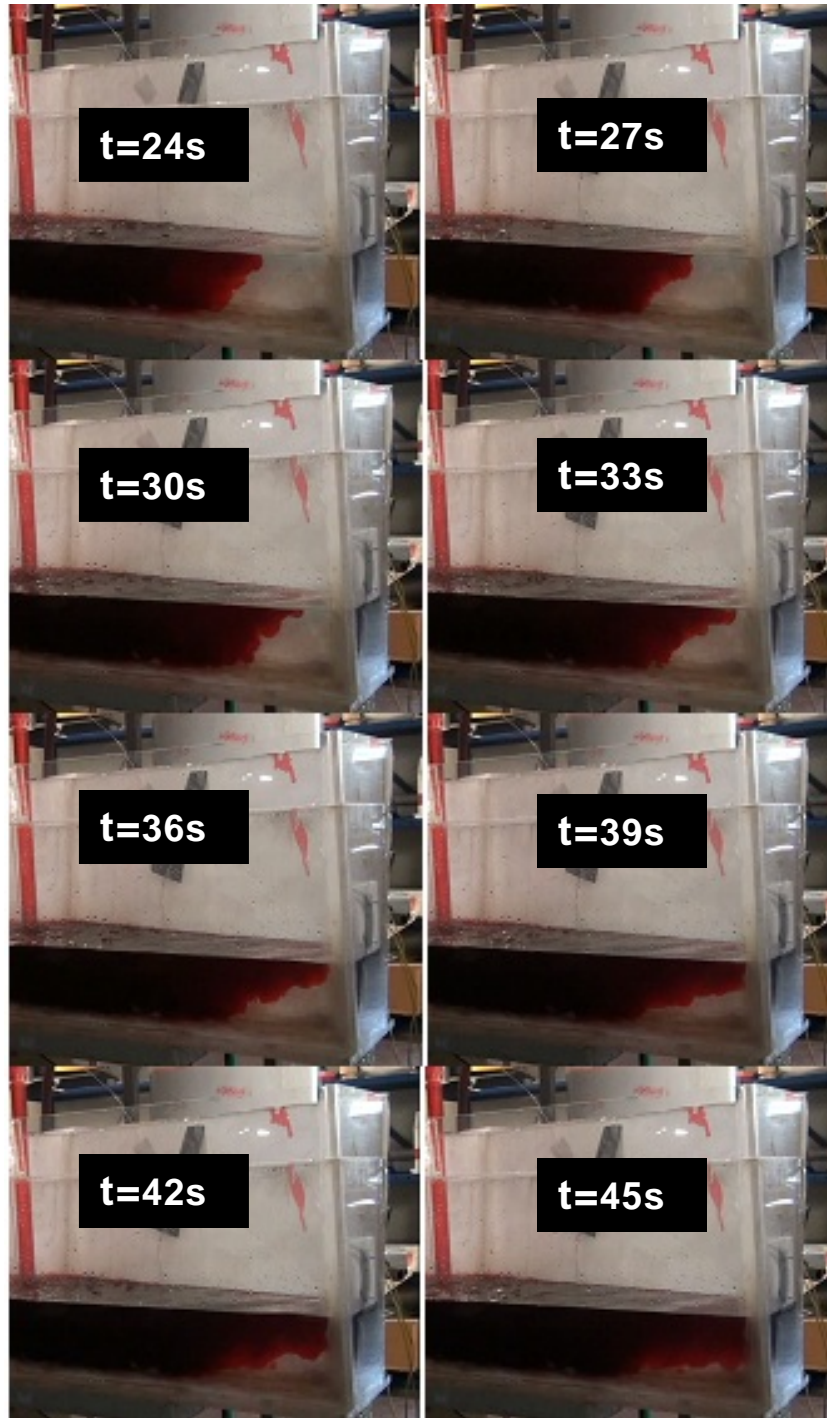


Figure-7.28(b) Tracer dispersion during a ladle change in the bare tundish for a step up of 15 degrees. $\Delta t = 3s$

The effects of buoyancy forces are visible towards the end of the tundish. So a step up of 10 or 15 degrees at the inlet can produce stronger natural convections near the extremities of the tundish, even during a ladle change operation. It would be interesting to see, the fluid flow patterns during a ladle change when the impact pad is present. Figures 7.29 and 7.30 represent the tracer mixing behaviour during a ladle change operation in the tundish fitted with the standard impact pad for step inputs of 5 and 10 degrees respectively. The presence of the pad mitigates the effect of the non-isothermal conditions. The tracer mixing behaviour is similar in both cases.

To summarize, ladle change operations involve higher turbulence within the tundish, resulting in faster mixing of the tracer. The inertial forces may be strong enough even near the extremities of the tundish and to see any effect of buoyancy forces, higher thermal step inputs are required. Presence of the impact pad creates a recirculation zone in the entry region and hence carries the hot fluid upwards, thereby diminishing the effects of natural convection. When compared with steady state casting operations, a small step up of 5 degrees can affect the flow in the bare tundish.

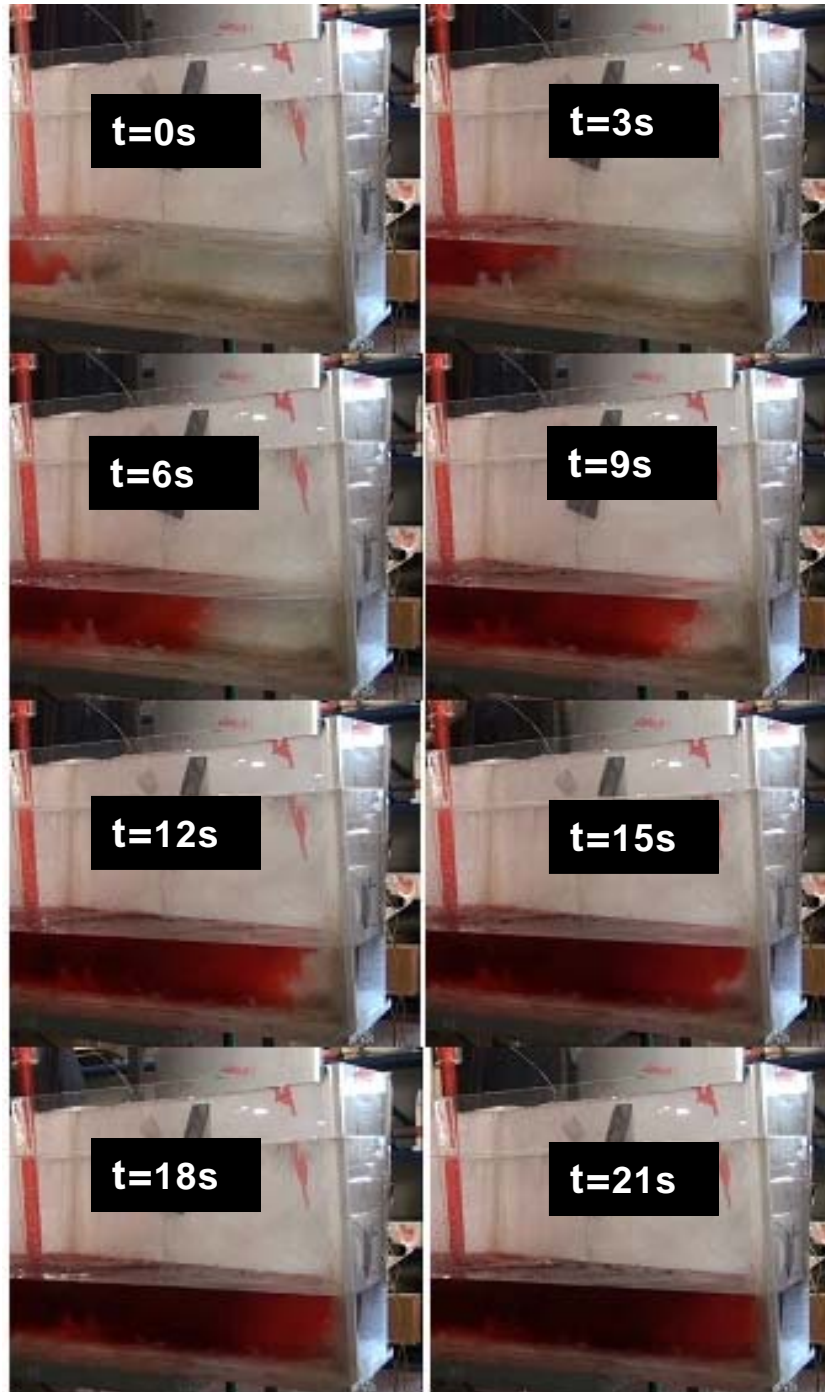


Figure-7.29 Tracer dispersion during a ladle change in the tundish with SIP for a step up of 5 degrees. $\Delta t = 3s$

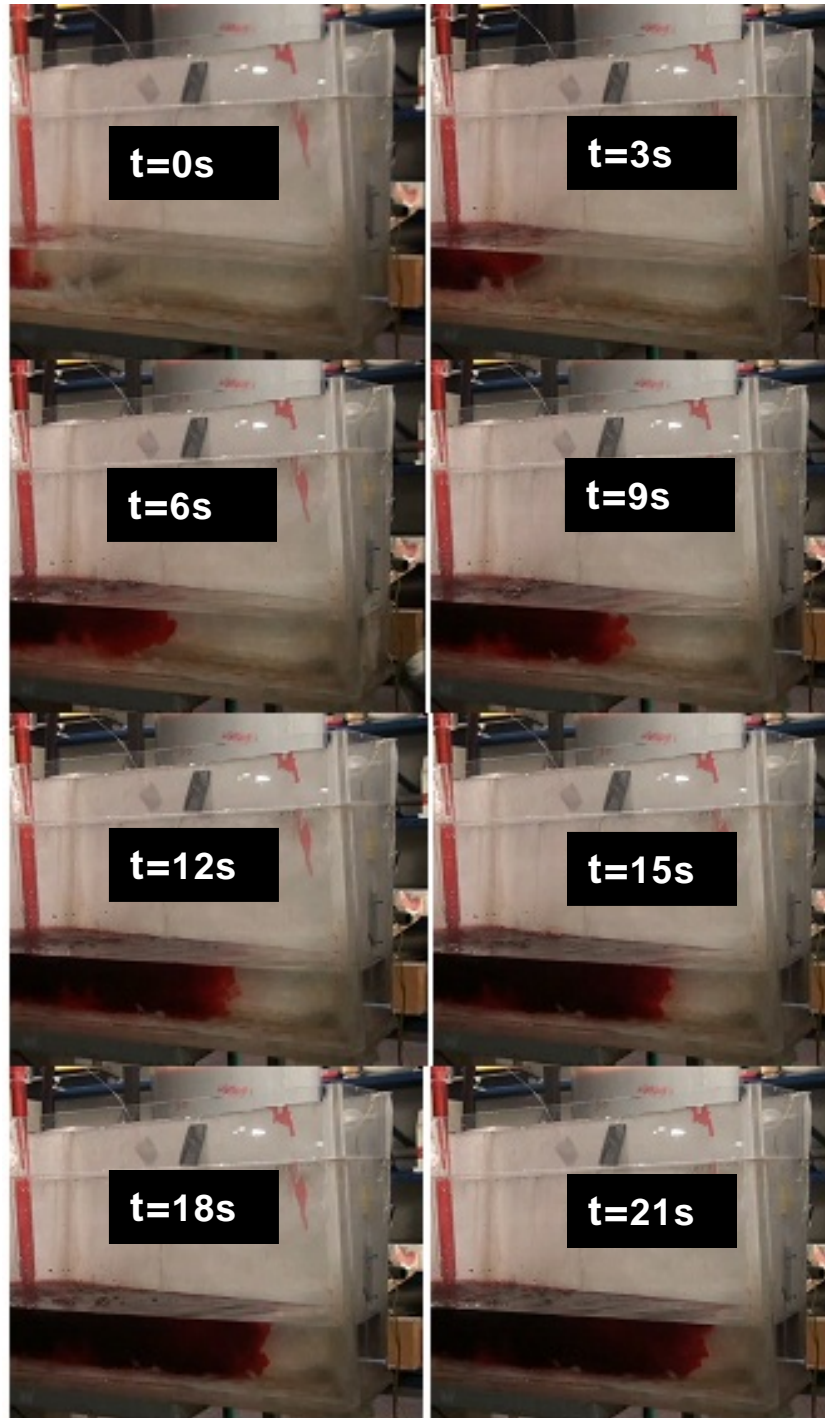


Figure-7.30 Tracer dispersion during a ladle change in the tundish with SIP for a step up of 10 degrees. $\Delta t = 3s$

7.4.5 Effect of heat losses from the tundish walls and free surface

One of the major reasons that give rise to non-isothermal conditions is the heat losses that take place from the walls and free surface of the tundish. So far, the heat losses from the walls and free surface had been neglected and only step inputs of hot (or cold) fluid had been considered. There was not data available to us for the heat losses occurring from the walls of the full-scale delta shaped tundish. However, some data are available in the literature and these were explored. For the numerical simulations, the temperature at the inlet was assumed to be constant throughout the ladle teeming time. In this way, the sole effect of the heat losses from the walls could be analyzed. However, in reality, the inlet temperature also drops by about 0.3-0.5 degrees per minute. The operating temperature of the tundish was assumed to be 1823K (1550⁰C) and the same temperature prevailed at the inlet. Following Joo and Guthrie's¹²⁸ work, a heat flux of -75kW m⁻² was set for the free surface. The negative value indicates a heat loss from the system. This value can vary a lot depending on the type of slag used on the top, or the grade of steel that is being cast. The heat fluxes from the walls were set to -2.6kW m⁻².The simulation was carried out for 30 minutes (1800 s) and the variation of outlet temperature was monitored at intervals of 60 s. Figure-7.31 below shows the variation

of output steel temperature, solely due to heat losses from the tundish walls and free surface.

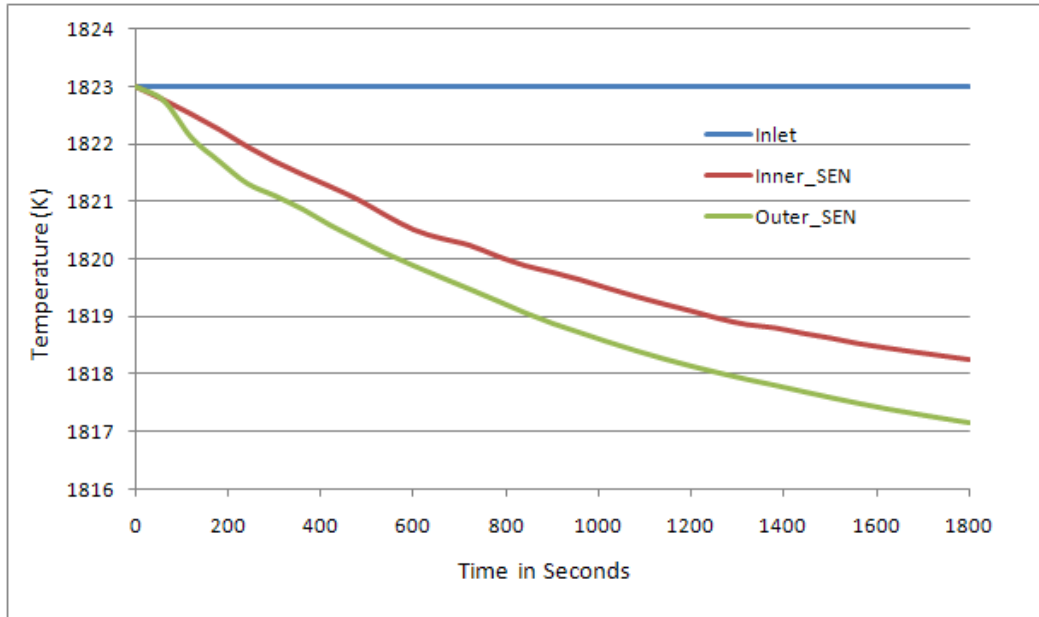


Figure-7.31 Variation of outlet steel temperature with time

The inlet temperature was always constant (1823K) throughout the 30 minutes. The temperature of the liquid metal coming out of the inner SEN drops to around 1818.26K at the end of 30 minutes which is a drop by approximately 5 degrees. The temperature of the steel exiting from the outer SEN drops by around 6 degrees after 30 minutes. The rate of decrease in temperature of liquid steel at the outlets was almost similar for the first 100 seconds. After that, the rate of temperature drop for the outer SEN was higher than that for the inner SEN. This is because of the fact that the outer SEN is closer to the wall and the melt near to the outer strand will have more heat losses than that near the inner SEN. In order to confirm,

the above fact, another simulation was carried out where, the heat flux from the free surface was decreased to 50 kW m^{-2} (-50 kW m^{-2}) and the heat flux from the walls was increased to 4 kW m^{-2} (-4 kW m^{-2}).

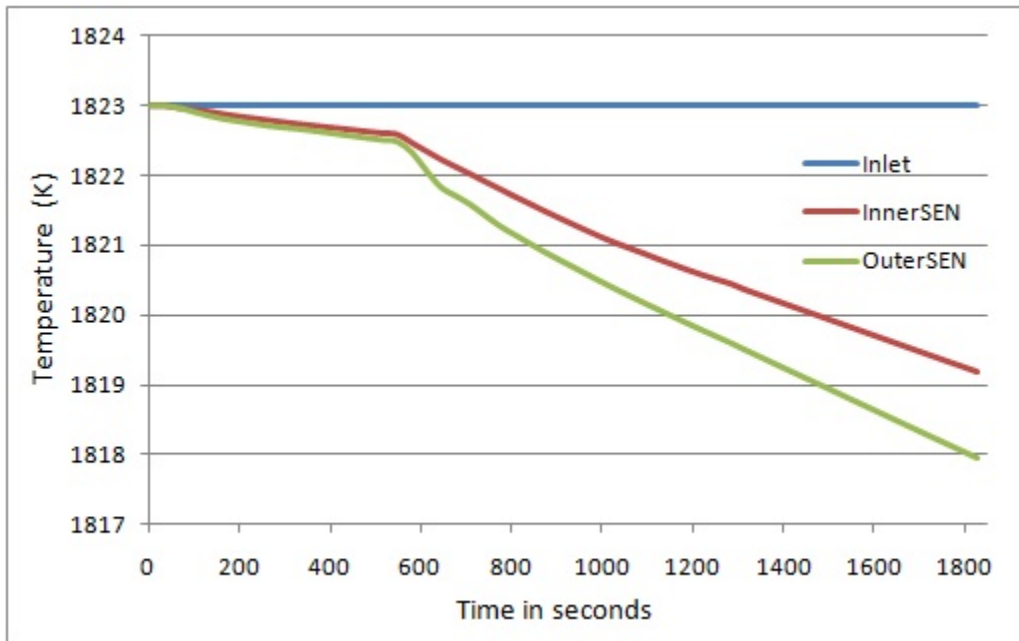


Figure 7.32 Variation of outlet steel temperature with time

The inlet temperature was always constant (1823K) throughout the 30 minutes. The results are presented in Figure 7.32. The temperature of the liquid metal coming out of the inner SEN drops to around 1819.18K at the end of 30 minutes which is a drop of approximately 4 degrees. The temperature of the steel exiting from the outer SEN drops by around 5degrees. The rate of temperature drop increased abruptly after about 550 seconds and that is evident

for both the inner and outer SENs. This may be attributed to the initial transient effects.

For both the above cases, the outlet steel temperature drops, because of heat losses from the walls, and the steel coming out of the outer SEN experiences a higher temperature drop than that at the inner SEN.

As seen from this study, heat losses from the walls and free surface can lead to a temperature difference of 4-5 degrees between the steel at the inlet and outlets, giving rise to non-isothermal conditions. If the literature^{7,127,129} is examined, the usual temperature drops are around 3-4 degrees under non-isothermal conditions..

For further studies, plant measurements need to be done in order to get accurate values of the heat losses from the walls and free surface of the tundish.

8.0 Conclusions and Recommendations

In the present doctoral thesis, physical and mathematical modelling of various transport phenomena, occurring in a tundish, were carried out and recommendations have been made which can help in improving the liquid metal output quality. Though experimental results have already been presented and discussed in the respective Chapters, important findings are summarized in this final Chapter.

When modelling, turbulent flows, the choice of the turbulence model is very important. It seen that the standard k- ϵ model does a good job when predicting bulk or gross properties and is in accordance with the opinions available in literature. Also, grid independency studies need to be done before performing any definitive mathematical modelling, as the results can be highly dependent on the mesh size.

Flow control devices greatly affect the fluid flow patterns in the tundish and their use can greatly enhance steel cleanliness. The standard QIT impact pad does a good job already in terms of inclusion floatation. Use of dams along with the standard impact pad may enhance the inclusion removal efficiency of the tundish. However, this is highly dependent on the height and position of the dam. The dams should be placed closer to the outer SEN. Placing any dam closer to the inner SEN degrades the steel quality. The use of smaller impact pads is also not recommended, as it results in very high values of RRI. Increasing the height of the standard impact pad, from its current height of 0.152 m to 0.30 m yields better results in terms of inclusion removal and can be used alone without the insertion of extra dams. The mathematical model used to analyze the different tundish configurations proved to be quite efficient and was in good agreement with experimental measurements.

Inert gas shrouding practices always helps to reduce ambient air aspirations into the ladle shroud. However, the amount of gas injected should be optimized. If too much inert gas is used, the gas bubbles entrain in the liquid and flow within the tundish. They form a rising bubble column just beneath the ladle shroud and results in an exposed 'eye'. The higher the volume fraction of inert gas used, the larger is the size of the exposed 'eye'. Larger exposed eye increases the probability of re-oxidation of the steel within the tundish. The mathematical model was robust and the indirectly predicted exposed 'eye' size was comparable to the experimentally measured one with errors less than 15%. However, when a real multiphase model was developed, the error reduced to less than 10%. Inert gas injections also affect the residence time distribution of the tundish.

The alignment of the ladle shroud can be a very important parameter in controlling the liquid metal quality. Slight mis-alignments of the shroud can result in more slag entrained in one of the strands of a multi-strand tundish during a ladle change operation. A submerged shroud operation would be better than the non submerged operation during a ladle change but practical difficulties do not normally permit for this. Assuming normally designed shrouds with a two-plate system is being used, the first measure is to minimise exposure times prior to re-submergence of the shroud, so as to limit the amount of slag entrainment. One technique would be to raise the

steel level in the tundish above the normal operating height (500mm in the case modelled), a few minutes before the end of a ladle pour. This allows time for the collector nozzle to be de-coupled from the emptied ladle, the turret rotated to the new ladle, and the collector nozzle re-fitted to the collector nozzle of the new ladle with a gasket. This procedure would be carried out such that the level of steel in the tundish would be just below the end of the shroud collector nozzle once ended. As soon as the level of steel within the tundish drops below the end of the ladle shroud, the new ladle should be opened immediately, and the ladle shroud quickly re-submerged. Ladle change times should be reduced from the current 3-4 minutes to 1-2 minutes.

Non-isothermal conditions are always inherent in the plant. The steel poured in from a new ladle is generally at a bit higher temperature than the existing liquid steel in the tundish. During steady state casting, i.e. when the liquid level remains constant in the tundish, for this step up condition, buoyancy forces are generated because of the temperature differences. In the jet entry region the inertial forces dominate because of high turbulence. The buoyancy forces become more prominent towards the ends of the tundish where the turbulence is lower. The flow patterns generated during a step up condition are perhaps favourable for inclusion float out, since the lighter hot water tends to rise upwards. On the other hand a step

down condition leads to stronger downward flows which in turn can worsen the liquid steel quality by entraining more inclusions into the shroud. Incorporation of flow modifiers like turbo-stops and impact pads mitigates the effects of the buoyancy forces. During a ladle change operation, the turbulence is very high because of the high refilling rate, and this requires higher thermal gradients to affect the flow. For steady state casting operations, a small temperature difference of 5 degrees leads to significant buoyancy driven flows, whereas during a ladle change, a minimum of 10-15 degrees temperature difference is necessary to produce strong natural convection. Heat losses from the walls and free surface of the tundish are also very important factors that give rise to non-isothermal conditions. The mathematical modelling predictions corresponded very well to our experimental results.

Finally, whenever, performing mathematical modelling, its validation with physical experiments is very essential and quantitative comparisons should be done wherever, possible. When using commercial CFD codes like ANSYS, it is also necessary to understand the underlying physics governing their operation and performance.

Future Work

1. The effect of flow modifiers on RTD and slag entrainment is an important subject that needs further study. All the eighteen configurations of the tundish should be considered and slag entrainment tests and residence time measurements should be performed.
2. As mentioned earlier, micro-bubbles could be very useful in cleaning up the steel from smaller inclusions ($<50\mu\text{m}$). Detailed experiments and in plant studies need to be performed in order to learn how to control the bubble size in real steel making practice.
3. The exposed 'eye' should be measured in real steel making tundishes and correlated to that measured in the water models.
4. For modelling of non-isothermal melt flows, plant measurements should be done to assess the heat losses from the walls and free surface of the tundish. The effect of non-isothermal melt flows on inclusion separation should be computed, and checked against ESZpas inclusion results.
5. The effect of the biased ladle shroud should be tested in the plant.
6. Direct Numerical Simulations and Large Eddy Simulations should be done during mathematical modelling, as they are

more realistic. They require extremely high computational memory and for that high performance computer clusters need to be used.

Most of the future work mentioned above will be taken up by the author during his post doctoral studies with the McGill Metals Processing Center and RTIT/QIT.

Contribution to Original Knowledge

Modelling of steel making tundish operations has been an active area of research for the last three decades, and a huge amount of information is now available in the literature. After doing the literature review, it was felt that there is still a lot to do, in terms of improving the processes for yielding better steel quality. The following items of this thesis are claimed to be original, and to have been performed for the first time.

1. A detailed study of the effect of different flow modifiers on inclusion removal efficiency has been done for the delta shaped four strand tundish. Eighteen different tundish configurations were considered together for the first time, and the best configuration was identified.
2. A new dimensionless number (G_u) has been proposed, which is an effective measure of steel cleanliness in terms of inclusion content.

3. For the first time, slag movements and fluid flow patterns were considered during inert gas shrouding. Three dimensional mathematical modelling and full and reduced scale water modelling were performed to study the fluid flow patterns and formation of the slag 'eye'.
4. Modelling of the exposed 'eye' in a tundish due to inert gas shrouding has been done for the first time in this doctoral study. A combined discrete phase plus VOF approach was performed to model the exposed 'eye' and was validated with experiments.
5. For the first time, the effect of ladle shroud alignment on liquid metal quality has been considered and studied
6. Detailed studies of non-isothermal melt flows in a delta shaped four strand tundish have been performed. All previous studies mostly involved single strand tundishes and mathematical modelling. For the first time, physical and mathematical modelling was applied simultaneously to study the effects non-isothermal conditions on melt flows during steady state casting and ladle change operations.

This doctoral thesis also resulted in the following journal publications:

1. "Physical and Mathematical Modelling to Study the Effect of Ladle Shroud mis-alignment on Liquid Metal Quality in a Tundish" Kinnor

Chattopadhyay, Mihaiela Isac and Roderick I.L.Guthrie, ISIJ International, Vol. 51 (2011), No. 5, pp. 759–768

2. "Physical and Mathematical Modelling of Inert Gas Shrouding in a Tundish" Kinnor Chattopadhyay, Mihaiela Isac and Roderick I.L.Guthrie, ISIJ International, Vol. 51 (2011), No. 4, pp. 573–580
3. "Applications of Computational Fluid Dynamics (CFD) in Iron and Steel Making"- Part 2, Kinnor Chattopadhyay, Mihaiela Isac and Roderick I.L. Guthrie, Ironmaking & Steelmaking, Volume 37, No 8, November, 2010 , pp. 562-569
4. "Applications of Computational Fluid Dynamics (CFD) in Iron and Steel Making"- Part 1, Kinnor Chattopadhyay, Mihaiela Isac and Roderick I.L. Guthrie, Ironmaking & Steelmaking, Volume 37, No 8, November, 2010 , pp. 554-561
5. "Vertical alignment of ladle shroud affects transient steel quality output from a multi-strand tundish" Kinnor Chattopadhyay, Liu Fengang, Mihaiela Isac and Roderick I.L. Guthrie , Ironmaking and Steelmaking , 38, (2011), pp. 112-118
6. "Physical and Mathematical Modelling of Steel Making Tundish Operations: A review of the last decade (1999-2009)" Kinnor Chattopadhyay, Mihaiela Isac and Roderick I.L. Guthrie, ISIJ International, Vol. 50, No.3,2010.pp 331-348
7. "Physical and Mathematical Modeling of Inert Gas-Shrouded Ladle

Nozzles and Their Role on Slag Behavior and Fluid Flow Patterns in a Delta-Shaped, Four-Strand Tundish” Kinnor Chattopadhyay, Mainul Hasan, Mihaiela Isac and Roderick I.L. Guthrie, Metallurgical and Materials Transactions B, Vol. 41B, No 1, 2010, pp225

REFERENCES

-
- ¹ Mazumdar, D., and Guthrie, R.I.L., *The Physical and Mathematical Modeling of Continuous Casting Tundish Systems*, ISIJ International, (1999) 39(6), pp 524-547.
- ² Guthrie, R.I.L., and Isac, M., *The Process Metallurgy of Ladle-Tundish-Mould Operations for Continuously Casting Slabs, Blooms and Billets*, Iron and Steel Making, (2003), pp 27- 32
- ³ Guthrie, R.I.L., *Engineering in Process Metallurgy*, Oxford University Press, (1992).
- ⁴ Tanaka, S., *Modelling Inclusion Behaviour and Slag Entrainment in Liquid Steel Processing Vessels*, PhD Thesis, McGill University, Montreal, Canada, 1989
- ⁵ Krishnapisharody, K., and Irons, G., *Studies of Slag Droplet Formation in Ladle Metallurgy: Part I*. Physical Modeling, ICS 2008, pp-367-374
- ⁶ Damle.C and Sahai.Y , *A Criterion for Water Modeling of Non-isothermal Melt Flows in Continuous Casting Tundishes*, ISIJ international, (1996) 36(6), pp 681-689
- ⁷ Sahai, Y., and Emi, T., *Tundish Technology for Clean Steel Production*, World Scientific Publication Co. Pte. Ltd. (2008)
- ⁸ Ghosh, A., *Secondary Steel Making, Principles and Applications*, CRC Press (2001)
- ⁹ Lopez-Ramirez, S., Barreto, J De J., Vite-Martinez, P., Serrano, J A Romero, Duran-Valencia, C., *Physical and Mathematical* 333

Determination of the Influence of Input Temperature Changes on the Molten Steel Flow Characteristics in Slab Tundishes, Metallurgical and Materials Transactions B, (2004) 35B(5), pp 957-966

¹⁰ Vargas-Zamora, A., Morales, R. D., Diaz-Cruz, M., Palafox-Ramos, J., Garcia, D. L., *Heat and Mass Transfer of a Convective-Stratified Flow in a Trough Type Tundish*, International Journal of Heat and Mass Transfer, (2003), 46(16); pp 3029-3039.

¹¹ Craig, K. J., De Kock, D. J., Makgata. K. W., De Wet, G. J., *Design Optimization of a Single-Strand Continuous Caster Tundish Using Residence Time Distribution Data*, ISIJ International, (2001) 41(10), pp 1194-1200.

¹² Solhed, H., Jonsson, L., Jonsson. P., *A Theoretical and Experimental Study of Continuous-Casting Tundishes Focusing on Slag-Steel Interaction*, Metallurgical and Materials Transactions B, (2002) 33B(2), pp 173-185.

¹³ Solhed, H., Jonsson, L., *An Investigation of Slag Floatation and Entrapment in a Continuous-Casting Tundish Using Fluid-Flow Simulations, Sampling and Physical Metallurgy*, Scandinavian Journal of Metallurgy, (2003) 32(1), pp 15-32.

¹⁴ Debroy, T., and Sychterz, J.A., *Numerical Calculation of Fluid Flow in a Continuous Casting Tundish*, Metallurgical and Materials Transactions B,(1985)16B, pp 497-504.

¹⁵ Launder, B.E., and Spalding, D. B., *Lectures in Mathematical Models of Turbulence*, Academic Press, NY, 1972

¹⁶ Yakhot, V., and Orszag, S. A., *Renormalization Group Analysis of Turbulence. I. Basic Theory*, J. Sci. Comput., (1986), 1, pp3.

¹⁷ Shih, T.-H., Liou, W.W., Shabbir, A., Yang, Z. and Zhu, J., *A New k - ϵ Eddy Viscosity Model for High Reynolds Number Turbulent Flows -Model Development and Validation*, NASA TM 106721,(1994)

¹⁸ Schwarze, R., Obermeier, F., Hantusch, J., Franke, A., Janke, D., *Mathematical Modelling of Flows and Discrete Phase Behaviour in a V-Shaped Tundish*, Steel Research, (2001) 72(5+6), pp 215-220.

¹⁹ Schwarze, R., Obermeier, F., Janke, D., *Numerical Simulation of Fluid Flow and Disperse Phase Behaviour in Continuous Casting Tundishes*, Modelling and Simulation in Materials Science and Engineering, (2001), 9(4); pp 279-287

²⁰ Qinfu, H., Zongshu, Z., *Comparison Between Standard and Renormalization Group k - ϵ models in numerical simulation of Swirling Flow Tundish*, ISIJ International, (2005) 45(3), pp 325-330.

²¹ Jha, P. K., Ranjan, R., Mondal, S. S. and Dash, S. K., *Mixing in a Tundish and a Choice of Turbulence Model for its Prediction*, International journal of Numerical Methods for Heat and Fluid Flow, (2003) 13(8), pp 964 – 996

²² Ilegbusi, O. J., *Application of Two Fluid Model of Turbulence to Tundish Problems*, ISIJ International, (1994) 34(9), pp 732-738.

²³ Jha, P. K., Dash, S. K., *Effect of Outlet Positions and Various Turbulence Models on Mixing in a Single and Multi Strand Tundish*, International Journal of Numerical Methods for Heat & Fluid Flow, (2002) 12(5), pp 560-584.

²⁴ Robert, A., Mazumdar, D., *Physical and Mathematical Modelling of Flow and Residence Time Distributions in Different Tundish Designs*, Steel Research, (2001) 72(3); pp 97-105

²⁵ Patankar, S. V., and Spalding, D. B., *A Calculation Procedure for Heat, mass and Momentum Transfer in Three Dimensional Flows*, International Journal of Heat and Mass Transfer, (1972) 15, 1787-1806

²⁶ Versteeg, H. K and Malalasekera, W., *An Introduction to Computational Fluid Dynamics: The Finite Volume Method*, McGraw-Hill, Loughborough University, (1995)

²⁷ Fan, C-M., Hwang, W-S., *Mathematical Modeling of Fluid Flow Phenomena During Tundish Filling and Subsequent Initial Casting Operation in Steel Continuous Casting Process*, ISIJ International, (2000) 40(11), pp 1105-1114.

²⁸ Odenthal, H-J., Pfeifer, H., Klaas, M., *Physical and Mathematical Modeling of Tundish Flows Using Digital Particle Image Velocimetry and CFD-Methods*, Steel Research, (2000) 71(6+7), pp 210-219.

²⁹ Sheng , D.Y., and Jonsson, L., *Two-Fluid Simulation on the Mixed Convection Flow Pattern in a Non-isothermal Water Model of Continuous Casting Tundish*, Metallurgical and Materials Transactions B, (2000) 31B (4), pp 867-875.

³⁰ Ahn, J. H., Lee, Jung-Eui, Yoon, J. K., *Analysis of mixed grade transition in continuous thin slab casting with EMBR* , International Conference on Processing Materials for Properties, Proceedings, 2nd, San Francisco, CA, United States, (2000), pp577-581.

³¹.Sinha, S.K, Godiwalla, K.M, Shaw, D.K., and Sivaramakrishnan, C.S., *Fluid flow behaviour in a water model tundish under open, submerged and modified inlet conditions*, Scandinavian Journal of Metallurgy, (2001) 30, Pg 103-107

³² Sahai.Y, *Modelling of Melt Flow in Continuous Casting Tundishes*, The Brimacombe Memorial Symposium, Vancouver, BC, Canada, (2000) pp 631-641

³³ Ferro, S.P., Principe, R.J., and Goldschmit, M.B., *A New Approach to the Analysis of Vessel Residence Time Distribution Curves*, Metallurgical and Materials Transactions B, (2001) 32B, pp1185 - 1193

³⁴ Gardin, P., Brunet, M., Domgin, J.F., and Pericelous, K., *An Experimental and Numerical CFD Study of Turbulence in a Tundish Container*, Applied Mathematical Modelling, (2002) 26, pp323-336

³⁵ Jha, P.K. and Dash, S.K., *Employment of different turbulence models to the design of optimum steel flows in a tundish*, International Journal of Numerical Methods for Heat and Fluid Flow, (2004) 14(8), pp 953-979

³⁶ Pardesi, R., Basak, S., Singh, A.K., Basu, B., Mahashabde ,V., Roy, S.K., and Kumar, S., *Mathematical Modeling of the Tundish of a Single-Strand Slab Caster*, ISIJ International, (2004) 44 (9) , pp 1534-1540.

³⁷ Kumar A., Koria S.C., and Mazumdar D., *An Assessment of Fluid Flow Modelling and Residence Time Distribution Phenomena in Steelmaking Tundish Systems*, ISIJ International, (2004) 44 (8), pp 1334 - 1341.

³⁸ Zamora, A.V., Morales, R.D., Diaz-Cruz, M., Palafox-Ramos, J., and Barreto, J .De J., *Inertial and buoyancy driven water flows under gas bubbling and thermal stratification conditions in a tundish model*, Metallurgical and Materials Transactions B, (2004) 35B, pp247-257

³⁹ Ramos-Banderas, A., Sanchez-Perez, R., Morales, R.D. Palafox-Ramos, J., Demedices-Gracia, L., and M. Diaz-Cruz, *Mathematical simulation and physical modeling of unsteady fluid flows in a water model of a slab mold*, Metallurgical and Materials Transactions B, (2004) 35B, pp449-460

⁴⁰ Tripathi, A. and Ajmani, S.K, *Numerical Investigation of Fluid Flow Phenomenon in a Curved Shape Tundish of Billet Caster* ,ISIJ International, 2005 45(11) , pp 1616-1625

⁴¹ Cho, M.J. and Kim, I.C., *Simple Tundish Mixing Model of Continuous Casting during a Grade Transition*, ISIJ International, (2006) 46(10), pp 1416-1420

⁴² Huang, X., and Thomas, B.G., *Intermixing model of continuous casting during a grade transition*, Metallurgical and Materials Transactions B, (1996) 27B,pp 617-632

⁴³ Alkishriwi, N., Meinke, M., and Schroder, W., *A large-eddy simulation method for low mach number flows using preconditioning and multigrid*, Comp. Fluids, (2006) 35(10), pp1126–1136

⁴⁴ Davila, O., Morales, R.D., and Gracia- Demedices, L., *Mathematical simulation of fluid dynamics during steel draining*

operations from a ladle, Metallurgical and Materials Transactions B, (2006) 37B, pp71

⁴⁵ Sankanarayan, R., and Guthrie, R.I.L, *Slag entraining vortexing funnel formation during ladle teeming: similarity criteria and scale-up relationships*, Ironmaking and Steelmaking, (2002) 29, pp 147-153

⁴⁶ Sankanarayan, R., and Guthrie, R.I.L, *A Laboratory Study of Slag Entrainment during Emptying of Metallurgical Vessels*, ISS Steelmaking Conf., (1992) 75, pp. 655-664

⁴⁷ Vayrynen, P. Vapalahti, S., Louhenkilpi, S., Clark, M. and Wagner, T., *Tundish flow model tuning and validation: steady state and transient casting situations*, STEEL SIM 2007, Austria

⁴⁸ Zorzut, M., Vecchiet, F. Kapaj, N., and Paderno, A., *Tundish Flow Optimization and Steel Grade Change Prediction*, BHM, 152. Jg.(2007), Heft 11, pp 355-360

⁴⁹ Alizadeh, M., Edris, H., and Shafyei, A., *Fluid Flow and Mixing in Non-Isothermal Water Model of Continuous Casting Tundish*, Journal of Iron and Steel Research, International. 2008, 15(2), pp7-13, 22

⁵⁰ Yun WANG, Yunbo ZHONG, Baojun WANG, Zuosheng LEI, Weili REN and Zhongming REN, *Numerical and Experimental Analysis of Flow Phenomenon in Centrifugal Flow Tundish*, ISIJ International, Vol. 49 (2009), No. 10, pp. 1542–1550

⁵¹ Warzecha, M., Merder, T., Pfeifer¹, H., and Pieprzyca, J., *Investigation of Flow Characteristics in a Six-Strand CC Tundish Combining Plant Measurements, Physical and Mathematical Modeling*, Steel Research International,(2010) 81(11), pp 987-993

⁵² Hamill, I., Lucas, T., *Computational Fluid Dynamics Modelling of Tundishes and Continuous Casting Moulds*, Fluid Flow Phenomena in Metals Processing, TMS Annual Meeting, San Diego, (1999), pp279-286.

⁵³ Joo, S., and Guthrie, R.I.L., *Heat flow and inclusion behaviour in a tundish for slab casting*, Canadian Metallurgical Quarterly, Vol 30, (1991), pp261-269

⁵⁴ Hulstrung, J., Zeimes, M., Au, A., Oppermann, W., and Redusch, G., *Optimization of Tundish Design to Increase the Product Quality By Means of Numerical Fluid Dynamics*, Steel Research, (2005) 76(1), pp 59-63

⁵⁵ Solorio-DIAZ G., Morales, R. D., Palafox-Ramos, J., Ramos-Banderas, A., *Modeling the Effects of A Swirling Flow on Temperature Stratification of Liquid Steel and Floatation of Inclusions in a Tundish*, ISIJ International, (2005), 45(8), 1129-1137

⁵⁶ Zhang, L., Taniguchi, S., Cai, K., *Fluid Flow and Inclusion Removal in Continuous Casting Tundish*, Metallurgical and Materials Transactions B, (2000) 31B(2), pp 253-266

⁵⁷ Javurek, M., Kaufmann, B., Zuba, G., Gittler, P., *Some New Aspects on inclusion Separation in Tundishes*, Steel Research, (2002) 73(5); pp 186-193

⁵⁸ B.G.Thomas and Hua Bai, *Tundish Nozzle Clogging - Application of Computational Models*, 18th Process technology Division Conference Proceedings, Vol 18. Iron and Steel Society, Warrendale, PA, 2001, pp 895-912

⁵⁹ Rogler, J. P., Heaslip, L. J., Mehrvar, M., *Inclusion Removal in a Tundish By Gas Bubbling*, Canadian Metallurgical Quarterly, (2004) 43(3), pp 407-415

⁶⁰ Nguyen, A.V., Ralston, J., and Schulze. H.J., *On modelling of bubble-particle attachment probability in flotation*, Int. J. Miner. Process., 1998, vol. 53, pp. 225-249

⁶¹ A. V. Kuklev, V. V. Tinyakov, Y. M. Yu, V. N. Gushchin, V. A. Ulyanin, V. G. Ordin, A. M. Lamukhin, A. A. Myasnikov., *Effectiveness of Refining Steel in a Tundish with Partitions* Metallurgist, 2004, Vol 48, Nos. 7-8, pp394

-
- ⁶² Rogler, J. P., Heaslip, L. J., Mehrvar, M., *Physical Modelling of Inclusion Removal in a Tundish by gas Bubbling*, Canadian Metallurgical Quarterly, (2005) 44(3),pp 357-368
- ⁶³ Rückert, A., Warzecha, M., Koitzsch, R., Pawlik, M., and Pfeifer, H., *Particle Distribution and Separation in Continuous Casting Tundish*, Steel Research International,(2009) 80(8), pp 568-574
- ⁶⁴ Dautre, D.; Guthrie, R.I.L.: U.S.Patent 4,555,662; *Method and apparatus for the detection and measurement of particulates in molten metal*; granted November 26th, (1985)
- ⁶⁵ Joo, S.; Guthrie, R.I.L.: *Inclusion behaviour and heat-transfer phenomena in steelmaking tundish operations: part I Aqueous modeling*; Metall. Matter. Trans. B, 24B, (1993), P.755
- ⁶⁶ Carozza, C.; Lenard, P. ; Sankanarayan, R.; Guthrie, R.I.L.: *Light Metals 1997 Métaux Légers Symposium*, 36th Annual Conference of Metallurgists; Sudbury, Ontario, (1997), P.185
- ⁶⁷ Li, M.; Guthrie, R.I.L.:*Liquid Metal Cleanliness Analyzer (LiMCA) in Molten Aluminum*; ISIJ Int.,41 , (2001), P.101
- ⁶⁸ Lopez-Ramirez, S., Morales, R.D., and Romero Serrano, J.A., *Numerical Simulation of the Effects of Buoyancy Forces and Flow Control Devices on Fluid Flow and Heat Transfer Phenomena of Liquid Steel in a Tundish*, Numerical Heat Transfer, Part A, (2000) 37(1) , pp 69-86
- ⁶⁹ Odenthal, H.J., Bolling, R., Pfeifer, H., Holzhauser, J.F., Wahlers, F.J. *Mechanism of fluid flow in a continuous casting tundish with different turbo-stoppers*, Steel Research, (2001) 72(11+12), pp 466-476.
- ⁷⁰ Morales, R.D., Diaz-Cruz, M., Palafox-Ramos, J., Ramirez, S.L., Barreto Sandoval, J.De J., Steel Research, 72(2001), No.1,pp 11-16
- ⁷¹ Bao, Y., Jang, W., Xu, B., Zhang, H., Journal of University Science and Technology, Beijing, (2002) 9(1), pp 13
- ⁷² Palafox-Ramos, J., Barreto, J. De J., Lopez-Ramirez, S., Morales, R. D., *Melt Flow Optimization Using Turbulence Inhibitors in Large Volume Tundishes*, Ironmaking and Steelmaking, (2001) 28(2), pp 101-109

⁷³ Morales, R. D., Lopez-Ramirez, S., Palafox-Ramos, J., Zacharias, D., *Mathematical simulation of effects of flow control devices and buoyancy forces on molten steel flow and evolution of output temperatures in tundish*, Ironmaking and Steelmaking, (2001) 28(1), pp 33 - 43

⁷⁴ K.H.Tacke and J.C.Ludwig: *Steel flow and inclusion separation in continuous casting tundishes*, Steel Research , (1987), 58, pp262-270

⁷⁵ Sinha, A.K., PhD Thesis, The Ohio State University, USA (1990)

⁷⁶ H.Nakajima, F.Sebo, S.Tanaka, L.Dumitru, D.J.Harris and R.I.L.Guthrie: *Tundish Metallurgy Vol I*, Steelmaking Conference Proceedings, ISS-AIME, 1986, 69, pp 705-716.

⁷⁷ Solorio-Diaz, G., Morales, R. D., Palafox-Ramos, J., Garcia-Demedices, L., Ramos-Banderas, A., *Analysis of Fluid Flow Turbulence in Tundishes Fed by a Swirling Ladle Shroud*, ISIJ International, (2004) 44(6), pp 1024-1032

⁷⁸ .Solorio-DIAZ G, Morales R D, Palafox-Ramos J, Ramos-Banderas A, *Modeling the Effects of a Swirling Flow on Temperature Stratification of Liquid Steel and Floatation of Inclusions in a Tundish*, ISIJ International, (2005), 45(8), pp 1129-1137

⁷⁹ B.E Launder and D. B. Spalding, *The Numerical Computation of Turbulent Flows*, Comput . Meth. Appl. Mech. Engng. 3, (1974),269

⁸⁰ S. H. Seyedein, M. Hasan, and A. S. Mujumdar, *Modelling of a single confined turbulent slot jet impingement using various $k - \epsilon$ turbulence models*, Applied Mathematical Modelling, (1994), 18, pp 526-537

⁸¹ Patankar, S. V. and Spalding, D. B., *A calculation procedure for heat, mass and momentum transfer in three-dimensional parabolic flows*, Int. J. Heat Mass Transfer., 15, (1972), pp 1787-1806

⁸² Versteeg, H. K and Malalasekera, W, *An Introduction to Computational Fluid Dynamics: The Finite Volume Method*, McGraw-Hill, Loughborough, (1995),pp 142

⁸³ ANSYS-FLUENT 12.0 User Guide

⁸⁴ Y. A. Buevich, *Motion resistance of a particle suspended in a turbulent medium*, Fluid Dyn., 1,(1966), pp119

⁸⁵ Hirt C.W.and Nichols B.D.; *Volume of fluid method for the dynamics of free boundaries*, Journal of computational physics, 39, 1981, pp. 201-225

⁸⁶ Kinnor Chattopadhyay, Mihaiela Isac and Roderick I.L. Guthrie, *Physical and Mathematical Modelling of Steelmaking Tundish Operations: A Review of the Last Decade (1999–2009)*, ISIJ Int., 50,(2010),331-348

⁸⁷ Yanping Bao, W.Jang, B.Xu, H.Zhang, Journal of University Science and Technology, Beijing,9, (2002), pp 13

⁸⁸ J. Palafox-Ramos, J. De J. Barreto, S. L. Ramirez, R. D. Morales, *Melt flow optimisation using turbulence inhibitors in large volume tundishes*, Ironmaking and Steelmaking, 28, (2001), pp101-109

⁸⁹ J. A. Morales Pereira et al. *Effect of Turbulence Inhibitors on Slag Emulsification in Continuous Casting Tundish*, (2001), Steelmaking Conference Proceedings, pp127- 137

⁹⁰ A.K.Sinha and A.Vassilicos, *Physical Modeling Study of Effect of a Turbulence Suppressor Device on Flow and Mixing in a Dual Strand Tundish*, (2001) Steelmaking Conference Proceedings, pp111- 125

⁹¹ Piccone, Sinha and Madden, *Intermix Trials at Gary No.2 Caster Using Different Tundish Configurations*,(2001)Steelmaking Conference Proceedings, pp101-110

⁹² S.L.Ramirez, J.De J. Barreto, J.Palafox-Ramos, R.D.Morales, D.Zacharias, *Modeling study of the influence of turbulence inhibitors on the molten steel flow, tracer dispersion, and inclusion trajectories in tundishes*, Met and Mat Trans B, 32B, (2001), pp 615-627

⁹³ A.A.Corona, R.D.Morales, M. Diaz-Cruz, J.Palafox-Ramos and H.R.Hernandez, *Modelling the effects of off-centered ladle streams on fluid flow of liquid steel in a slab tundish*, Steel Research, 73, (2002), pp 438- 444.

-
- ⁹⁴ A.A.Corona, R.D.Morales, M. Diaz-Cruz, J.Palafox-Ramos and L.Garcia. Demedices, *Thermal Stratification of Steel Flow in Tundishes with Off-Centred Ladle Shrouds Using Different Flow Control Designs* , Can Met Quart, Vol 42, No. 4, pp 455-464, 2003
- ⁹⁵ A.R.Banderas, R.D.Morales, .Garcia. Demedices, and M. Diaz-Cruz, *Mathematical Simulation and Modeling of Steel Flow with Gas Bubbling in Trough Type Tundishes*, ISIJ Int ,43, (2003), pp 653- 662
- ⁹⁶ P.Kovac, J.Kijac, V.Masek, P.Marek, P.Kalmar and K.Michalek, *Steel Cleanliness Improvement Through Tundish Configuration Optimizing*, METALLURGIJA, 42 (2003), pp 249-255
- ⁹⁷ LIU Jin-gang, YAN Hui-cheng, LIU Liu and WANG Xin-hua, *Water Modeling of Optimizing Tundish Flow Field*, Jour. of Iron and Steel Res Int, Vol 14, No.3,(2007), pp14-20
- ⁹⁸ H.B.Kim, *Modelling of transport phenornena in a delta shaped four strand tundish*, PhD Thesis, McGill University, Montreal, Canada, 2003
- ⁹⁹ S. Ray, *On application of physical and mathematical modelling to predict tundish performance*, PhD Thesis, McGill University, Montreal, Canada, 2009
- ¹⁰⁰ A.Chakraborty, M.Isac and R.I.L. Guthrie “*Results of RRI tests on standard QIT impact pad with 2 inch using the new McGill online aqueous particle detection system*”, Technical report for QIT, Jan 27, 2009
- ¹⁰¹ Kim, H.B., *Modelling of two phase gas-liquid flows in ladle shrouds*, Master of Engineering Thesis, McGill University, Montreal, Canada
- ¹⁰²D. Bolger, R. I. L. Guthrie, D. H. M. Kings, R .A. Sommers, and J. D. Usher, *Steelmaking Conference Proceedings of ISS*, Pittsburgh, (1996), 481
- ¹⁰³ Bai, H., and Thomas, B.G., *Effects of Clogging, Argon Injection, and Continuous Casting Conditions on Flow and Air aspiration in Submerged Entry Nozzles*, Metallurgical and Materials Transactions B, (2001) 32B, pp707- 722

-
- ¹⁰⁴ Evans, G.M., Rigby, G.D., Honeyands, T.A., He, Q.L., *Gas Dispersion Through Porous Nozzles into Down-Flowing Liquids*, Chemical Engineering Science, (1999) 54, pp 4861-4867
- ¹⁰⁵ Bai, H., and Thomas, B.G., *Turbulent Flow of Liquid Steel and Argon Bubbles in Slide-Gate Tundish Nozzles: Part I. Model Development and Validation*, Metallurgical and Materials Transactions B, (2001) 32B, pp 253 - 267
- ¹⁰⁶ Bai, H., and Thomas, B.G., *Turbulent Flow of Liquid Steel and Argon Bubbles in Slide-Gate Tundish Nozzles: Part II. Effect of Operation Conditions and Nozzle Design*, Metallurgical and Materials Transactions B, (2001) 32B, pp 269 - 284.
- ¹⁰⁷ CFX4.2 Users Manual, AEA Technology, Pittsburgh, PA, 1997.
- ¹⁰⁸ Li Tao WANG, Qiao Ying ZHANG, Chen Hong DENG and Zheng Bang Li, *Mathematical Model for Removal of Inclusion in Molten Steel by Injecting Gas at Ladle Shroud*, ISIJ International, (2005) 45(8), pp. 1138-1144
- ¹⁰⁹ Qiao Ying ZHANG, Li Tao WANG and Zhi Rong XU, *A New Method of Removing Inclusions in Molten Steel by Injecting Gas from the Shroud*, ISIJ Int. 46 (2006), pp.1177-1182
- ¹¹⁰ Jung-Soo CHO and Hae-Geon LEE, *Cold Model Study on Inclusion Removal from Liquid Steel Using Fine Gas Bubbles*, ISIJ Int., 41,(2001), pp.151-157
- ¹¹¹ Lalhua WANG. Hae-Geon LEE and Peter HAYES, *A New Approach to Molten Steel Refining Using Fine Gas Bubbles*, ISIJ Int., 36,(1996),pp17-24
- ¹¹²Xiaofeng ZHENG. Peter C. HAYES and Hae-Geon LEE, *Particle Removal from Liquid Phase Using Fine Gas Bubbles*, ISIJ Int., 37,(1997), pp 1091- 1097
- ¹¹³ Korla, S.C., and Srivastava, S.C., *Residence Time Distribution of Steel Melt Due to Argon Shrouded Stream Pouring in a Tundish*, Steel Research, (1999), 70(6) , pp. 221- 226
- ¹¹⁴ K. Chattopadhyay, M. Hasan, M. Isac and R. I. L. Guthrie, *Physical and Mathematical Modeling of Inert Gas-Shrouded Ladle Nozzles and Their*

Role on Slag Behavior and Fluid Flow Patterns in a Delta-Shaped, Four-Strand Tundish, Metall. Mater. Trans. B, 41B, (2010), pp. 225-233

¹¹⁵ K. Krishnapisharody and G. A. Irons: *A Study of Spouts on Bath Surfaces from Gas Bubbling: Part I. Experimental Investigation*, Metall. Mater. Trans. B, 38B, (2007), pp. 367-375

¹¹⁶ K. Krishnapisharody and G. A. Irons: *A Study of Spouts on Bath Surfaces from Gas Bubbling: Part II. Elucidation of Plume Dynamics*, Metall. Mater. Trans. B, 38B, (2007), pp. 377-388

¹¹⁷ K. Krishnapisharody and G. A. Irons, *An Extended Model for Slag Eye Size in Ladle Metallurgy*, ISIJ International, Vol. 48 (2008), No. 12, pp. 1807–1809

¹¹⁸ Baokuan LI, Hongbin YIN, Chenn Q. ZHOU, and Fumitaka TSUKIHASHI, " *Modeling of Three-phase Flows and Behavior of Slag/Steel Interface in an Argon Gas Stirred Ladle*" ISIJ International, Vol. 48 (2008), No. 12, pp. 1704–1711

¹¹⁹ M. Peranandhanthan and D. Mazumdar, *Modeling of Slag Eye Area in Argon Stirred Ladles*, ISIJ International, Vol. 50 (2010), No. 11, pp. 1622–1631

¹²⁰ D. Mazumdar and R. I. L. Guthrie: *Modeling Energy Dissipation in Slag-Covered Steel Baths in Steelmaking Ladles*, Metall. Mater. Trans. B, 41 (2010), pp. 976-989

¹²¹ Carlos A. LLANOS, Saul GARCIA-HERNANDEZ, J. An´gel RAMOS-BANDERAS, Jose de J. BARRETO and Gildardo SOLORIO-DIAZ , *Multiphase Modeling of the Fluid dynamics of Bottom Argon Bubbling during Ladle Operations*, ISIJ International, Vol. 50 (2010), No. 3, pp. 396–402

-
- ¹²² H. Solhed, L. Jonsson, P. Jonsson: *A theoretical and experimental study of continuous-casting tundishes focusing on slag-steel interaction*, Metall. Matter. Trans. B., 33B, (2002), pp. 173 - 185
- ¹²³ H. Solhed and L. Jonsson: *An investigation of slag floatation and entrapment in a continuous-casting tundish using fluid-flow simulations, sampling and physical metallurgy*, Scand. J. Metall.,32, (2003), pp. 15-32
- ¹²⁴ H.B.Kim, M.Isac and R.I.L.Guthrie:*Physical modelling of transport phenomena in a delta-shaped, four strand tundish with flow modifiers*, Steel Res. Int., 76, (2005), pp. 53-58
- ¹²⁵ S. Ray, M. Isac, R.I.L. Guthrie, A. Beaulieu, M. Gagne: AISTech 2008 Conference Proceedings, Continuous Casting/Process Technology, AIST, Warrendale, PA, (2008),51
- ¹²⁶ K. Chattopadhyay, L. Fengang, M. Isac and R. I.L. Guthrie: *Effect of vertical alignment of ladle shroud on transient steel quality output from multistrand tundish* , Ironmaking and Steelmaking, Vol 38, No. 2, 2011, pp. 112-118
- ¹²⁷ Chakraborty, S. and Sahai, Y.: *Effect of holding time and surface cover in ladles on liquid steel flow in continuous casting tundishes*, Metall. Trans. B, 1992, 23B, pp. 153-167
- ¹²⁸ S. Joo, J. W .Han, and R.I.L. Guthrie, *Inclusion behavior and heat-transfer phenomena in steelmaking tundish operations: Part II. Mathematical model for liquid steel in tundishes*, Metall. Matter. Trans. B, 24B, (1993), pp. 767 - 777
- ¹²⁹ Damle, C. and Sahai, Y.: *A Criterion for Water Modeling of Non-isothermal Melt Flows in Continuous Casting Tundishes*, ISIJ International, 1996, 36, pp. 681-689
- ¹³⁰ Mehdi Alizadeh, Hossein Edris and Ali Shafyei, *Fluid Flow and Mixing in Non-Isothermal Water Model of Continuous Casting Tundish*, Journal of Iron and Steel Research International, 2008, 15(2), pp 7-13, 22

¹³¹ D. Y. Sheng and Lage Jonsson, *Investigation on the Convection Pattern of Liquid Steel in the Continuous Casting Tundish by Theoretical Analysis, Water Model Experiment and CFD Simulation*, MEFOS, S 97125, Lulea, Sweden

¹³² Baosteel Group Co., Company Publications, *Numerical Simulation of The Coupled Fluid Flow and Heat Transfer and Optimization of Flow Control Devices in A Six-strand Tundish*, Technical Report, 2005-12-29,
http://www.baosteel.com/group_e/07press/ShowArticle.asp?ArticleID=40

¹³³ R D Morales, J de J Barreto, S López-Ramirez, J Palafox-Ramos and M Diaz-Cruz, *Mathematical simulation of the influence of buoyancy forces on the molten steel flow in a continuous casting tundish*, Modelling Simul. Mater. Sci. Eng., 2000, Vol. 8, pp 781-801

¹³⁴ ALEXANDER BRAUN, MAREK WARZECHA, and HERBERT PFEIFER, *Numerical and Physical Modeling of Steel Flow in a Two-Strand Tundish for Different Casting Conditions*, Metal Mater Trans B, 2010, 41 B pp 549 - 559

¹³⁵ YUJI MIKI and BRIAN G. THOMAS. *Modeling of Inclusion Removal in a Tundish*, Metal Mater Trans B ,1999, 30B, pp 639-654

¹³⁶ D. Y. SHENG and LAGE JONSSON, *Investigation of Transient Fluid Flow and Heat Transfer in a Continuous Casting Tundish by Numerical Analysis Verified with Non isothermal Water Model Experiments.*, Metal Mater Trans B, 1999, 30B, pp 979-985

¹³⁷ D. Y. SHENG and LAGE JONSSON, *Two-Fluid Simulation on the Mixed Convection Flow Pattern in a Non isothermal Water Model of Continuous Casting Tundish*, Metal Mater Trans B, 2000, 31B, pp 867-875

¹³⁸ Ray, S.K., Isac, M., Guthrie, R.I.L., and Gagne, M. *A comparative study of isothermal and non-isothermal modeling of flows in tundishes*, AISTech - Iron and Steel Technology Conference Proceedings , Volume 1, 2009, pp. 1151-1162